DISSERTATION

ION TRANSPORT, SENSING APPLICATIONS, AND REDOX GRADIENT FORMATION: AN ELECTROCHEMICAL STUDY OF ELECTRONICALLY CONDUCTING POLYMERS

Submitted by

Corey A. Salzer

Department of Chemistry

In partial fulfillment of the requirements

for the Degree of Doctor of Philosophy

Colorado State University

Fort Collins, Colorado

Spring 2002

COLORADO STATE UNIVERSITY

October 26, 2001

WE HEREBY RECOMMEND THAT THE DISSERTATION PREPARED UNDER OUR SUPERVISION BY COREY A. SALZER ENTITLED ION TRANSPORT, SENSING APPLICATIONS, AND REDOX GRADIENT FORMATION: AN ELECTROCHEMICAL STUDY OF ELECTRONICALLY CONDUCTING POLYMERS BE ACCEPTED AS FULFILLING IN PART THE REQUIREMENTS FOR THE DEGREE OF DOCTOR OF PHILOSOPHY.

Committee on Graduate Work

Advisor

Department Head

ABSTRACT OF DISSERTATION

ION TRANSPORT, SENSING APPLICATIONS, AND REDOX GRADIENT FORMATION: AN ELECTROCHEMICAL STUDY OF ELECTRONICALLY CONDUCTING POLYMERS

Conducting polymers are a unique class of materials that exhibit very interesting electronic characteristics. The ease of modification of the polymers and their physical and electronic properties make these very attractive materials for a large number of applications. Conducting polymers have been studied for use in light emitting devices, as sensing materials, for drug delivery, and antistatic coatings. Fundamental to most of the polymers potential applications is the occurrence of ion transport in and out of the polymer material during oxidation and reduction processes.

In Chapter Two, a rotating ring-disk electrochemical method is applied to the study of ion transport in films of poly(pyrrole). Many researchers have examined the nature of ion flux in conducting polymers, but the methods they employed have drawbacks to the quantitative, *in situ* measurement of the ion transport occurring in the polymers. We present a means of surmounting the shortcomings of the other methods of analyzing ion transport in conducting polymers and give insight into the nature of ion flux in poly(pyrrole) films.

Chapters Three and Four report on the use of poly(3,4-diphenylpyrrole) films as a sensing material for chlorinated hydrocarbons. Chapter Three employs impedance

spectroscopy as a tool to monitor capacitance and resistance changes of the polymer that occurs upon interaction of the film with dichloromethane in an aqueous environment. These impedance changes were used to sense the presence of dichloromethane. Chapter Four uses the di-substituted polymer films as the sensing material in a vapor sensor possessing selectivity for small, chlorinated hydrocarbons. Here, changes in film resistance occur as a result of a charge transfer complex between the polymer and the analyte vapor. The direction and magnitude of the resistance change is used to identify the vapor.

In Chapter Five, chemically locked redox gradients are formed in ruthenium- and iron-based redox polymers. Thermally polymerizable anions were incorporated into the polymers for polymerization with pendant acrylate groups on the redox polymer. The intent was to permanently lock the redox gradients in the film; thus improving upon the on the thermally locked gradients formed in similar films by other researchers.

Corey Alan Salzer
Chemistry Department
Colorado State University
Fort Collins, CO 80523
Spring 2002

COPYRIGHT PAGE

Chapter 2, Part I and Chapter 2, Part II have been previously published. The copyright information for the two publications are listed below, respectively.

QUANTITATIVE IN SITU MEASUREMENT OF ION TRANSPORT IN POLYPYRROLE/POLY(STYRENESULFONATE) FILMS USING ROTATING RING-DISK VOLTAMMETRY

C. Michael Elliott.*,⊗ Corey A. Salzer,⊗ and Susan M. Hendrickson[a]
Department of Chemistry
Colorado State University
Ft. Collins, CO 80524

*Corresponding author
⊗Colorado State University
[a]Present address: Davidson College, Davidson, North Carolina 28036

QUANTITATIVE IN SITU STUDIES OF IONIC DOPING OF POLYPYRROLE EMPLOYING ROTATED RING-DISK ELECTRODE VOLTAMMETRY

C. Michael Elliott*,⊗ and Corey A. Salzer⊗
Department of Chemistry
Colorado State University
Ft. Collins, CO 80524

*Corresponding author
⊗Colorado State University

ACKNOWLEDGEMENT

I would like to thank my research advisor Dr. C. Michael Elliott and the members of Dr. Elliott's research group. Their patience and assistance have made this work possible. I would also like to thank my family for their loving support throughout my education.

TABLE OF CONTENTS

LIST OF TABLES

LIST OF FIGURES

LIST OF SCHEMES

LIST OF ABBREVIATIONS

3-SPA$^-$	3-Sulfopropyl acrylate
4,4'-DEAB	4,4'-dicarbo(acrylatoprop-1-oxy)-2,2'-bipyridine
4,4'-PAB	4,4'-(pentyl-1-acrylato)-2,2'-bipyridine
A$^-$	Anion
BArF$^-$	Tetrakis(3,5-bis(trifluoromethyl)phenyl)borate
bpy	Bipyridine
C$^+$	Cation
Cc$^+$	Bis(cyclopentadienyl)cobalt(II)
CMP$^+$	1-Methyl-3-cyanopyridinium
DMP$^+$	1,3-Dimethylpyridinium
DMSO	Dimethylsulfoxide
EC	Electrochemical-chemical reaction steps
E_{disk}	Disk potential
E_{ring}	Ring potential
EQCM	Electrochemical quartz crystal microgravimetry
f_{C^+}	Fraction of doping change due to C$^+$
IDA	Interdigitated array
$i_d(t)$	Total disk current
I_P	Ionization potential
$i_{r,0}$	Background ring current
i'_r	Instantaneous corrected ring current

$i_r(t)$	Total ring current
$i_r'(t)$	Corrected ring current
poly(EDOT)	Poly(3,4-ethylenedioxythiophene)
PPN^+	Bis(triphenylphosphoranylidene)ammonium
pPy	Poly(pyrrole)
pSS^-	Poly(4-styrenesulfonate)
p(DPP)	Poly(3,4-diphenylpyrrole)
R_A	Resistance in air
RRDE	Rotating ring-disk electrode
R_V	Resistance in vapor-saturated air
SECM	Scanning electrochemical microscopy
SS^-	Styrenesulfonate
SSCE	Saturated sodium calomel electrode
TBA^+	Tetrabutylammonium
TEA^+	Tetraethylammonium
TMA^+	Tetramethylammonium
Tos^-	*p*-toluenesIfonate
XPS	X-ray photoelectron spectroscopy
Z	Impedance of a circuit
Z'	Real impedance component
Z"	Imaginary impedance component
|Z|	Impedance modulus
θ	Phase angle

$\Delta R/R$	Relative resistance change

CHAPTER 1

General Background of Organic Conducting Polymer Materials

INTRODUCTION

Organic conducting polymers comprise a unique class of conducting materials that have received increasing attention from physicists and chemists alike since the early 1970s. The draw to these materials lies in their electronic and ionic conduction, the ready modulation of their physical and chemical properties, and their use in a wide range of applications. Such materials, (i.e., poly(pyrrole), poly(aniline), and poly(thiophene)), have found applications in sensors[1-12], charge storage devices[13-18], coatings[16,18], and membranes[19-22]. Optimization of these materials requires a thorough understanding of the electronic conduction process and physical properties of such materials given a range of environmental conditions and chemical modifications.

Conduction in Organic Conducting Polymers. The fundamental characteristic of organic conducting polymers leading to electronic conductivity is the extensive conjugation of π-orbitals along the polymer backbone. The high degree of conjugation in such linear polymers results in molecular orbital energies that overlap and form band-like electronic structures with a band gap between the HOMO (π) and LUMO (π^*) (see Figure 1.1).[23] In the neutral film, the band gap is quite large. Thus, the neutral state of the

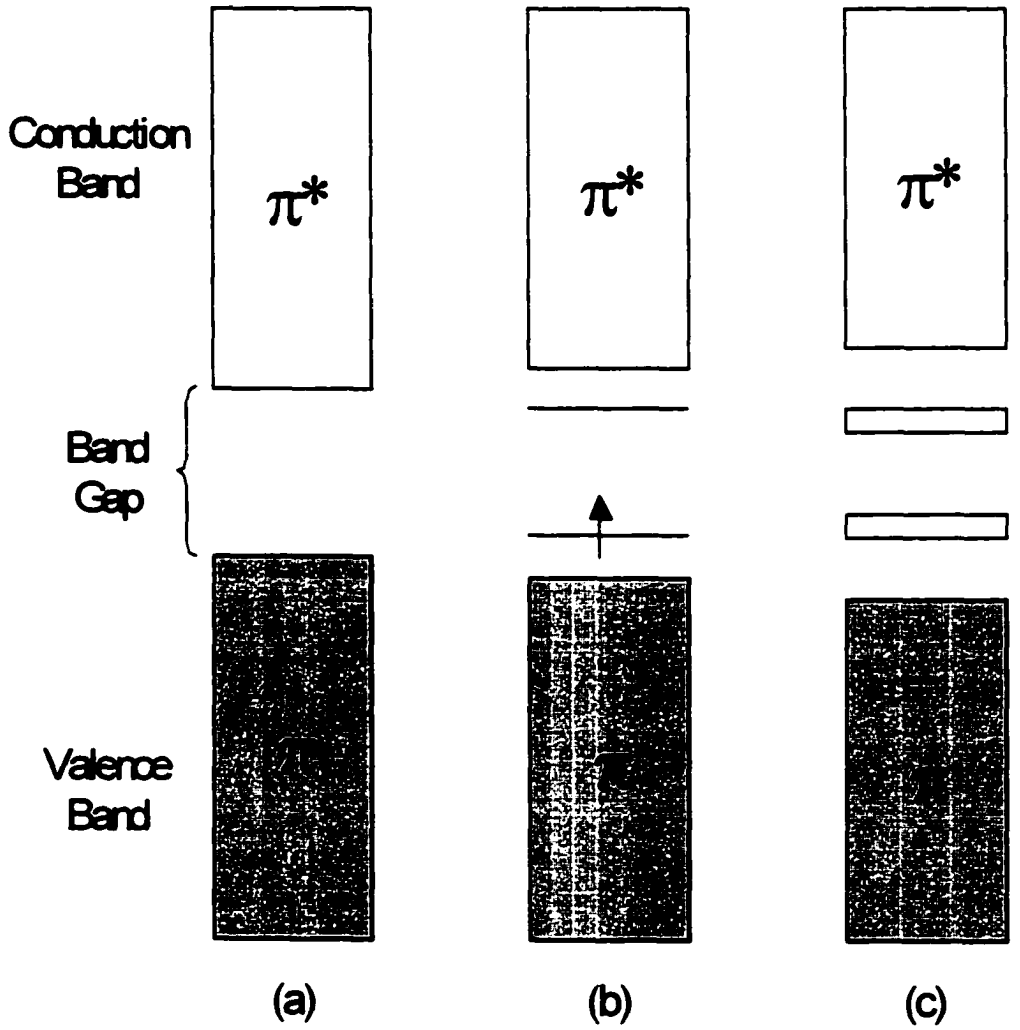

Figure 1.1. Diagram showing the band structure of a conducting polymer as it becomes increasingly oxidized. (a) Neutral polymer. (b) Polaron formation. (c) Bipolaron formation at high levels of polymer oxidation. The bands shown in (c) are empty.

polymers is electrically insulating. However, 'doping' of the films (a term borrowing from semi-conductor terminology), can manipulate the band structure of the polymers. This change in the band structure is intimately related to the electrochromic properties and the conductive state of the films. Conductivities of several of these materials can be quite significant, approaching that of true metals[24,25] (see Table 1.1).

The term 'doping' in the context of conducting polymers refers to the introduction of charge defects on the polymer material. These defects occur in the form of a charge transfer complex between the polymer backbone and a counterion, or 'dopant'. These defects take on different forms depending on polymer type and degree of oxidation. Most organic conducting polymers undergo p-doping, but a few can also be n-doped.[16] This discussion will be limited to p-doping in polymers, particular poly(pyrrole).

P-doping in conducting polymers such as poly(pyrrole) is actually an oxidation process, either by chemical or electrochemical means, which results in the formation of cations on the conjugated backbone of the polymer. Doping promotes energy levels and eventually bands (at higher oxidation states) into the band gap[26,27] (Figure 1.1b and 1.1c).

Initial oxidation (or p-doping) of the polymer creates radical cations (spin ½) on the polymer backbone. These radical cation species, known as polarons, are the charge carriers responsible for electronic conductivity at low oxidation levels[26] (see Fig. 1.1b). For higher levels of polymer oxidation, it is energetically favorable for polarons to combine; forming a dication species called a bipolaron (two cations separated by 3 to 5 monomer units, spin 0).[26] These electronic species are thought to be analogous to a Cooper pair as discussed in superconductor theory.[26] Both defect types are associated

Material	Conductivity, $\Omega^{-1}cm^{-1}$
Copper	10^{6}
Graphite	10^{4}
Poly(acetylene)	200-1000
Poly(paraphenylene)	500
Poly(pyrrole)	40-200
Poly(thiophene)	10-100
Glass	10^{-11}
Nylon	10^{-15}

Table 1.1. List of common conducting polymers and materials with their conductivities. (Adapted from references 24 and 25)

with a lattice distortion of the polymer backbone and are also the mobile charge carriers, not electrons, in these types of polymers.[26] Thus, electronic conduction in organic conducting polymers involves movement of charge as polarons and bipolarons *along* the polymer backbone. Polymer strand lengths are typically small with respect to film thicknesses. Therefore, bulk conduction is also believed to involve the intra-chain and fibril motion of these carrier species.[28] This differs from redox polymers where conduction occurs via electron hopping between redox centers connected by an insulating organic polymer backbone (Figure 5.1, Chapter 5 of this text).[29]

Maintaining charge neutrality is, of course, necessary in the oxidized polymer. This occurs by the incorporation of counterions (i.e., dopants) from the electrolyte solution during oxidation of the polymer. For a p-doped film, anions are present in the films' oxidized state. This doping process will be discussed at length below.

Polymer Growth and Formation. Polymerization and growth of conducting polymers is typically accomplished by two methods: chemically or electrochemically. The former involves the chemical oxidation of the monomer by oxidizing agent such as $FeCl_3$, AsF_5, or any other suitable oxidizing agent. The oxidized monomers react to form bulk polymeric materials. Chemical synthesis has the advantage of ease of production and low cost, particularly in scale up production. This method is especially attractive for commercial processes. The synthesized material can be shaped into films[30] or drop cast to form films from a solution of polymer in an appropriate solvent.[30,31] Chemical polymerization is also useful for polymer formation on non-conductive surfaces and on colloidal particles.[30,32,33]

Commonly, polymerization is achieved by electrochemical anodic polymerization onto an electrode surface compatible with the applied potentials for film growth (i.e., gold, platinum, glassy carbon, or indium tin oxide coated glass). The insoluble polymer adheres to the surface of the electrode in the form of a film. This is a useful arrangement for electrochemical investigations. Polymer membranes can also be formed by growth of polymer onto gold grid or other porous electrode arrangements.[20]

Scheme 1.1 shows a proposed[34] electrochemical oxidation of heterocyclic conducting polymers, in this case, pyrrole. Loss of one electron from a monomer unit results in formation of a radical cation. This species can either react with another oxidized pyrrole unit or react with a neutral monomer and, with the loss of two protons, produce the dimer. Due to the lower oxidation potential of the dimer as a result of the molecules' increased conjugation and ability to stabilize its oxidized form, the growth of larger oligomers and extended polymer chains is favored. This is not the only proposed mechanism for polymerization of pyrrole. In a review by Sadki et al., a number of mechanisms are reported, each with reasonably supportive evidence.[34] The actual mechanism is still a topic of controversy.

Mechanism aside, electrochemical growth methods: galvanostatic, potentiostatic, or potential cycling, provide several favorable polymer growth features. Films of the polymer can be grown rapidly and to desired size (i.e., area) and thickness. Thickness of the polymer may be controlled through the monitoring of the charge passed during oxidation. Approximately 2.2 electrons are consumed per polymerization event of

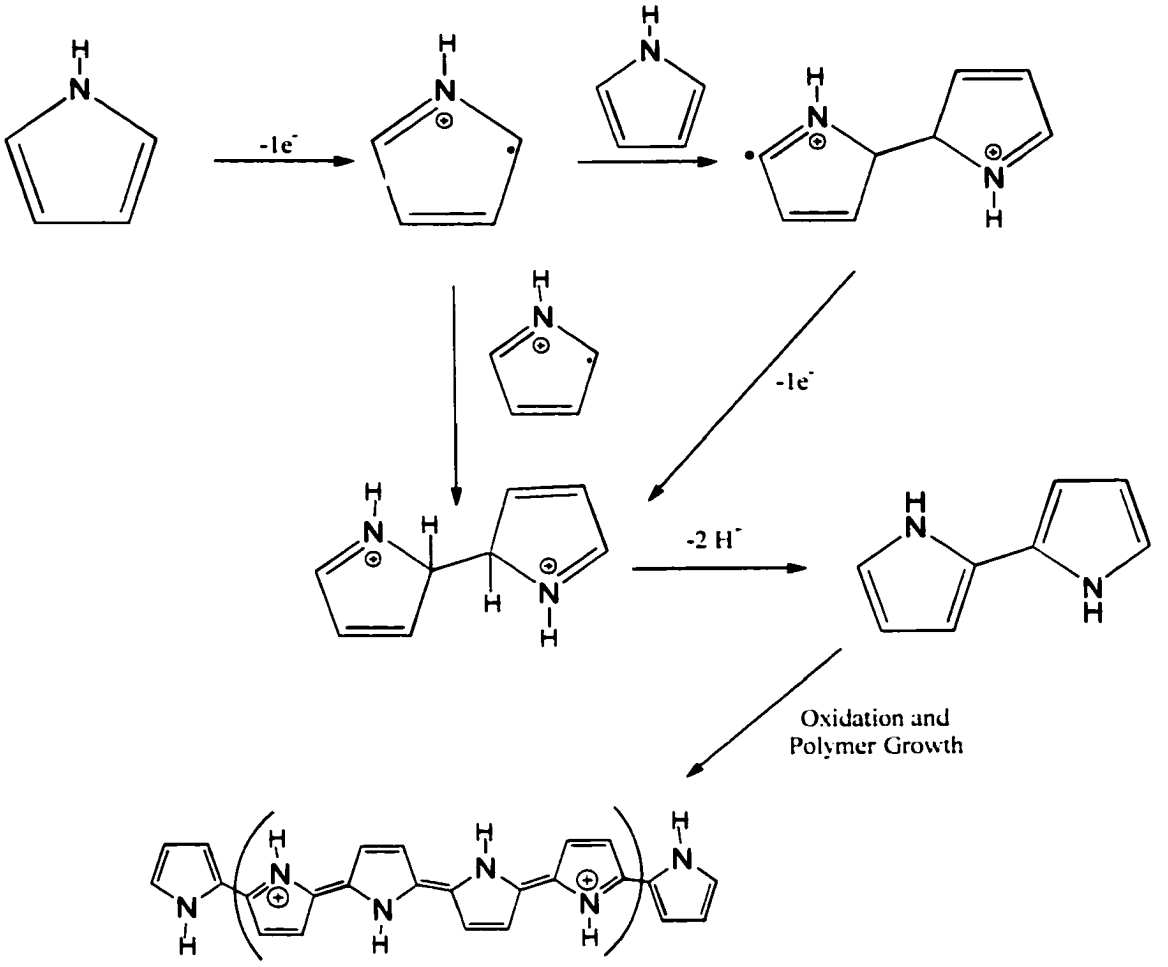

Scheme 1.1. A proposed mechanism for the electrochemical synthesis of poly(pyrrole).

poly(pyrrole): 2 electrons for polymerization and 0.2 electrons for partial positive charge on polymer backbone.[35] Thus, the moles of monomer consumed for film formation can be measured by knowing the charge passed during film formation and electrode area. Correlation of the data with profilometry or other thickness profiling data can be used to monitor the thickness of the electropolymerized films.[13]

Electrochemical growth also provides for a wide range of dopant inclusion during growth. This can be advantageous with respect to manipulation of film properties since the incorporated ion can significantly affect film characteristics such as morphology, conductivity, and work function.[36,37] Electrochemical polymerization, in comparison to chemical oxidation polymerization, allows for both rapid polymer preparation and greater control of film growth.

Modification of Film Properties/Behavior. The chemical and physical properties of conducting polymers such as poly(pyrrole) and poly(thiophene) can be readily modulated with the addition of substituents to the monomer unit. Through the use of appropriate substituents, properties of conducting polymers such as conductivity, morphology, solubility, and electrochromic behavior of conducting polymers can be customized for various applications.[38-43] The substitution of phenyl groups at the 3- and 4-positions of pyrrole will greatly change the properties of the polymer. The presence of the phenyl groups eliminates β,β-coupling of the monomers during film growth, sterically hinders the alignment of the phenyl rings in a polymer strand affecting conductivity, and changes the films solvation characteristics.[44] As will be discussed in Chapter 3, this change in solvation affects the redox switching of the polymer films which can be a useful characteristic for a sensor.[44]

The conductivity of poly(thiophene) can be manipulated with the addition of a single substituent. Waltman et al., report the addition of a methyl group to the 3-position on thiophene yields a 100-fold increase in conductivity of the polymer.[17,44] The conductivity of poly(3-methylthiophene) was shown to increase by five orders of magnitude in comparison to poly(thiophene) prepared under identical conditions!

In another example, the oxidation potential and optical properties can also be modulated by addition of a bridging substituent to the monomer. Polymers of the substituted thiophene, EDOT (3,4-ethylenediethoxythiophene), have very different properties from those of unsubstituted thiophene polymers. The addition of electron donating groups at the 3,4-positions drastically reduces the oxidation potential of the polymer. EDOT also has one of the lowest band gap energies of conducting polymers, about 1.6 eV; as a result the monomer is blue in color compared to the transparent thiophene solutions.[45] Films of poly(EDOT) can range from sky blue to transparent depending upon oxidation state.[45] Commercial uses of this polymer have included antistatic coatings and charge storage.[46]

The choices of solvent and counterion have also been shown to have considerable influence upon the conducting polymer characteristics. Changing the counterion incorporated in a film during polymerization has been noted to affect the resulting film morphology of the polymer and the nature of the counterion motion that occurs in the film during redox cycling.[37] In other cases, the counterion can even influence the facility of polymerization, as will be demonstrated in Chapter Four of this thesis. Solvent choice can affect the behavior and characteristics of the films as well. The solvent used for film growth and electrochemical studies can affect film morphology and counterion transport

behavior.[40,47-49] In one case, the vapor sensing capabilities of a polymer film were more selective for methanol vapors when the polymer was grown from a methanol solution instead of acetonitrile.[50]

Ion Transport. Electrochemical switching between the conducting (oxidized) and insulating (reduced) states of a conducting polymer requires the concomitant motion of counterions for maintaining charge neutrality. It is reported that the rate of redox switching is often limited by the facility of the appropriate ion motion in the polymer films.[48,51] Slow migration rates of dopant ions can impede the rate at which a desired oxidation state can be attained by the polymer. Since many of the polymer applications involve the redox switching of the polymer, an extensive amount of the research in the field of conducting polymers has involved the study of ion transport processes in various polymers under a variety of environments and conditions. However, the type of ion transport process that occurs in a particular film cannot yet be predicted with absolute certainty, as many variables exist that can affect the doping process.

As mentioned above, the oxidative growth of conducting polymers like poly(pyrrole) involve the inclusion of dopant anions for neutralization of the positive charge carriers. If the dopant anion is readily mobile, subsequent electrochemical reduction of the polymer will result in the expulsion of the dopants into the electrolyte solution. Re-oxidation of the film will require passage of anions from solution to charge sites in the polymer. This is depicted in Scheme 1.2a. A predominance of anion transport occurring for charge compensation is commonly reported for polymers doped

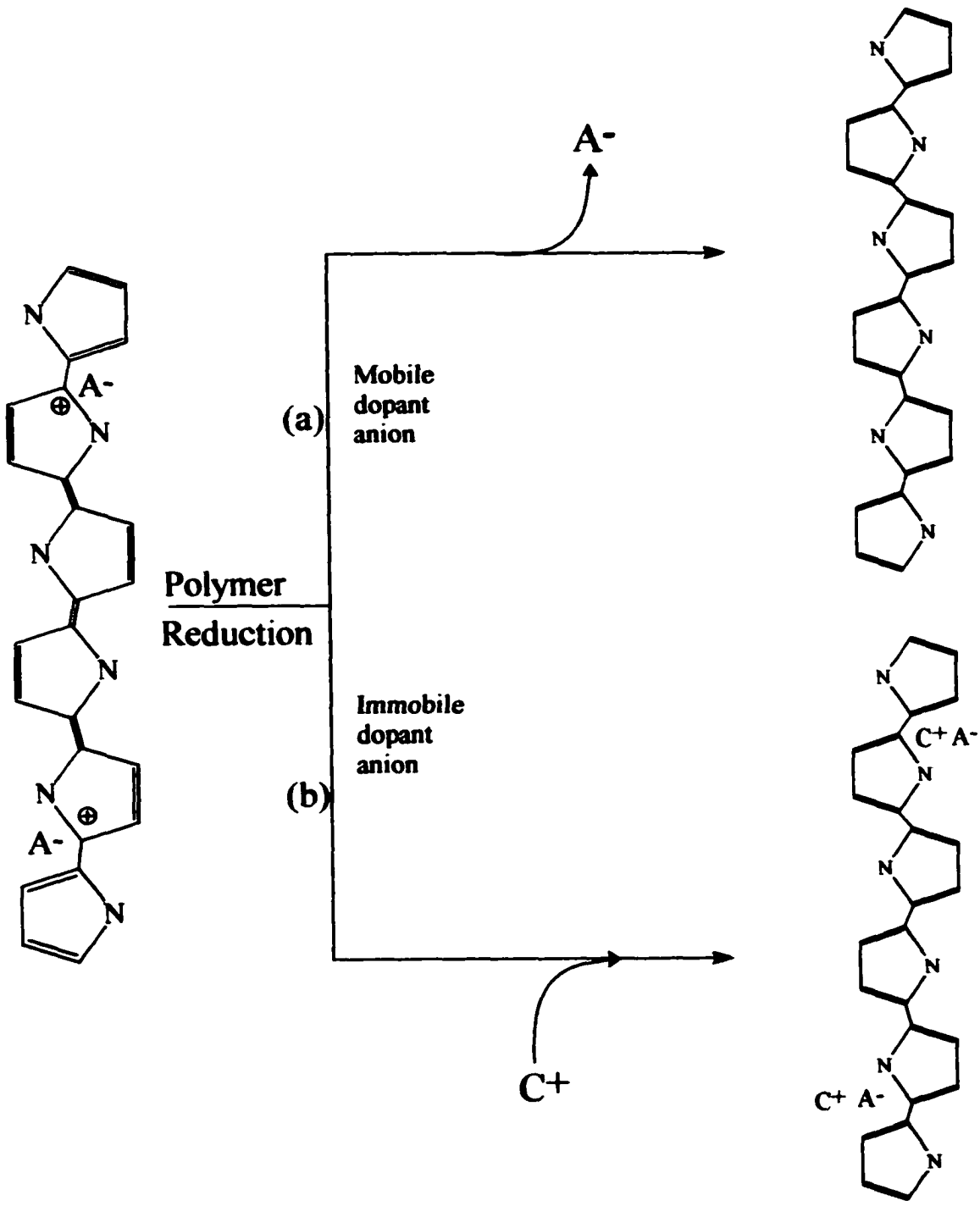

Scheme 1.2. Possible ion transport in poly(pyrrole) films during redox cycling in electrolyte solution. (a) shows the loss of an anion upon polymer reduction and (b) shows the influx of a cation to compensate trapped anions during film reduction.

with small and readily mobile anions such as BF_4^- and ClO_4^-.[6,17,22,38,43,48,52] Doping only by anions is one of the limiting regimes for describing the doping process. In these instances, dopant anions are readily mobile, sterically unencumbered, and have low ion pair dissociation energy with the cationic sites on the polymer backbone.

The other limiting case involves the exclusive motion of cations to compensate charge in the polymer. This is often seen in composite polymer films. These are polymer films that are doped with very large or polymeric anions, such as dodecylsulfonate[53] or poly(styrenesulfonate).[48,54] Upon oxidative growth, the anionic dopants become sterically trapped inside the conducting polymer. In the oxidized state, the positive charge of the film (i.e., polarons and bipolarons) is compensated by the entrapped anions (Scheme 1.2b). Reduction of the positive charge on the film requires the influx of cationic species from the electrolyte solution to charge compensate the incorporated anionic sites. Re-oxidation expels the cations leaving the large anion to compensate the charge on the polymer.

Although it is often reported that ion transport in conducting polymer films occurs by one of the two limiting ion transport regimes, there are cases in which more complex, mixed ion transport behavior is noted. These involve the combined motion of both cations and anions. Smyrl et al. reported charge compensation by both anions and cations in composite poly(pyrrole)/poly(stryenesulfonate) films occurring in separate potential regions of the film voltammetry.[55] During the anodic potential sweep, the charge neutrality is maintained by the expulsion of cations (i.e., Li^+, Na^+, and Mg^{2+}) at less positive potentials. Anion flux (ClO_4^-) into the film follows the cation expulsion at the

most positive potentials during the anodic sweep. Zhong and Doblhofer reported a similar trend with poly(pyrrole)/dodecylsulfate films cycled in KCl solutions.[56]

The occurrence of mixed ion transport can be noted in non-composite poly(pyrrole) films as well. J. R. Reynolds et al. found poly(pyrrole)/sulfonate films cycled in aqueous CsCl to expel/intake Cs^+ at potentials more negative than +200 mV vs. Ag/AgCl and intake/expel Cl^- at potentials positive of +200 mV.[57] Similar behavior was reported for poly(pyrrole)/nitrate films cycled in neutral and basic (pH=12) aqueous $NaNO_3$ solutions.[58]

Poly(pyrrole) films grown with chloride or bromide counterions have been found to demonstrate mixed ion transport character in certain aqueous systems.[59-61] Other researchers have found solvent/film dependence for the dominant ion transport characteristic of a film.[47,48,62] Poly(pyrrole)/chloride films in acetonitrile were found to have small, mobile cations, such as Na^+, Cs^+, and Li^+, dominate the charge compensation whereas anion motion of ClO_4^- or Cl^- dominated in aqueous systems. This dependence is explained by solvation of the various ions and the polymer as well as by ion dissociation energies between the anions and the positive charges on the polymer. The readily mobile anion (in this case ClO_4^-) may be immobilized in pPy/Cl^- films by changing the solvent system. By such means, the researchers could impart cation transport to a polymer that undergoes anion dominant transport in a different solvent system.[47]

Analysis Methods of Ion Transport Processes. A number of analytical techniques have been employed to study ion transport in conducting polymers, including impedance spectroscopy,[48,63] X-ray photoelectron spectroscopy (XPS),[48,60,64] luminescence techniques,[57,65] and scanning electrochemical microscopy (SECM).[59] These

methods are usually combined with electrochemical methods such as cyclic voltammetry or coulometry. However, the most commonly used approach is to monitor *in situ* mass changes of the polymer by means of Electrochemical Quartz Crystal Microgravimetry (EQCM).[35,55,57,58,60,61] EQCM is a method by which small changes in the oscillation frequency of a quartz crystal electrode are measured and related to small mass changes (i.e., nanograms) of the electrode. A polymer films deposited onto one of the quartz electrodes can be redox cycled in an electrolyte solution and, by monitoring the change in the vibrational frequency of the electrode, the change in film mass can be ascertained. The change in mass of a polymer, due at least in part to ion influx/efflux, is then correlated to the change in polymer oxidation state obtained from its voltammetry or coulometry. The advantages of EQCM are its high sensitivity to mass changes and *in situ* capabilities. However, it suffers from a lack of selectivity in identifying specific dopants and in differentiating solvent molecules from ions.[59,65] Each of the other approaches listed above has its own advantages and limitations as well. For instance, luminescence is selective and sensitive, but is limited to ions which luminesce, and consequently, are typically rather large. On the other hand, XPS can be used to examine a wide array of ions, but lacks the ability to measure ion transport *in situ*. Both luminescence and SECM suffer from the fact that the polymer must be charged with the probe ion prior to voltammetric scanning. Consequently, subsequent to the first scan, transport of the probe ion is convoluted with supporting electrolyte cation and anion transport.

The following chapter reports on the ion transport characteristics of poly(pyrrole) and poly(pyrrole)/poly(styrenesulfonate) composite films monitored with a rotating ring-disk electrochemical approach. The intent of the work was to develop the rotating ring-

disk as a means of quantitatively identifying the doping process *in situ* in a range of conducting polymers and environmental conditions.

Chapters 3 and 4 present the results from studies of 3,4-disubstituted poly(pyrrole) films as a sensing material in vapor and liquid phases. The polymer demonstrates unique selectivity for chlorinated organic molecules in solution and as vapors. It is shown that the nature of the counterion and the ion transport behavior is important for the material as a sensing medium.

Chapter 5 reports on the initial attempts at forming permanent, chemically locked, redox concentration gradients in conducting redox polymers. Again, an understanding of ion transport properties in these conducting polymers is crucial to the success of the project.

CHAPTER 2, PART I

Quantitative In Situ Measurements of Ion Transport in Composite and Non-Composite Films of Poly(pyrrole) Using Rotating Ring-Disk Voltammetry

INTRODUCTION

At least two prior attempts to use rotating ring-disk electrode (RRDE) voltammetry to measure ion flux across a conducting polymer/solution interface have been reported. Aizawa and coworkers[66] monitored the oxidation of Br^- at the ring electrode while a poly(pyrrole) film on the disk was redox-cycled in 0.10 M NaBr/water:acetonitrile(1:1). Despite efforts to quantitate this data, these results are of only qualitative value because NaBr was the sole electrolyte in solution. Migration of Br^- was neglected in their data treatment. Earlier yet, Pickup and Osteryoung[67] used RRDE voltammetry to monitor Cl^- flux from poly(pyrrole) in a very slightly basic (i.e., a slight excess of Cl^-) $AlCl_4^-$ molten salt. In contrast to the work of Aizawa and coworkers, this data was quantitatively useful since $[Cl^-] << [AlCl_4^-]$. Unfortunately, as these authors were also able to show, Cl^- was not the only dopant ion in the polymer; consequently, it was not possible to determine exactly which ions were participating in the charge

compensation process. As we will demonstrate below, the type of difficulties encountered in these earlier studies can be avoided altogether with the right combination of dopant ion(s) and background electrolyte. Moreover, it is possible with this technique to quantitatively account for all of the ions participating in polymer doping level changes *in situ* and in real time.

BACKGROUND

Before considering how RRDE voltammetry can be applied to polymer doping studies, it is instructive to review how this technique is employed to study so-called ***EC*** reactions in solution.[68] Consider the following hypothetical ***EC*** reaction:

$$\textit{E}: \quad O + e^- \rightarrow R$$

$$\textit{C}: \quad R \xrightarrow{k} Z$$

Typically, the electrochemical reaction, ***E***, is initiated at the disk. The ring potential is adjusted to give a mass-transport-limited reoxidation of R back to O. Because of the electrode rotation, the R formed at the disk is hydrodynamically transported across the insulating gap towards the ring where it can be reoxidized. Was it not for the chemical step, which irreversibly consumes some of the fraction of the R before it reaches the ring, the ring and disk currents would be related by equation 1.

$$-(i_r)/(i_d) = N \qquad (1)$$

The quantity N is a constant called the collection efficiency and its value is determined solely by the physical construction of the RRDE electrode (i.e., the disk area and the dimensions of the insulating gap and the ring)[68] (Appendix I). When there is follow-up chemistry, as reaction ***C*** above, some of the R is irreversibly consumed before reaching

the ring; therefore the current ratio on the left side of eq. 1 becomes less than N. The disk-to-ring transit time, and thus the chemical reaction time, is determined in a mathematically well-defined way by the rotation rate of the electrode.[68] Without going to unnecessary detail, the numerical value of the chemical rate constant, k, can be obtained by considering how the ratio of the ring limiting current to the disk limiting current, i_r/i_d, changes as a function of rotation rate. Of relevance here is the fact that the voltammetry of an electroactive polymer film on the disk of an RRDE is related to the mass-transport-limited voltammetry of the dopant ion(s) at the ring. This relationship is closely analogous to how the disk and ring voltammetry of O and R, respectively, are related in this hypothetical ***EC*** reaction in solution.

Prior to discussing how the currents are related, the unique constraints imposed on the experiment by the polymer/dopant system need to be addressed. Two requirements are made of the dopant redox chemistry by the fact that the voltammetry of the dopant ion (or ions) is to be used to quantify the polymer/solution interfacial ion flux. First, the dopant ion must be electrochemically inactive over the entire potential range applied to the polymer; and second, it must give mass-transport-limited voltammetry at the ring within the solvent window. Moreover, if multiple types of dopant ions are to be considered, their voltammetry must also be sufficiently separated in potential to avoid simultaneous reduction (*vide infra*). In general, either cationic or anionic dopants (or both) could be probed as long as the above criteria are satisfied. In order to simplify initial studies, singly charged dopant ions are preferred. This simplifies the calculations involved. For example, a singly charged anion will compensate a single positive charge in the film. Thus one oxidation event in the film can be compensated by a single anion.

A divalent anion could compensate cationic sites in the film or it is also possible to compensate only a single oxidation site and carry along a cation from solution. If this were the case, a clear picture of the transport behavior of the film would be difficult to ascertain. That is, cation motion may be erroneously attributed to charge compensation of the polymer backbone and the total amount of anions involved in charge compensation could vary significantly from cycle to cycle.

In addition to the dopant ions, the solution must contain an inert supporting electrolyte to eliminate migration effects. However, that supporting electrolyte cannot participate in polymer doping otherwise, any effort to quantitatively correlate the disk current with total ion transport would be pointless. Fortunately, differences in ion size can be used effectively to discriminate against doping by the supporting electrolyte ions. For example, the supporting electrolyte cation employed in this study, bis(triphenylphosphoranylidene)ammonium (PPN^+), is sufficiently large so that it is widely excluded from entering the polymer (Figure 2.1). *It is the use of this sterically excluded electrolyte that circumvents the problems encountered in earlier attempts to quantitate dopant ion flux by RRDE.*[66,67]

As stated above, RRDE voltammetry can, in principle, be used to monitor flux of cations, anions, or both. The present work focuses only on cationic doping in poly(pyrrole)/poly(styrenesulfonate) composites. Anion and cation contributions will be addressed in Part II of this chapter. When pyrrole is polymerized in the presence of poly(styrenesulfonate) (pSS^-), the pSS^- polyanion is irreversibly incorporated into the polymer structure.[35,54,55] The large polyanion becomes physically entrapped within the

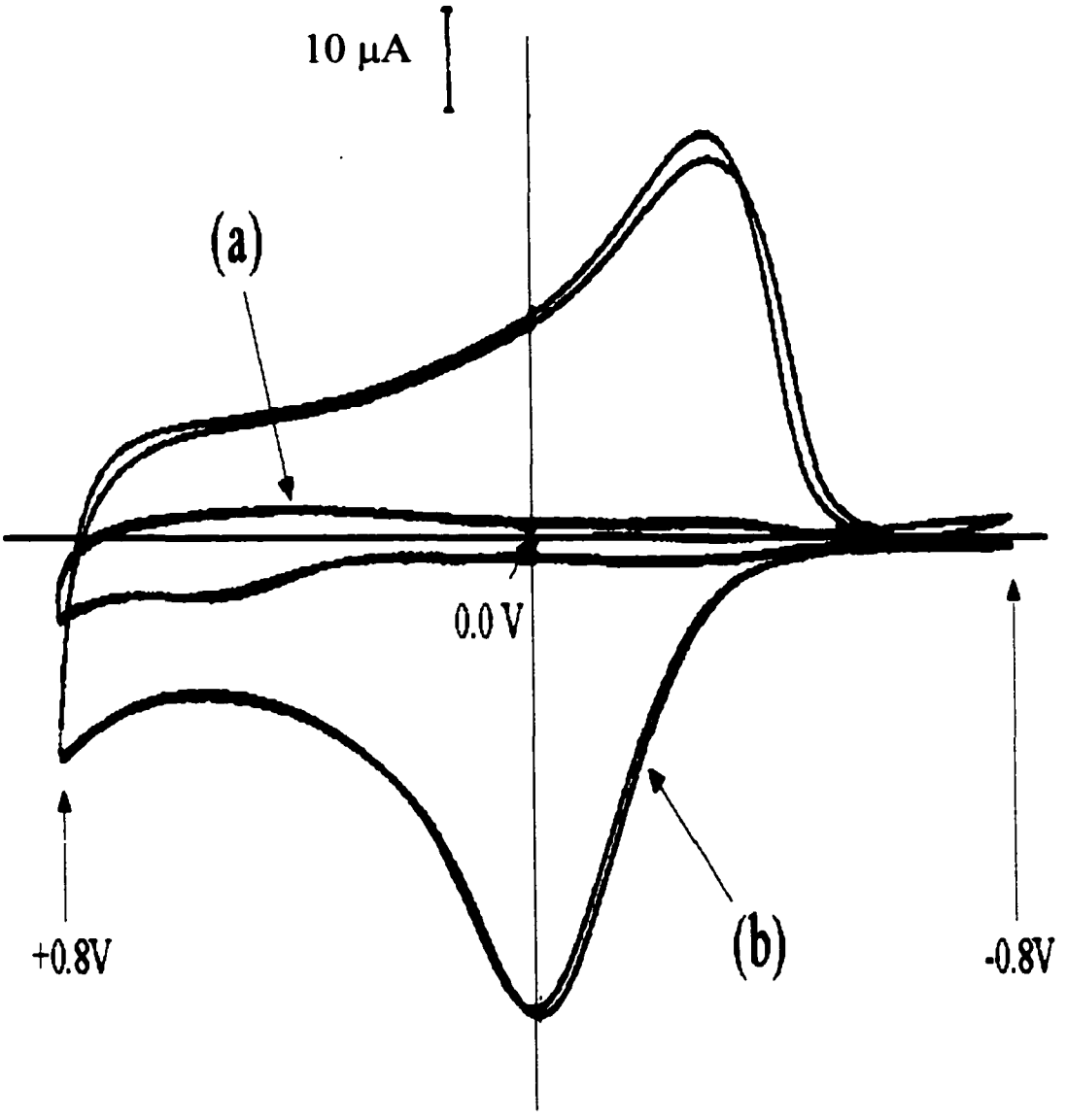

Figure 2.1. The above shows the cyclic voltammetry of a pPy^{+}/pSS^{-} film cycled in (a) 50 mM $PPNPF_6$ in acetonitrile and in (b) 50 mM tetrabutylammonium hexafluorophosphate. The film was electrochemically deposited on the platinum disk of the RRDE. A silver psuedo-reference electrode was used with a platinum wire auxiliary. The scan rate was 50 mV/s.

structure of the poly(pyrrole) film. Since pSS^- cannot leave the polymer upon subsequent redox cycling, charge neutrality is maintained predominantly by cation influx and efflux:

$$pPy^+/pSS^- + e^- + C^+ \leftrightarrow pPy/pSS^-C^+$$

In these experiments, the potential of a pPy^+/pSS^- coated disk is typically scanned between 0.00 V and –1.1 V. The range is sufficient to convert the polymer successively from fully reduced (-1.1 V) to significantly oxidized (0.00 V). Voltammograms of pPy^+/pSS^- obtained in electrolyte solutions of typical composition for a RRDE study are shown in Figure 2.2. The features of these voltammograms are similar to those of poly(pyrrole) voltammograms obtained in more standard electrolyte solutions such as tetraethylammonium chloride or sodium tetraphenylborate.[35,69]

In the RRDE experiment, the ring electrode potential is chosen to be well onto the mass-transport-limited current plateau of the dopant cation (C^+) reduction.[70] Consequently, in the ideal case, a constant, time-independent current, $i_{r,0}$, should pass at the ring in the absence of any polymer voltammetry at the disk.

Here the doping experiment deviates from the classical solution ***EC*** study. In the ***EC*** case, R is not present in bulk solution so there is no current at the ring unless R is being produced at the disk. By contrast, in the absence of any redox process at the disk, C^+ is present in bulk solution for the RRDE studies and produces a constant current ($i_{r,0}$) at the ring. When the polymer doping level changes, the concentration of C^+ reaching the ring changes, causing the ring current to deviate from $i_{r,0}$. It is the difference between $i_{r,0}$ and the total ring current, $i_r(t)$, which is quantitatively related to the total disk current, $i_d(t)$. Consider a positive potential scan of the disk starting at a value where the pPy^+/pSS^- film is fully reduced (e.g., -1.0 V). As the polymer becomes progressively

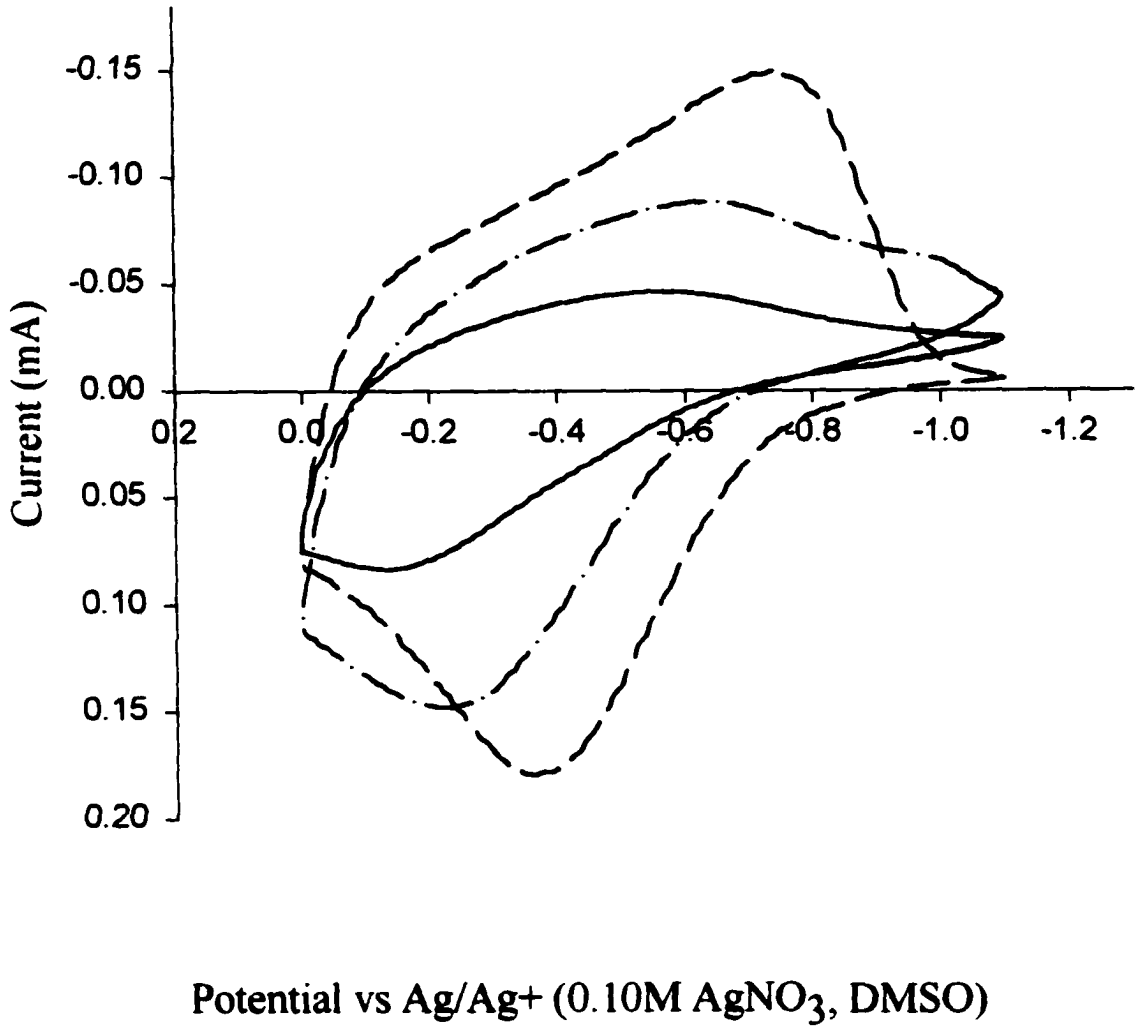

Figure 2.2. Cyclic voltammograms of pPy^{-}/pSS^{-} films (grown under identical conditions) cycled in acetonitrile solutions of 2 mM dopant cation and 50 mM PPNTos: cobalticinium(Cc^{+}, solid line); 1-methyl-3-cyanopyridinium (CMP^{+}, dash-dot); 1,3-dimethylpyridinium (DMP^{+}, dash only).

more oxidized, electrons are being removed from the polymer and enter the electrode. For charge neutrality to be maintained either cations must be ejected into solution or anions from solution must enter the polymer. If it is assumed for the present that only cation doping occurs in pPy^+/pSS^-, every electron removed from the polymer releases a cation into solution (Figure 2.3a). From the point of view of the ring electrode, the act of releasing C^+ from the polymer is indistinguishable from creating C^+ electrochemically at the disk (as was the origin of the R being formed at the disk in the ***EC*** experiment). The difference in the two experiments is, again, that in the ***EC*** studies the only source of R is electrochemistry at the disk; in the doping experiment C^+ released from the polymer adds to the constant flux of C^+ from the bulk solution, thus increasing $i_r(t)$ over $i_{r,0}$. An identical argument can be made for the reductive potential scan of the disk except that in that case C^+ enters the polymer (Figure 2.3b), reducing its concentration at the ring and causing the measured absolute ring current $i_r(t)$ to drop below $i_{r,0}$. If the corrected ring current, $i_r'(t)$, is defined as:

$$i_r'(t) = i_r(t) - i_{r,0} \qquad (2)$$

a relation analogous to eq.1 exists which takes the form:

$$-i_r'(t)/i_d(t) = N \qquad (3)$$

When the doping change is accomplished exclusively by C^+, the collection efficiency in eq. 3, N, is the same as in eq. 1. Just as deviations of the current ratio from N signal a non-zero rate of follow-up chemistry for an ***EC*** process, deviations in the current ratio in eq. 3 from N signal that C^+ is not the sole ion participating in changing the polymer doping level.[71] The fraction of the doping change that *is* due to C^+, a value denoted as

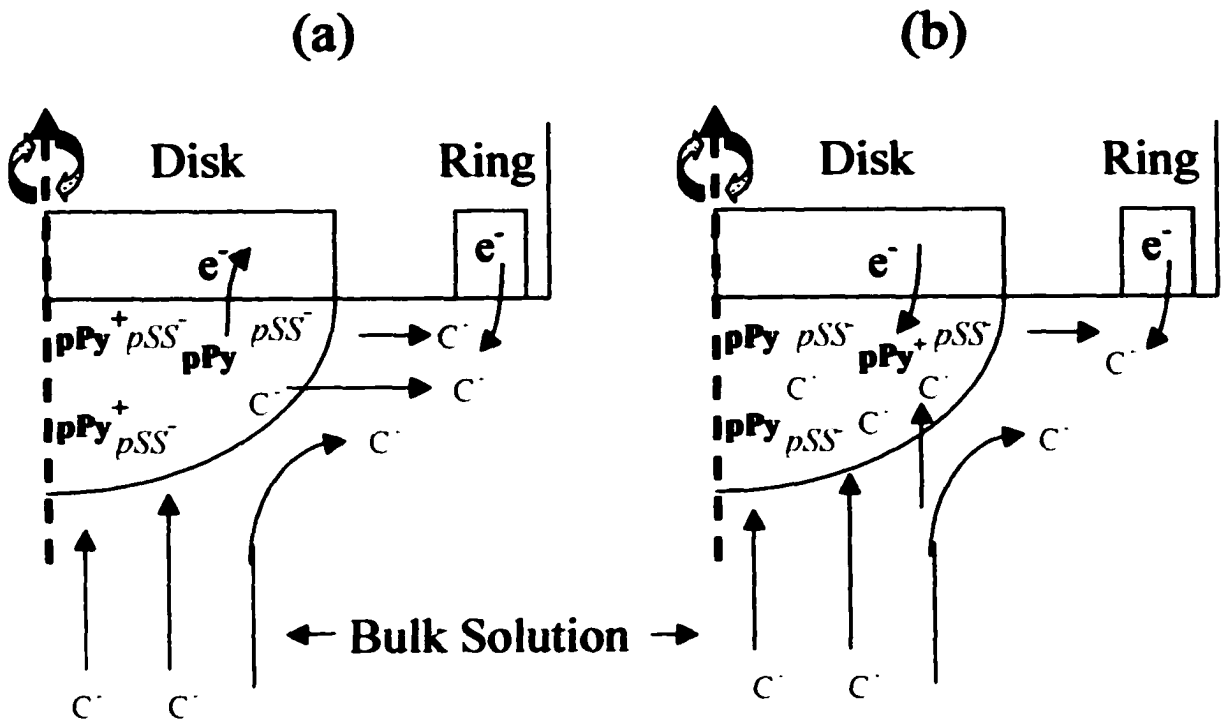

Oxidation of film expels dopant cations. The reduction current at the ring increases; indicating the undoping of the film.

Reduction of the film requires the influx of cations to compensate charge of the trapped anions. Decrease in the cations passing to the ring causes drop in ring current.

Figure 2.3. Diagram demonstrating the cation transport process that occur in the pPy^+/pSS^- films on the RRDE with rotation of the electrode.

f_C^+, can be determined by dividing the left side of eq. 3 by the right and setting this equal to f_C^+, namely:

$$f_C^+ = (1/N)(-i_r(t)/(i_d(t))(4)$$

EXPERIMENTAL

Chemicals and Equipment. All chemicals except as noted below were purchased from Aldrich and used as received. Pyrrole was purified by distillation under nitrogen. Bis(triphenylphosphoranylidene)ammonium *p*-toluenesulfonate (PPNTos) was prepared by combining aqueous solutions of PPNCl and sodium *p*-toluenesulfonate. PPNTos precipitates out of the combined solution as a white solid. The PPNTos was filtered, rinsed with distilled water, and dried under vacuum. The dried product was subsequently recrystallized from methanol/water and from dichloromethane/ethyl acetate. In each case, small white crystals formed which were filtered from the solution and washed, respectively, with either distilled water or ethyl acetate. The rinsed solid was dried under vacuum overnight.

Tetraethylammonium poly(4-styrenesulfonate) (TEApSS) was prepared via dialysis (Spectra/Por® Membrane MWCO: 6-8,000 Spectrum Medical Industries, Inc. Los Angeles) from tetraethylammonium bromide (TEABr) and poly(sodium 4-styrenesulfonate) (NapSS) in distilled water. Aqueous solutions of TEABr and NapSS were combined. The molar amount of TEABr was in excess of the NapSS (ca. 2.5 g) by two fold. The mixture was sealed in a dialysis tube, which was then submerged in distilled water for 48 hours. After this time, the tube had swollen and become taut. External water in the container was changed, and to it, several grams of TEABr were

added. The dialysis tube remained in the stirred solution for 48 hours. This external solution was then replaced with pure distilled water, which was replenished several times over a span of 48 hours. The tube was removed from the container, rinsed with distilled water, and the contents poured into a flask. The presence of bromide in the solution was tested with aqueous silver nitrate. The absence of a precipitate indicated the dialysis was complete. The aqueous solution was taken to dryness on a rotary evaporator leaving a tan film on the flask walls. By dissolving the product in a minimum of absolute ethanol and slowly re-evaporating the ethanol on the rotary evaporator, a tan, solid coated the flask walls, which could readily be removed. Once removed, the material was further dried under vacuum. Finally, this procedure is general for preparing acetonitrile soluble $R_4N^+pSS^-$ salts when R is hexyl- or smaller (for R larger than hexyl- see ref 125).

1-Methyl-3-cyanopyridinium hexafluorophosphate ($CMPPF_6$) was prepared by dissolving 3-cyanopyridine in acetonitrile and adding dropwise, a stoichiometric amount of iodomethane. The reaction mixture was refluxed for 4 hours and then allowed to cool to room temperature. The iodide salt (CMPI) formed as a yellow solid upon cooling. It was filtered and recrystallized from acetonitrile to yield yellow, needle-like crystals. The CMPI was then dissolved in water and excess of ammonium hexafluorophosphate added. The solution was cooled in a refrigerator until white needle-like crystals formed. This mixture was filtered and the solid, $CMPPF_6$, was washed with cold water and then dried for 12 hrs. under vacuum. 1,3-Dimethylpyridinium hexafluorophosphate ($DMPPF_6$) was synthesized in a similar manner starting with 3-picoline in place of 3-cyanopyridine. The half-wave potentials for the reduction of CMP^+ and DMP^+ were determined from steady-state voltammetry at the Pt ring of the RRDE. The values for CMP^+ and DMP^+ were

calculated to be −1.13 V and −1.70 V, respectively vs. a Ag/Ag^+ (0.10 M $AgNO_3$, DMSO) reference electrode. The measurements were made in acetonitrile solutions containing 2 mM electroactive cation and 50 mM PPNTos.

The bis(cyclopentadienyl)cobalt(II) hexafluorophosphate ($CcPF_6$) was purchased from Aldrich and was used as received. The half-wave potential was determined as above and calculated to be −1.21 V vs. a Ag/Ag^+ (0.10 M $AgNO_3$, DMSO) reference electrode.

An EG&G Princeton Applied Research Model 173 potentiostat/galvanostat with a Model 175 digital coulometer was used for film growth (*vide infra*). A Pine Instruments RDE4 bipotentiostat, modified to provide a potential range of ±5V, was utilized for the ring-disk electrochemistry. Electrode rotation was accomplished using a Pine Instruments PIR electrode rotator. Data acquisition was accomplished using a program, written in ASYST, provided by Professor Daniel Buttry of the Department of Chemistry, University of Wyoming. The program was modified locally (Appendix II). A BAS 100B Electrochemical Workstation was used for the chronocoulometry experiments.

Cells and Electrodes. The electrochemical cells used in film growth and in ring-disk experiments were each single compartment cells and were employed in three- and four-electrode configurations, respectively. The working electrode was a custom designed platinum ring-platinum disk electrode purchased from Pine Instruments. The disk electrode had a 2.6 mm radius. The radius to the inside of the ring was 4.0 mm and the radius to the outside of the ring was 4.3 mm. This gave a large ring-disk gap width of 1.4 mm (Figure 2.4). The counter electrode was a platinum wire coil. A Ag/Ag^+ (0.10 M

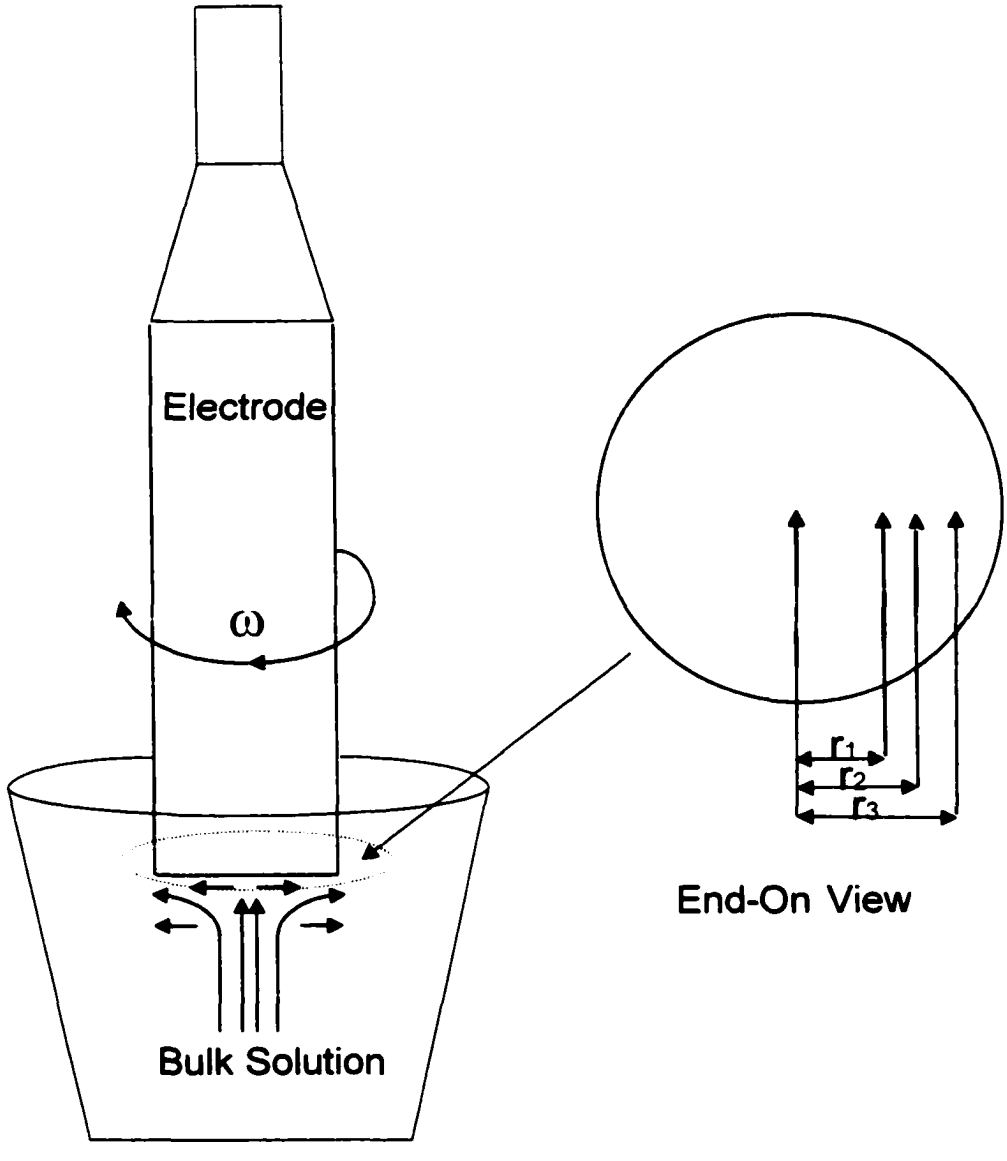

Figure 2.4. Diagram showing the configuration and dimensions of the rotating ring-disk electrode utilized in these studies. r_1=2.6mm, r_2=4.1mm, and r_3=4.3mm.

$AgNO_3$, DMSO) reference electrode was employed for film growth and for some of the ring-disk experiments; however, more typically, a Ag pseudo-reference electrode was utilized in the RRDE experiments. All potentials are reported relative to the Ag/Ag^+ (0.10 M $AgNO_3$, DMSO) electrode.

Film Growth. Composite poly(pyrrole)/poly(styrenesulfonate) films were grown potentiostatically at +0.8V; a potential located well into the oxidation region of the pyrrole monomer. The acetonitrile growth solution was 1.0 M in pyrrole and 0.10 M in TEApSS and was stored at 0°C under Argon between uses. The extent of film growth was determined from the charge passed during polymerization. All films were grown with the passage of 15 mC. This gave film thicknesses on the disk (area: 0.071 cm^2) of ca. 300 nm according to published estimates of film deposition thickness with respect to the charge passed during potentiostatic formation.[13] Following film polymerization, the working electrode was removed from the growth solution and rinsed with copious amounts of acetonitrile. The electrode and film were then placed into the rotator and positioned in the RRDE cell. Shape and peak magnitudes of the polymer's cyclic voltammetry were used to qualitatively verify film quality.

Solutions. All solutions used for analysis of cation transport in the composite films were prepared in the same manner. The total concentration of electroactive cation(s) in solution was maintained at 2.0 mM. The concentration of the PPNTos supporting electrolyte was 50 to 54 mM. Acetonitrile was used as the solvent in all electrochemical experiments.

Current Decay Correction. In the discussion leading up to eqs. 2-4, the results from the RRDE experiment were treated as ideal. In practice, the total excursion of the

$(i_r(t) - i_{r,0})$ is typically only ca. 10% of the value of $i_{r,0}$. Therefore, if $i_{r,0}$ were not rigorously constant, significant errors would be introduced into the data treatment. In actual experiments, ring current data is collected over many cycles of the disk potential requiring between 5 and 10 minutes. Over such extended periods, changes to the ring electrode surface often resulted, which were sufficient to cause the value of $i_{r,0}$ to slowly, and monotonically, decrease. This decrease is typically small in absolute terms, but is large enough to make eqs. 3 and 4 unusable as previously defined. To deal with this problem, the time dependence of the background current at the ring was determined and the constant value of $i_{r,0}$ in eq. 2 replaced with the time dependent function, $i_{r,0}(t)$ thus, redefining $i_r'(t)$ in eqs. 3 and 4:

$$i_r'(t) = i_r(t) - i_{r,0}(t) \qquad (2')$$

To approximate the function $i_{r,0}(t)$, the points where $i_d(t)$ crossed the zero-current axis were determined over the course of multiple cycles of the disk potential. When $i_d(t)$ = 0.00 mA, no net change in polymer doping can be occurring; thus, the concentration of C^+ at the ring should be exactly its bulk concentration. It follows then that $i_r(t)$ at these points equal values of $i_{r,0}(t)$. The ring current data for the points where $i_d(t)$ = 0.00 mA, (as a function of potential or time) were quite adequately fit to a simple quadratic function (Figure 2.5). This function was then used to generate values of $i_{r,0}(t)$ at the intervening potentials (times).

RESULTS AND DISCUSSION

Cyclic Voltammetry. Films of pPy^+/pSS^- give stable, reproducible voltammetry with each of the three electroactive cation dopants examined. The general shape of the

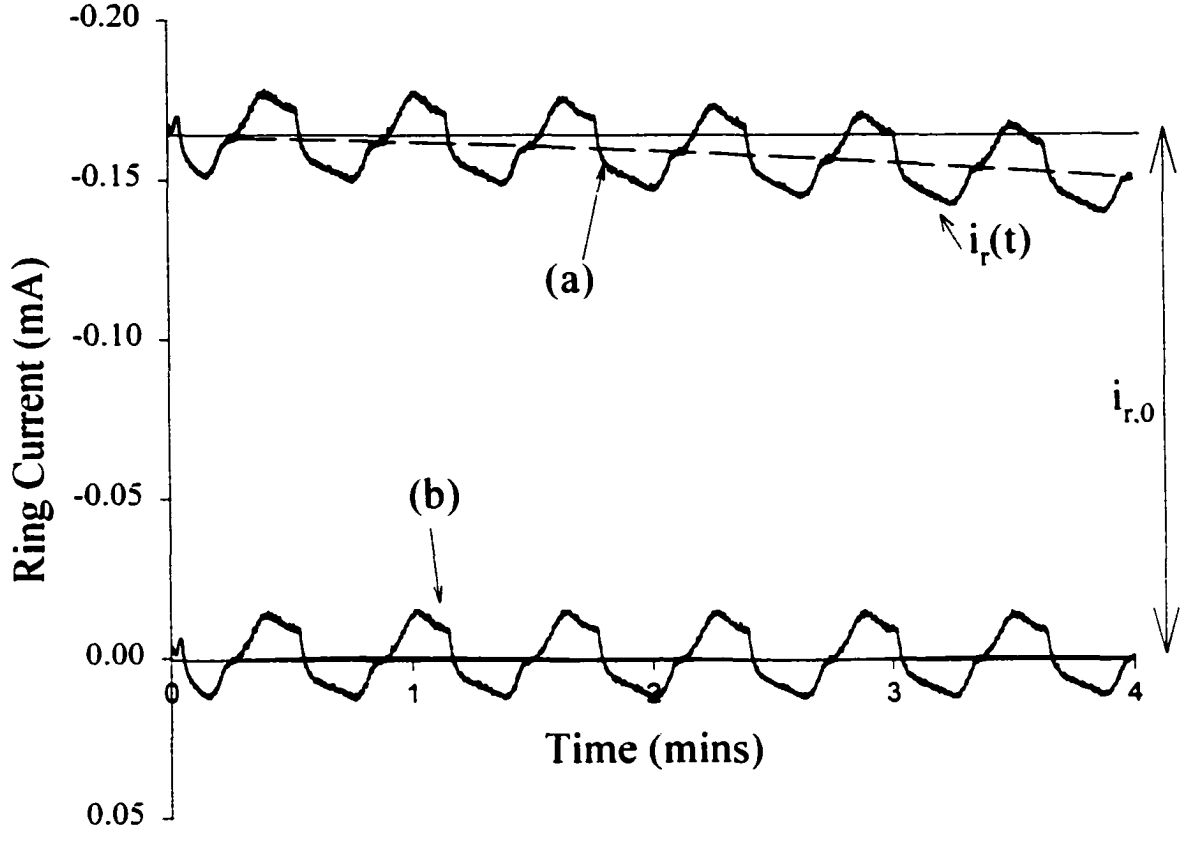

Figure 2.5. Diagram demonstrating the correction of ring data for current decay caused by electrode fouling and the subtraction of the background current, $i_{r,0}$. The dashed line is the calculated fit used for correction of the decay and background current. (a) shows the recorded ring current without correction for the current decay caused by fouling and the value of the background current. (b) shows the resulting ring current after correction.

voltammograms are as expected; however, the total charge passed for a given film during redox cycling is different for the different dopant cations. Comparison of the voltammograms in Figure 2.2 shows that the amount of charge passed follows the order $DMP^+ > CMP^+ > Cc^+$. The peak potentials of the voltammograms are also dopant dependent; the less charge passed, the more positive the peak potentials for a given film.

Single Dopant Ion Transport Measurements. Figure 2.6 shows both the $i_r(t)$ and $i_d(t)$ data for a pPy^+/pSS^- film cycled repeatedly between 0.0 and −1.1 V in a solution containing DMP^+. The ring potential is held at −1.9 V giving a mass-transport-limited reduction of DMP^+. The qualitative response for pPy^+/pSS^- films is similar to that shown in Figure 2.6 regardless of which electroactive dopant is being studied. The current response of the polymer is stable and centered about the zero current axis. The value of $i_{r,0}$ at the beginning of the experiment is represented in the upper part of Figure 2.6 by a solid line. Over the course of this experiment (ca. 4 mins.), the background current at the ring decays by roughly 10%. The dashed line labeled $i_{r,0}(t)$ is the time dependent background current obtained as described in the experimental section. The corrected ring current response calculated from eq. 2′, $i_r'(t)$, is less than, and has the opposite sign from, the disk current, $i_d(t)$. From consideration of eq. 4, when $f_C^+ = 1$ $i_r'(t)$ should be smaller than $i_d(t)$ by exactly a factor equal to the collection efficiency, N (i.e., 0.12).

Typically, for each individual dopant ion studied the value of f_C^+ obtained from eq. 4, within experimental error, is equal to unity. A visually informative way of displaying the current data is in the form of a conventional cyclic voltammogram. When $f_C^+ = 1$ a plot of $-N(i_r')$ should exactly overlay the disk voltammetry; when $f_C^+ < 1$ the plot of $-N(i_r')$ will be smaller than i_d by f_C^+. Figure 2.7 contains an overlay plot of i_d and

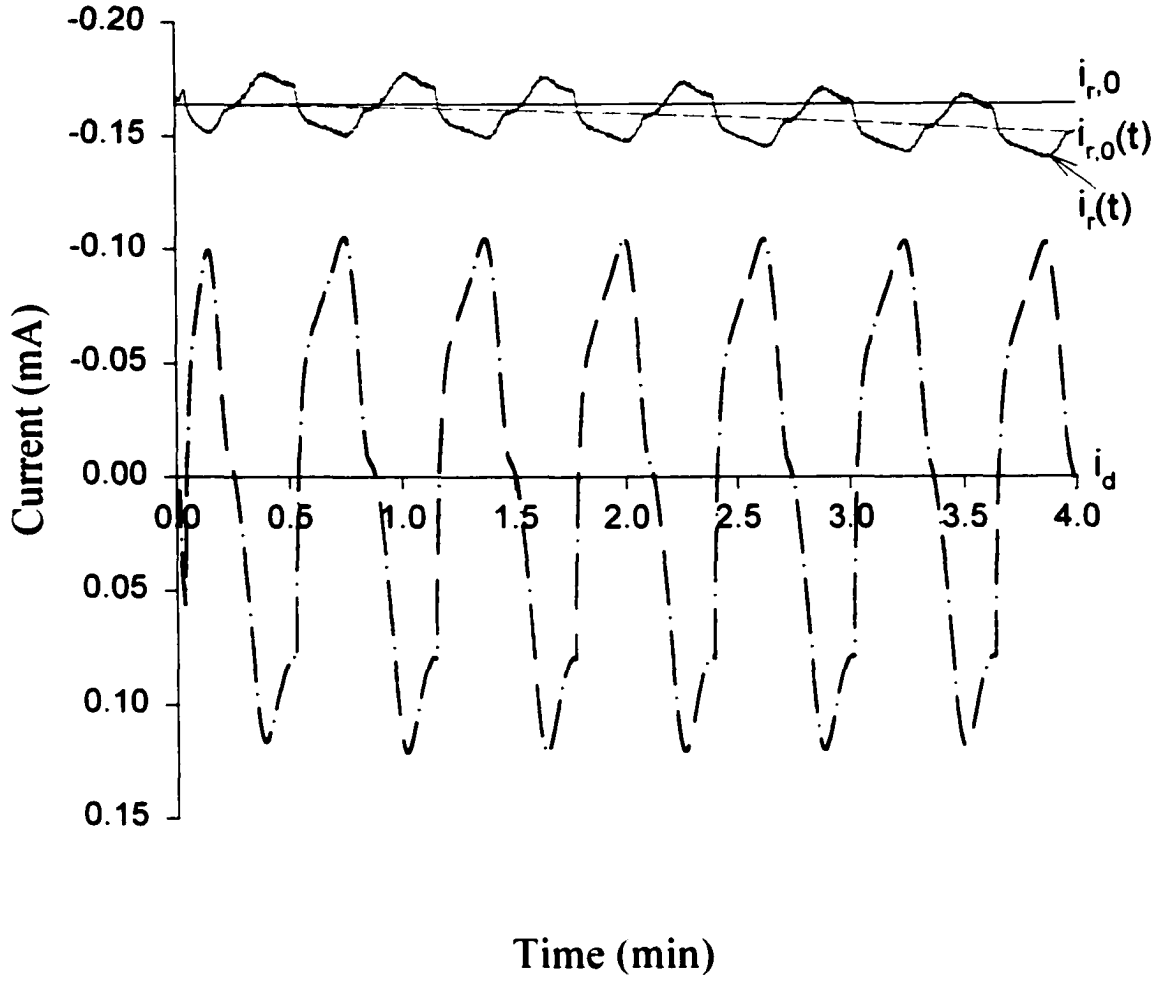

Figure 2.6. Current vs. time plot for a pPy^{+}/pSS^{-} film on the disk electrode ($i_d(t)$, dash-dot line) in an acetonitrile solution of 2 mM $DMPPF_6$ and 50 mM PPNTos cycled between 0.0 and −1.10V and the simultaneously recorded mass-transport-limited ring current for the reduction of the DMP^{+} ($i_r(t)$, solid line). The dashed line shows the background current fit used to correct the ring current data for the current decay and the background current. Electrode rotation rate was 400 rpm.

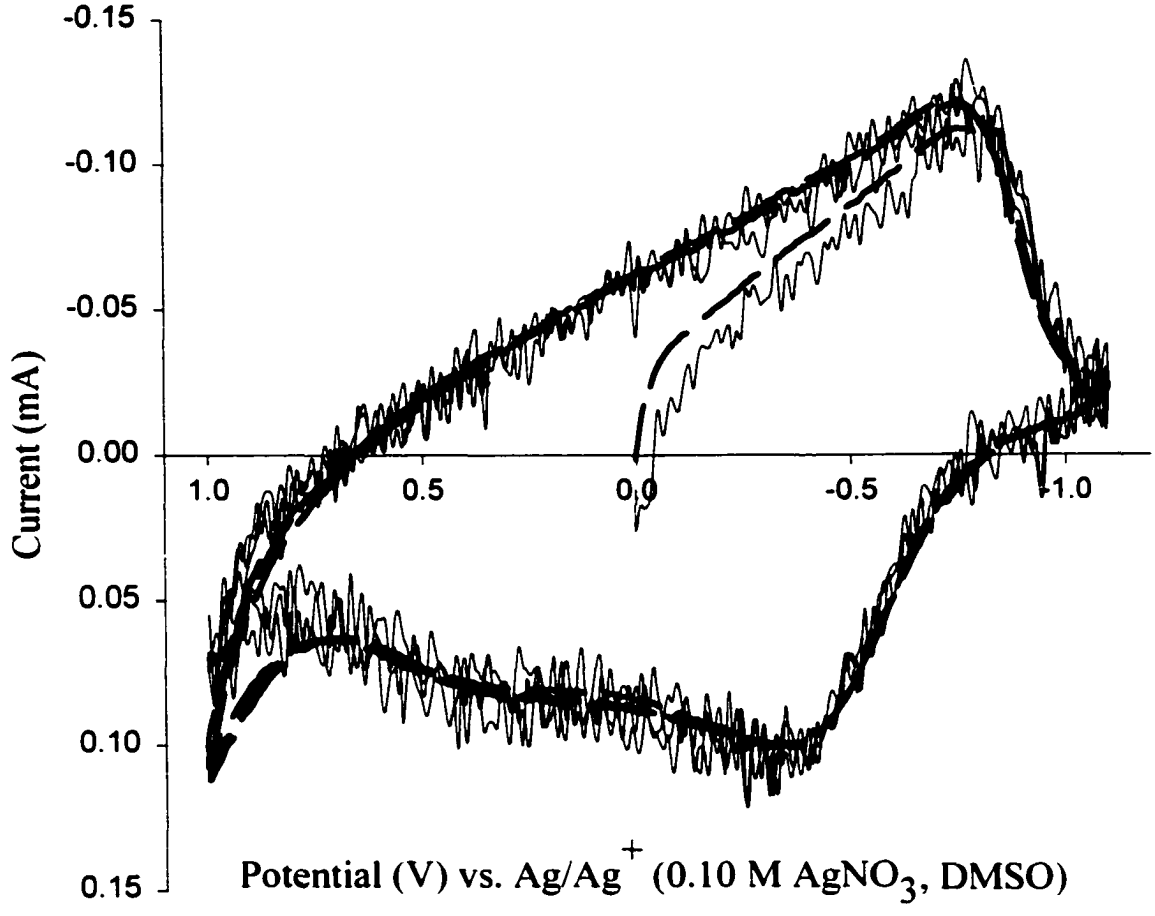

Figure 2.7. Plot of i_d (dashed line) and $-i'_r/N$ (solid line) vs. E_{disk} for a pPy^+/pSS^- film (disk) cycled in an acetonitrile solution of 2 mM $DMPPF_6$ and 50 mM PPNTos. E_{ring} was held at -1.9 V in the mass-transport-limited reduction of DMP^+. Electrode rotation rate was 400 rpm.

$-N(i_r')$ for three multiple scans of the disk potential. Once steady state is obtained the two currents correlate, within experimental error, over all but the most positive part of the three scans. Only when the potential goes positive of ca. +0.8 V do the two plots deviate. Positive of +0.8 V on both the positive- and negative-going scans $i_d > -Ni_r'$ indicating $f_{C^+} < 1$. Recall that the pPy^+/pSS^- films were grown potentiostatically at +0.8 V. Cycling the potential positive of +0.8 V therefore oxidizes the polymer beyond the state in which it was grown. Consequently, there is insufficient negative charge from the pSS^- to compensate the additional positive charge injected into the film; thus, additional anions from solution must enter the film to maintain charge balance.

Doping Competition Studies. Studies with each of the individual electroactive dopants demonstrate that, at potentials negative of +0.8 V, these pPy^+/pSS^- composite films undergo doping changes exclusively via cation transport. Having established this fact, we were interested in how the various cations compete in the doping process. Such competition studies would be virtually impossible via techniques such as EQCM, but they are straightforward employing the RRDE experiment.

We chose to consider two pairs of cations: DMP^+ vs. Cc^+ and DMP^+ vs. CMP^+. The other possible combination, CMP^+ vs. Cc^+, was not considered because the reduction potentials of the cations are too close to allow detection of each cation independently.

In the competition studies, the potential of the disk electrode was cycled in a series of solutions in which the relative concentrations of the two dopant cations was varied but their sum was held constant. Figure 2.8 shows a progression of voltammograms in solution containing 2.0 mM total electroactive cation ($[CMP^+]+[DMP^+]$) as the relative fractional concentration of CMP^+ is varied from 1.0 to

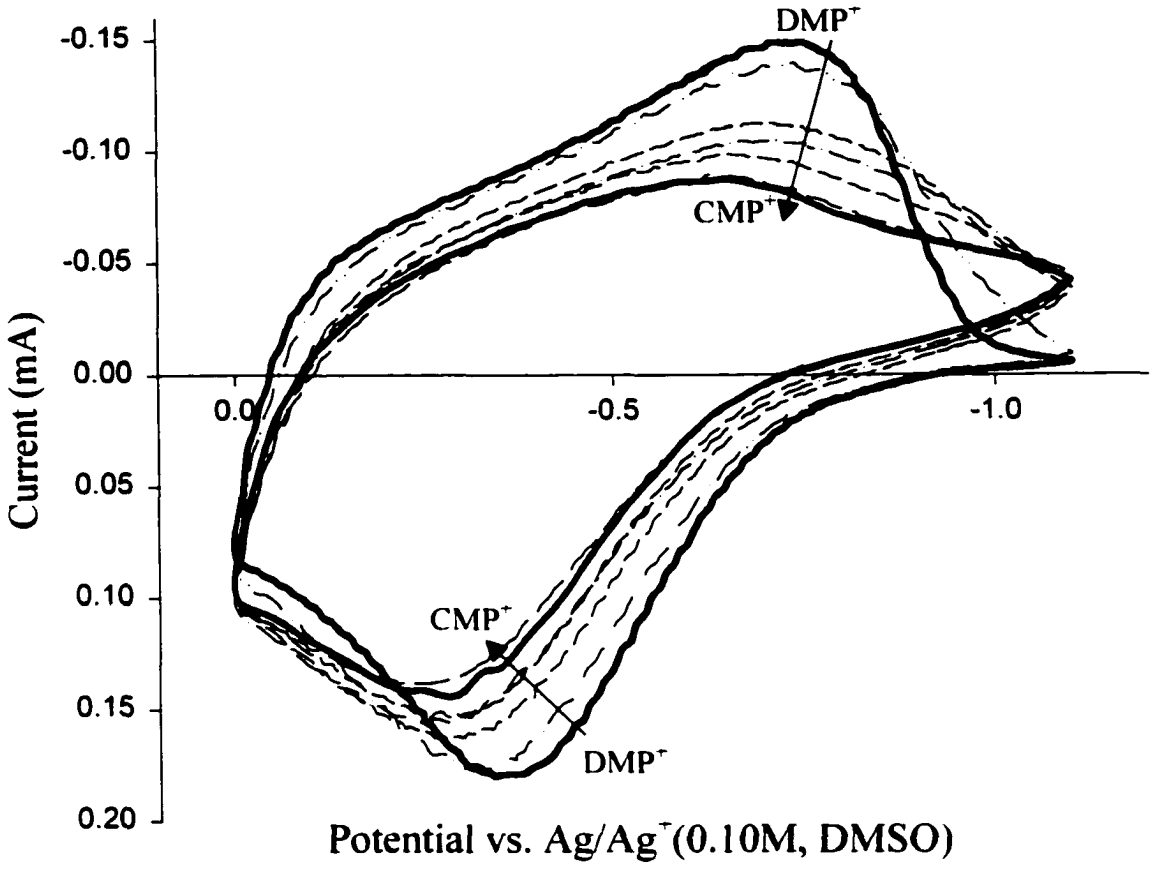

Figure 2.8. Cyclic voltammograms showing the change in the current response of a pPy^+/pSS^- film as the solution is progressively change from pure CMP^+ (inside solid curve) to pure DMP^+(outside solid curve). Each solution was 50 mM in PPNTos and the total dopant ion concentration ($[CMP^+]$ + $[DMP^+]$) was kept at 2 mM. Electrode rotation rate was 400 rpm.

0.0. Consistent with the voltammograms shown in Figure 2.2, the amount of charge passed increases, the voltammogram becomes more peak-shaped, and the peak shifts to more negative potentials. Somewhat surprisingly, the shape of the disk voltammogram proved to mildly dependent upon the order in which the polymer was exposed to the two dopant cations. If the solution was changed progressively from one of pure DMP^+ to one of pure CMP^+, the shape of the final voltammogram differed moderately from that obtained from a film exposed only to CMP^+. Apparently, cycling the oxidation state of the polymer in a solution containing DMP^+ causes irreversible changes in the film, i.e., film morphology. When the reverse order of cation exposure is used, as depicted in Figure 2.8, the voltammograms at each extreme (i.e., DMP^+ only and CMP^+ only) are the same as if the film had been exposed only to the respective electrolyte. Similar results were observed in Cc^+ and DMP^+ competition studies. Consequently, for the majority of the data reported here, the film was exposed to DMP^+ last. Irrespective of the film history and the order of electrolyte exposure, the relative fraction of the doping level change due to each dopant cation in a given mixture appears to depend only on the ratio of the dopant cation concentrations in solution (*vide infra*).

When the potential of the disk is cycled, the rate of change of polymer doping (as reflected by the disk current) changes over the coarse of the experiment. From eq. 4, the fractional doping-change rate due to a given cation (or combination of cations) can be calculated at every point in the voltammogram. When multiple dopant cations are present in solution, there is no *a priori* reason that f_C^+ for each cation remains constant at all doping rates (currents). Nonetheless, under most circumstances, f_C^+ remains constant within experimental error over the entire potential scan. There are two situations when

f_C^+ was observed to change during a potential sweep: (1) when the potential is taken positive of where the film was grown (as discussed previously) and (2) when the flux of the lower concentration cation during the anodic sweep is insufficient to provide the required degree of doping. To determine if sufficient cation flux exists, one need only compare the ratio $i_{r,0}/i_d$ to the electrode parameter $\beta^{2/3}$. The value β, like the collection efficiency, N, is specific for each RRDE and is determined by electrode geometry.[66,72]

For the reduction of the polymer at the disk not to be cation-flux-limited, the following must be true:

$$i_{r,0}/i_d > \beta^{2/3} \qquad (5)$$

In experiments where the solution contained a single dopant cation at 2 mM, $i_{r,0}/i_d$ was always at least a factor of ca. 2.5 greater than $\beta^{2/3}$. In the mixed electrolyte experiments, the doping rate can become flux limited for the less concentrated component (ca. <10%). In this situation, f_C^+ for both cations was observed to vary during the anodic scan. Fortunately, this situation arises only when one component is present in a very small relative concentration.[73]

Since f_C^+ was determined to be effectively constant over the entire polymer voltammogram, except as considered above, it has a value characteristic of each set of concentrations in the binary mixtures. Figure 2.9 is a plot of f_C^+ vs. percent solution concentration of the most easily reduced cation of each pair (i.e., the solid triangles for f_{CMP}^+ in the CMP^+/DMP^+ pair and the solid circles for the f_{Cc}^+ in the Cc^+/DMP^+ pair). The open triangles and circles along the horizontal line at $f_C^+ = 1.0$ represent the combined doping by both cations obtained from eq. 4 by potentiostating the ring in the mass transport-limited reduction of both dopant cations of the pair. Within experimental

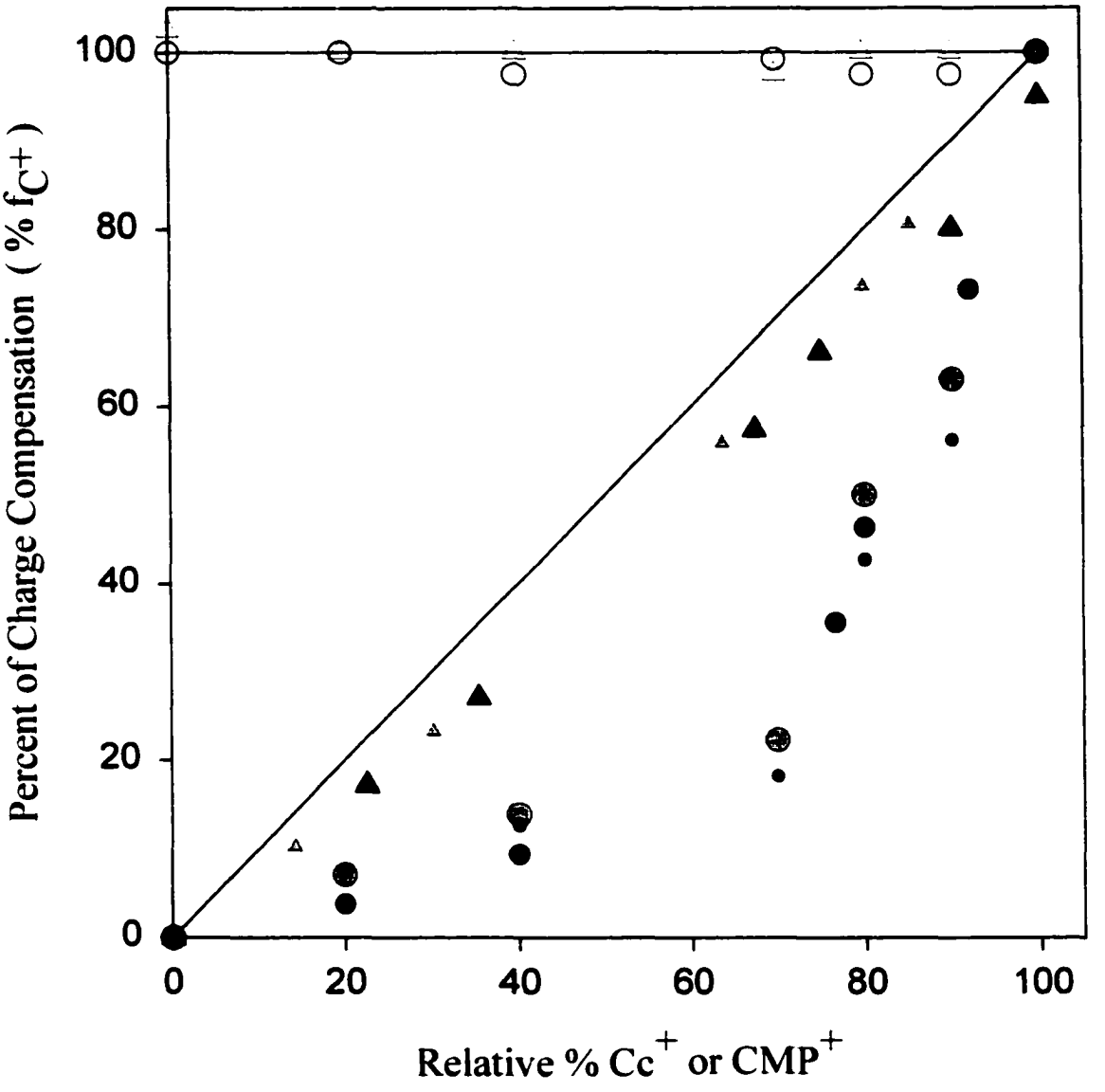

Figure 2.9. Results of doping competition studies for CMP^+ vs. DMP^+ (triangles) and Cc^+ vs. DMP^+ (circles). The diagonal line represents the case of no doping preference between the cations. The ordinate is percent f_{C^+} for the more easily reduced ion (i.e., either CMP^+ or Cc^+). The abscissa is the relative fraction of the same ion in solution. The horizontal line at the top of the plot indicates values having a total $f_{C^+} = 1$(i.e.; accounting for all doping occurring in film). Departure of the data from the diagonal line indicates a preferential doping in the film by DMP^+.

error, the total doping change of the polymer can be accounted for by the electroactive cations. The different sizes of the data symbols delineate data obtained from different, yet identically grown, pPy^+/pSS^- films. Finally, for none of the data presented in Figure 2.9 was the doping rate limited by flux of either ion to the polymer surface.

When there is no preference for one cation over the other, the fractional contribution to the doping, f_C^+, of each cation should exactly correspond to its fractional solution concentration. All data would then lie on the diagonal line in Figure 2.9. For both pairs of cations represented in the Figure 2.9, all data points lie below the diagonal line indicating a preference for DMP^+.

Based on molecular models,[74] the Cc^+ is roughly cylindrical in shape with a long axis dimension (measured from a corner of one cyclopentadiene through the cobalt to the far corner of the other ring) of ca. 5.6 Å. The length from center-to-center of the two cyclopentadiene rings is 4.6Å and the diameter of each ring is 4.2Å. DMP^+ is more nearly the shape of an oblong disk with a long axis dimension of ca. 6.6 Å (measured form carbon-to-carbon of the two methyl groups) and a short axis dimension of ca. 4.9 Å. Given their physical dimensions, one might anticipate a preference for DMP^+ based simply on size. In fact, the data in Figure 2.9 demonstrates a strong preference for the smaller DMP^+ cation over Cc^+. For example, when the relative solution concentration of Cc^+ is 70%, it is responsible for less than 20% of the polymer doping change!

While the Cc^+/DMP^+ pair was studied because of difference in size, the CMP^+/DMP^+ pair was studied because of differences in reduction potential (CMP^+ is ca. 700 mV easier to reduce than DMP^+). Assuming initially both ions to be the same size, we presumed any doping preference in this pair would reflect electronic differences in the

ions (e.g., charge-transfer interactions between the cation and the pyrrole sites). Consideration of the data shown in Figure 2.9 (triangles) shows that there is indeed an obvious preferential doping, but it is for the more electron rich DMP^+. Consideration of charge transfer interaction predicts the opposite. While the physical size of the bare cations does not suggest a steric preference, allowing for differences in solvation might. The "effective volume" would include solvent molecules carried along with the doping cation. This would be seen to increase the steric effects due to the necessity of greater film swelling. CMP^+ incorporates a nitrile function (like the solvent) while DMP^+ is distinctly hydrophobic around its entire periphery. Therefore, postulating differences in the "effective volume" of these two cations is reasonable and may explain the preferential partitioning of DMP^+.

The RRDE experiments, which generated the data in Figure 2.9, confirm preferential doping of pPy^+/pSS^- by DMP^+. What these experiments do not address is whether the origin of the preference is kinetic, thermodynamic, or some combination of both. Examination of the voltammograms taken in Cc^+ and CMP^+ electrolyte included in Figure 2.2 show that the polymer continues to reduce after the –1.1 V switching potential is reached. Even at a sweep rate as low as 50 mV/s, the polymer is not entirely at equilibrium in these electrolytes, at least at the most reducing potentials. In order to develop a more quantitative picture of the doping kinetics, potential step chronocoulometry experiments were conducted for a pPy^+/pSS^- film in solutions that were each 50 mM in PPNTos and 2 mM in one of the electroactive cations. In these experiments, the potential of the polymer was stepped between 0.0 V, where the film is partially oxidized, and –1.1 V where, in the DMP^+ case at least, the polymer appears to

be fully reduced. During each experiment, the disk was rotated at 400 rpm to ensure that the rate of reduction was not limited by cation flux to the polymer-solution interface. The charge-time responses for the first 32 seconds of a reductive potential step are shown in Figure 2.10 for each cation. In none of the electrolytes has the polymer reached its equilibrium doping level. In fact, it was found that the DMP^+ charge response attains a quasi steady-state at ca. 53 seconds while the CMP^+ takes ca. 122 seconds and Cc^+ takes ca. 137 seconds. The final value for the charge passed, however, is the same for each of the cations. It is obvious from this data that there is a significant difference in the rate of doping by the three cations; this being fully consistent with the different shapes of the cyclic voltammograms in Figure 2.2. Slowing the scan rate to 5 mV/s yields voltammograms that are more nearly the same shape and size. Unfortunately, as scan rate decreases, the signal-to-noise of the ring current also decreases. At scan rates much below 50 mV/s, the S/N becomes so poor that measurements of changes in doping level are unreliable.

It is instructive to report that the chronocoulometric experiments on conducting polymers, such as the one illustrated in Figure 2.10, are plagued by iR drop problems, especially in regards to quantitative doping measurements. This is particularly evident when comparisons are made between different films and/or electrolyte solutions. As reported by Lacroix et al.[75] and Kalaji et al.[76] the transients measured, especially at macroelectrodes, are particularly effected by iR drop problems due to large solution and film resistances. With respect to the data presented here, there were most definitely influences of such resistances occurring in our system. This is inconsequential, however,

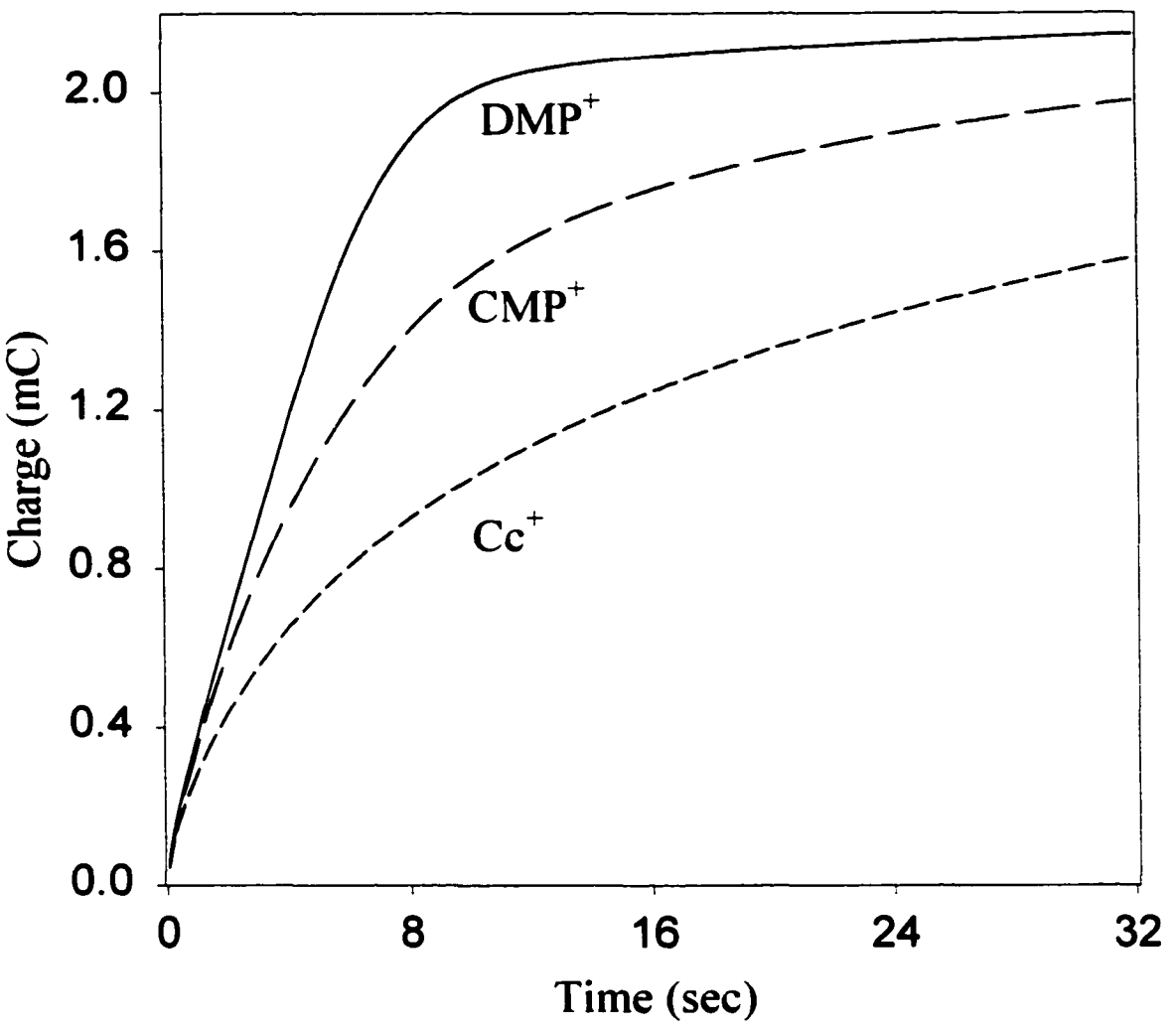

Figure 2.10. Chronocoulometry for a pPy^{+}/pSS^{-} film (charge passed by reduction of the polymer) on the disk of the RRDE with rotation at 400 rpm. The potential step is from 0.0 to -1.10 V. Each solution was 2 mM in electroactive cation and 50 mM in PPNTos.

as we were concerned only with the *difference* in charging rates in the film for systems in which only the electroactive cation is varied. The variation of the cation should have little affect on the overall solution conductivity, thus the uncompensated solution resistance should have been essentially unchanged. The intrinsic film resistance should have also gone essentially unchanged for the experiments as identical films were used. Thus the trend we saw *repeatedly* for the charging time of the film could then be assumed to be due to the variants in the cation mobility in the film or across the solution/film interface. Variation in ion mobility in the films has been suggested in terms of ion size by a later report by Kalaji et al. in terms of anion transport in polyanaline films.[77] The trends in peak shifts and magnitudes in the voltammetry of the films as a result of variously sized counter-anions were qualitatively identical to trends in our data.

While the chronocoulometry and slow-scan CV results demonstrate that there is a major kinetic component to the preferential doping at 50 mV/s scan rates, these experiments do not rule out the possibility of concomitant thermodynamic preferences. In an effort to obtain some qualitative information on the equilibrium doping state, a pPy^+/pSS^- film was held at –1.10 V in 1:1 solutions of each doping ion pairs (1 mM concentration of each of the two ions) for 10 minutes. Here, the thermodynamically favorable ion can predominantly compensate for charge sites in the film. Measurement of f_C^+ for expulsion of the ions in the first scan with comparison of f_C^+ for subsequent cycles can provide insight into the possibility of thermodynamic preferences. The potential of the disk was then scanned in the positive direction. On this first anodic scan, the value for f_{CMP}^+ and f_{Cc}^+ were slightly greater (relative to f_{DMP}^+) than predicted by the data in Figure 2.9. These values are ca. 25% larger on the first scan compared to

subsequent scans. In some instances, a greater f_{CMP^+} was measured compared to f_{DMP^+} on the first anodic scan. While there is no way to determine if, even after 10 minutes, the film has reached a true partition equilibrium, these results do suggest that if there is a thermodynamic preference for DMP^+, it is smaller than the kinetic preference.

Given the absence of any other compelling explanations, it seems reasonable to conclude that steric factors are responsible for the kinetic preference of pPy^+/pSS^- films to dope with DMP^+ in both pairs of ions. The Cc^+ unarguably occupies a larger volume than does the DMP^+ and it is slower to pass through the film. For the CMP^+/DMP^+ case there is only a slight preference for the later dopant, which is consistent with steric differences in the two cations based on differential solvation.

CONCLUSION

We have demonstrated the utility of rotating ring-disk voltammetry in quantitating studies of ion transport in conducting polymer films. In the past, pPy^+/pSS^- has been assumed, without real direct proof, to undergo only cation doping. With judicious selection of the supporting electrolyte and the dopant cation(s), we have been able to show by RRDE voltammetry that this assumption is entirely correct under conditions similar to those used in previous studies. Moreover, we have shown that RRDE voltammetry can provide quantitative, *in situ* information on competitive ion doping processes.

CHAPTER 2, PART II

Quantitative *In Situ* Studies of Ionic Doping of Poly(pyrrole) Employing Rotating Ring-Disk Voltammetry

INTRODUCTION

During the electrochemical oxidation of pyrrole to form electrode bound films of poly(pyrrole) (pPY), ions are incorporated to maintain charge neutrality. In order to change the redox state of the polymer film, these counterions (i.e., dopants) must exchange between the polymer and solution. In the specific case of poly(pyrrole), anion flux is expected to dominate doping changes, provided the anions are readily mobile. If they are not, cation flux can become involved and can even become dominant. In other words, immobile anions within poly(pyrrole) (or any analogous polymer) can be charge compensated during polymer reduction by cation uptake. In fact, as we will show subsequently, under the right conditions, fluxes of anions and cations can occur simultaneously at the polymer solution/interface during changes in the doping level.

The pPy/pSS^- films, which were discussed in the previous section, represent a limiting case for doping characteristics in these conducting polymer films. In that scenario, the ion flux during redox cycling of the films was exclusively due to mobile cations. The incorporation of the large, immobile anion, pSS^-, entrapped within the polymer matrix, is the reason for such doping properties. The use of that particular composite film simplified the ion transport and greatly assisted in verifying the RRDE

technique. The other limiting case, with regards to the ion transport processes in poly(pyrrole) films, is the occurrence of anion-dominated flux during redox cycling (refer to Scheme 1.2a). This is found in situations where anionic dopants can move freely and readily through the polymer and across the polymer/solution interface. Typically, these films are grown from solutions that contain small anions (i.e., PF_6^-, BF_4^-, ClO_4^-) and are cycled in solutions containing similarly small and mobile anions.[48,54] However, the doping level changes in such conventional non-composite organic conducting polymers (e.g., poly(pyrrole) doped with small anions such as PF_6^-) can be considerably more complex than in composite polymers containing entrapped anions (e.g., the pPY^+/pSS^- films described in the above section) because, as we will demonstrate, it is possible for both cations and anions to be involved. Moreover, doping ion profiles typically depend upon the identities of the ions available,[48,78] the potential applied to the polymer,[69] and its history. Consequently, doping studies involving these types of polymers present a much more formidable challenge. In principal, however, the same RRDE approach used successfully to quantitate doping changes in pPy^+/pSS^- can be adapted to study other polymers. What is required is the ability to independently monitor both cation and anion fluxes.

In the following, results from doping studies on non-composite, electrochemically-grown films of poly(pyrrole) are present. A collection of different electrolyte ions has been considered. In some instances only the anion or the cation was electrochemically active, but in others both dopant ions in solution were electroactive. *To our knowledge these latter measurements constitute the first successful attempt at quantitatively and independently following the fluxes of both anion and cation dopants in*

real time during the voltammetry of a single conducting polymer film. The requirements imposed by the RRDE experiment on the redox chemistry of the probe ions limits the selection available for the studies presented here. For poly(pyrrole), the same reducible methylpyridinium cations utilized in our earlier studies of pPY^{+}/pSS^{-} composites are appropriate. The selection of acceptable probe anions, unfortunately, is also narrow. However, both chloride and bromide meet all of the required criteria. That is, the ions are electroactive inside the solvent window but outside of the potential window used to cycle the polymer, have stable redox chemistry, and readily pass in and out of the film structure.

EXPERIMENTAL

Chemicals and Equipment. All chemicals used for this study were purchased from Aldrich. Pyrrole was distilled under nitrogen prior to use and was stored in the dark at 0°C. Bis(triphenylphosphoranylidene)ammonium tetrakis(3,5-bis(trifluoromethyl) phenyl)borate (PPNBArF) was prepared via metathesis from the chloride and potassium salts of the respective ions. The PPNBArF salt is shown in Diagram 2.1.

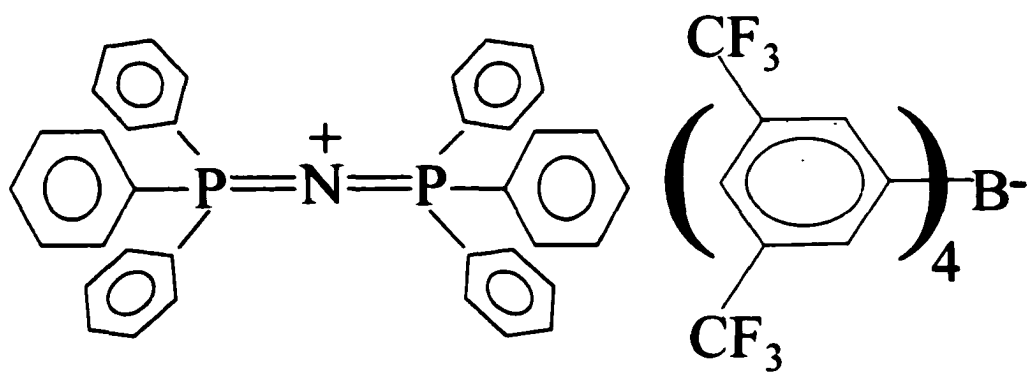

Diagram 2.1. Structure of the PPNBArF salt.

A solution of PPNCl in hot methanol was quickly added to an equimolar amount of potassium tetrakis(3,5-bis(trifluoromethyl)phenyl)borate (KBArF) also dissolved in hot methanol. Immediately upon mixing, a grainy white solid forms. After the solution cooled the solid was removed via filtering and recrystallized from tert-butanol. The product was filtered, rinsed with tert-butanol, and dried several hours under vacuum.

Synthesis of KBArF followed a slight modification of a literature procedure for the synthesis of NaBArF. In our procedure, 3,5-bis(trifluoromethyl)benzyl magnesium bromide was reacted with borontrifluoride etherate instead of sodium tetrafluoroborate.[79] The crude product was converted to the potassium salt using potassium carbonate instead of sodium chloride.

The crude KBArF solid was recrystallized as follows. The solid was dissolved in a minimum of ether. To the solution, chloroform was added to about five-times excess (by volume with respect to the ether solution). The ether was then slowly removed from the solution via rotoevaporation. The resulting chloroform solution was cooled to 0°C in a freezer. An orange solid crystallized out of the solution. The liquid was decanted off the solid and the solid dried at room temperature under vacuum. The dried orange solid was then dissolved in a minimum of hot methanol. Distilled water was then added to the hot methanol solution until the solution has only a slightly cloudy appearance. This solution was then placed in the freezer overnight. A fine white precipitate formed in the solution, which was separated from the solvents by centrifugation. The liquid was decanted and the white solids collected.

The white solids collected still contained impurities as identified by nmr spectroscopy. The entire recrystallization procedure was repeated several times until the pure KBArF was obtained.

PPNBr was prepared by stoichiomeric addition of NaBr to a solution of PPNCl in acetone. After 6 hours of stirring, a fine solid (sodium chloride) is present in the flask. The mixture was filtered and the solution collected. The solution was then rotovaped to dryness leaving a white solid (PPNBr) in the flask. The PPNBr was recrystallized from ethylacetate/2-propanol. The resulting crystals were dried under vacuum.

1-Methyl-3-cyanopyridinium tetrakis(3,5-bis(trifluoromethyl)phenyl)borate (CMPBArF) was prepared by combining stoichiometric amounts of KBArF and $CMPPF_6$ in hot distilled water. The resulting solid was filtered and rinsed with distilled water. The solid was recrystallized from methanol/water. An analogous process was used for preparation of 1,3-dimethylpyridinium tetrakis(3,5-bis(trifluoromethyl)phenyl)borate (DMPBArF). The synthesis of $CMPPF_6$ and $DMPPF_6$ has been reported in the previous section of this chapter.

Cells and Electrodes. The electrochemical cells used in film growth and in ring-disk experiments were each single compartment cells and were employed in a three- or four-electrode configuration, respectively. The platinum ring-disk working electrode employed here has previously been described in detail above. A platinum wire was used for the counter electrode and a Ag/Ag^+ (0.10 M $AgNO_3$, DMSO) reference electrode was employed for film growth. For the ring-disk experiments, a 3 mm diameter Ag disk pseudo-reference electrode (-90 ± 50mV vs SSCE) was utilized. This reference electrode

was epoxied into the center of the bottom of the cell to minimize iR effects (see Figure 2.11).

Film Growth. Films were grown to a variety of thicknesses potentiostatically, galvanostatically, and by potential cycling. Different electrolyte anions were considered (e.g.: *p*-toluenesulfonate (Tos^-), hexafluorophosphate (PF_6^-), or tetrafluoroborate (BF_4^-)) as well as different solvents (propylene carbonate and acetonitrile). Very little variation was found in the doping behavior among films produced under each of these conditions. Consequently, poly(pyrrole) films described herein were grown potentiostatically at +0.8 V vs Ag/Ag^+(0.10M $AgNO_3$/ DMSO) from acetonitrile solutions of pyrrole (0.2M) and the tetraethylammonium salt (0.2M) of Tos^-, PF_6^-, or BF_4^-. The extent of film growth was determined by the coulombs passed during polymerization (15 mC, except where noted). Following film growth, the working electrode was removed from the growth solution with the polymer in an oxidized state. The film and electrode were rinsed with copious amounts of acetonitrile and immediately transferred to the RRDE cell.

Cyclic Voltammetry. All voltammetry was performed with rotation of the working electrode at 400 rpm. Unless otherwise stated, a scan rate of 50 mV/sec was employed.

Scanning Electron Microscopy. Scanning electron micrographs (SEM) were taken using a Phillips model 505 SEM. Sample films for imaging were grown onto platinum foil electrodes of approximately identical area. Film thicknesses were monitored with a coulometer and were grown identically as above. The films, in an oxidized state, were dried prior to examination. Gold was sputtered on the films to a thickness of 20 nM prior to imaging.

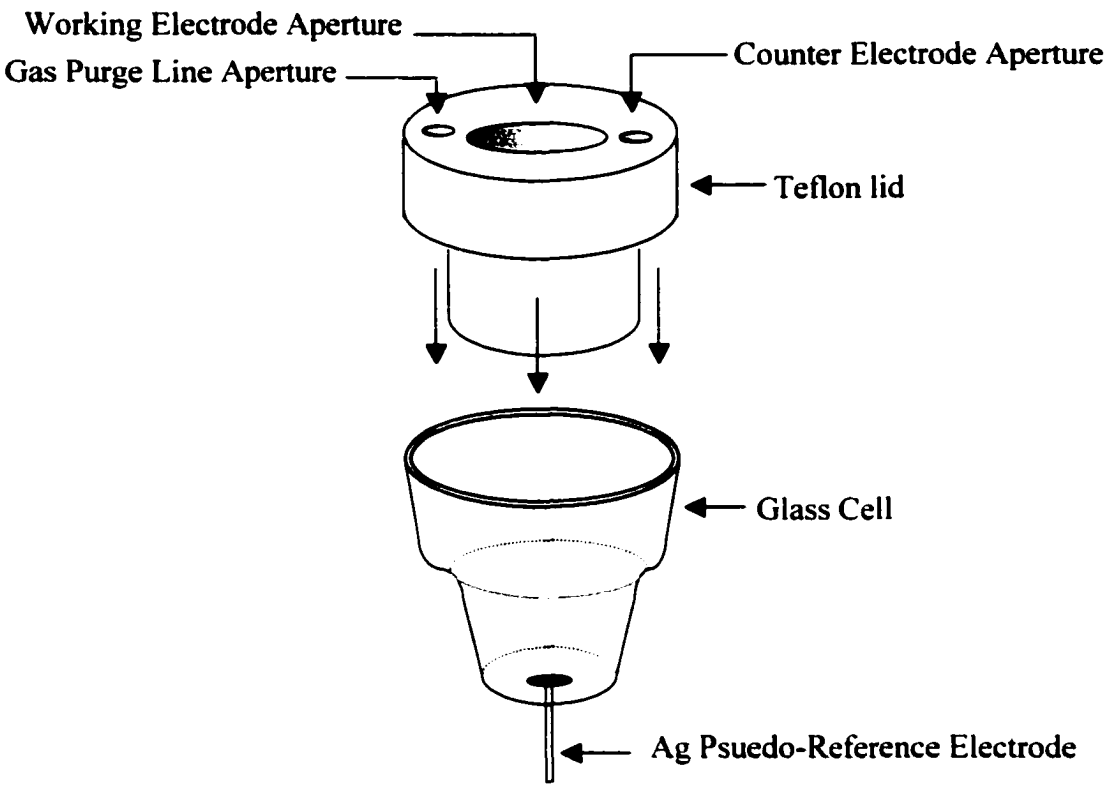

Figure 2.11. Diagram of electrochemical cell for RRDE experiments.

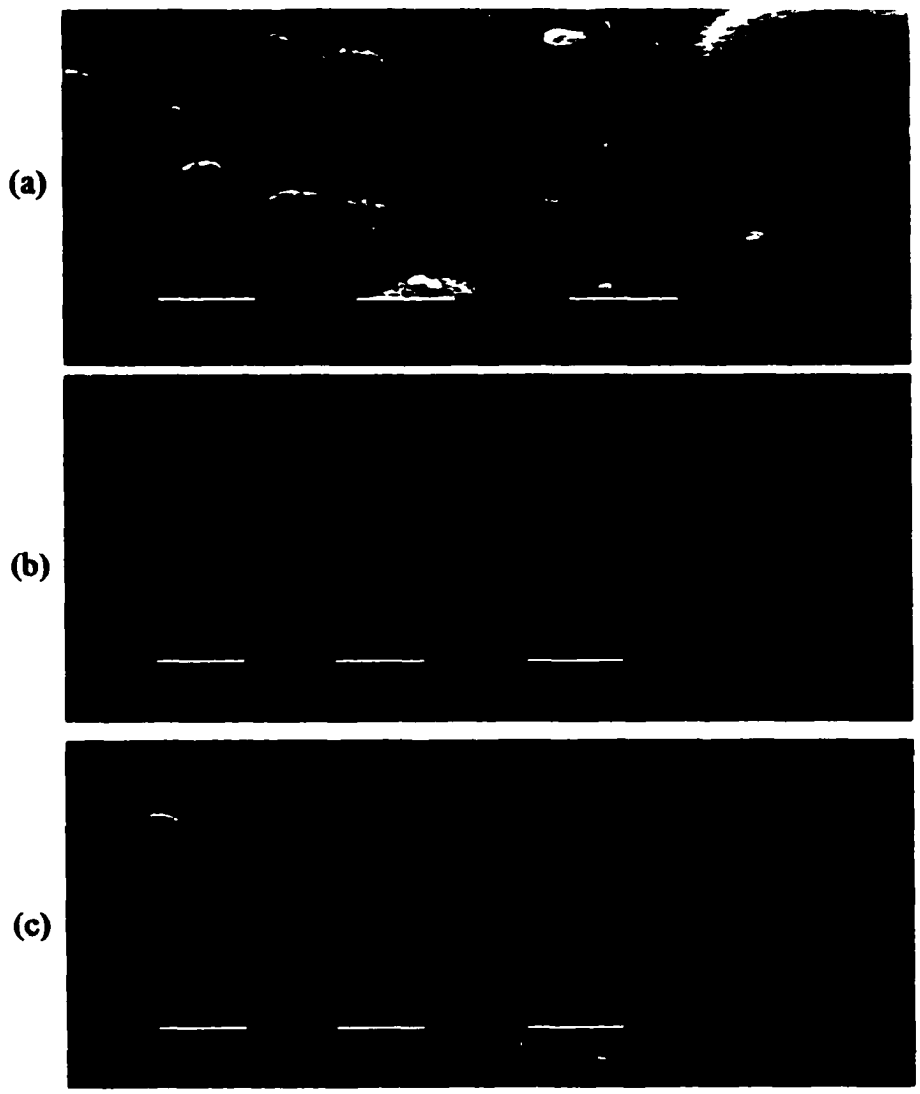

Figure 2.12. Scanning electron micrographs of (a) pPy/BF_4, (b) pPy/pSS, and (c) pNMPy/BF_4.

two films are structureless and smooth. In contrast, the poly(pyrrole) film consists of interpenetrating pitted nodules ranging in size down from ca. 1μm diameter.

Voltammetry of Poly(pyrrole) in PPNBArF Electrolyte. The solid curve (a) in Figure 2.13 is a voltammogram of a typical poly(pyrrole) film in acetonitrile containing 50 mM PPNBArF. The voltammogram exhibits two obvious pairs of waves; one centered at about -0.25 V and a broader pair centered at 0.10 V. Under identical conditions pPY^{+}/pSS^{-} and poly(N-methylpyrrole) yield featureless voltammograms with small magnitude currents characteristic of double layer charging (Figures 2.1a and 2.14). In contrast, the charge passed by poly(pyrrole) films in PPNBArF electrolyte is a significant percentage of the total charge capacity of the film indicating that the PPN^{+} and the $BArF^{-}$ ions are only partially excluded from the bulk of the polymer (vide infra).

Electroactive Cation Doping-CMP^{+}. Figure 2.15 shows the polymer voltammetry at the disk (solid curve, a) and the quantity related to the ring current, $-i^{*}_{r}(t)/N$, for CMP^{+} reduction (dotted curve, c) during the first potential scan after introducing CMP^{+} to a solution of 50 mM PPNBArF. The presence of this small cation initially produces only modest changes in the film voltammetry. The major consequence is an immediate increase in the magnitude of the disk current for the process at ca. –0.3 V with very little change in the wave at more positive potentials (cf. Figures 2.13a and 2.15a). Note that there is no involvement of CMP^{+} in the polymer doping at potentials positive of 0.0 V. From the ring current data in Figure 2.15, it is evident that the entire increase in current at the disk can be attributed to CMP^{+} doping in the polymer. With continued potential cycling, the wave at –0.3 V diminishes and finally disappears after about ca.10 cycles. Concomitantly, the changes in ring current reflected by the quantity

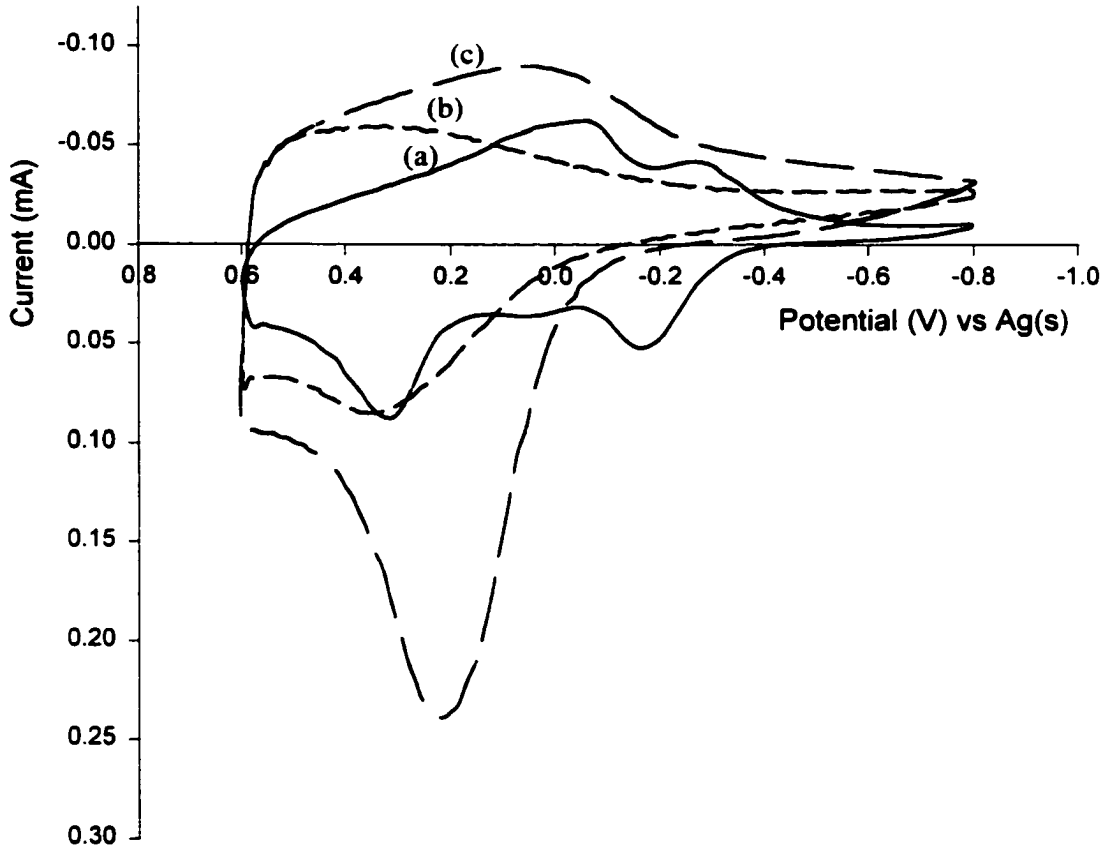

Figure 2.13. Steady state cyclic voltammograms of a pPy^{+}/PF_6^{-} film at a Pt disk in different combinations of electrolyte. The film is cycled in acetonitrile solutions of 50 mM PPNBArF (a), in 50 mM PPNBArF/2 mM PPNBr (b), and in 50 mMPPNBArF/2 mM PPNBr/2 mM CMPBArF (c).

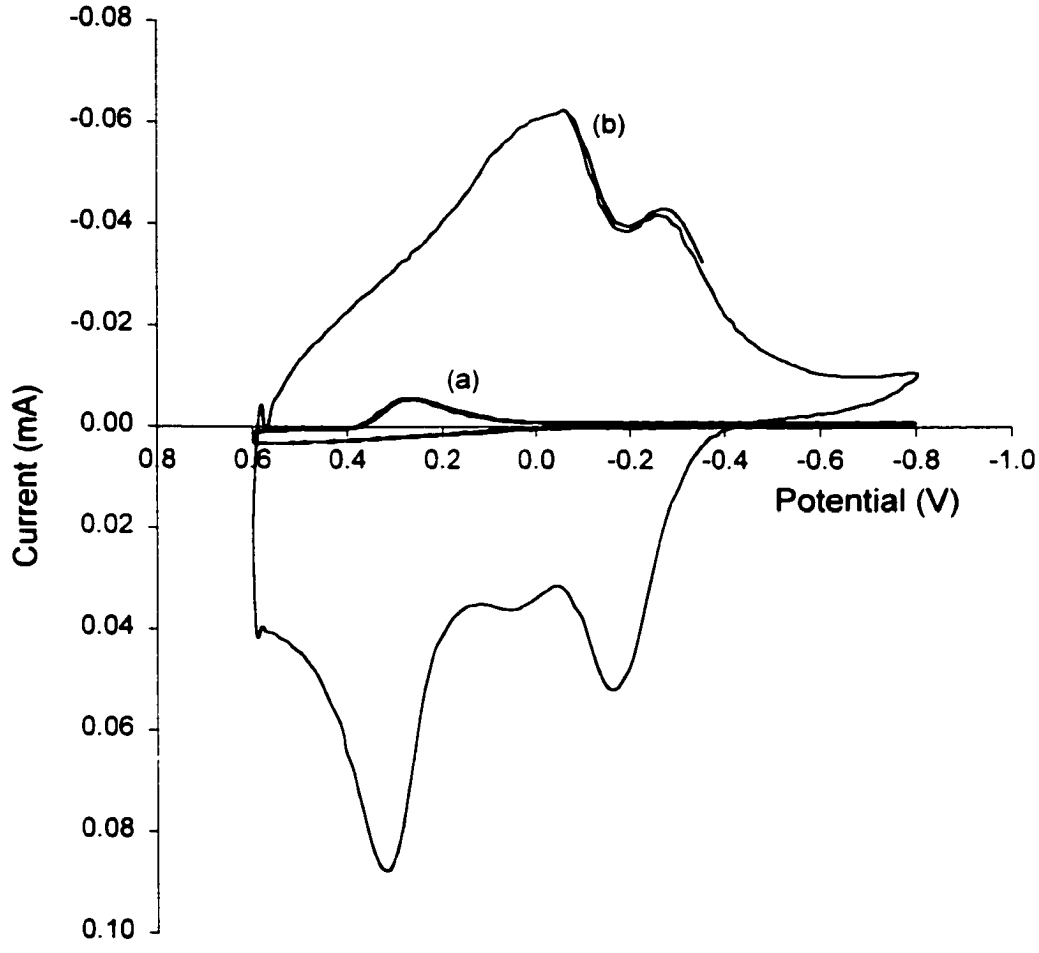

Figure 3.2.14. Cyclic voltammograms for (a) $pNMPy^{+}/BF_4^{-}$ and (b) pPy^{+}/PF_6^{-} films cycled in acetonitrile solutions of 50 mM PPNBArF. Only a small current response can be noted for the $pNMPy^{+}/BF_4^{-}$ film at potentials more positive than 0.0 V.

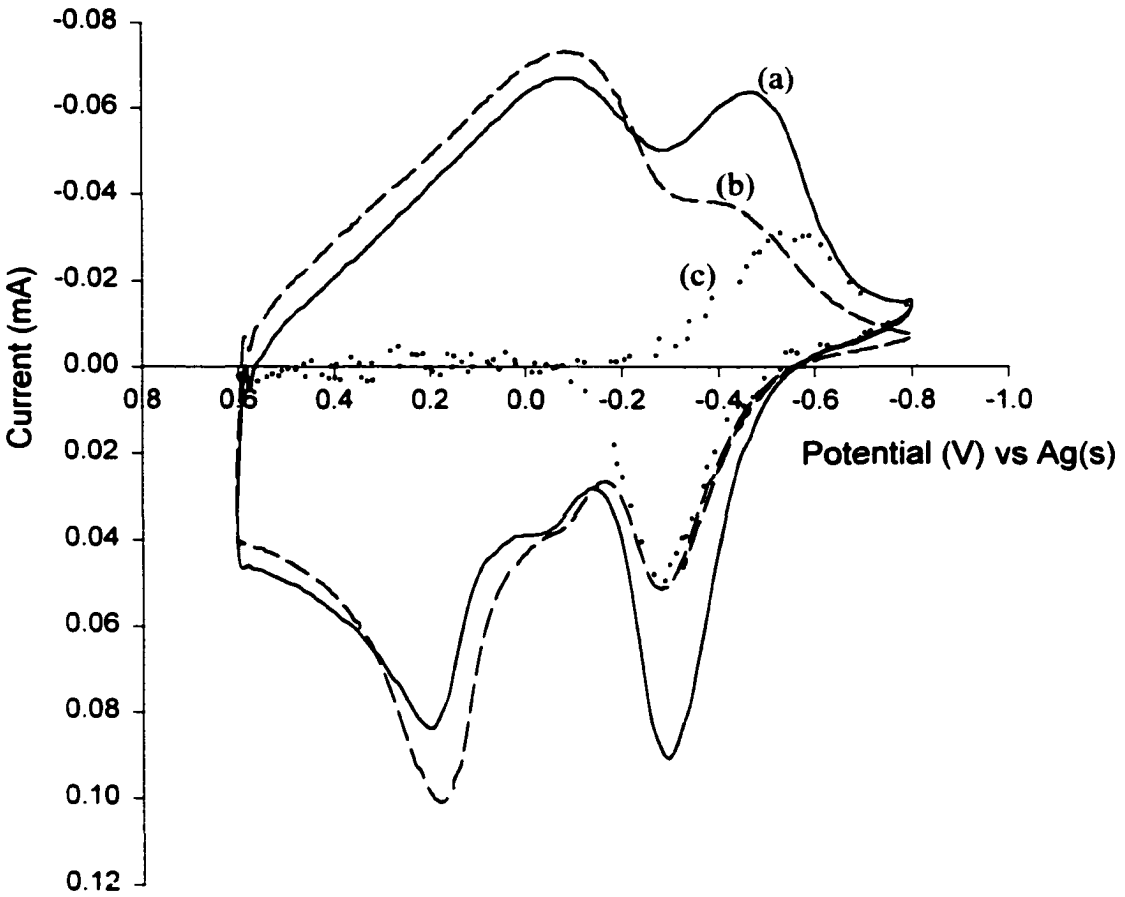

Figure 2.15. The solid line (a) shows the first cycle of the voltammetry of a pPy^{+}/BF_4^{-} film in 50 mM PPNBArF/acetonitrile solution after addition of 2mM CMPBArF. Prior to the addition of CMPBArF, the film was cycled in 50 mM PPNBArF/acetonitrile until stable voltammetry was obtained. The dashed line (b) is the fifth cycle after addition of CMPBArF which clearly shows the change in the film voltammetry with continued cycling. The dotted line (c) is a plot of the quantity, $-i'_r(t)/N$, for the reduction of CMP^{+} correlating with the solid line disk voltammogram (a).

$-i'_r(t)/N$ shows that doping by CMP^+ diminishes as well, eventually reaching zero. Finally, as the wave at –0.3 V decreases, both the oxidation and reduction currents at more positive potentials increase (Fig. 2.15b).

Electroactive Anions-Cl^- or Br^-. Contrasted with the minor changes in the poly(pyrrole) voltammetry brought about by the addition of CMP^+, introduction of PPNBr or PPNCl causes profound changes that are evident by comparison of curves (a) and (b) in Figure 2.13. The voltammogram of the film becomes rather featureless with a broad oxidation peak at ca. 0.4 V. The wave on the reduction scan is also very broad extending past the negative potential limit back into the anodic sweep. This type of behavior, as will be discussed in more detail subsequently, is indicative of slow ion transport within the polymer. A typical measurement of $-i'_r(t)/N$ for the doping by a halide is shown in Figure 2.16. Although the ring voltammetry shows a significant amount of charge compensation by the halide, there is obviously additional doping by electrochemically inactive ion(s); otherwise the magnitude of $-i'_r(t)/N$ and disk current (dashed and solid curves in Figure 2.16, respectively) would be identical.

Electroactive Cation and Anion-CMP^+ and Cl^-. Figure 2.13c demonstrates the effect on the poly(pyrrole) voltammetry of adding CMP^+ into a solution already containing Cl^-. When the CMP^+ is added, the total charge capacity of the film within the voltage range scanned approximately doubles and a relatively sharp peak at ca. 0.2 V develops on the anodic scan. Additionally, the cathodic current at negative potential increases.

Figure 2.17 shows $-i'_r(t)/N$ for CMP^+ reduction (2.17b) and of Cl^- oxidation (2.17c) for a typical poly(pyrrole) film that has been potential-cycled to steady state in

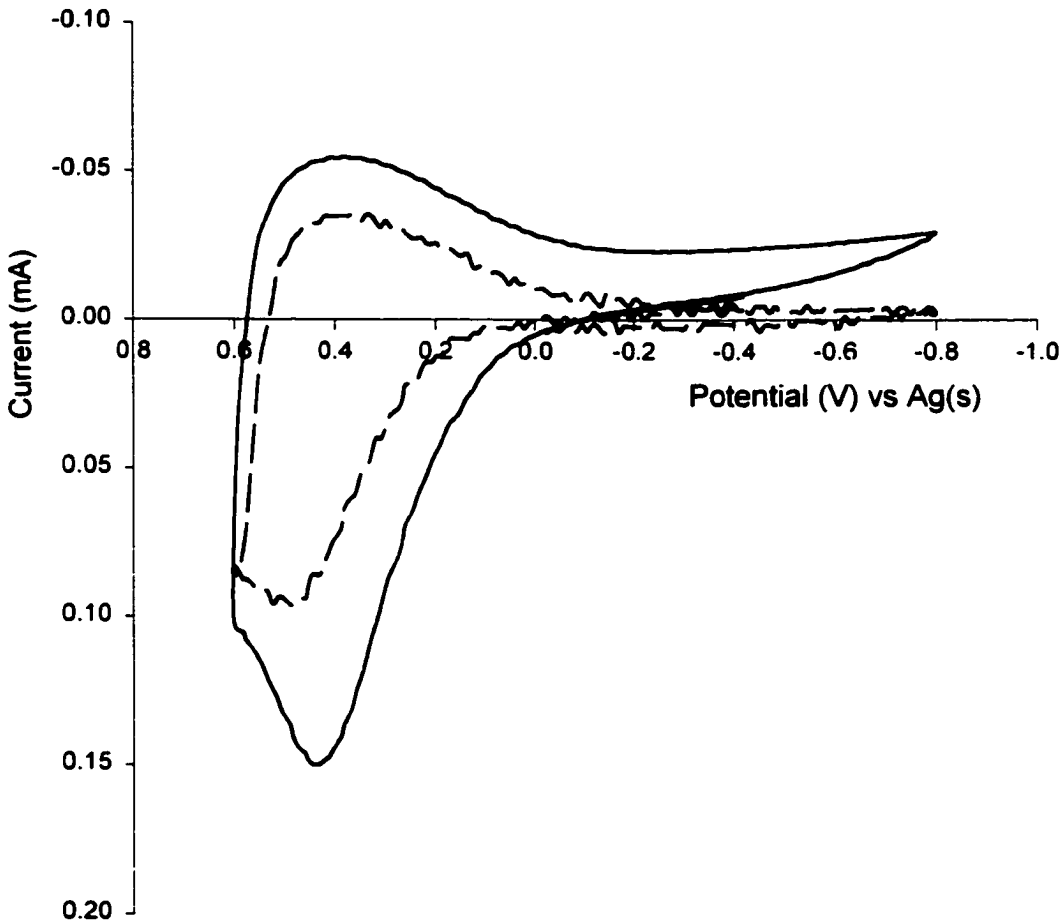

Figure 2.16. The solid line shows the current response for a pPy^{+}/PF_6^{-} film cycled in an acetonitrile solution of 50 mM PPNBArF/2mM PPNCl. The oxidation of Cl^{-} at the ring electrode (presented as $-i'_r(t)/N$) is given by the dashed line.

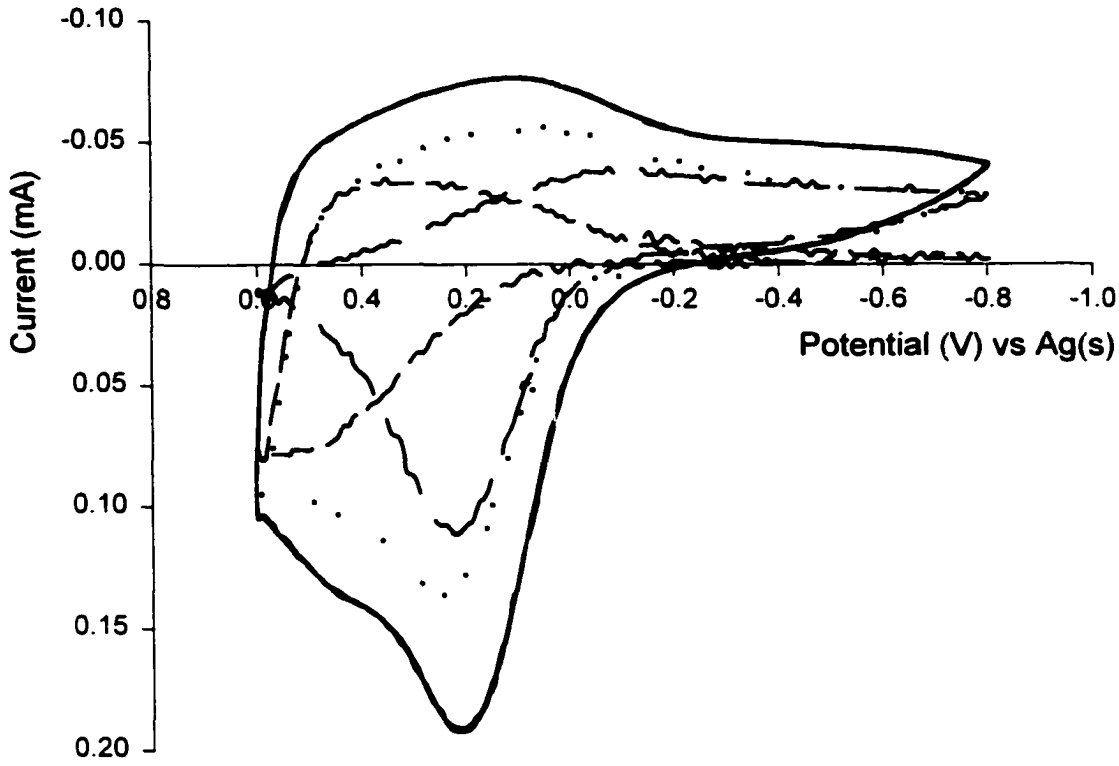

Figure 2.17. The current response of a pPy^{+}/PF_6^{-} film cycled in an acetonitrile solution of 50 mM PPNBArF/2 mM CMPBArF/2 mM PPNCl is shown by the solid line voltammogram (a). The current response, $-i'_r(t)/N$, for CMP^{+} reduction and for Cl^{-} oxidation at the ring, are given by the long-dashed (b) and short-dashed (c) voltammograms, respectively. The dotted-line voltammogram (d) shows the sum of the CMP^{+} and Cl^{-} contribution to the film doping. Note the relationship of shape and magnitude of this voltammogram (d) with the total film voltammetry (a). The voltammogram of the film (a) and the total electroactive ion voltammogram (d) do not exactly overlay as a result of partial doping by PPNBArF.

acetonitrile solution containing 2 mM CMPCl and 50 mM PPNBArF. Negative of ca. 0.0 V the doping change is predominantly due to CMP^+. In fact, except at the positive extreme of the potential scan, the doping change shows a considerable contribution from CMP^+. Chloride doping only becomes significant at the most positive potentials (E > 0.4 V).

Electrochemically Inactive Cations---TAA^+(tetraalkylammonium). Various electrochemically inactive cations (tetrabutyl-, tetrapropyl-, and tetramethylammonium) were added to background electrolyte solutions as Cl^- salts. The resulting film voltammetry depends on which cation is present. Adding TBACl produces similar voltammetry to that obtained in PPNCl electrolyte (cf. Figure 2.13b). Adding TMACl, on the other hand, results in voltammetry at both the disk and ring (for Cl^- oxidation) similar to that obtained from CMPCl (cf. Figure 2.17a and c), indicating that TMA^+ participates in the doping much like CMP^+. The intermediate sized tetrapropylammonium cation showed voltammetry that initially behaves similar to TBA^+ but becomes more like TMA^+ after long cycle times.

Electrochemically Inactive Lipophilic Anion-PF_6^-. Addition of $CMPPF_6$ into the background electrolyte solution results in polymer voltammetry qualitatively similar to that in CMPBArF (cf. Figure 2.15 and Figure 2.18) except that more CMP^+ doping is evident. The pair of peaks at ca. –0.3 V (Figure 2.18) initially grows in magnitude, but then decreases with time until they are no longer observable. The evolution of the CMP^+ voltammetry tracks the growth and disappearance of this peak just as it did for CMPBArF.

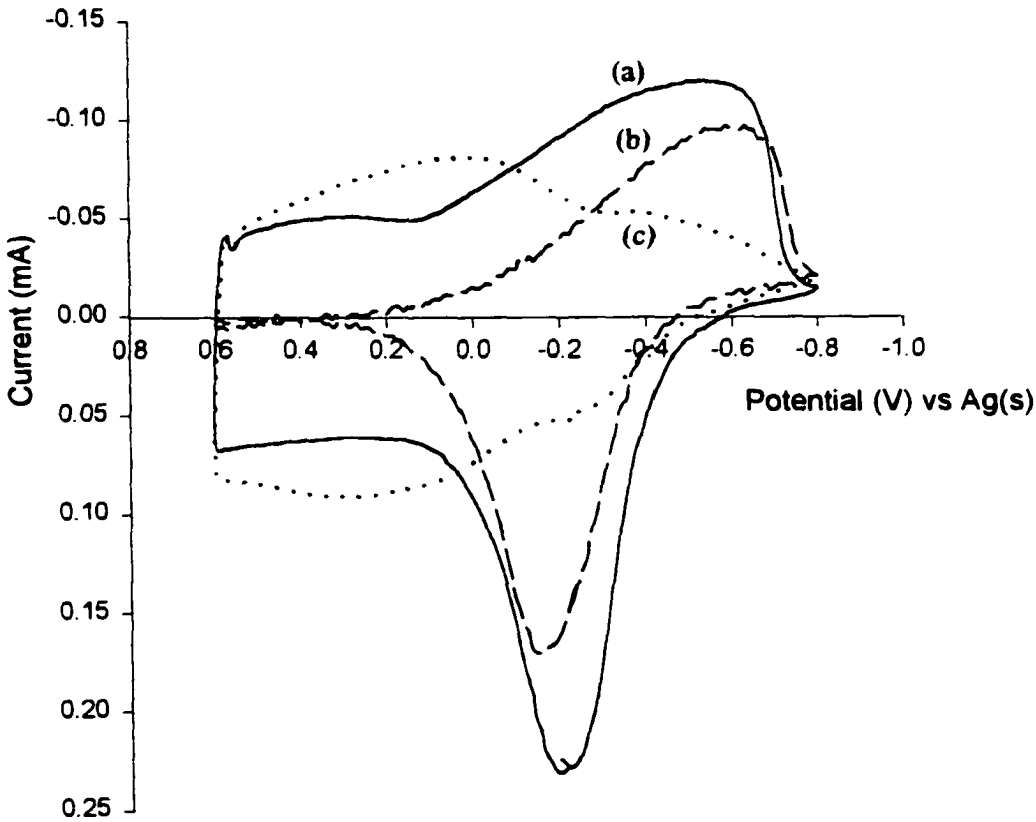

Figure 2.18. The voltammetric response of a pPy^{+}/Tos^{-} film cycled in an acetonitrile solution of 50 mM PPNBArF/2 mM $PPNPF_6$ is given by the solid line (a). The ring current response, $-i^{+}_{r}(t)/N$, for the reduction of CMP^{+} for the first cycle after addition of CMPBArF (2 mM) is plotted by the dashed line (b). The dotted line (c) is the disk current response after ca. 10 cycles.

DISCUSSION

Considering the scanning electron micrographs of the three polymer films shown in Figure 2.12, only poly(pyrrole) has resolvable structure at these magnifications. Also, poly(pyrrole) is the only one of these three polymers that exhibits any significant redox activity in PPNBArF electrolyte. Typically, the total integrated charge passed by a poly(pyrrole) film cycled over the potential region between 0.6 and –0.8 V vs Ag/Ag^+ is about 60% as large in PPNBArF electrolyte as in an electrolyte composed of a smaller, more mobile ions such as $TMAPF_6$. The increased charge capacity with $TMAPF_6$ shows that there are some polymer redox sites (roughly 40%) accessible only to smaller ions. The linear relationship between the scan rate and the peak currents of the polymer voltammetry in PPNBArF electrolyte, however, indicates that ion transport within the polymer is rapid, at least for scan rates in the range of 25 to 100 mV/s (Figure 2.19)

From the CV data and the SEM images we can now make some reasonable inferences about the nanoscopic structure of these poly(pyrrole) films. For there to be rapid transport of PPN^+ and $BArF^-$ within the polymer, channels must exist which are several times the diameter of the ions; otherwise, we would expect slow ion transport which would show up in the scan rate dependence of the polymer CV. Furthermore, slightly more than half of the total redox centers must be close enough to the walls of these channels to be charge compensated by ions in the channels. The remaining sites are not so close but some fraction of these (maybe all) can be rapidly accessed by smaller TMA^+ and PF_6^- ions. This model is consistent with the SEM image (Figure 2.12a) that shows a porous structure that, based on the CV results, must extend down to the dimension of 10's of angstroms. Likewise, the featureless SEM images of pPY^+/pSS^-

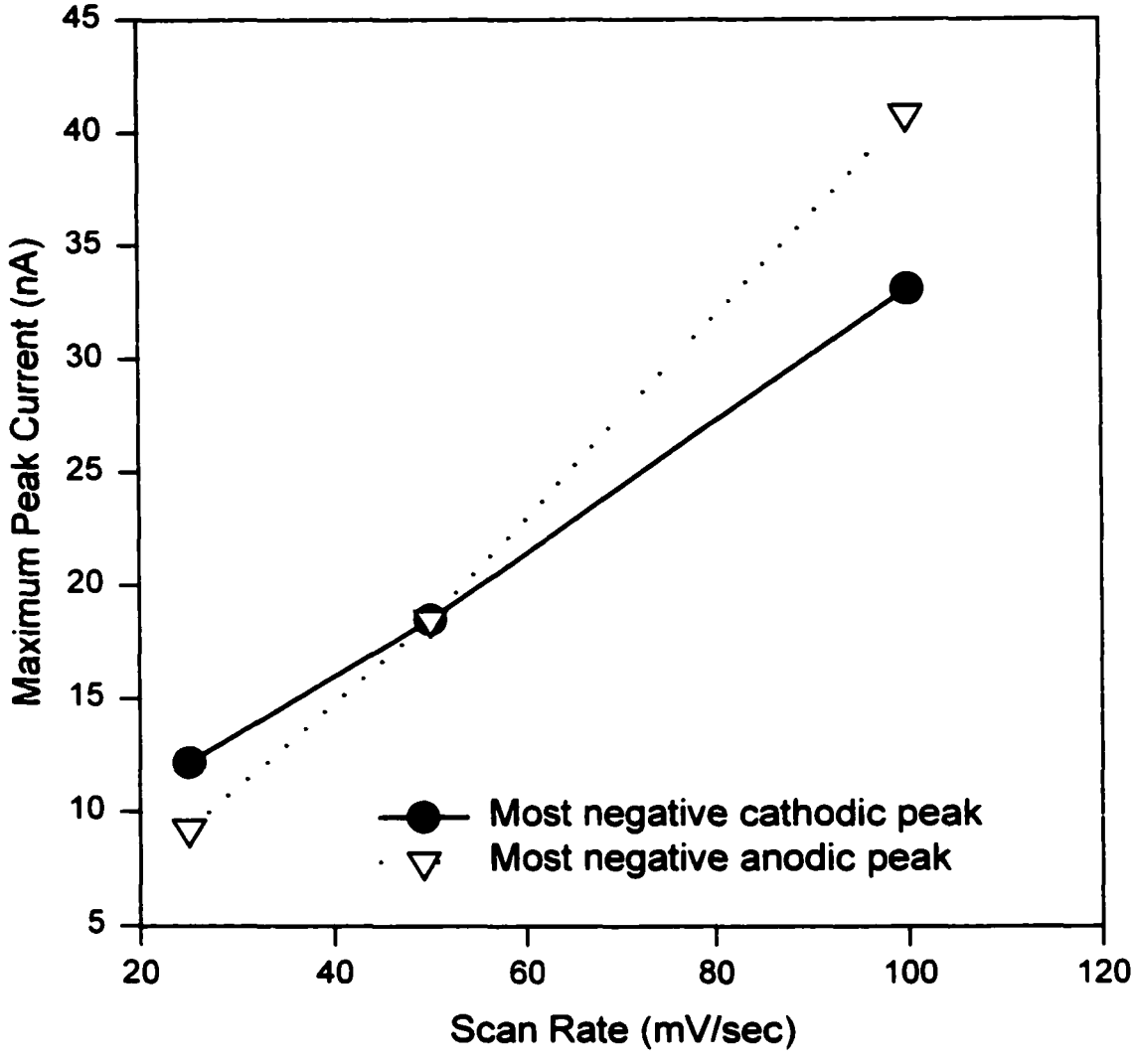

Figure 2.19. The plots in the figure show the linear relationship of the peak current response with respect to the scan rate for pPy^{+}/pSS^{-} films cycled in acetonitrile solutions of 50 mM PPNBArF.

and poly(N-methylpyrrole) are consistent with their lack of electrochemistry in PPNBArF electrolytes.

The initial increase in polymer current resulting from the addition of CMPBArF quantitatively tracks the polymer incorporation of CMP^+ (cf. Figure 2.14). For CMP^+ (or any cation) to participate in doping requires the presence of "fixed" anionic sites within the polymer. Since the charge on the poly(pyrrole) backbone is either neutral (when fully reduced) or positive (when oxidized), these negatively charged sites must result from anions that were entrapped during the growth process. Thus, when the poly(pyrrole) is reduced, cations from solution incorporate to balance the negative charge of the entrapped anion. For reasons that are not transparent, these sites are the most difficult ones to be reduced and easiest to be oxidized (i.e., they have the most negative redox potential). The similarity in the general shape of the polymer voltammograms in Figures 2.13a and 2.15a suggest that a significant number of these trapped anion sites are close to the surface of the nanoscopic pores and can thus be compensated by PPN^+. Interestingly, the very process of repeated doping and undoping with CMP^+ (or other small cations) modifies the polymer structure in a way that releases the entrapped anions. Once this is accomplished, no further CMP^+ doping is evident from the ring current. In contrast, cycling the polymer in PPNBArF alone gives steady state voltammetry of the types observed in Figure 2.13a where there is an obvious stable cation-doping peak at –0.3 V. Also, addition of tetramethylammonium ion (TMA^+) to solution causes very similar changes in the polymer voltammetry to those observed with addition of CMP^+. This suggests that the behavior of CMP^+ is not unique, but rather, it is a general "small cation" effect. In contrast to TMA^+, the addition of modestly larger cations, such as

tetrabutylammonium, produce no changes in the polymer voltammetry; thus indicating that it is excluded from sites accessible to CMP^+ and TMA^+ (ostensibly, because of size).

As described previously, when CMP^+ is introduced with a small, lipophilic anion such as BF_4^-, PF_6^-, or Tos^-) rather than as the $BArF^-$ salt, the interaction between CMP^+ and the polymer are qualitatively similar to those observed for the case of CMPBArF. The only difference is that the amount of CMP^+ doping is initially larger. Essentially the same steady state voltammetry results from each of these anions; namely, the current-potential profile is broadened and the charge capacity, especially at more positive potentials, is increased. This increased charge capacity must reflect the greater number of redox sites accessible to the smaller anions. Therefore, we conclude that, at steady state, some combination of small anion and $BArF^-$ is responsible for *all* charge compensation changes of the polymer (i.e., no cation participation).

The addition of PPNX to solution, where X^- is Br^- or Cl^-, produces dramatically different changes in the polymer voltammetry relative to, for instance, $PPNPF_6$. On the first anodic cycle after introducing PPNX to solution, ca. 30% more charge is passed during the polymer oxidation than passes on the subsequent re-reduction cycle (Figure 2.20). After the first exposure to X^- at positive potentials, visible examination of the film color indicates that the polymer never fully reduces again. In other words, roughly one third of the X^- that enters the film on the first oxidation cycle does not come back out. Also, as is evident from Figure 2.16, no significant amount of X^- (in this specific case, Cl^-) participates in doping changes negative of ca. -0.1 V despite considerable current being passed at the disk.

As pointed out in the results section, addition of CMP^+ (or other small organic

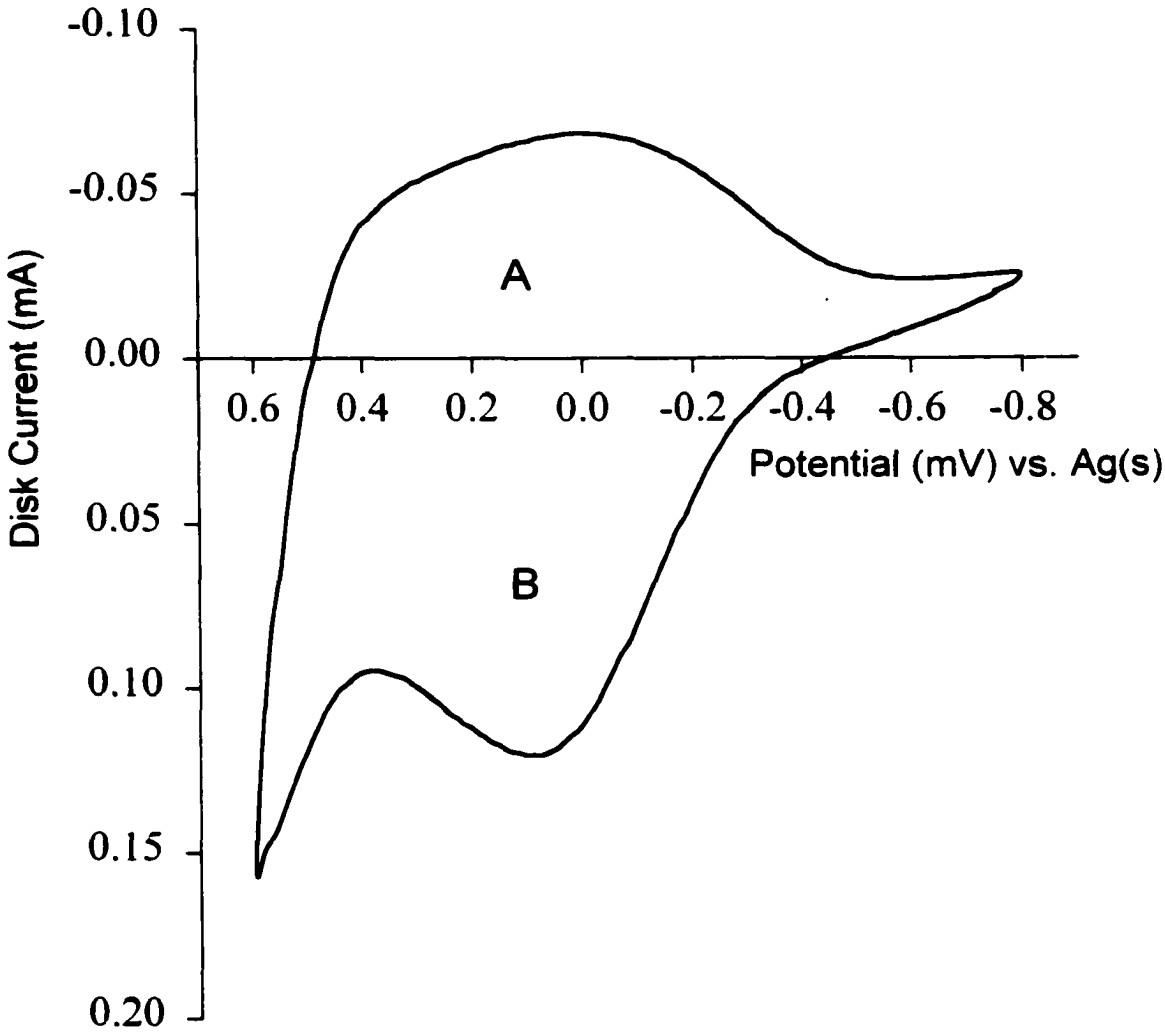

Figure 2.20. The first cycle of the voltammetry of a pPy-PF_6^- film after 5 mM PPNCl was added to the 50 mM PPNBArF/acetonitrile solution. The electrode rotation rate was 400 rpm. By cut-and-weigh methods, the ratio of the charge passed in the anodic sweep was compared to the charge passed in the following cathodic sweep via comparison of mass ratios of area A and area B. The average value of area A was 0.33g and the value of area B was 0.45g; indicating more charge was passed in the first anodic scan than was passed in the subsequent cathodic sweep.

cations, e.g., TMA^+) to a solution already containing X^- results in a roughly two-fold increase in the total charge capacity of the film (cf. Figure 2.13). Interestingly, adding CMP^+ causes virtually no change to the shape or magnitude of the doping profile of X^-; all of the additional charge capacity can be attributed to CMP^+ doping (cf. Figure 2.13 and 2.17). Figure 2.17 is typical of the steady state voltammetry obtained with CMP^+ and X^- present in solution. Both ions contribute to the doping change, which is in contrast to the behavior of CMP^+ in the presence of PF_6^-, BF_4^-, or Tos^- where there is no cation participation at steady state.

Earlier in this chapter, the linear relation of the scan rate and the peak current of the poly(pyrrole) voltammetry was invoked to argue that, in the absence of X^-, ion transport within the film is facile. Ions of both charges appear to move rapidly within whatever polymer domain(s) are accessible to them (determined by their size). The initial irreversible uptake of X^- eliminates this rapid ion transport within the polymer. This is demonstrated by the fact that on the positive going scan potentials up to ca. -0.2 V *cathodic* current continues to flow (Figure 2.16, solid line). Such behavior is consistent with the redox process having become mass-transport-limited; that is, the film is not equilibrated to the redox potential due to the slow incorporation or transport of the counterions. Since the quantity $-i'_r(t)/N$, shown in Figures 2.16 and 2.17 for halide oxidation, give no indication that X^- is participating in doping changes in this potential range, presumably charge balance is being maintained by cation uptake. The ring voltammetry in Figure 2.17 corroborates this assertion, as evidenced by the contribution of CMP^+ in this potential region. It would appear that the initial irreversible uptake of Cl^- dramatically alters the structure of the polymer in a way that profoundly affects ion (and

presumably solvent) transport into and/or through the polymer.

Another unusual feature of the polymer voltammetry in CMPX electrolyte is the existence of significant potential regions, during both the anodic and cathodic scans, where both CMP^+ and X^- are simultaneously participating in the doping change. For example, from approximately 0.2 to 0.6 V on the anodic scan in Figure 2.17 significant up take of Cl^- and loss of CMP^+ are simultaneously occurring. Clearly a simple Donnan-exclusion model is incapable of explaining such complex behavior.

From all of the various RRDE data collected here we can begin to construct a model that can explain the redox behavior of poly(pyrrole) in contact with X^- electrolyte. Before doing so, it is useful to recount briefly the major findings of our earlier RRDE study of pPY^+/pSS^- films. Succinctly put, all doping changes in these composite films are *quantitatively* due to small cation (e.g., CMP^+) transport. When the films are first grown electrochemically, pSS^- polyanions are irreversibly incorporated. Subsequently, when the poly(pyrrole) backbone is reduced the influx of small cations into the polymer is the only mechanism available to maintain charge neutrality.

The doping behavior of poly(pyrrole) in PPNX or CMPX electrolytes is probably best characterized (phenomenologically, at least) as being hybrid between the doping behavior of pPY^+/pSS^- composites and that of the other small-ion systems considered here (e.g., $CMPPF_6$). The fraction of X^- that irreversibly enters the film on the first anodic scan behaves similar to pSS^-; i.e., they serve as permanent negative charges that do not leave the polymer on the time scale of the experiment. To reduce those cationic sites on the poly(pyrrole) that are associated with these "fixed" X^- sites, requires that some other cation enter the film to balance the charge. The remaining "mobile" X^- can

move out of the polymer to maintain charge neutrality. If the only cation in solution is PPN^+ only a relatively small quantity of these ions can enter the now-more-restricted pore structure of the polymer on the time scale of the experiment. The mobile X^- ions, on the other hand, can come and go as redox changes of the polymer require; thus they dominate the doping change when PPN^+ is the only cation available. When a small cation such as CMP^+ is introduced into solution, it can more easily and quickly enter the polymer. Thus all of the sites compensated by "mobile" X^- can still undergo reduction, but additionally, a significant fraction of poly(pyrrole) sites compensated by "fixed" X^- can now also be reduced because CMP^+ can enter the polymer to replace the oxidized cationic poly(pyrrole) sites. Interestingly, the sites associated with the "fixed" X^- are the easiest to oxidize and hardest to reduce. In other words, starting at the most reducing potentials, it is thermodynamically easier to expel CMP^+ than to incorporate additional X^-

.

Finally, the uptake of X^- by the polymer is only "irreversible" to the extent that the film remains in contact with X^--containing electrolyte. Transferring the film back into a solution of PPNBArF restores the original shape of the voltammogram. (i.e., as in Figure 2.13 or 2.15). The polymer also regains the capability of being fully reduced at negative potentials after several potential cycles in the new electrolyte.

CONCLUSION

We have shown that RRDE voltammetry is a useful tool in quantitatively mapping the complex changes in the ionic composition of poly(pyrrole) films under conditions of electrochemical control. By considering electrolyte solutions containing

various combinations of electrochemically active probe ions and electroinactive ions, a wide range of solution electrolyte conditions can be investigated. Contrary to preconceived expectations, the method by which the poly(pyrrole) films are grown (i.e., potentiostatically, galvanostatically or via potential cycling) has practically no effect on the doping behavior.[81] Instead, the doping behavior is entirely dominated by the nature and combination of ions available to the films from the electrolyte solution. In the presence of small organic cations and lypophilic anions, for example, anion transport dominates doping changes at steady state (which is the same behavior typically reported by others who have studied similar films by indirect methods). However, prior to reaching steady state both ion-types are involved.[48,54,82] In contrast, electrolytes containing small, hard anions (i.e., Br^- and Cl^-) drastically (but reversibly) alter the doping profile of poly(pyrrole) and probably alter its nanoscopic structure. These anions enter the polymer and, in part, become entrapped such that cation doping is required to discharge (reduce) the poly(pyrrole) sites with which the entrapped anions are associated. Finally, electrochemically-grown films of poly(pyrrole) have a porous structure that is clearly evident from SEM images; moreover, that porosity extends down to the dimensions of the electrolyte ions. Otherwise, large electrolyte ions such as PPN^+ and $BArF^-$ would be sterically excluded from the bulk of the polymer, as they are by pPY^+/pSS^- and poly-N-methylpyrrole.[78]

The major limitation of the RRDE approach lies in the fact that, for the dopant ions to be directly monitored, they must be electrochemically active within the solvent window but inactive over the potential range of the polymer. This is admittedly a non-trivial constraint because it significantly reduces the number of dopant ion candidates for

study. That caveat notwithstanding, we have found in preliminary work, that by using mixtures of electroactive and non-electroactive ions, it is often possible to gain considerable *in situ* information on doping by electroinactive ions. This can be accomplished by considering the difference between the total doping requirement of the polymer and the part due to the electroactive dopant.

CHAPTER 3

Impedance-Based Solution Phase Sensing of Small Organic Molecules Using Thin Films of Poly(3,4-Diphenylpyrrole)

INTRODUCTION

A particularly interesting and rapidly growing field of study is the development of sensing methods based on electrically conducting polymers. The use of organic conducting polymers as transducer materials for detection and quantification of a wide array of analytes has been reported. The two primary areas of investigation are in the development of materials and devices for sensing of biologically significant analytes (i.e., glucose and urea) in aqueous media and the sensing of vapors and gases. Sensing methods using conducting polymers are typically based upon changes in polymer properties through interaction with a target analyte; for example, changes in mass,[83-86] resistance,[2,86-89] work function,[36,50,90] and conductance[91] have all been considered. Additionally, their low cost, their ease of production, and the ease with which their properties can be modified by adding substituents to the monomer make these materials very attractive for sensing applications.

The concepts and data presented herein will demonstrate the sensing capabilities of one specific conducting polymer, poly(3,4-diphenylpyrrole), p(DPP), (Figure 3.1)

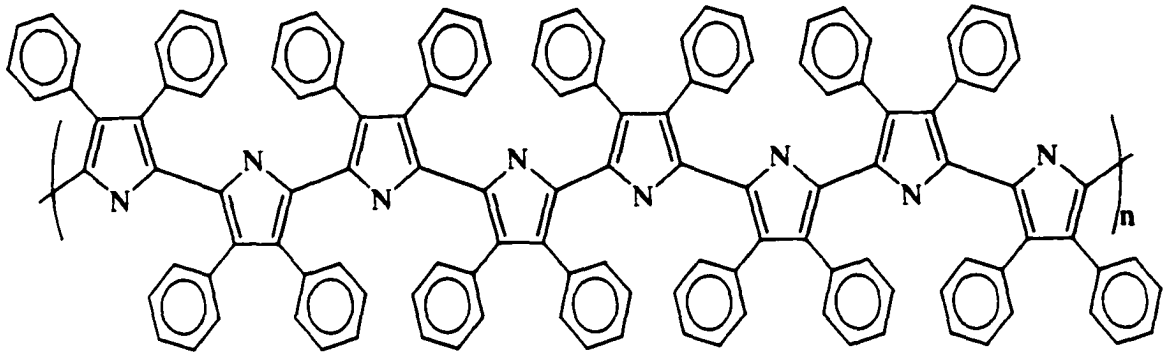

Figure 3.1. Structure of poly(3,4-diphenylpyrrole). The polymer as shown is in the neutral (undoped) state.

through monitoring changes in its impedance.

BACKGROUND

Solution Phase Sensors Employing Conducting Polymers. The use of conducting polymers for solution phase sensing is less common than their use in sensing of gases. Nonetheless, it will be shown that there exists a range of innovative uses for this class of materials in solution phase sensors. The most common solution application of these materials has been in the development of biosensors. In most cases, the conducting polymer serves as a medium for the entrapment of an enzyme and as the transducer for conversion of a chemical interaction to an electronic signal. These sensors are very analyte specific due to the selective properties inherent to the enzymes.

The above approach has been employed with a variety of biological molecules, but none more so than for the redox enzyme glucose oxidase for development of glucose sensors.[3,5,91-94] Glucose oxidase is typically entrapped in a conducting polymer film and interaction with glucose in the presence of oxygen results in the formation of peroxide and gluconic acid by the catalyzed oxidation of glucose.[5,95] These changes in the chemical environment can either directly affect the electronic properties of the conducting polymer film or they can induce redox chemistry upon the polymer with the formation of certain reaction products. The stoichiometric relation between products (and their subsequent redox reactions) and the glucose in solution produces quantitative sensing capabilities in this type of sensor.

A specific example of the type of sensor considered above is illustrated by the work of Sung et al. In their work, glucose oxidase was covalently bound to a polymeric

anion, poly(2-acrylamido-2-methylpropane sulfonic acid). The polymer/polyanion-enzyme was then electrochemically incorporated into a conductive poly(pyrrole) film on an electrode surface.[93] The enzyme/polymer composite film on the working electrode was held at a constant potential. The signal response was in the form of a change in the current measured at the electrode. Thus, amperometric detection resulted from electrochemical oxidation of the peroxide produced during the reaction of the entrapped glucose oxidase with glucose from solution. At potentials as low as 0.3 V vs. Ag/AgCl, signals were produced for glucose concentrations up to 20 mM with response times less than 30 seconds. Others have reported detection limits reaching 50 mM using glucose-containing poly(aniline) films on microelectrodes.[91]

In sensing of biological molecules using some entrapped enzymes, the reaction products of the interaction of the enzyme and the target molecule change the pH within the film. The conductivity of poly(aniline) is pH sensitive and a signal was measured as a change in film resistance. A range of molecules has been detected in this manner including peroxide,[96] penicillin,[97] ascorbate,[98] and cholesterol[8,92]. One interesting study employed an array of individual enzyme/polymer sensors in order to simultaneously identify three different biological molecules present in solutions.[91] Here, each poly(aniline) film composing the array contained a different enzyme. Product formation from an enzymatic reaction changed the pH environment of the film designed to target a particular analyte. Signals were produced by changes in the conductivity of the films. It was proposed that an array of various selective sensors could result in an "electronic tongue".[91]

Other properties of conducting polymers have been exploited for analyte sensing. Recognizing the electrochromic dependence of poly(aniline) on pH, Talaie et al. devised a unique pH sensor.[98] Using a bilayer of poly(aniline) grown on a poly(pyrrole)-coated platinum electrode, the investigators correlate solution pH with film resistance and the visible color. This method was applicable throughout the entire pH range, but the response was not linear. At best, the technique could determine an approximate pH (within a couple pH units) by either film resistance or color.

Similar ion sensing has been reported using electrochemically deposited composite films of poly(3-methylthiophene)/poly(dibenzo-18-crown-6) on a low melting point alloy electrode.[99] These films were employed for the potentiometric sensing of sulfide ions in aqueous solutions. The measured potential change was attributed to interaction of the dibenzo-18-crown-6 moieties with HS^- or S^{2-} adsorbed within the film matrix. The ion-exchange process leads to an unbalanced charge distribution. This method was found to be highly selective towards HS^- and S^{2-} from a large range of common anions.

Feldheim et al. demonstrated a more direct sensing method with conducting polymers. The researchers noted a significant cathodic shift in the redox potential of poly(N-methylpyrrole) occurred when certain neutral organics were introduced into an aqueous solution.[41] This shift was exploited for the direct amperometric detection of small chlorinated hydrocarbons.[44] To this end, films of poly(N-methylpyrrole) were electrochemically deposited onto an electrode surface. Absorption of small chlorocarbons such as dichloromethane and chloroform into the film caused reversible swelling of the polymer and a concomitant change in the polymer doping level. With the

polymer held at constant potential, a current spike resulting from the doping level change was related to the concentration of the chlorocarbon present in solution. This method allowed quantitative determination of the concentration of dichloromethane in aqueous solutions between 1 mg/mL to 10 ng/mL. Although the film response was not entirely specific to small, chlorinated hydrocarbons the interaction with chlorocarbons produced the most sensitive responses. Other organics such as tetrahydrofuran and acetone elicit qualitative similar responses but the magnitude was significantly smaller.

The work presented in this chapter stems from a report by Feldheim et al. regarding the study of the structure-function relationship between conducting polymers and various organic solvents.[44] The particular film employed by Feldheim et al. was poly(3,4-diphenylpyrrole). The addition of aromatic substituents was found to have a significant and interesting impact upon the polymer's electrochemistry. A dramatic on/off switching of the film voltammetry in aqueous systems was demonstrated. In pure aqueous solutions containing 0.10 M $NaClO_4$ the films gave no electrochemical response over a large potential range. However, bubbling dichloromethane-saturated N_2 through the aqueous solution could turn on the film voltammetry. Bubbling with pure N_2 purged the dichloromethane from solution and turned the voltammetry off again. This bubbling process could rapidly and reversibly introduce and purge the organic solvent into and out of the solution.

We concluded that this on/off behavior of the pDPP voltammetry might be used for the purpose of directly sensing dichloromethane in aqueous solutions. In the reports by Feldheim et al.,[44] flow-injection amperometry was employed to detect current responses of pDPP resulting from interaction with dichloromethane. An oxidative

potential was applied to a pDPP film in an aqueous electrolyte solution. Since the solution contained no dichloromethane, the doping level of the film could not equilibrate to the applied potential. When an aqueous sample containing dichloromethane passed over the film, the pDPP swelled, facilitating ion transport. The resulting anodic current spike signaled the presence of dichloromethane. After passage of the injected sample, dichloromethane diffused out of the polymer, trapping the added counterions. Upon repeated injections, Felheim et al. found a decrease in the signal response by the film as the film equilibrated to the doping level dictated by the applied potential. After six injections of a dichloromethane-saturated solution, the response decayed to less than 4% of the initial value. This diminishing response is unsatisfactory for practical sensing purposes.

In the present work, the on/off behavior of the pDPP film's electrochemistry was also utilized for sensing dichloromethane. However, unlike the amperometric study by Feldeim et al.,[44] the a.c. impedance of the pDPP was monitored. In this experiment, a small amplitude potential perturbation was applied to a film held at a resting potential. Thus, the film's doping level remains essentially constant. This eliminates problems associated with the decay of the amperometric signal reported above. Using ac impedance techniques, changes in pDPP film conductivity could be measured as changes in film resistance and capacitance; that is, the signal would occur as a change in film impedance.

Impedance Spectroscopy. Although an in-depth coverage of impedance spectroscopy and impedance theory is beyond the scope of what is possible here, a brief

background will be given on concepts pertinent to the work presented. For a more thorough explanation of impedance techniques, please refer to references listed herein.

According to Ohm's law, the resistance in an electrical system is proportional to the applied potential and inversely to the current ($R = E/i$). This is specific for the case of a direct current system where the current is impeded only by resistive circuit components.[101] In alternating current (ac) systems, Ohm's law becomes $Z = E/i$, where Z is the impedance of the circuit. Capacitors as well as resistors, impede the current flow in an ac circuit.[101] It is the capacitive and resistive components of the film that will be useful in the sensor study presented here.

In the ac technique, a small amplitude sinusoidal potential is applied over a dc potential. The dc potential sets up an equilibrium redox position on the system while the sinusoidal potential wave perturbs the equilibrium at various frequencies (Figure 3.2a). The resulting current is measured. The current response through a pure resistor of resistance R is $i = A\sin(\omega t)/R$, and the current through a pure capacitor of capacitance C is $i = AC\sin(\omega t + \pi/2)$.[101] In these equations, A is the amplitude and ω is the frequency (in radians per second) of the sinusoidal potential. Inspection of these equations show that the current response due to these elements differ in the phase angle, (ωt) and ($\omega t + \pi/2$), with respect to the applied potential.[101] The phase angle, θ, is the angle between the current vector and the applied potential. Thus, the current response of a purely resistive component will be in phase with the applied potential wave, $\theta = 0$, whereas a purely

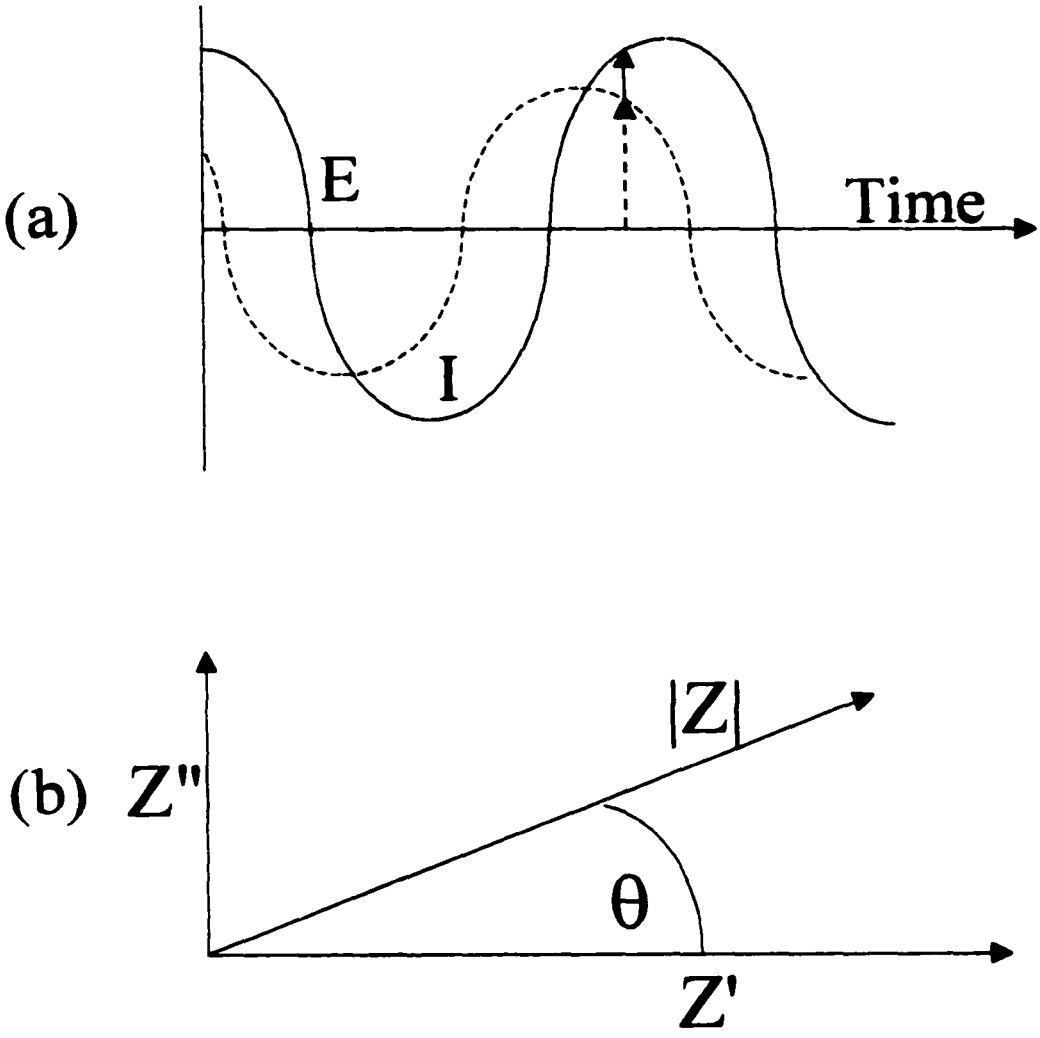

Figure 3.2. (a) Diagram demonstrating the applied sinusoidal potential perturbation (solid curve) to the electrochemical system. The dashed curve represents the resulting current response. The response is shown out-of-phase and having a smaller amplitude form the applied potential waveform. (b) A vector diagram showing the impedance relationships.

capacitive element will have a current response which lags the applied potential by 2π (90°).

Along with the phase angle, the magnitude of the impedance, or modulus, ($|Z|$) is also measured. Representation of this data is defined in terms of a real component ($|Z'|$) and an imaginary component ($|Z''|$) (see Figure 3.2b). These correspond to resistive and capacitive components, respectively. An impedance response is then described as a modulus and a phase angle.

There are two common formats for presenting impedance spectra. Impedance 'spectra' are plots of the impedance response to a range of applied potential frequencies. The most common formats for presenting impedance data are the Nyquist plot and the Bode plot. The Nyquist plot has the log of the imaginary impedance, Z'', on the ordinate and the log of the real impedance, Z', on the abscissa. In a Bode plot, the modulus of the impedance is on the abscissa and the frequency (in Hertz) is on the ordinate. An analogous format of the Bode plot compares the phase angle to the frequency. These plot formats can provide resistance, capacitance, and overall impedance information about the system being studied.

Studies utilizing ac impedance as a detection method commonly use Nyquist and Bode plot formats. Wide frequency range spectra are used for the determination of changes in physical values based on spectra shape. These are unappealing methods for real-time studies because the frequency of the applied perturbation varies with time, constantly changing the experimental conditions. It was desired that sensing for chlorocarbons in aqueous solutions should take the form of a real-time detection method.

Real-time detection has been demonstrated with impedance techniques in a previous sensor[102] and a similar approach is used here.

For the real-time sensing of a dichloromethane-containing sample, data are obtained at a single frequency instead of a range of frequencies. The values obtained represent the magnitude of the impedance $|Z|$, where $|Z| = [(Z')^2 + (Z'')^2]^{1/2}$. Plotting |Z| vs. data point number results in a series of inverted peaks (valleys) that indicate the presence of a chlorinated hydrocarbon. It is crucial to mention that the data presented here are only an *approximate* plot of $|Z|$ vs. time. The temporal separation of the data points is not exact as a result of the averaging method employed by the ac impedance instrument used in these studies. The instrumental limitations are such that true time plots were unavailable. The software used was not specifically designed for collecting impedance data with respect to time; the time dependence in typical impedance experiments was explored with frequency variations of the applied potential perturbation. However, the data points were found to be temporally spaced close enough such that the plots do not distort the true response. For the data presented here, the time between data points differ by only a few seconds to ensure a comparable set of plots.

A steady, reproducible response of the films towards dichloromethane was desired. For optimization of the responses, a study of the effects of the variable parameters was necessary. These parameters included, but were not limited to, the resting potential of the film, the film thickness, film growth conditions, frequency of the potential oscillation, flow rate, concentration of sample, the nature and concentration of the supporting electrolyte species, and cell thickness. The large number of available

adjustable parameters makes optimization of the system tedious. Some of the parameters have been studied and the results are discussed below.

EXPERIMENTAL

Chemicals. All chemicals except as noted below were purchased from Aldrich and used as received. Sodium perchlorate was dried under vacuum with heating to remove excess water prior to use. Distilled water (340 $k\Omega cm^{-2}$) was used as is. Optima grade acetonitrile purchased from Fisher Scientific was used for polymer growth solutions. 3,4-diphenylpyrrole (3,4-DPP) had been previously synthesized in our group.[25] Purification of the 3,4-DPP monomer was accomplished via sublimation. A white solid was collected on the cold finger of the sublimation apparatus and a black tar-like material left in the bottom of the sublimation vessel. Purified 3,4-DPP was stored in darkness under argon at 0°C. If stored at room temperature or in the presence of light, the monomer turned yellow and produced poor films.

Cells and Electrodes. For the static-solution experiments, a simple one-compartment cell was used in a three-electrode set-up. A glassy carbon button electrode (3mm in diameter) was employed for these studies. An SSCE electrode was used for the reference electrode. A platinum wire was used as the auxiliary electrode.

A model CC-5 thin layer cell and cabinet were purchased from Bioanalytical Systems (BAS). The working electrode, also purchased from BAS, contained two independently addressable glassy carbon disks (3mm in diameter) embedded into a PEEK block (Figure 3.3). The disks are positioned parallel to each other in reference to the direction of solution flow. The stainless steel casing of the cell comprised the auxiliary

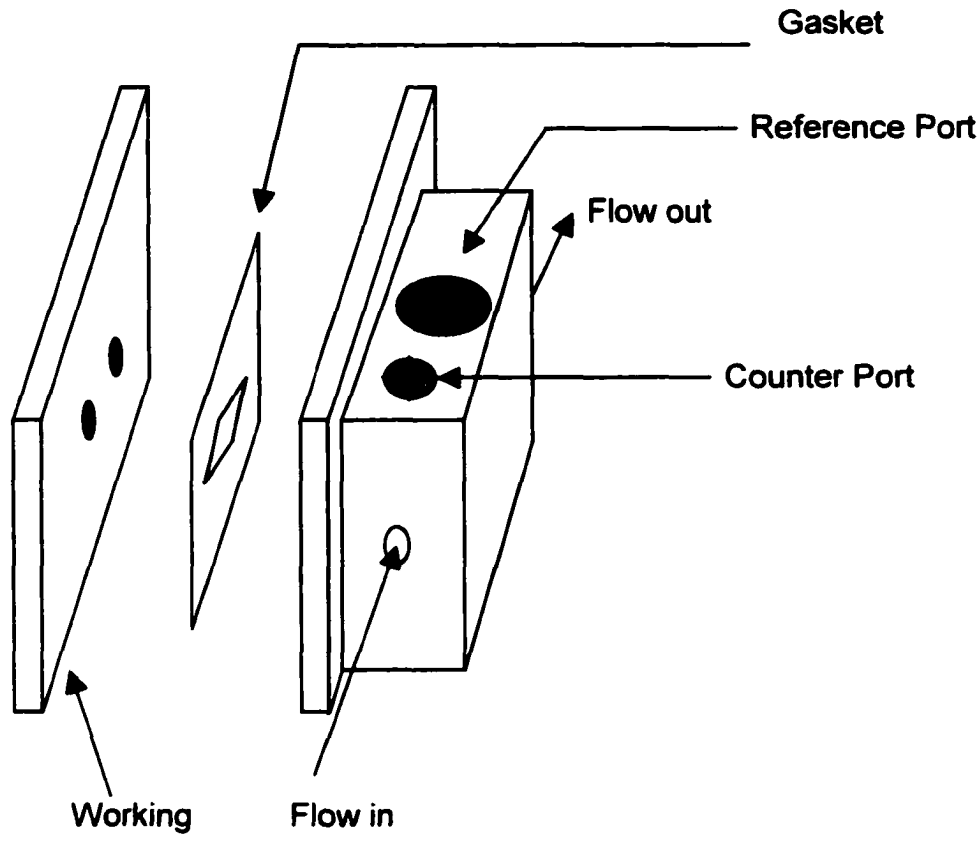

Figure 3.3. Diagram of the working electrode and cell used in the flow injection analyzer.

electrode in the BAS cell. A BAS RE-4 Ag^{+}/AgCl reference electrode was employed in the cell.

Inserting gaskets of different thickness between the working electrode and the stainless steel auxiliary electrode plate could modulate the volume of the cell. The shape of the cell compartment was determined by the gasket design as well. In these experiments the compartment had a diamond shape with a long axis of 16 mm and a short axis of 7 mm. Typically a Teflon gasket with a thickness of 50 μm was employed. This gave a cell volume of approximately 28 μL. The working electrodes were positioned in the center of the long axis of the cell gasket. The solution inlet and outlet ports located in the stainless steel casing of the cell were positioned at either end of the gasket's long axis. During use, the cell and electrodes are mounted in the CC-5 faraday case.

Sample injection was facilitated with the use of a 100 μL sample loop in conjunction with a 6-port injection valve (Rheodyne Model 7125). Sample solutions could be injected into the sample loop and released into the solution stream as desired. Flow of solution through the cell was accomplished by a gravity feed. This produced the best flow characteristics with this cell. Typical flow rates ranged from 25 to 75 μL/min.

Instrumentation. Film growth and cyclic voltammetry were performed with an EG&G Princeton Applied Research Model 173 potentiostat/galvanostat in conjunction with a Princeton Applied Research Model 179 digital coulometer. Data was recorded on a Yokagawa 3023 X-Y chart recorder. AC impedance was performed with an ACM AC Impedance Spectroanalyzer (ACM Instruments, United Kingdom). The instrument was operated with a PC computer and customized software. The operating program had been

specially modified by ACM Instruments to allow for manual control of the resting potential.

Film Growth and Solutions. Poly(3,4-diphenylpyrrole) films were grown onto the working electrodes via potentiostatic polymerization. A potential of +700 mV (vs. $Ag/AgNO_3$ (0.10 M $AgNO_3$, DMSO)) was used for all film growth. The growth solutions contained 0.10 M 3,4-DPP and 0.10 M $NaClO_4$ in acetonitrile. A J-tube was used for film growth on the working electrode employed in the dynamic solution experiments (Figure 3.4). Measuring the coulombs passed during polymerization monitored the film growth. Films were grown with the passage of 3 mC (ca. 43 mC/cm^2).

The background solution in the dynamic-solution experiments was aqueous 0.10 M $NaClO_4$. Aqueous solutions of 0.10 M $NaClO_4$ were saturated with dichloromethane by addition of the organic liquid to the aqueous electrolyte solution several days prior to use. An excess of the dichloromethane was ensured by visibly noting the presence of the two liquid phases. For quantitative detection experiments, solutions were prepared as fractional concentrations of the dichloromethane-saturated aqueous electrolyte solution. This was accomplished by diluting the concentrated solution (ca. 1 mg/ml) with additional aqueous 0.10 M $NaClO_4$ solution. These samples were prepared prior to each experiment in order to minimize a change in concentration of the organic in solution.

RESULTS AND DISCUSSION

Cyclic Voltammetry. Voltammetry of the $pDPP/ClO_4^-$ films was investigated to ensure that current responses were obtained similar to those reported by Feldheim et al.

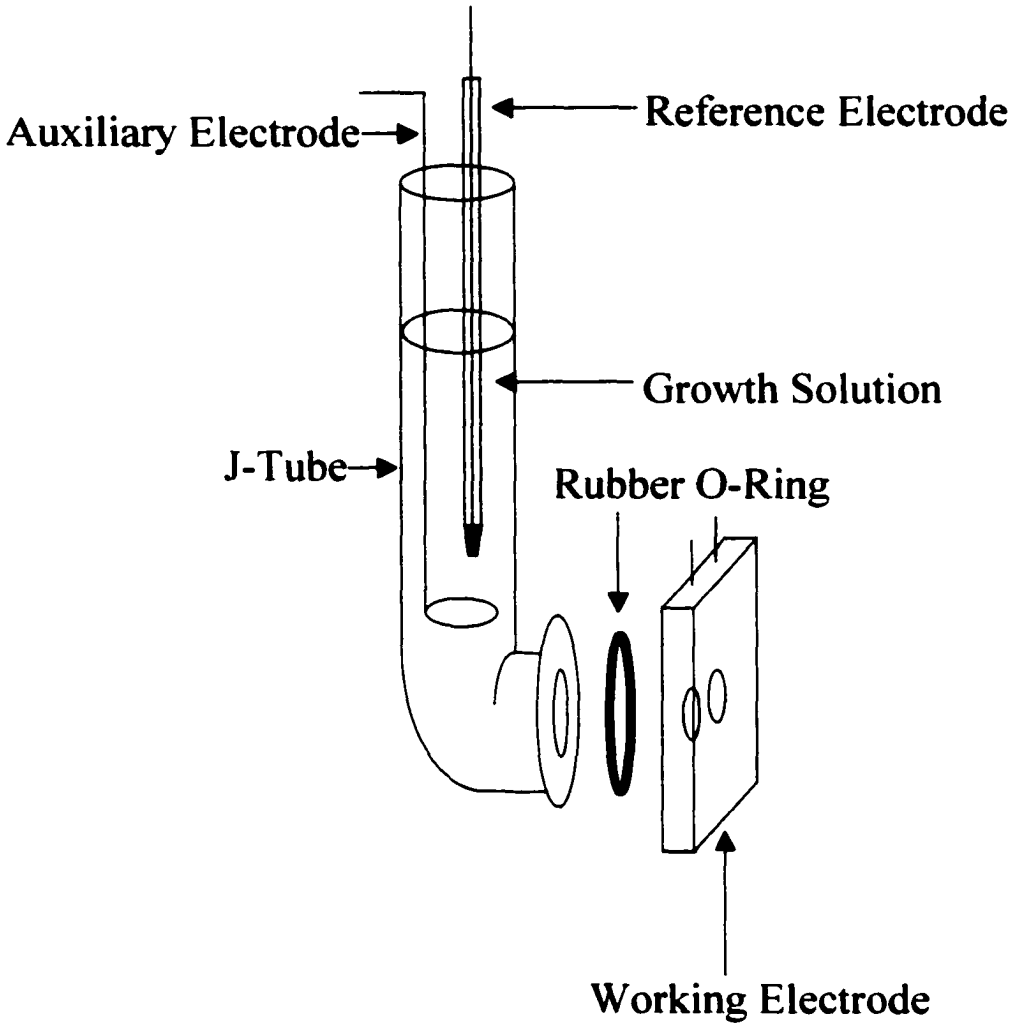

Figure 3.4. Diagram of J-tube cell used for pDPP film growth and static solution electrochemical experiments.

A film on a glassy carbon working electrode was first cycled in an aqueous 0.10 M $NaClO_4$ solution. As expected, there was no significant current response between -0.5V and +0.6 V vs. SSCE (Figure 3.5a). Dichloromethane-saturated nitrogen gas was then bubbled through the electrolyte solution while continuously cycling the film potential. The first three potential cycles produced responses that only slightly change in shape and current magnitude. However, subsequent cycles show marked increases in the current response of the film. Steady-state voltammetry (Figure 3.5b) was attained after ca. 6 minutes. At steady state, the film voltammetry had sharp, well-defined peaks. The shape of the steady-state voltammetry was identical to that reported by Feldheim et al. Purging the solution with pure nitrogen gas restored the original voltammetry (Figure 3.5a). This process of on and off switching of the films electrochemistry was entirely repeatable.

Impedance Measurements in Static Solutions. AC impedance spectra taken in static solution provided a view of the broad behavior of the films' impedance response. Potential perturbation frequency scans were performed on pDPP/ClO_4^- films from 1000 Hz to 1 Hz. The amplitude of the potential perturbation was set at 8 mV for the scans. The equilibrium resting potential of the films was +350 mV vs. SSCE. As indicated by the voltammetry in Figures 3.5a and 3.5b, this potential should provide a large difference in the impedance response by the film in the presence and absence of dichloromethane. Impedance measurements were alternately performed in either pure solutions of aqueous 0.10 M $NaClO_4$ or solutions saturated with dichloromethane.

The data from the scans were analyzed in three formats. Consider first the Nyquist plot (Figure 3.6a). The impedance response for the film in the electrolyte solution containing dichloromethane is represented in the plot by the open triangles. It is

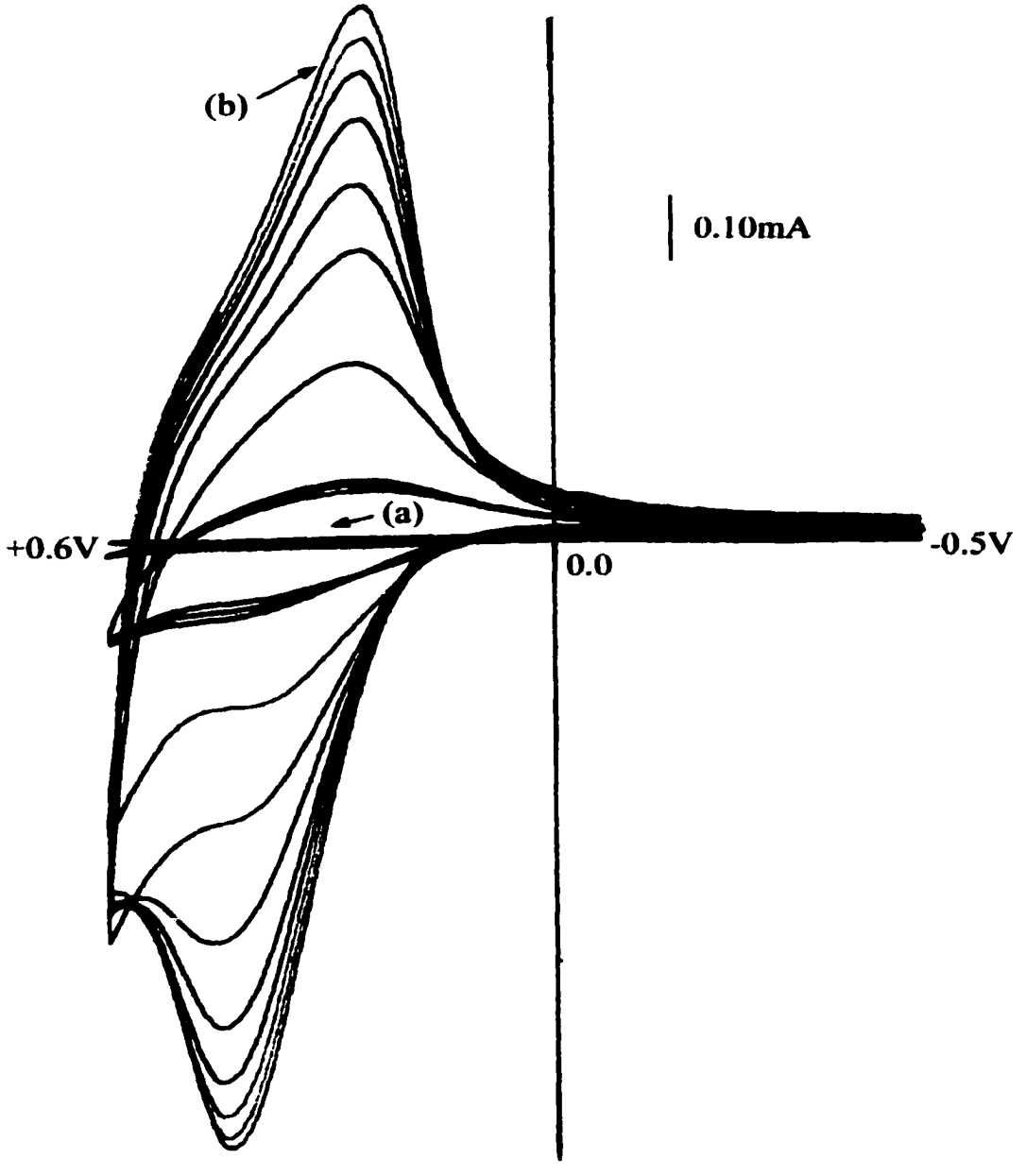

Figure 3.5. Cyclic voltammogram of pDPP/ClO_4^- film on a glassy carbon electrode in 0.10M $NaClO_{4(aq)}$ solution. The arrow (a) shows response of the film without dichloromethane (DCM) present. The largest trace (b) shows the response afterbbling N_2/DCM for several minutes. The intermediate lines show the growth of the response. The potentials shown are vs. an SSCE reference electrode.

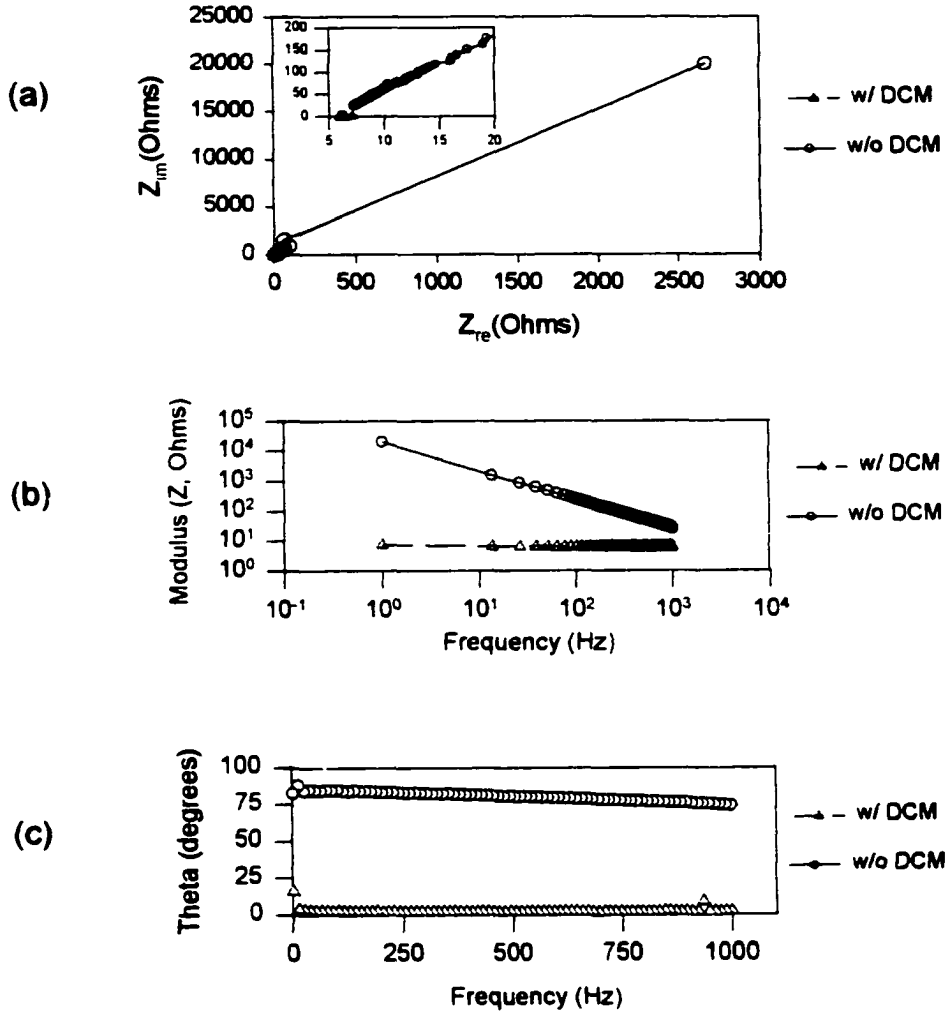

Figure 3.6. AC impedance data for a pDPP film in a static cell. The solution was 0.10M $NaClO_4$(aq); both with and without dichloromethane present. (a) Nyquist plot, (b) Bode plot, (c) Bode-θ plot. The inset in the Nyquist plot clarifies the responses at low impedance values.

evident in Figure 3.6a that there was no capacitive (Z_{im}) contribution to the impedance when dichloromethane was present. Only a resistive component (Z_{re}) was noted; having a value of ca. 6 Ω over the entire frequency scan. In contrast to this, the film response in pure aqueous electrolyte (open circles) shows significant changes in both real (resistive) and imaginary (capacitive) impedance. At all values of the applied frequency (which is only implicitly evident in Figure 3.6a), the capacitive and resistive values were greater for the film in pure aqueous solutions than for the films exposed to the dichloromethane-saturated solutions.

A second format for displaying impedance data was the Bode plot (Figure 3.6b). Here the log of the frequency was plotted against the log of the modulus of the impedance ($|Z|$). For the film in dichloromethane-saturated aqueous $NaClO_4$ solution, the modulus of the impedance remained unchanged (with a value of ca. 6 Ω) over the entire frequency spectrum. Recall that the Nyquist plot indicated that the impedance of ca. 6 Ω. The impedance measured in this case was entirely due to a resistive component: there was no significant capacitive contribution to the film impedance. The Nyquist plot demonstrated only a modest change in the real and imaginary impedance values of the film in pure aqueous electrolyte solutions. However, the modulus of the impedance in the Bode plot changed by more than three orders of magnitude in the field of the applied frequencies. The difference in the two plots in Figure 3.6b is dramatic. At the highest frequency, a 5-fold difference in the magnitude of the impedance modulus of the film is noted between the two plots. At the lowest frequency of 1 Hz, the difference in the plots was more than 10,000 Ω.

The third format used to analyze the impedance response of the films was the Bode-θ plot (Figure 3.6c). Here the frequency was plotted versus the phase angle of the response. Figure 3.6c shows a large difference in the phase angle response between the film in the pure aqueous electrolyte solution and the dichloromethane-saturated solution. For the system having dichloromethane present, the phase angle is nearly in phase (or 0°) over the entire frequency range. This indicates the film behaved as a pure resistor. This of course agrees with the data presented in Figure 3.6a and 3.6b. Without dichloromethane present, the phase angle of the response lags behind the perturbation by ca. 75° at high frequencies and increases to about 85° at the lowest frequency. This indicates a predominance of capacitive effects in the film. Recall that the impedance response by a pure resistor is in phase (0°) with the sinusoidal perturbation whereas a pure capacitor will lag behind the perturbation (out of phase) by 90°. A combination of resistive and capacitive effects will result in intermediate values of θ.

The above plots readily demonstrate the differences in the impedance characteristics of the films in aqueous solutions with and without dichloromethane present. When the film was exposed to dichloromethane, there was only a small change in the film impedance. The Nyquist and the Bode-θ plots identify the impedance to be primarily resistive; there appears to be no capacitive component influencing the impedance in this frequency range. Thus, it should not be surprising that the current responds rapidly to the applied potential perturbation. As discussed earlier, the presence of the dichloromethane allows for the facile redox switching of the film along with the simultaneous ion transport. The value of the resistive component was small and likely corresponds to solution resistance in the cell and intrinsic film resistance.

In the pure aqueous $NaClO_4$ solutions, the contribution to the impedance value was a combination of a resistive component and a large capacitive component. The inability of the film's oxidation state to change with the potential perturbation due to blocked ion transport yields a capacitor-like structure at the working electrode. Ion migration can occur to and from the polymer/solution interface, but no significant faradaic process results. Thus, the impedance plots in Figure 3.6 show the dominance of a capacitive component in the system. The sensing capabilities of these films are based primarily on the changes in capacitive behavior.

Other resting potentials were investigated to see if the difference in the impedance response of the film could be further improved from that shown in Figure 3.6. For resting potentials ranging from +400 mV to +600 mV, the impedance responses were similar to those noted in the above examples. However, the magnitude of the impedance modulus for some of the compared spectra (i.e., with or without dichloromethane) increased over the entire frequency spectrum and slight variations in the impedance *difference* were noted in some of the films (Figure 3.7). These changes in the impedance responses shown by the Bode plots seemed to be primarily due to variations in the impedance response of the films in pure aqueous electrolyte solutions. As seen in Figure 3.6, capacitance influences dominate the impedance response of the films when dichloromethane was absent from the solutions. Changes in capacitance values from one film to the next likely exist. Sources of the additional capacitance could be physical variations in the polymer films.

A negative rest potential was employed to see how the impedance characteristics respond to the potential perturbation. From the cyclic voltammogram in Figure 3.5 it is

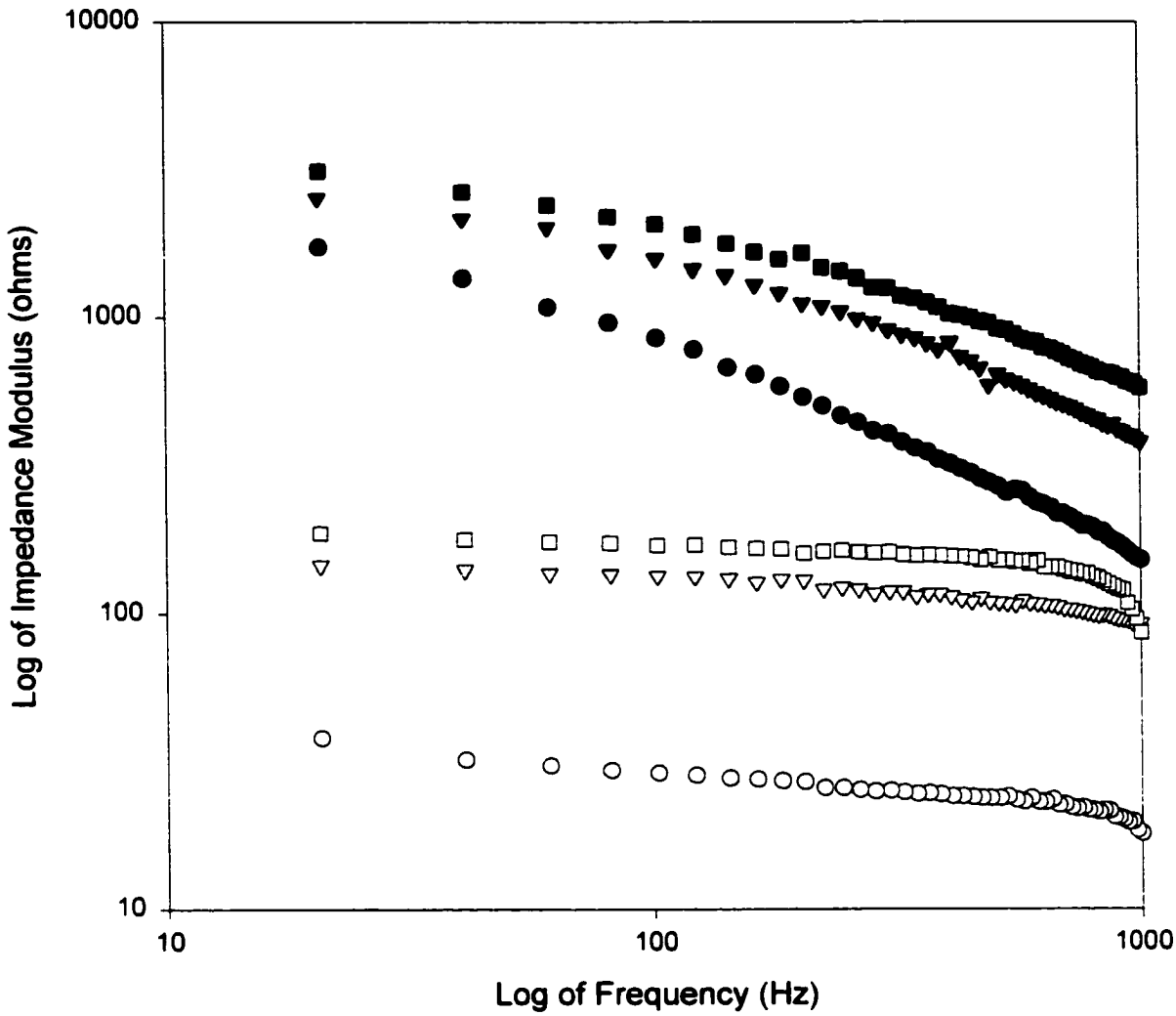

Figure 3.7. Sets of impedance spectra for a pDPP film equilibrated to various positive potentials. The spectra were taken in solutions of 0.10M $NaClO_4$(aq) both with (open data points) and without (filled data points) dichloromethane. The rest potentials used were +400mV (triangle), +500mV (squares), and +600mV (circles).

evident that no current passed at –200 mV, regardless of the solution composition. Using a pDPP/ClO_4^- film equilibrated to –200 mV, an 8 mV potential perturbation was applied over a frequency range from 100 Hz to 1 Hz. This was performed in aqueous electrolyte solutions with and without dichloromethane. It should not be surprising that the plots show only a small difference in magnitude between runs in pure aqueous $NaClO_4$ solution and in dichloromethane-saturated solution. At –200 mV, the film is insulating and no faradaic process should occur at the film. Both situations produced plots having large capacitive components.

In Figure 3.8 we see that all six spectra have large values of impedance modulus (500-1000 Ω) over the entire frequency range. For the spectra of the film in dichloromethane-saturated solution, impedance values are slightly larger than those values measured for the film in pure aqueous $NaClO_4$ solution. This trend is opposite of that for film impedance spectra taken at positive rest potentials (see Figure 3.7). At a rest potential of –200 mV, the potential perturbation of 8 mV could not significantly change the electronic properties of the films; the polymer thus remained in an insulating state and no faradaic processes occurred. The film impedance was comprised of large capacitive and resistive components regardless of the composition of the electrolyte solution. The larger impedance values for the open-circle plots in Figure 3.8 are predominantly due to increased solution resistance when dichloromethane was present. As a result, there was additional impedance contribution for those spectra.

It is easy to see from the Bode plot in Figure 3.6b that the large difference in the impedance modulus could be used to sense for dichloromethane. By holding the potential perturbation at a low frequency, a large change in the impedance modulus

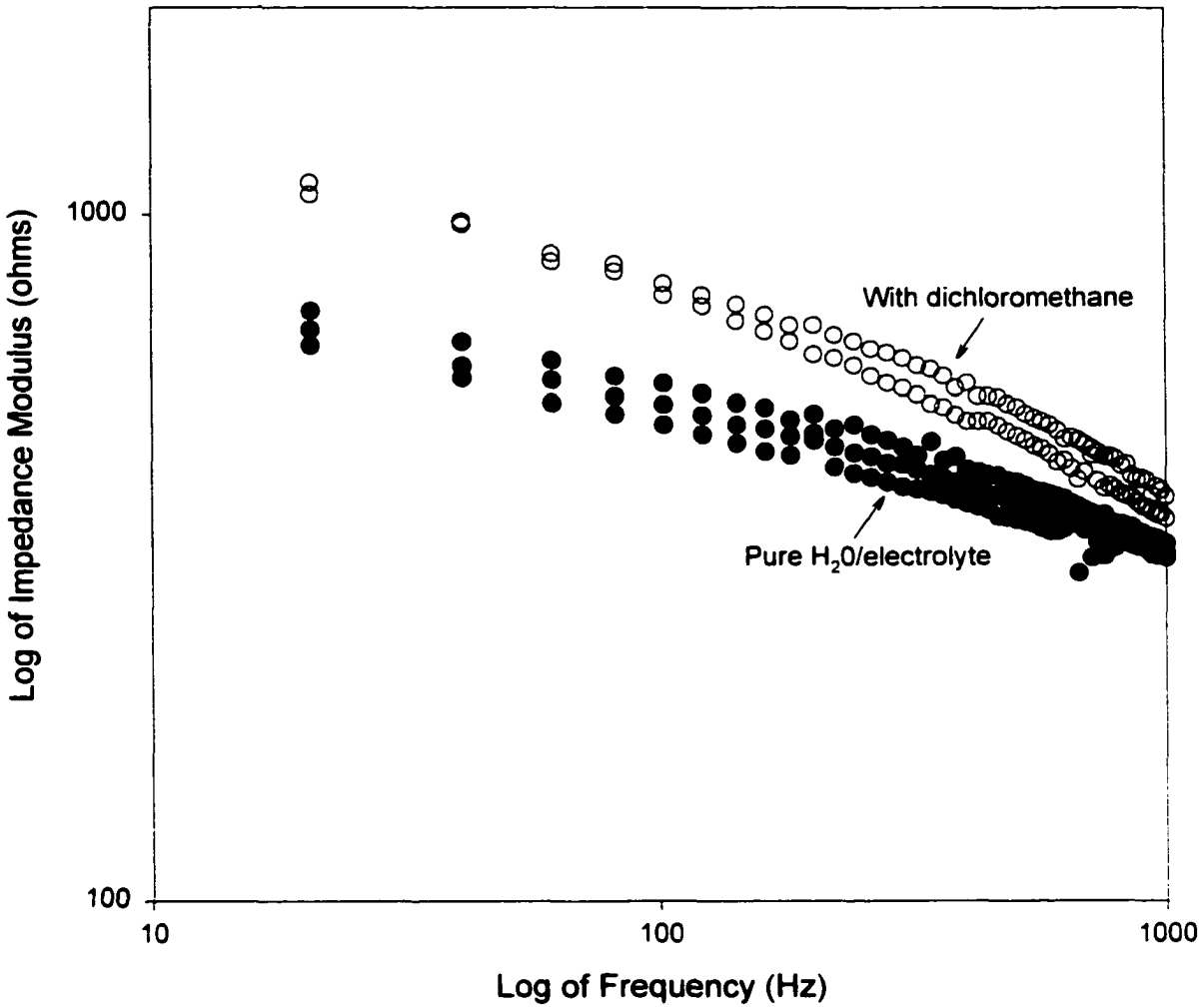

Figure 3.8. Bode plot showing spectra of pDPP films equilibrated at –200 mV. The open circle spectra are for films in electrolyte solution containing dichloromethane and the filled circle spectra were taken in pure aqueous 0.10 M $NaClO_4$ solutions.

would occur with introduction or loss of dichloromethane from solution. For these experiments, a frequency of 100 Hz was chosen. There were two factors influencing this choice. First, the particular frequency gave a large impedance difference between the spectra in Figure 3.6b. Secondly, in using this frequency, a significant number of measurements could be taken on a reasonable time scale for the detection of a sample in the dynamic-solution experiments. With necessary data averaging to minimized noise, a frequency of 100 Hz for our instrumentation produces approximately one data point every 12 seconds. A lower frequency would give a larger signal response based on the data in Figure 3.6b, but the time needed to collect enough data per run would also increase. In order to get enough data points to identify the sample, extremely slow flow rates would be necessary. Slower flow rates would allow for increased diffusion of the sample plug in the flow system and a decrease in the resolution of the signal.

Background Impedance Response in Flow Cell. Figure 3.9 shows a plot of the average background impedance modulus of a bare glassy carbon electrode used in the flow injection analyzer. The background solution of aqueous 0.10 M $NaClO_4$ had a flow rate of 64 μL/min. The electrode was held at +400 mV vs. SCE while an 8 mV potential perturbation was applied at a frequency of 100 Hz. A 100 μL sample of aqueous 0.10 M $NaClO_4$ saturated with dichloromethane was injected into the flow stream at data point 30. Multiple runs were performed taking 80 data points for each run. Based on the increased impedance noted in the open-circle plots in Figure 3.8, it was expected that there would be an increase in the impedance measured at the bare glassy carbon electrode as the injected sample passed by the working electrode. Here too the increase in impedance modulus would be due to an increase in the solution resistance of the cell.

All impedance plots collected in the background experiments showed noisy responses despite the use of the internal data averaging by the impedance instrument. The data from five runs were averaged in Figure 3.9 to see if a single response peak could be identified. A peak can be noted at ca. data point 40. However, given the small magnitude of this response and the large error bars, any change in the cell impedance of the solution due to the presence of ca. 1 mg/ml of dichloromethane in the aqueous carrier solution is negligible. The source of the noise in the background impedance measurements has not been identified or further improved beyond that shown in Figure 3.9.

Impedance Spectra of 3,4-DPP Films in Flow Cell. Similar to the experiments with the static cell, impedance spectra were obtained for the 3,4-DPP films in the flow cell over a frequency range of 1000 Hz to 1 Hz. The films were set at rest potentials identical to those used in the static-solution experiments. The spectra were taken in flowing solutions (ca. 60 μL/min) of either pure aqueous 0.10 M $NaClO_4$ or aqueous 0.10 M $NaClO_4$ saturated with dichloromethane. For films at a rest potential of –200 mV, identical impedance behavior was noted as Figure 3.10. The film impedance was slightly larger when dichloromethane was present as a result of additional solution resistance, but the plots nearly overlap.

With films equilibrated to positive rest potentials, the spectra in Figure 3.11 show larger impedance difference between runs taken with and without dichloromethane in the flow solution. As in the analogous static-solution experiments, the spectra for films in pure aqueous $NaClO_4$ solutions have larger impedance values over the frequency range than for solutions saturated with dichloromethane. The plots in Figure 3.11 have an order

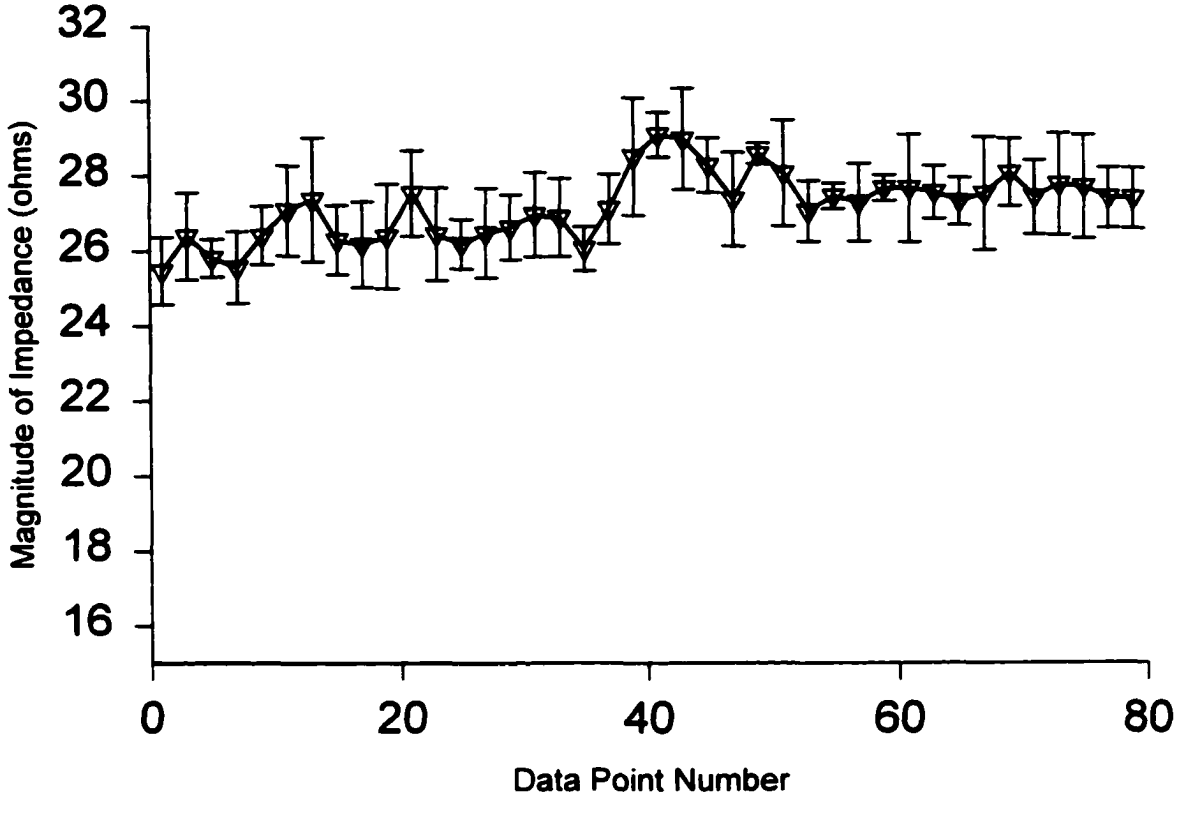

Figure 3.9. Plot of average background impedance modulus of bare glassy carbon electrode in flow injection analyzer. Background solution was 0.10M $NaClO_4$(aq). A 100μL sample saturated with dichloromethane was injected at data point number 30 for each run. The calculated standard error is shown for each data point.

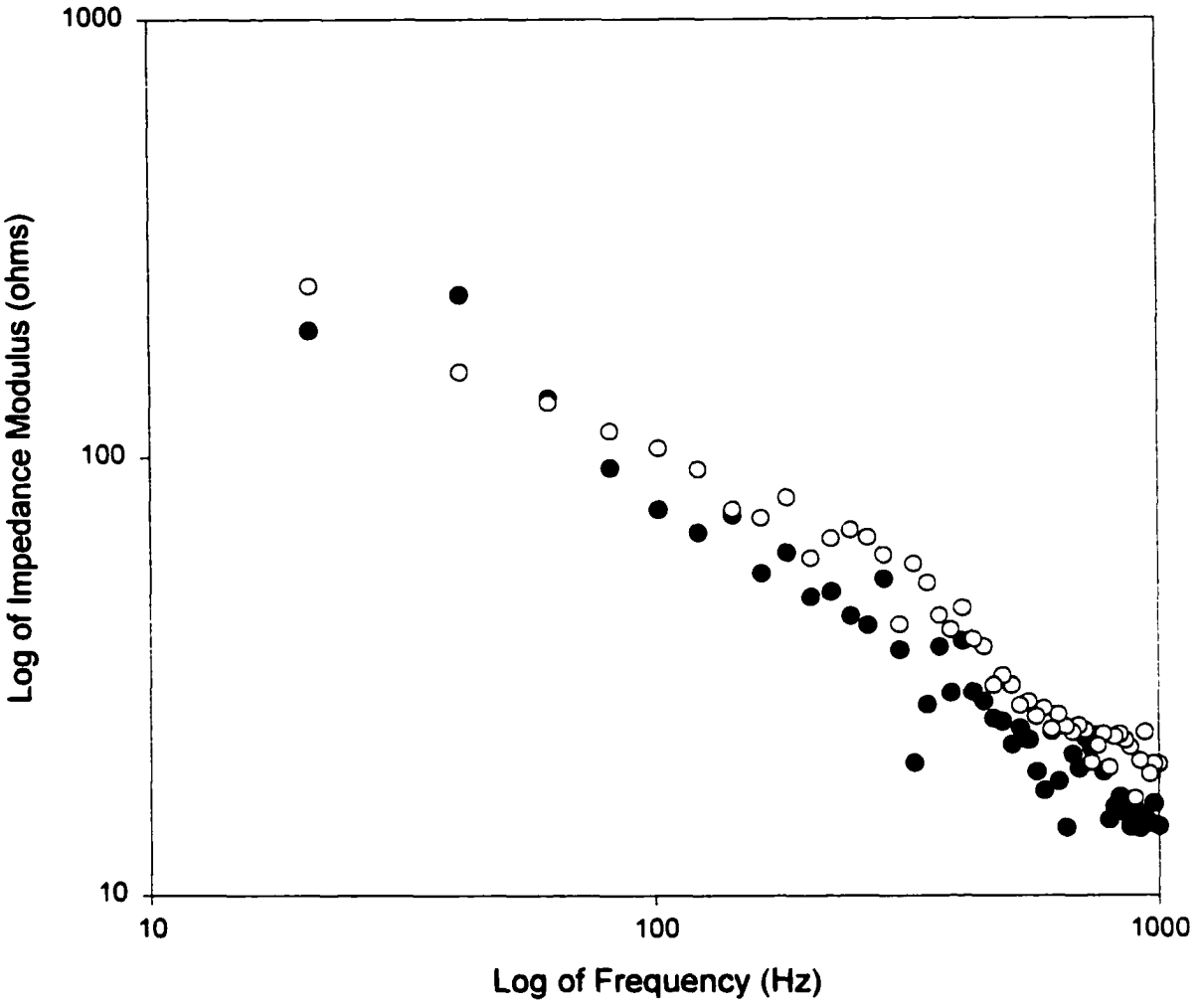

Figure 3.10. Bode plot showing spectra of pDPP films on glassy carbon electrodes in the flow cell. The spectra were taken in aqueous 0.10M $NaClO_4$ solutions saturated with dichloromethane (open circles) and without dichloromethane (filled circles). The rest potential of the films was –200mV. The flow rate was ca. 0.08 ml/min.

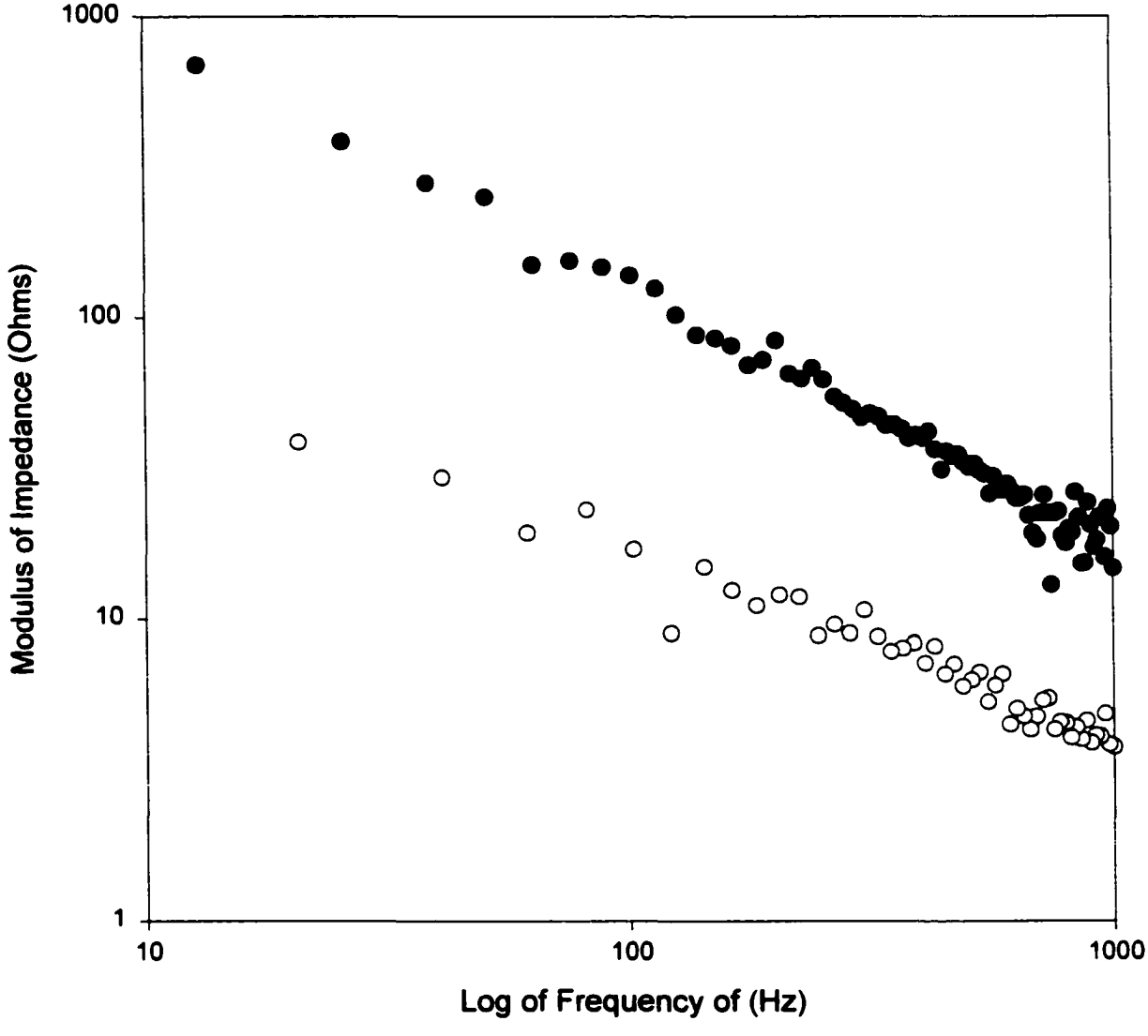

Figure 3.11. Bode plot showing spectra of pDPP film on a glassy carbon electrode in the flow cell. The spectra were taken in aqueous 0.10M $NaClO_4$ solutions saturated with dichloromethane (open circles) and without dichloromethane (filled circles). The rest potential of the films was +400mV. The flow rate was ca. 0.08ml/min.

of magnitude difference at the lowest frequency while having a 5-fold difference at the highest frequency. These differences were slightly smaller than those in the static cell runs. At 100 Hz, the static-solution experiments gave a 1.3 *order of magnitude* difference between the impedance spectra taken with and without dichloromethane present. With flowing solutions, the change was 0.96 order of magnitude. The source of the decreased impedance difference is unknown.

Further examination of the Bode plots revealed a greater amount of noise in the flow-solution data than the static-solution data. Unfortunately, the noise could not be improved beyond that noted in the above figures. The increase noise may be due to physical changes in the film resulting from mechanical influences by the flowing solution.

Single Frequency Detection of Dichloromethane in a Flow Cell. When monitoring the impedance modulus at a single frequency, the impedance response to a dichloromethane-saturated sample appears as a drop in the value of the background impedance (Figure 3.12). From film to film, a wide range of background impedance values was measured. Typically, values were between 200 and 300 ohms, but values as high as 25 kΩ have been recorded. The range of background impedances was a bit surprising as the films were identically grown and identical experimental conditions employed. Fortunately, the relative change in the impedance given by a signal response was more consistent from film to film. This relative signal response to a dichloromethane-saturated aqueous $NaClO_4$ solution was typically a change of 0.8 to 1.0 orders of magnitude with respect to the value of the background impedance. This allowed ready identification of the signal response.

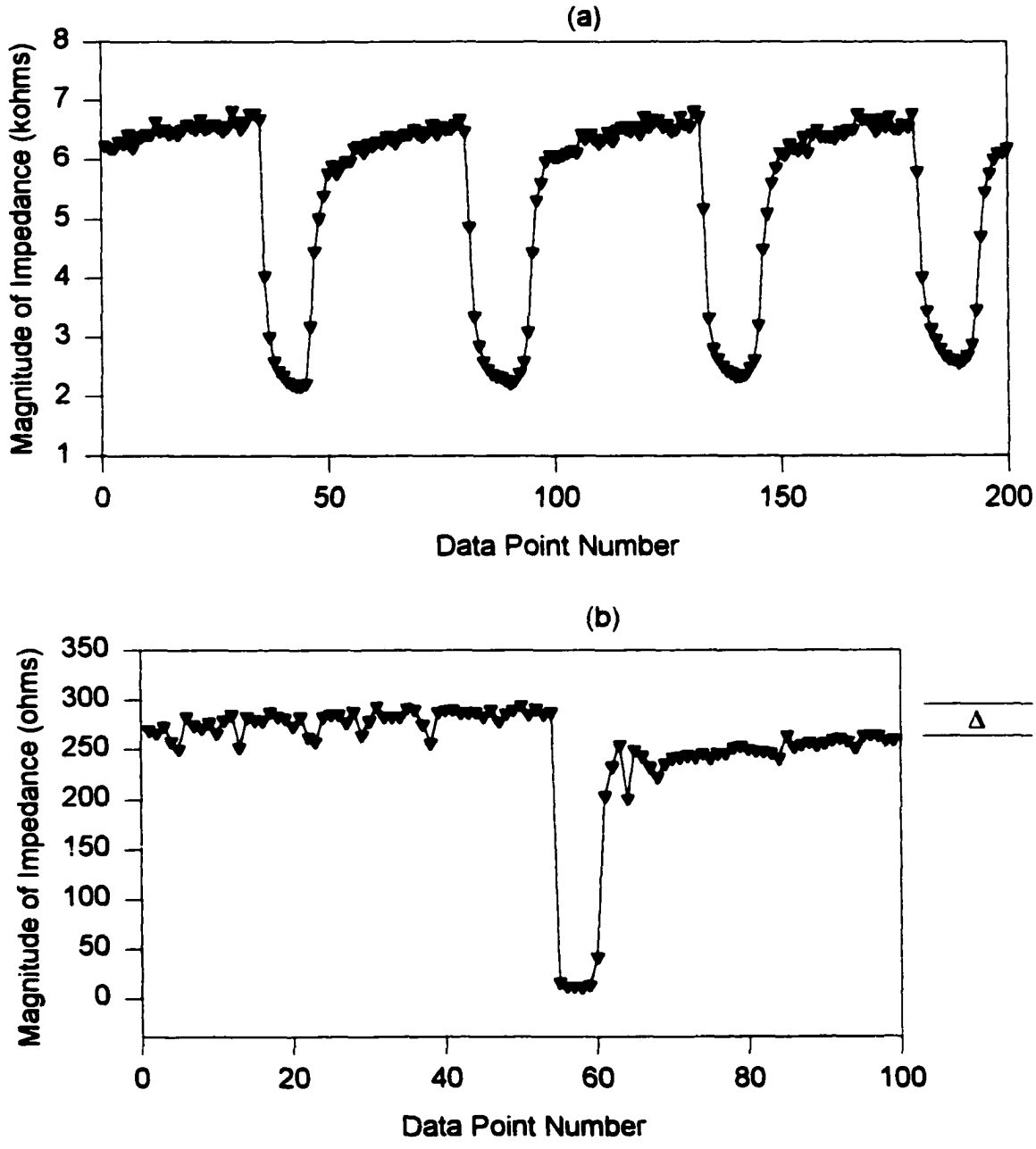

Figure 3.12. Impedance response of pDPP films in the flow cell to injections of 0.10M $NaClO_4$(aq) samples saturated with dichloromethane. The decrease in the magnitude of the film impedance signals the presence of the dichloromethane. The background carrier solution was 0.10M $NaClO_4$(aq). The reproducibility of the signal is demonstrated in (a). A change in the baseline impedance, Δ, after sample detection is noted in (b). The frequency of the 8mV potential perturbation was 100Hz in both plots shown.

The signal responses upon repeated injection of dichloromethane-containing samples were well defined and repeatable. Some initial decay in the peak magnitude was noted (see Figure 3.12a) but after a few injections of the dichloromethane samples, the response stabilized. Any decay in the peak response was typically only a small percentage of the overall relative signal.

The background impedance was seen to change in some of the films after passage of the dichloromethane-saturated sample. The background impedance has been noted to both increase and decrease from its original value. However, the change was usually rather small with respect to the magnitude of the initial background impedance. This change was likely due to structural changes in the film caused by repeated swelling and shrinking of the polymer. Although the change was typically less than ca. 20% of the original background impedance, this made the total signal response less repeatable for successive sample measurements. Many of the films did, however, demonstrate little change in the background impedance value or the magnitude of the signal response over hours of film use with numerous injections.

In order to optimize the detection of dichloromethane by the films, parameters such as flow rate and cell thickness were varied. Both the cell volume and the flow rate were independently varied to see if changes occurred in the magnitude of the signal or in the background noise.

Flow rates were varied from 0.076 ml/min to 0.023 ml/min. The only notable effect was a broadening of the signal response at lower flow rates. That is, the minimum impedance reached by the signal did not change, but was only maintained longer before

returning to the background value. This was simply a result of a longer exposure time of the film to the dichloromethane in a sample.

Adjusting the cell volume was accomplished by changing the gasket thickness between the working electrode and the cell body. Adding or removing gaskets could produce a range of thickness between 50 and 640 μm. Correspondingly, the cell volume could range between ~28 μL to ~360 μL. Changing in cell volume in these experiments did not produce any notable differences in the signal response of the films to dichloromethane-saturated samples.

Quantitative Impedance Detection of Dichloromethane in Aqueous Solutions. Film impedance responses to different dilutions of dichloromethane-saturated aqueous $NaClO_4$ solutions were examined in both static- and dynamic-solution systems. The static-solution experiments were performed with films grown onto the glassy carbon working electrode used in the flow cell. The cell employed for these static-solution experiments was identical to that shown in Figure 3.4. The resting potential of the films was +400 mV vs. SSCE and a potential perturbation of 8 mV was applied at a frequency of 100 Hz. Each data set was made up of ca. 100 data points. This corresponded to a run time of ca. 20 minutes. Impedance measurements were made in a range of relative concentrations of dichloromethane. The film impedance in each solution was measured and the response plotted against the percent concentration of dichloromethane relative to a saturated solution. A number of these runs can be seen in Figure 3.13. These values were then normalized against impedance value of the film in pure aqueous electrolyte and the corresponding data averaged together. The resulting plot is shown in Figure 3.14. The plot showed that there was no significant impedance change in the film with

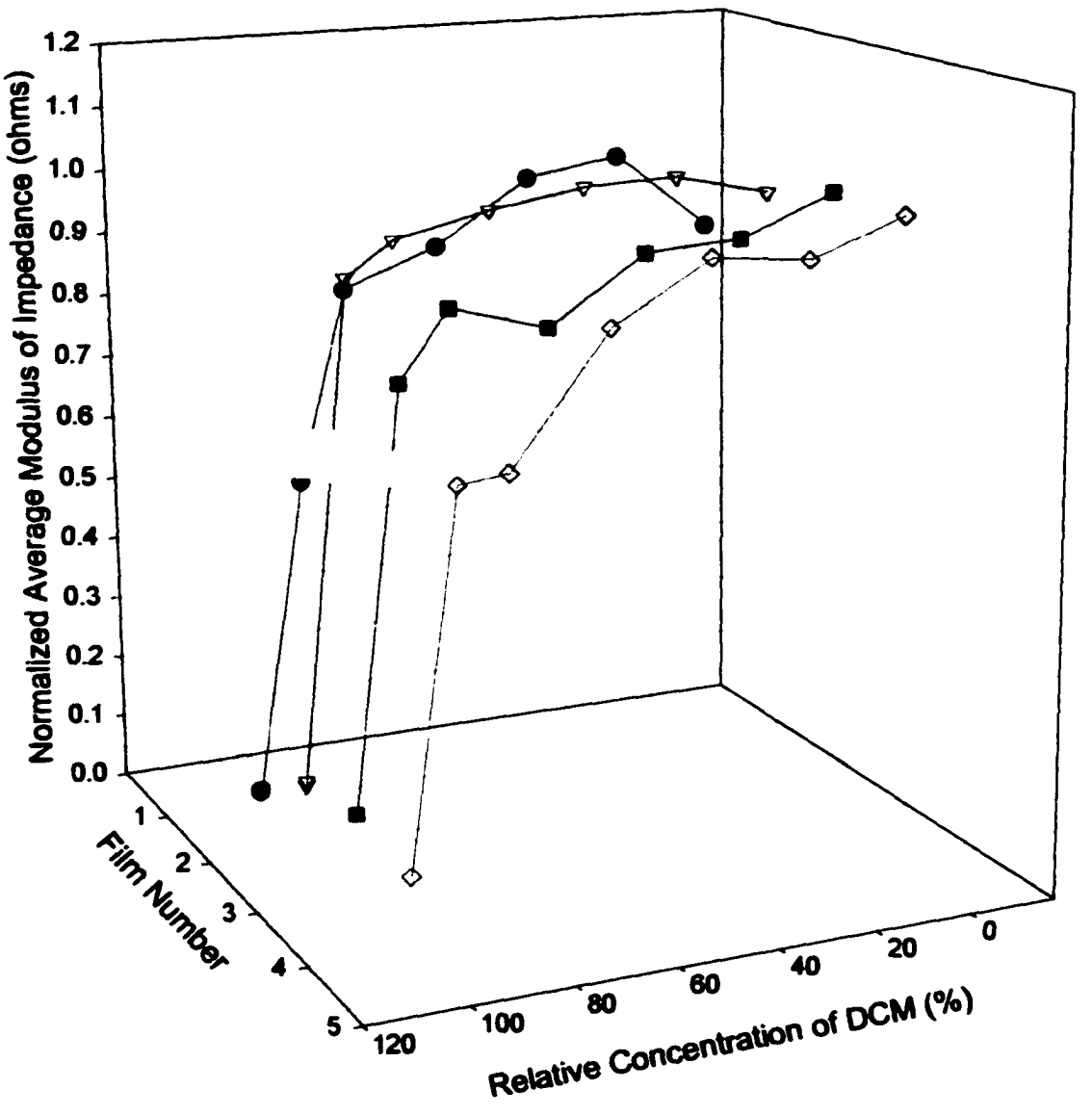

Figure 3.13. The above shows plots for the impedance response of pDPP films on glassy carbon electrodes to various relative concentrations of dichloromethane in 0.10M $NaClO_4$ solution. The data was taken in a static solution environment.

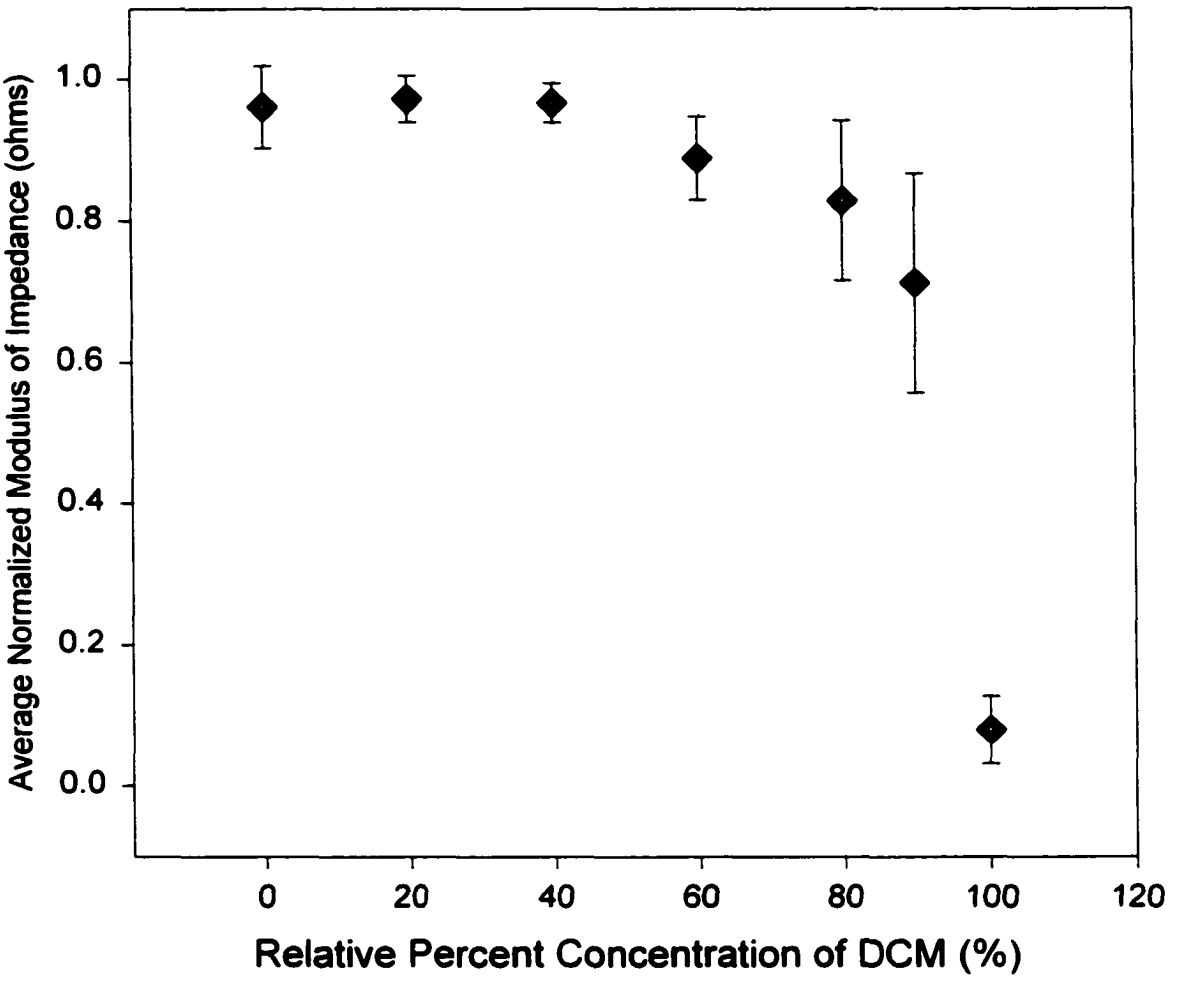

Figure 3.14. The average normalized data from Figure 3.13 is shown. A dramatic increase in the impedance response in the static system is noted past ca. 60% relative concentration of dichloromethane. Error bars are shown for the average normalized data.

solutions containing less than ca. 60% saturated concentration of dichloromethane. Only at 60%, is the impedance of the film affected by the presence of the dichloromethane.

Quantitative detection of dichloromethane in the flow cell was performed by measuring the change in the background impedance of the film due to the passage of an aqueous sample containing dichloromethane. The samples were diluted to various fractional concentrations of the dichloromethane-saturated solution as done in the above static-solution experiments. Samples were prepared fresh for each run and were 100 μL as determined by the sample injection loop. Different relative concentrations were injected in random order and multiple injections of each concentration were used with each film. The magnitude of an impedance response was measured from the impedance background value to the peak of the signal. Normalization of the response values was done by assigning a value of one to the signal response for the dichloromethane-saturated sample. Figure 3.15 shows the average normalized response of the films to the various sample concentrations. The plot shows basically an on/off behavior of the film impedance. There was no significant impedance change up to a relative concentration of 40%; and above 80%, the impedance signal was essentially unity.

Unfortunately, in regards to sensing of dichloromethane, both static and dynamic methods did not yield any sign of sensing the chlorinated hydrocarbon below 50% of the dichloromethane-saturated aqueous solution. This corresponds to a detection limit of ca. 500 ppm. This limit is about two orders of magnitude less sensitive than the purge-trap/GC method used by the EPA.[103]

Instead of responding in a manner which would allow for the quantitative determination of the chlorinated hydrocarbons, the polymer demonstrated an interesting

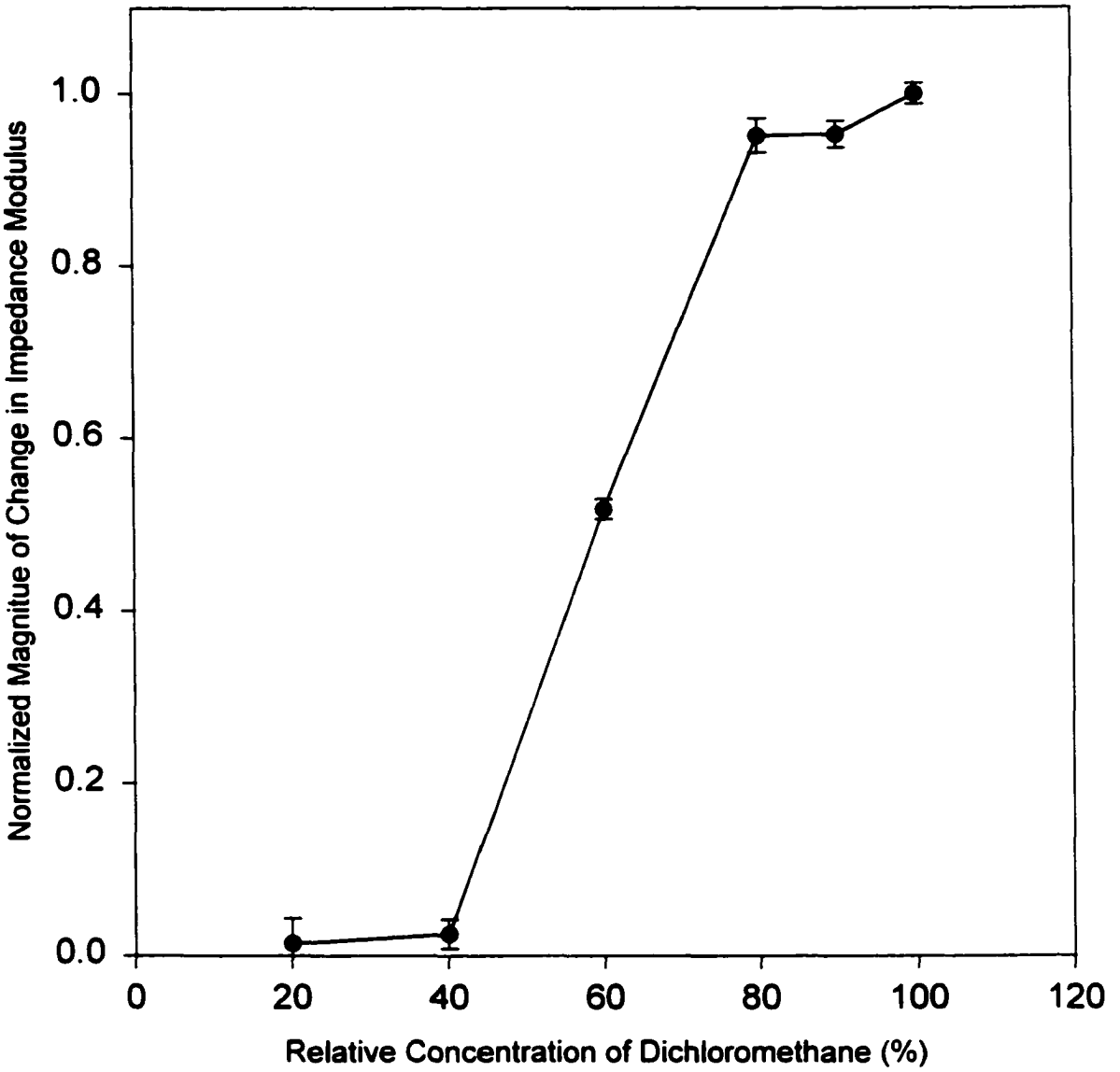

Figure 3.15. The above plot shows the quantitative detection of the saturated dichloromethane samples in the flow cell using pDPP films on glassy carbon electrodes. The data shows a large increase in the change in impedance signal beyond ca. 50% relative concentration of dichloromethane. Error bars are shown.

"on/off" impedance behavior towards dichloromethane concentration. This was clearly shown in Figure 3.15. For dichloromethane concentrations less than ca. 500 ppm (i.e., 50% relative concentration) there was little change in the film impedance; that is, the actual film impedance remained large and highly capacitive in nature. At dichloromethane concentrations greater than ca. 500 ppm the film impedance change increases dramatically and the measured change is near unity at dichloromethane concentrations above ca. 70%. Only a narrow range of dichloromethane concentrations (between 50% and 70%) produced impedance changes between ca. 0 and 1 (see Figure 3.15).

A detection limit of ca. 500 ppm was also noted in the static solution systems. However, the impedance of the films does not show such a dramatic change for solutions having dichloromethane concentrations greater than ca. 500 ppm as noted in Figure 3.15. Instead the impedance decreased more gradually with increasing dichloromethane concentration. The source of this difference in the response between the flow cell method and the static solution method is unknown at this time.

In either case, it is likely that the dichloromethane still enters the polymer from solutions less than 500 ppm of the chlorinated hydrocarbon, given the polar nature of the aqueous solution environment and the hydrophobic nature of the polymer. However, the fact that we see very little impedance change in the film until a relatively large concentration of dichloromethane is in solution suggests that there is a minimal degree of swelling of the polymer that must occur before facile ion transport may take place and the capacitive nature of the polymer breaks down. Until that degree of swelling occurs, the film impedance remains large. At or above the concentration of dichloromethane needed

to swell the film sufficiently (ca. 500 ppm for these films), the ion transport turns "on" and the impedance drops dramatically. Greater concentrations of dichloromethane do not further decrease the film impedance. The capacitive component has already been eliminated and only a small resistive component remains.

CONCLUSIONS

The direct sensing ability of poly(3,4-DPP) films for dichloromethane in aqueous solutions was found to be limited. For dichloromethane-saturated samples (ca. 1 mg/ml), the impedance response was large and repeatable. However, the response of the films was highly non-linear with concentration and effectively absent for dichloromethane below about 500 ppm in the aqueous solutions. Above or below this concentration there was little quantitative difference in the impedance responses. Essentially, the film behaves as an "on/off" detector for dichloromethane in aqueous solutions. This "on/off" behavior, however, gives some insight into the nature of the swelling/ion transport relationship in these films.

The use of the ac impedance approach was found to be quite successful in overcoming the charge trapping that led to the decay of sensing capability of the pDPP films in a previous report.[44] By inducing small potential perturbations about a set redox state, the sensing capabilities of the films for the dichloromethane-saturated samples were found to be repeatable and stable with time. Also, the impedance data for the films gave additional insight into the mechanism by which the film senses the chlorocarbon in the aqueous systems. Swelling of the film results in a more facile exchange of counterions, which permit the rapid change in the redox state of the films. Only small resistive effects

are noted for the oxidized films. Without the presence of the chlorocarbon, the film behaved like a capacitor, suggesting restricted motion of counter ions in the film and inability of the film to electrochemically respond to the applied potential perturbations.

CHAPTER 4

Vapor-Phase Sensing by Poly(3,4-Diphenylpyrrole) Films For Various Organic Vapors

INTRODUCTION

The use of organic conducting polymers as transducer materials in sensors has been widely reported and is finding applications in both solution and vapor sensing.[12,44,104-106] The previous chapter discussed the use of an organic conducting polymer film, poly(3,4-diphenylpyrrole) (pDPP), for sensing dichloromethane in an aqueous system. The polymer had previously shown unique interaction with dichloromethane and other small, chlorinated hydrocarbons.[44,107] In the process of investigating the ability of pDPP films to sense dichloromethane in the liquid phase, it was noted that no work has been published with regards to pDPP films used as a sensing material for gases. Because of the unique selectivity noted by pDPP for small, chlorinated hydrocarbons in the liquid phase,[44] it was believed similar selectivity might be noted for the interaction between the polymer film and chlorinated hydrocarbon vapors. This chapter will present preliminary data demonstrating the vapor sensing

capabilities of pDPP films on interdigitated array electrodes by monitoring changes in film resistance.

BACKGROUND

Sensing devices employing organic conducting polymer films, e.g., poly(pyrrole), poly(aniline), and poly(thiophene), are typically based on monitoring changes in the films' electronic properties upon interaction with the analyte vapor molecules. This includes signals produced by changes in a film's work function,[50,90] impedance,[102,106] or resistance[88,108,109]; the latter of these being more common.

Resistance changes of conducting polymer films due to exposure to organic vapors has been well documented in recent literature.[2,89,110] For monitoring the film resitance, the film must span between two leads separated by an insulating gap. This has been accomplished in similar sensing studies by using various electrode designs.[2,12,89,110-112] A suitable configuration, which is employed in these studies, is the interdigitated array (IDA) electrode (see Figure 4.1). Here, the "fingers" of the two combs of conducting material are interspaced and each comb is independently electrically addressable.

Figure 4.1. An Interdigitated Array

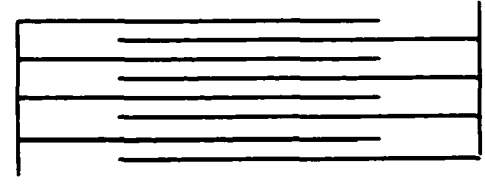

A polymer can be grown on the electrode surface such that the film bridges the insulating material and provides electrical contact between the two combs. In this way

one can measure the resistance of the film directly with an ohmmeter or by monitoring current between the finger sets at a given potential.

The process by which the analyte vapors affect the change in the electronic properties of the films is generally accepted as being a result of a degree of electron transfer between the polymer backbone and the analyte molecules.[111] The conductivity of the polymer is modulated by the formation of a weak charge-transfer complex between the polymer and the absorbed analyte molecules. This then, affects the concentration of dopant sites on the polymer backbone (i.e., polarons and bipolarons). Changing the doping level of the polymer will result in an increase or decrease in the electron mobility in the films, and thus change the film conductivity. Physical changes, induced by the absorption of the analyte molecules, also contribute to the change in the film resistance. Swelling of the polymer can increase resistance by effectively increasing the electron hopping distance between polymer strands. Repeated swelling and shrinking of the polymers can result in cracking and loss of adhesion to an electrode surface. The exact manner in which a particular analyte will affect the conductivity of a polymer film is difficult to predict. It appears from several reports that it is a balance between several properties of the film and the target analyte.[111,113] These properties can include the oxidation state of the polymer, the dielectric constant of the analyte, the incorporated dopant anion, and the dryness of the film, to name a few.

One of the attractive features of conducting polymer materials is their ease of modification in ways that potentially can affect their sensing characteristics. These include, but are not limited to, modifying the monomer (e.g., addition of substituents), changing the growth solution electrolyte, changing the solvent, and changing the method

employed for film growth (i.e., chemical or electrochemical). To give an example, Josowicz reported that changing the solvent from which a poly(pyrrole) film was polymerized from acetonitrile to methanol, enhanced the sensitivity of the film to methanol vapor.[111] Bartlett et al. demonstrated the effect of a substituent upon a polymer's film sensing properties.[108] There, significant differences in the conductivity changes and response times of poly(pyrrole) and poly(N-methylpyrole) films toward identical analyte vapors were noted. Freund and Lewis show in another example, that addition of various plasticizers to poly(pyrrole) films produced different resistance changes in the films.[112] By appropriate modifications of the polymer and its growth conditions, desired properties could be imparted, thus improving sensitivity and selectivity toward an analyte vapor.

Much of the reported work involving organic conducting polymers as vapor sensors describe stand-alone sensing devices. These involve the use of a single film for detection purposes. Unfortunately, these sensors lack a high degree of selectivity needed to differentiate a large range of vapors or gases. However, forming large sensor arrays has circumvented this shortcoming. Here, multiple sensor components having slightly different response characteristics towards a particular analyte vapor simultaneously produce individual responses. Through the use of complex pattern recognition systems, the combined response can readily differentiate a large number of analyte vapors from each other. Sotzing et al. have demonstrated an excellent example of such a device. The array was composed of poly(3,4-ethylenedioxy)thiophene-poly(styrenesulfonate) polymers combined with a range of chemically different insulating polymers.[88] By comparison of the combined resistance changes in the individual sensors of the array, a

large number of solvent vapors were readily identified. Other array-type sensors utilized conducting polymer films containing various plasticizers or dopant anions.[87,112] An example of the latter has been used for the analysis of the head space of beer.[87]

Investigation of the sensing properties of poly(3,4-diphenylpyrrole) (pDPP) films will hopefully contribute to the range of response characteristics exhibited by conducting polymers and give insight to the structure-response characteristics of this polymer as there is no reported work in this area using pDPP.

EXPERIMENTAL

Chemicals. All solvents were purchased from Fisher, Scientific and used as received. All salts were purchased from Aldrich and used as received. 3,4-DPP was previously synthesized in our group[25] and purification was described in Chapter 3, Part 1 of this text.

Cells and Electrodes. Single-compartment glass cells were used for film growth, film voltammetry, and as vapor chambers. The IDA working electrodes were purchased from Abtech Scientific, Inc (Richmond, VA). The electrodes consisted of platinum patterned on a glass substrate. A variety of arrangements were obtained which have different gap width between fingers, different finger lengths, and a different number of fingers composing the array. The finger height (as measured from the glass substrate) for all the IDAs was reported to be 0.10 μm. The gap distance between fingers varied from 5 μm to 15 μm. A number notation gives the physical arrangement for a certain IDA. For example, the numbers 0525.3 denote that the IDA has a 5 μm gap between fingers, there are 25 fingers on each comb (50 fingers total make up the IDA), and the fingers are 3 mm in length. The finger and gap width of the IDAs are reported to have identical

dimensions.[114] A clip produced in our lab accomplished electrical contact to the IDAs. The reference electrode used was a Ag/Ag^+ ($AgNO_3$, DMSO). *Note that the Fc/Fc^+ redox couple had a value of +140 mV versus this reference electrode.* The counter electrode was a platinum wire coil.

Polymer growth. pDPP films were electrochemically grown onto the IDA electrodes. A constant potential of +0.8 V was employed. Growth solutions were 0.10 M in monomer and 0.10 M in electrolyte with acetonitrile (Fisher, Optima grade) as the solvent. Monitoring the amount of charge passed during the electrochemical polymerization process controlled film thickness. The films produced for these studies were grown with the passage of either 3 or 6 mC of charge.

Once a film was grown, it was left to dry overnight in the air for about 18 to 24 hours. After drying, the resistance of the film was measured with an ohmmeter to ensure that the films had adequately shorted the finger sets together. The measured film resistance values were found to vary significantly from film to film. The variations likely arise from differences in film thickness, degree of film contact on the IDA electrode, or film morphology.[84]

Scanning Electron Microscopy. Scanning electron micrographs (SEM) were taken using a Phillips model 505 SEM. Films for imaging were grown onto platinum IDA electrodes under identical conditions as those used for sensing. All films were equilibrated to +250 mV and dried overnight prior to examination. A 15 nm thick layer of gold was deposited onto the films via physical vapor deposition prior to imaging.

Electrochemical Instrumentation. For film growth and cyclic voltammetry, an EG&G Princeton Applied Research Model 173 potentiostat/galvanostat was employed in

conjunction with a Princeton Applied Research Model 179 digital coulometer. Data was recorded on a Yokagawa 3023 X-Y chart recorder. To measure resistance changes of the films upon exposure to a vapor, a simple setup was employed that allowed repeatable exposure to vapor-saturated air and pure air. For measurement of the film resistance in vapor-saturated air, the electrode was placed in a vial with a liquid sample such that is was poised about 1 cm from the liquid surface and 1 cm from the lid of the vial. The IDA was simply removed from the vial for measurement of the film resistance in air; during which time the lid remained on the vial to maintain a saturated headspace above the solvent. The setup is diagramed in Figure 4.2..

RESULTS

Film Growth on IDAs. The electrolytes used in the growth solutions include $LiClO_4$, $LiCF_3SO_3$, tetraethylammonium perchlorate ($TEAClO_4$), tetrabutylammonium p-toluenesulfonate (TBATos), and tetrabutylammonium poly(styrenesulfonate) (TBApSS). These electrolytes contain anions of various size and composition. Because of this, they may impart different response characteristics to the films when incorporated during polymer growth. Many previous studies with conducting polymer "chemiresistor sensors" have commonly employed small anions such as ClO_4^- and BF_4^- as dopants.[6,87,89] These anions allow rapid growth of polymer films with good electronic properties. However, it has been reported that stronger films (i.e., having greater tensile strength or greater resistance to cracking) could be formed with triflate and tosylate ions instead of a smaller anion such as ClO_4^-.[37] Also, the mechanical properties, such as tensile strength, may be improved by the use of a polymeric anion such pSS^-. Improving the strength of

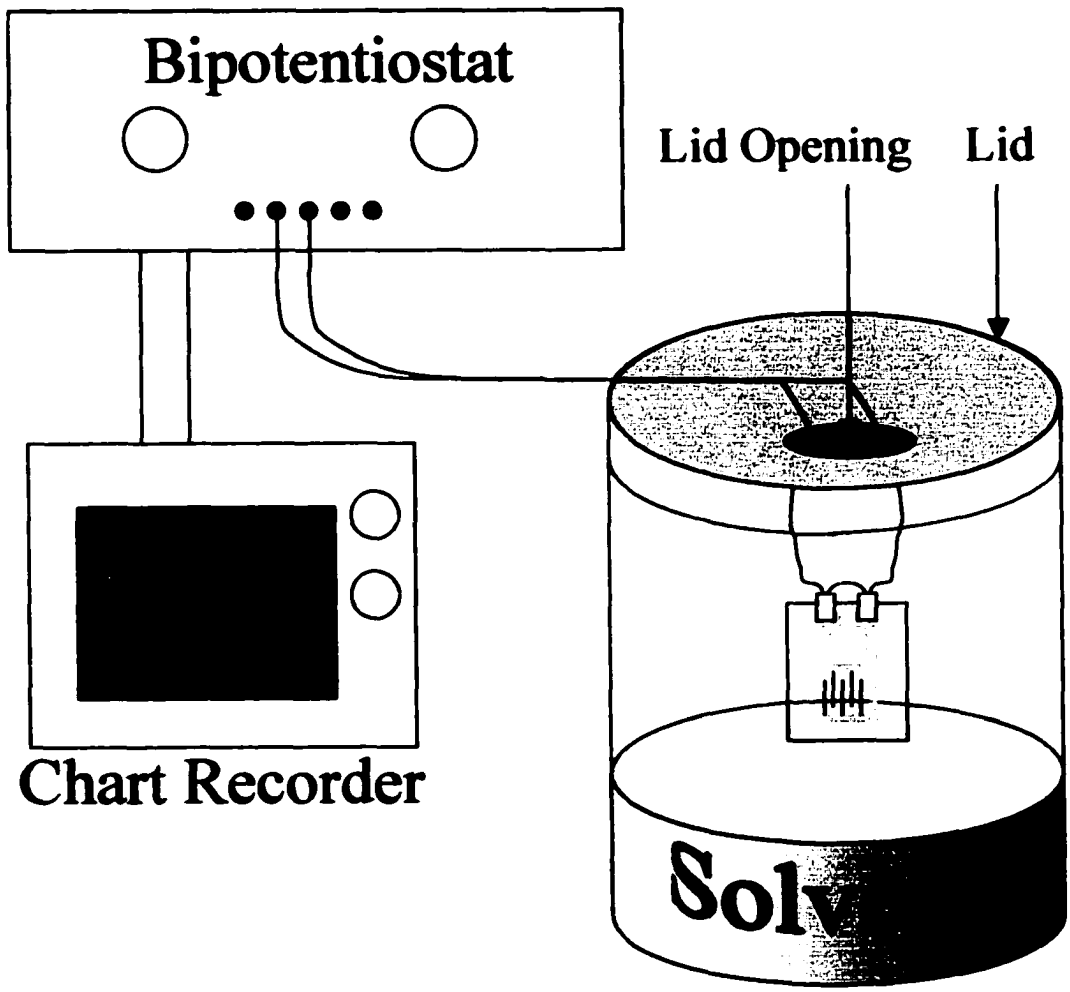

Figure 4.2. Instrumental setup for measuring current responses of pDPP films to air and vapor-saturated air.

the films could help to maintain film integrity during repeated cycles of swelling and shrinking.

The electrochemical growth of pDPP films was found to be dependent upon the electrolyte anion present in the growth solution. Growth solutions containing electrolytes such as $LiClO_4$, $TEAClO_4$, and $LiCF_3SO_3$ readily produced films of pDPP. However, attempts to electrochemically produce pDPP films doped with Tos^- or pSS^- counterions were fruitless. No film formation on the IDA electrodes, regardless of the dimensions of the finger gaps, was noted when employing these anions as the electrolyte.

Oxidation of the monomer did occur, as indicated by the passage of charge. With the aid of a magnifying mirror, small black strands of polymer could be seen drifting from the IDA electrode surface during attempts at film growth. Presumably, some polymer growth was occurring but the oligomers were sufficiently soluble in the growth solution and did not adhere to the electrode surface. Attempts to electrochemically produce films of pDPP with Tos^- or pSS^- dopants onto 2 mm diameter Pt button electrodes were also unsuccessful.

Interestingly, poly(pyrrole)/Tos^- and poly(pyrrole)/pSS^- films were readily grown on both the Pt IDA electrodes and the Pt button electrodes from these electrolytes. The inability to electrochemically produce pDPP/Tos^- or pDPP/pSS^- films may be a consequence of the β, β'-disubstituted monomer interaction with the electrolyte and the resulting oligomer solubility.

Film Voltammetry of pDPP/ClO_4^- Films in $LiClO_4$/Acetonitrile. Figure 4.3 shows the rapid and reversible voltammetric behavior of the pDPP/ClO_4^- film on a Pt IDA electrode. The $E_{1/2}$ of the film was +218 mV and the peak separation was typically

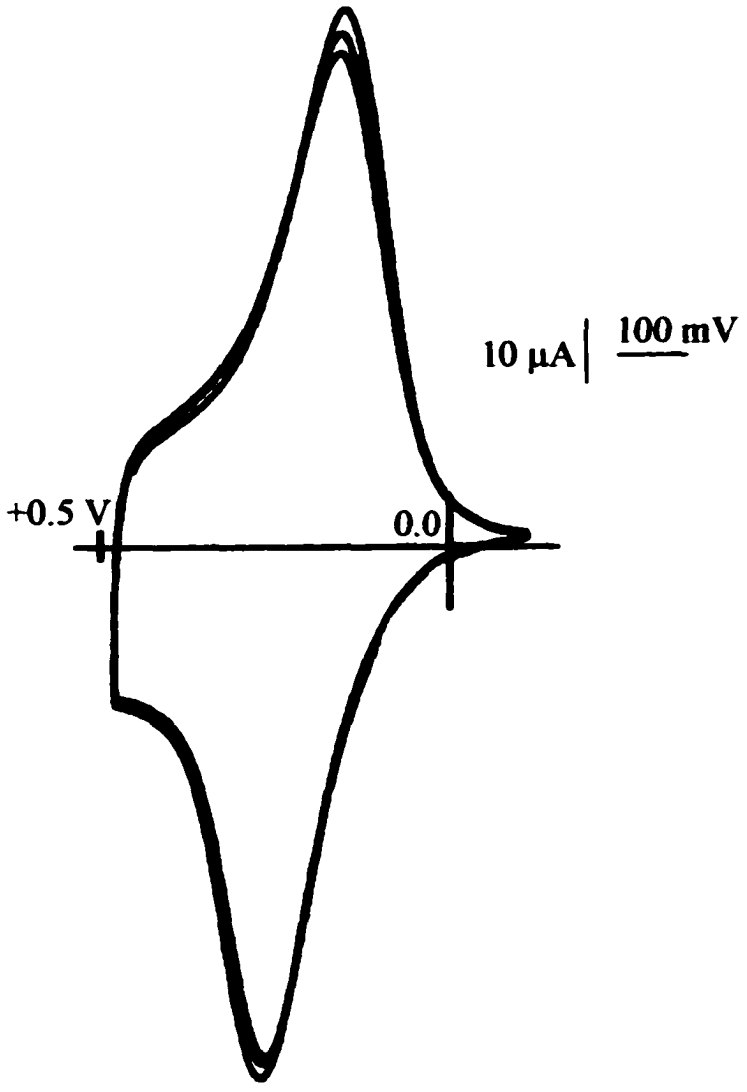

Figure 4.3. Cyclic voltammogram of pDPP/ClO_4^- film on Pt IDA. 6 mC were passed for growth of the film onto the 1025.3 IDA. The electrolyte solution was 0.10 M $LiClO_4$ in acetonitrile. The scan rate was 50 mV/s.

between 100 and 125 mV for the films. This was noted regardless the amount of polymer deposited. Recall that two deposition amounts, 3 or 6 mC, were used for film growth. By this, none of the films used in these studies were very thick. Thick conducting polymer films have been reported to result in poor response times of the films to the vapor analyte.[87,108]

Film Voltammetry of pDPP/$CF_3SO_3^-$ Films in $LiCF_3SO_3$/Acetonitrile. The pDPP/$CF_3SO_3^-$ films reveal marked differences in voltammetry in comparison to the pDPP/ClO_4^- voltammetry shown above. Figure 4.4 shows the voltammograms for two pDPP/$CF_3SO_3^-$ films. Although both show large, sharp current responses and reversible redox behavior, we find larger ΔE_p values when compared with the voltammetry in Figure 4.3. Voltammogram (a) in Figure 4.4 shows a ΔE_p of 290 mV and voltammogram (b) has a ΔE_p of 360 mV. One can also see that at the negative switching potential, there was still a significant reductive current being passed in both films. Voltammogram (b) passed more current at the negative switching potential than was noted in voltammogram (a). The values of ΔE_p and the current magnitude at the negative switching potential indicate that there was a slow step involved in the redox process in this system. It is likely due to inhibited flux of the $CF_3SO_3^-$ dopant ions into and out of the film as a result of sterics or differences in the pDPP/ClO_4^- and pDPP/$CF_3SO_3^-$ film structure. The larger ΔE_p and larger current at the negative switching potential in Figure 4.4b is due to a thicker film resulting from an IDA having a smaller effective area than in Figure 4.4a. That is, a thicker film will result on an IDA having a smaller effective area compared to a larger effective area given the deposition of equivalent amounts of polymer.

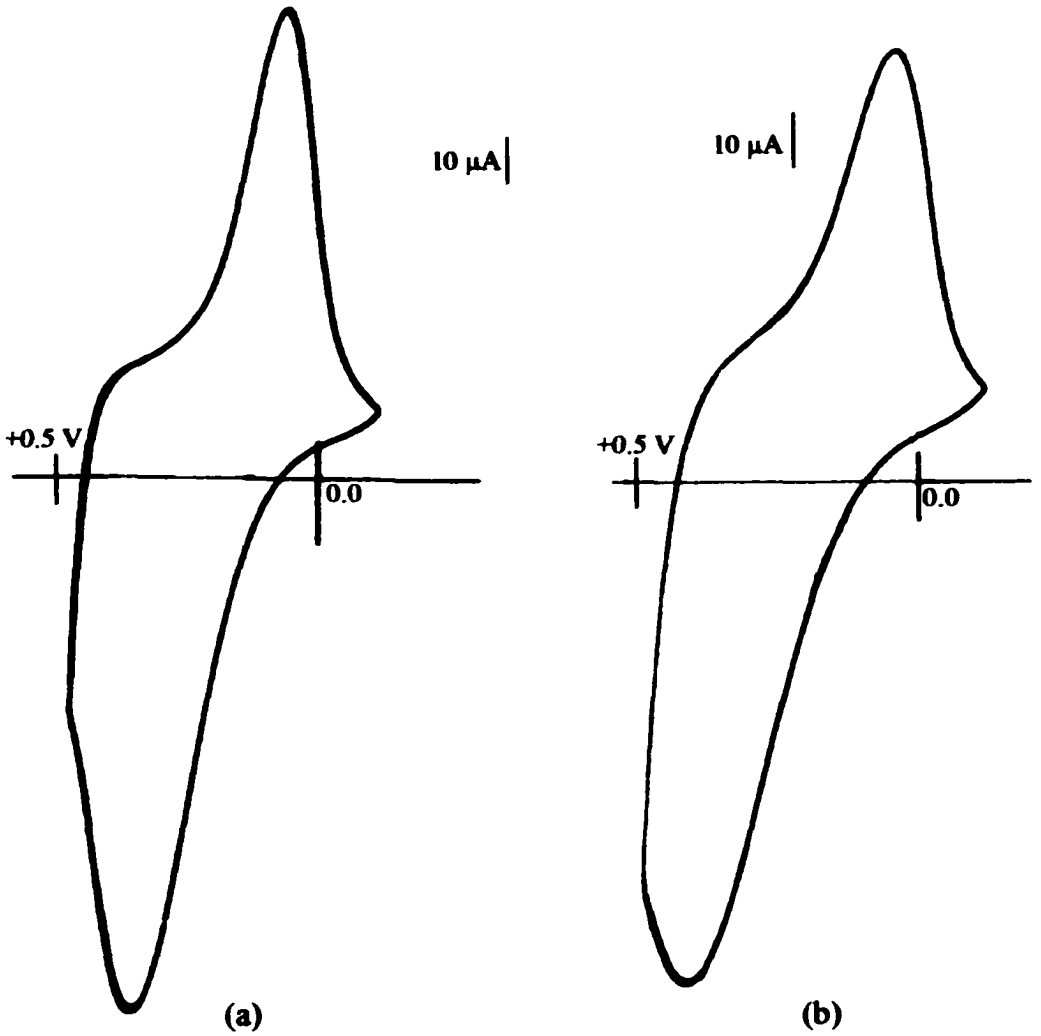

Figure 4.4. Cyclic voltammograms of pDPP/$CF_3SO_3^-$ films cycled in 0.1 M $LiCF_3SO_3$/Acetonitrile at 50 mV/s. Voltammogram (a) employed a 1525.3 IDA and voltammogram (b) used a 0525.3 IDA. Both films were grown with the passage of 6 mC.

Voltammetry of the pDPP/$CF_3SO_3^-$ and the pDPP/ClO_4^- films in an electrolyte solution containing a small, readily mobile anion, such as PF_6^-, supports the hypothesis of slow ion transport of the $CF_3SO_3^-$. Figure 4.5 shows the voltammetry of both film types cycled in a 0.10 M $TBAPF_6$/acetonitrile solution. The voltammetry of the films were nearly identical and both were similar to the pDPP/ClO_4^- films cycled in 0.10 M $LiClO_4$/acetonitrile solutions. Both voltammograms show sharp redox peaks, reversible redox chemistry, similar ΔE_p and $E_{1/2}$ values, and have only small redox currents at the negative switching potential. The PF_6^- ions readily pass in and out of the films in order to maintain electroneutrality in the films. The differences in the voltammograms in Figures 4.3 and 4.4 are thus believed to be due to sterically inhibited motion of the $CF_3SO_3^-$ anion in the films. The difference in voltammetry, however, does not imply that the films are structured identically. The slow ion transport may be a result of differences in film density or the degree of cross-linking of the polymers.

Freshly grown pDPP films were equilibrated to +250 mV in acetonitrile solutions containing either 0.10 M $LiClO_4$ or 0.10 M $LiCF_3SO_3$; corresponding to the films' respective growth-solution electrolyte. At +250 mV, both films should be highly oxidized and be in a highly conductive state as seen in the voltammograms in Figures 4.3 and 4.4. After allowing the films to dry over night to ensure evaporation of excess solvent, the dry films were biased between ±1 V by connecting both reference and counter leads from the potentiostat to one set of IDA fingers and the working lead to the other. Figure 4.6 shows a typical current-voltage curve of a dry film, which showed that the films behave as a pure resistor in the potential range of ±1 V. This was advantageous

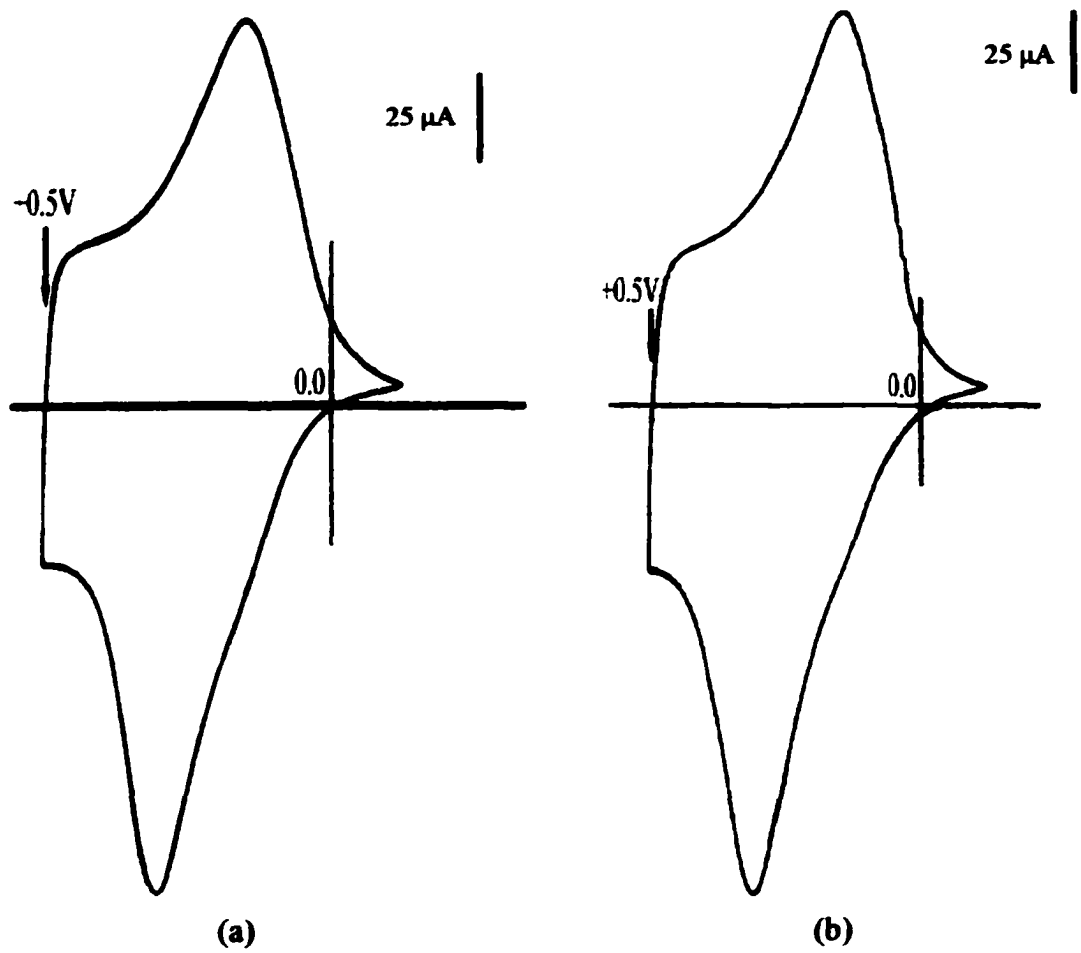

Figure 4.5. Voltammogram (a) is from a pDPP/$CF_3SO_3^-$ film and voltammogram (b) is from a pDPP/ClO_4^- film. Both voltammograms are the result of cycling the films in 0.10 M $TBAPF_6$/acetonitrile solutions at 50 mV/s. Both films were grown with the passage of 6 mC onto 0525.3 IDAs.

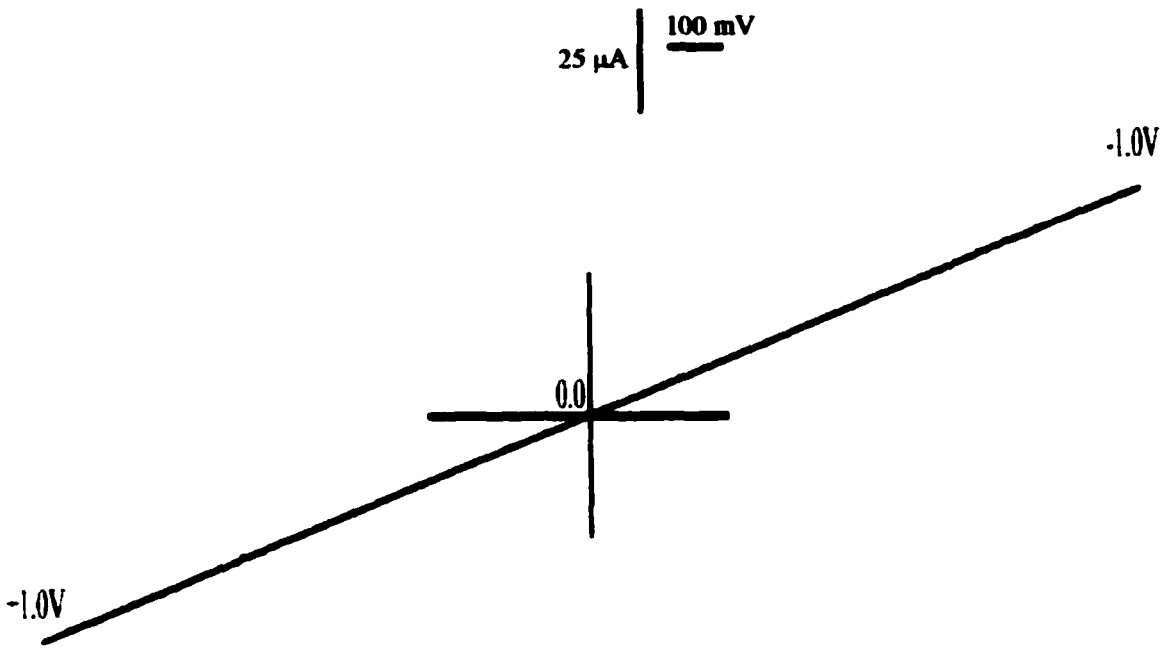

Figure 4.6. The cyclic voltammogram of a dry pDPP/ClO_4^- film. The film was grown with the passage of 6 mC onto a 1525.3 IDA. The scan rate was 50 mV/s. The reference and counter leads were both attached to one of the finger sets on the IDA and the working lead attached to the other finger set. Several cycles are shown in the voltammogram.

as it allowed for straightforward determination of resistance changes from the current data recorded in the experiments.

Scanning Electron Micrographs of pDPP Films. Figure 4.7 and Figure 4.8 are micrographs of the two different types of pDPP films grown in this study. Both films were noted to have a rough composition made up of polymer nodules. The pDPP/$CF_3SO_3^-$ films show a random dispersion of nodules throughout the IDA finger region with a large conglomeration of nodules along the periphery of the IDA. The nodule sizes range from ca. 10 to 50 μm in diameter. This rough, nodular formation has been reported for poly(pyrrole) films by others.[84,115] The fingers of the IDA are readily visible in the image in Figure 4.7a.

The pDPP/ClO_4^- film in Figure 4.8a also shows small nodule formation on the IDA region of the electrode, but the nodules are much smaller and are formed in a greater density than those seen in Figure 4.7a. However, it appears in Figure 4.8a that the bulk of the polymer is in the center region of the IDA as a thick spongy-looking mass. The mass is ca. 50 μm thick and covers ca. 50% of the IDA area. The large border region of film nodules noted in Figure 4.7a was not present in Figure 4.8a.

High magnification of the pDPP/$CF_3SO_3^-$ film showed a fuzzy structure of polymer covering the platinum fingers of the IDA and the gap between the fingers (Figure 4.7b). The step created by the glass substrate and the platinum finger can be noted in the image. Figure 4.8b shows the high magnification of the pDPP/ClO_4^- film. The fuzzy fine structure was not identified in these films as evidenced in the micrograph. Figure 4.9 is a micrograph of a section of clean, uncoated platinum IDA. The overall structure was very smooth with the exception of a bumpy region around the platinum;

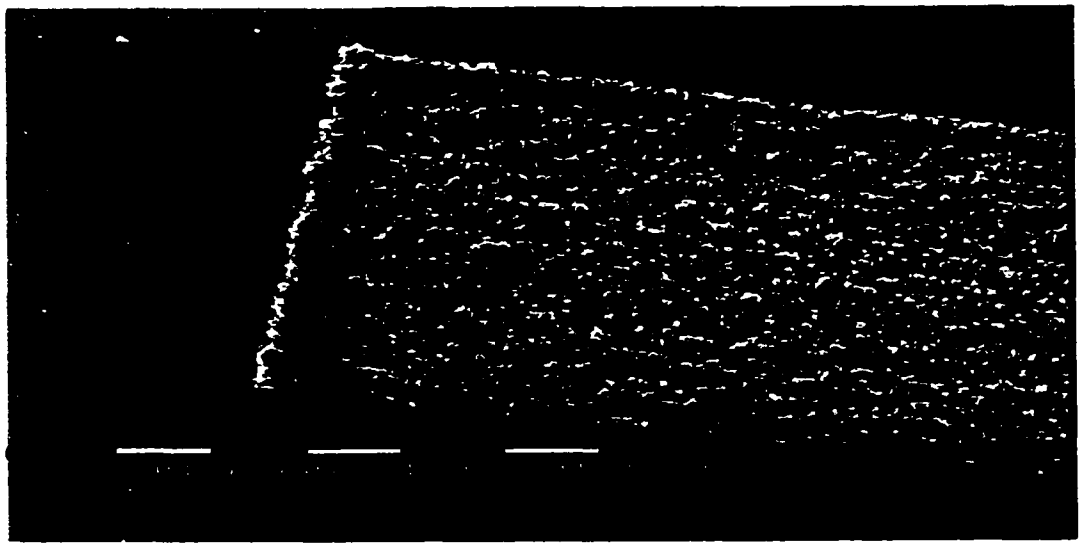

(a)

(b)

Figure 4.7. The above SEM images are for a dry pDPP/$CF_3SO_3^-$ film on a 0525.3 IDA. The oxidation state of the film was equilibrated to +250 mV. The film was grown with the passage of 6 mC.

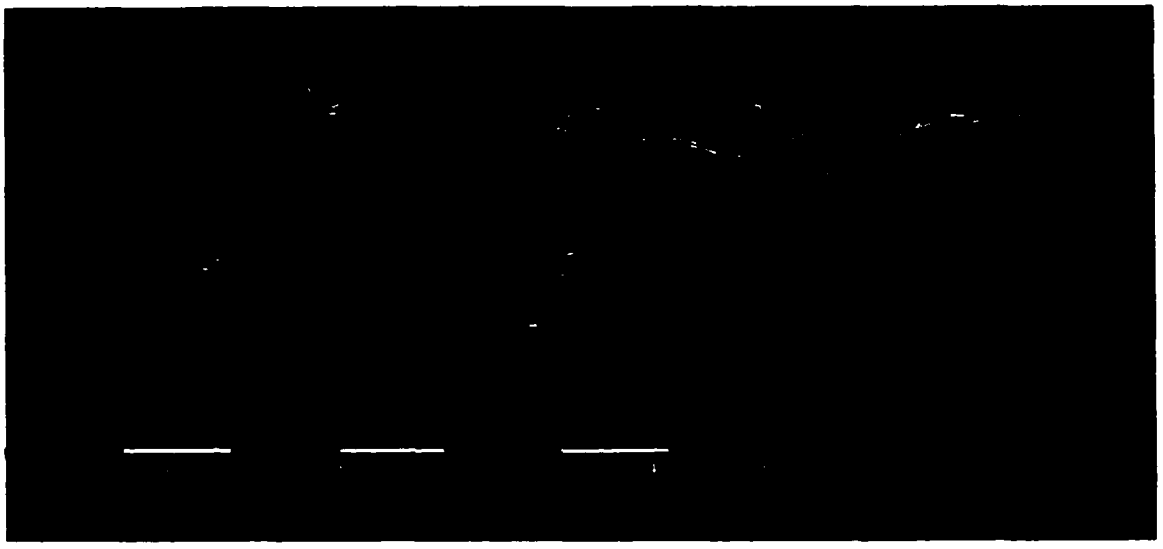

(a)

(b)

Figure 4.8. The above SEM images are for a dry pDPP/ClO_4^- film on a 0525.3 IDA. The oxidation state of the film was equilibrated to +250 mV. The film was grown with the passage of 6 mC.

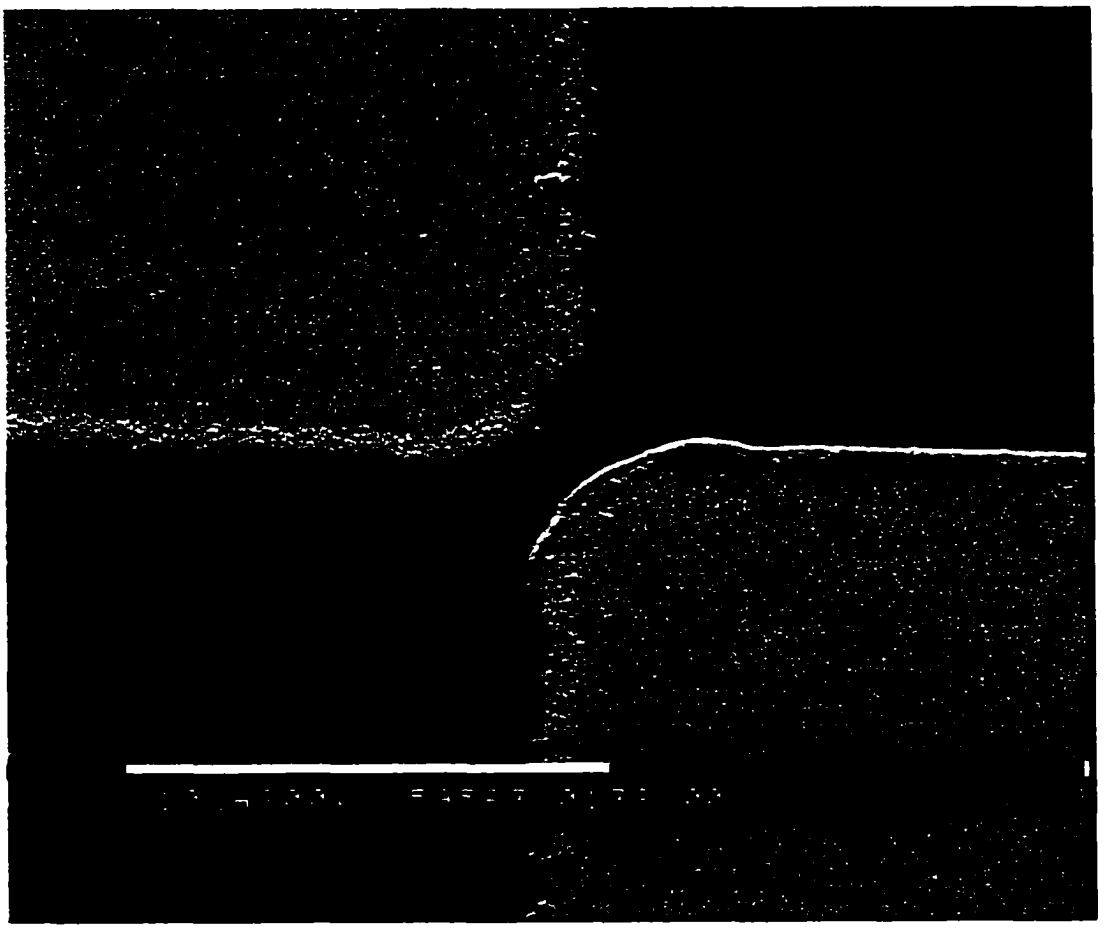

Figure 4.9. SEM of a region of a clean and bare platinum IDA electrode. The surfaces in the upper left and lower right portions of the image are platinum regions and the other portions are the glass support.

which is presumably an artifact of the IDA production. The fine structure in Figure 4.8b looks similar to that in Figure 4.9. Conclusive data on the existence of a fine structure film for the pDPP/ClO_4^- films was not obtained. The SEM images suggest the surface was lacking a carpeting of polymer, but the cyclic voltammograms (vide supra) and the quality of vapor sensing responses (vide infra) suggest good film formation, coverage, and contact with the electrodes.

Resistance of Dry pDPP Films in Air. The current measured between the finger sets of the IDA electrodes with a 250 mV bias applied was recorded on a chart recorder for the dry pDPP films. As film resistance is the parameter typically monitored for vapor sensing with these materials, current responses were converted to resistance values and will be discussed as such. For the dry films, the initial resistance values (i.e., prior to any exposure to analyte vapors) were found to vary over a wide range. The dry film resistances in ambient air at room temperature (ca. 27°C) ranged from ca. 100 ohms to several kilohms. There appeared to be no correlation between the initial resistance value and either the film thickness or IDA size used in these studies. Other researchers have noted this randomness in film resistance from one film to another.[7,88,109]

Relative Resistance Change of pDPP/$CF_3SO_3^-$ Films to Organic Vapors. The pDPP/$CF_3SO_3^-$ films were exposed to vapors of five different organic solvents. The conductivity changes upon repeated exposure to the vapor-saturated air and ambient air are shown in Figure 4.10. Initial inspection of the plots shows that the film responses are repeatable and can be clearly identified. With the exception of dichloromethane, the response time of the resistance change occurs rapidly for the vapors presented here. Exposure to all but the dichloromethane vapors produced responses that reach a stable

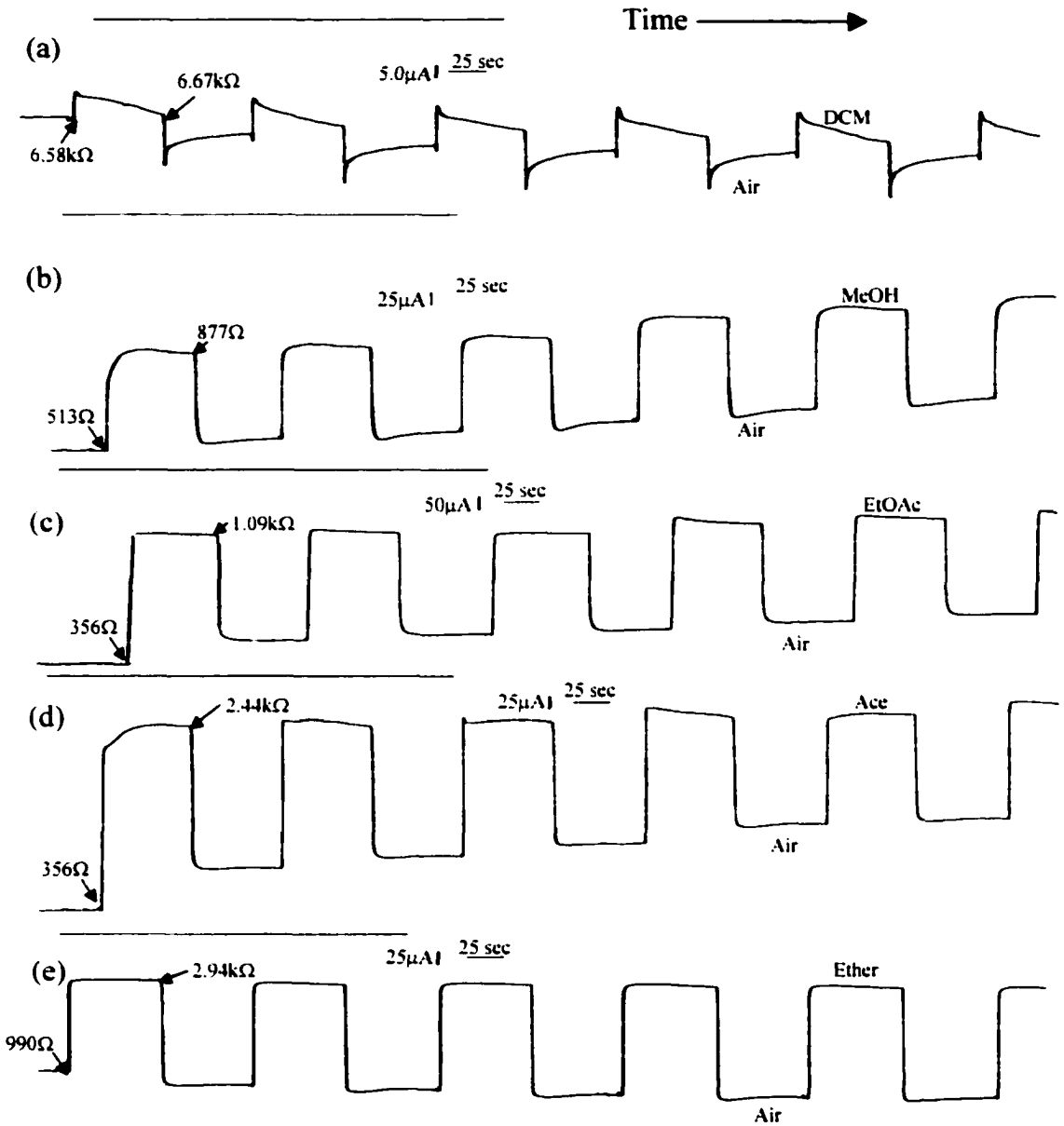

Figure 4.10. The above plots show the current response of the pDPP/$CF_3SO_3^-$ films with alternating exposure to air and vapor-saturated air. Corresponding resistance values are shown for the first peak response in each plot. The horizontal line above each plot is the open circuit reference point used to determine the current and resistance changes of the film. The dried film was equilibrated at +250 mV. The plots show the film response to (a) dichloromethane, (b) methanol, (c) ethyl acetate, (d) acetone, and (c) ether.

value in ca. 30s. In nearly all cases, 90% of charge was noted to pass in less than 10 seconds. The resistance response for the film alternately exposed to dichloromethane vapor and air (Figure 4.10a) shows a resistance response that quickly spikes and then decays with time. This response behavior distinguishes the dichloromethane effects on the film resistance from the other solvent vapors. For the other solvents, the alternating solvent/air exposure resulted in square-shape resistance responses. In all cases, the resistance response to the vapor and air was symmetrical, as seen in Figure 4.10. Qualitatively, both vapor absorption and desorption occurred quickly with the films.

It is important to note that exposure to all of the solvent vapors in Figure 4.10 were seen to *increase* the film resistance relative to ambient air at room temperature.

Some of the plots in Figure 4.10 show a change in the baseline resistance of the film (as defined by the initial resistance of the film in air) with repeated exposure to vapor. The sensing of methanol by pDPP/$CF_3SO_3^-$ (Figure 4.10b) shows the most dramatic change in the film baseline resistance. The baseline resistance decreases by over 100 Ω in ca. 10 minutes of testing. The changes in the films' baseline resistances seemed irreversible, as they did not settle back to their original values, even after an hour of drying in air. Fortunately, this transient baseline resistance did not affect the relative response of the film resistance change.

To quantitatively compare the resistance responses of the films to the different organic vapors, relative resistance changes, ΔR/R, were calculated. ΔR/R is defined as $(R_{Air} - R_{Vapor})/R_{Air}$. Figure 4.11 demonstrates how the resistance values used in calculating the ΔR/R values were measured from plots like those shown in Figure 4.10. The first data point is $(R_A - R_V)/R_A$, the second data point is $(R'_A - R'_V)/R'_A$, and so on.

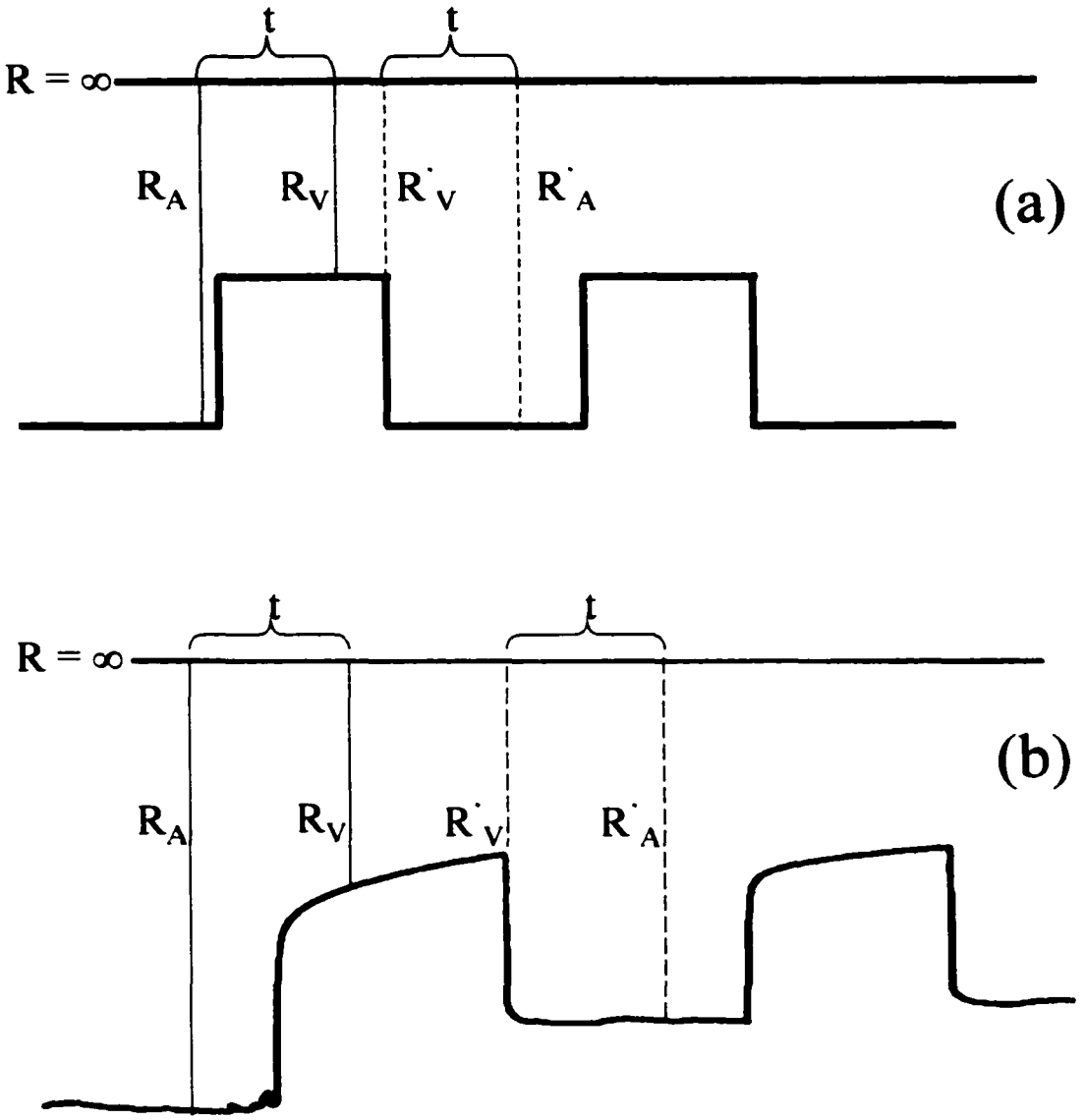

Figure 4.11. The above diagrams demonstrate the measurement of the current values used to calculate the resistance values used for determination of the relative resistance ($\Delta R/R$) change in the films. The upper diagram (a) shows measurements taken for an ideal response and the lower diagram (b) shows the measurements on a real response. The time (t) was identical (i.e.. 30 sec) for measurement of all resistance values.

Ideally, ΔR/R would be identical to ΔR'/R' (Figure 4.11a). Relative resistance values are used since the absolute film resistances varied to such a large degree from film-to-film. Using relative resistance values to define the signal response is commonly employed with organic conducting polymer films chemiresistor sensors.[7.10]

Figure 4.12 shows the average ΔR/R values calculated from response plots like those in Figure 4.10. These average ΔR/R plots included data from films of different thickness on IDAs of various dimensions. Two key trends are noted in Figure 4.12. First, the average ΔR/R value for films repeatedly exposed to vapor and air does not change drastically from one measurement to the next. Second, there is a distinct difference in the magnitude of the average ΔR/R values. It is easy to see that the responses by methanol and dichloromethane can readily be differentiated from each other and from the other three solvent vapors, based on the average ΔR/R values. The ΔR/R responses of the films to ether, ethyl acetate, and acetone vapors were nearly the identical and cannot be resolved from each other.

Table 4.1 shows the average relative response of the pDPP/$CF_3SO_3^-$ films to the various vapors. The data in the table shows that the relative resistance values could be used to differentiate several of the vapors from each other. The data include films deposited on IDA electrodes of various finger gap dimensions and films grown by the passage of 3mC or 6mC. There did not appear to be any obvious influence on the relative resistance values due to use of the various IDA electrodes and the amount of charge passed for film growth.

Relative Resistance Change of pDPP/ClO_4^- Films to Organic Vapors. Figure 4.13 shows the resistance responses for various pDPP/ClO_4^- films to the alternating

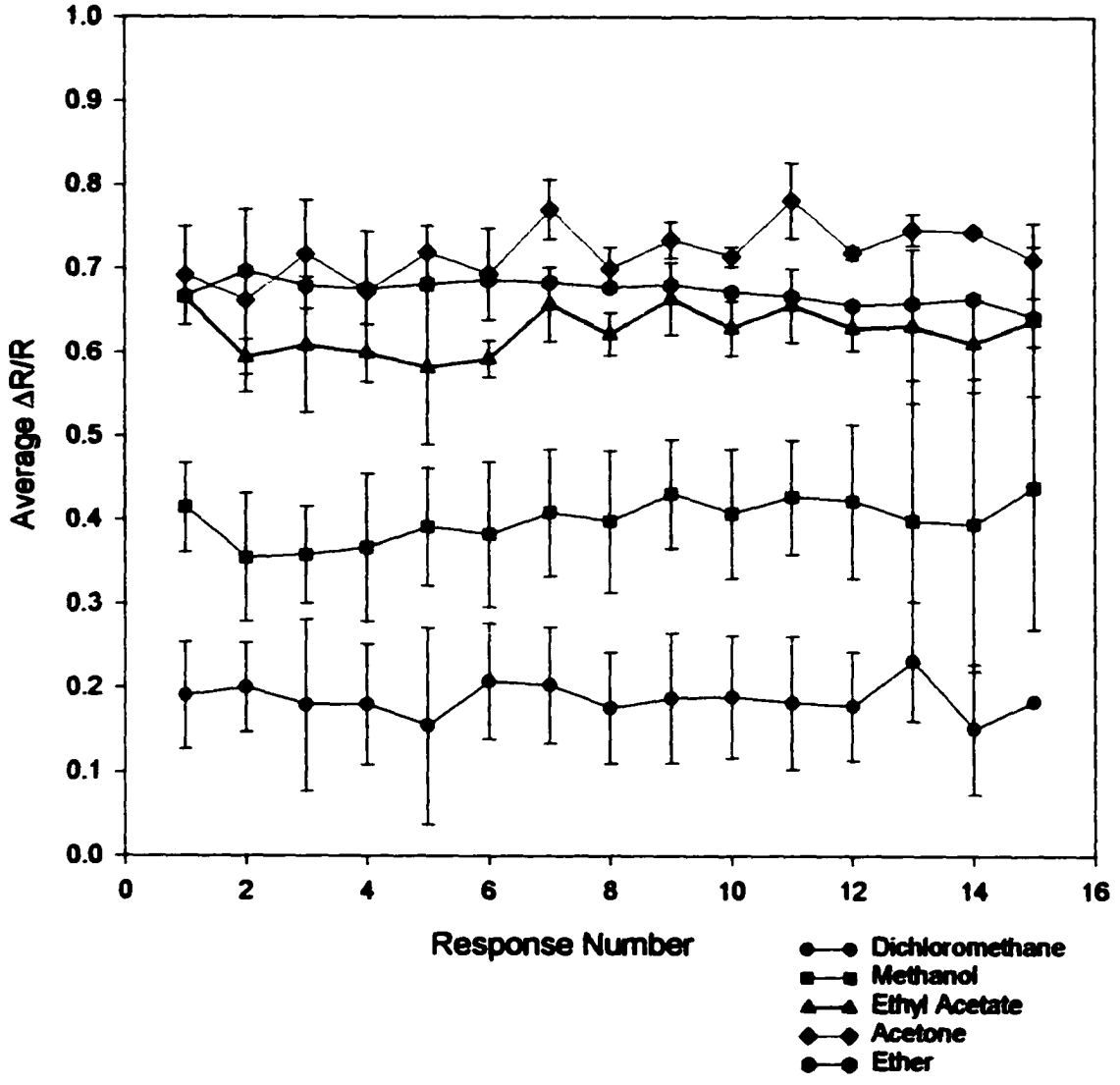

Figure 4.12. The figure shows the average ΔR/R for a number of pDPP/$CF_3SO_3^-$ films on IDA electrodes of various dimensions. The data was calculated from plots like those shown in Figure 3.2.10; thus the ΔR/R values are plotted versus response number. Each data point in the plots for the above figure corresponds to a change in the film resistance as seen in the plots in Figure 3.2.10.

		<ΔR/R>					
Film/Counter Anion	Film Growth	DCM	MeOH	EtOAc	Ace	Ether	ΔR_{DCM}
pDPP/ClO_4^-	Yes	-.034±0.018	0.55±0.070	0.59±0.014	0.54±0.029	0.43±0.019	(-)
PDPP/$CF_3SO_3^-$	Yes	0.19±0.020	0.40±0.026	0.63±0.027	0.72±0.033	0.67±0.014	(+)
PDPP/Tos^-	No	———	———	———	———	———	———
PDPP/SS^-	No	———	———	———	———	———	———

Table 4.1. Table shows the average ΔR/R values for the interaction of the pDPP films and the tested solvent vapors.

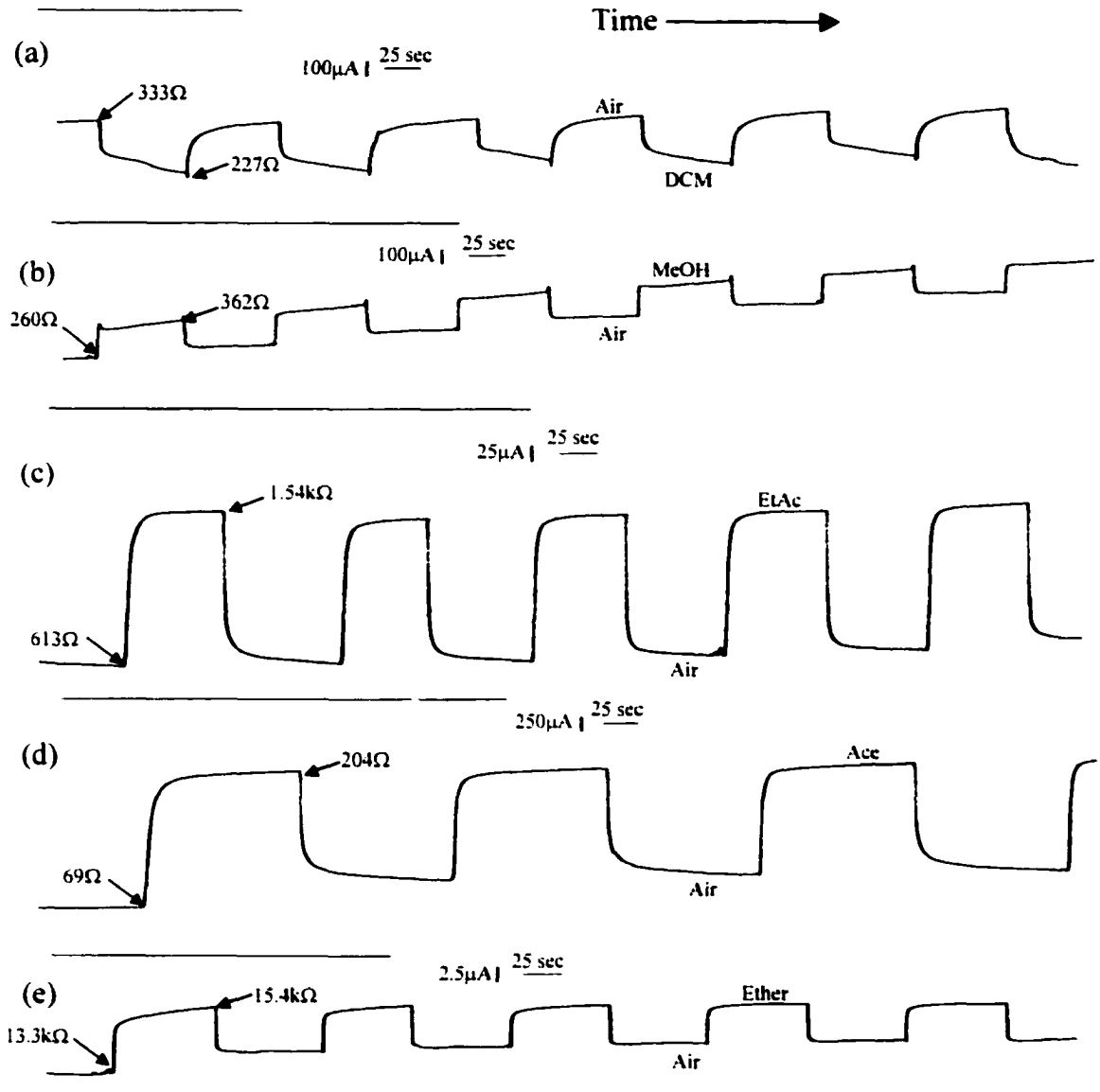

Figure 4.13. The current-time plots show the response of the pDPP/ClO_4^- films with alternating exposure to air and vapor-saturated air. Resistance values are shown for the first peak response in each plot. The horizontal line above each plot is the open circuit reference point used in determination of the current and resistance changes in the film. The dried film was equilibrated at +250 mV. The plots show the film response to (a) dichloromethane, (b) methanol, (c) ethyl acetate, (d) acetone, and (e) ether.

exposure of the vapor-saturated air and ambient air. At first glance, the responses of the films appear similar to those shown for the pDPP/$CF_3SO_3^-$ films in Figure 4.10. The resistance changes also display step-like peaks and gave repeatable responses. There are, however, several differences in these plots compared to those in Figure 4.10.

First, and most obvious, is the difference in the film response to dichloromethane vapor. The pDPP/ClO_4^- films did not show the spike and decay in the film resistance change noted with the pDPP/$CF_3SO_3^-$ films (Figure 4.10a). Instead, pDPP/ClO_4^- films produce a fast initial change followed by a slower resistance change that approached a maximum value. This film behavior is more akin to the film responses with exposure to the other solvent vapors tested here.

Second, whereas the pDPP/$CF_3SO_3^-$ film resistance was seen to increase upon exposure to the dichloromethane vapor (Figure 4.10a), the pDPP/ClO_4^- films show a *decrease* in the film resistance (Figure 4.13a). None of the other four organic solvent vapors examined had this effect on the film resistance.

Third, the resistance change to nearly all the vapors tested occurred more slowly than those seen with the pDPP/$CF_3SO_3^-$ films (Figure 4.10). The plots show that a steady-state resistance value was not attained in the span of ca. 60 seconds. With the exception of plot (b) in Figure 4.13 involving the interaction of the methanol vapor with the pDPP/ClO_4^- film (which show rapid and stable resistance changes), the other plots show a rapid resistance change followed by a slower, steady change in the film resistance. Plot (d) in Figure 4.13 was recorded on a slightly slower time scale so as to more clearly portray the slower response behavior just described above.

As in Figure 4.10, the plots in Figure 4.13 also show changes in the baseline resistance of the films upon repeated exposure to the solvent vapors. The transient baseline value for the film repeatedly exposed to methanol vapor is particularly obvious. The other vapors did not change the baseline resistance of the films in Figure 4.13 as dramatically as did methanol within the span of ca. 10 minutes.

Relative resistance values for the film response of the pDPP/ClO_4^- to the five organic vapors were calculated and are plotted in Figure 4.14. The figure shows that $\Delta R/R$ values of the films were clustered closely around 0.5. The film response to dichloromethane vapor is the exception. The $\Delta R/R$ value for the film interaction with dichloromethane vapor shows an average response of ca. –0.3. The average value has the opposite sign from the other plots since the resistance of the films decreased upon exposure to the dichloromethane vapor. Table 4.1 lists the average relative resistance responses of the various films to the organic vapors studied here.

Relative Resistance Change of pDPP/ClO_4^- Films to Small, Halogenated Organic Vapors. Given the unique directional behavior of the resistance change of the pDPP/ClO_4^- films exposed to the dichloromethane vapor (seen in Figure 4.13 and Figure 4.14), these films were exposed to a series of small, halogenated organic vapors. Figure 4.15 shows the resistance responses of a pDPP/ClO_4^- film exposed to four chlorinated hydrocarbons, two brominated hydrocarbons, and water vapor. All vapors were saturated in air at ca. 25°C. All pDPP/ClO_4^- films produced similar responses to the vapors as those shown in Figure 4.15. The plots clearly show that the film resistance decreases with exposure to all of the chlorinated vapors. The magnitude of the response was seen to vary for the different chlorinated solvents and there was little change in the baseline

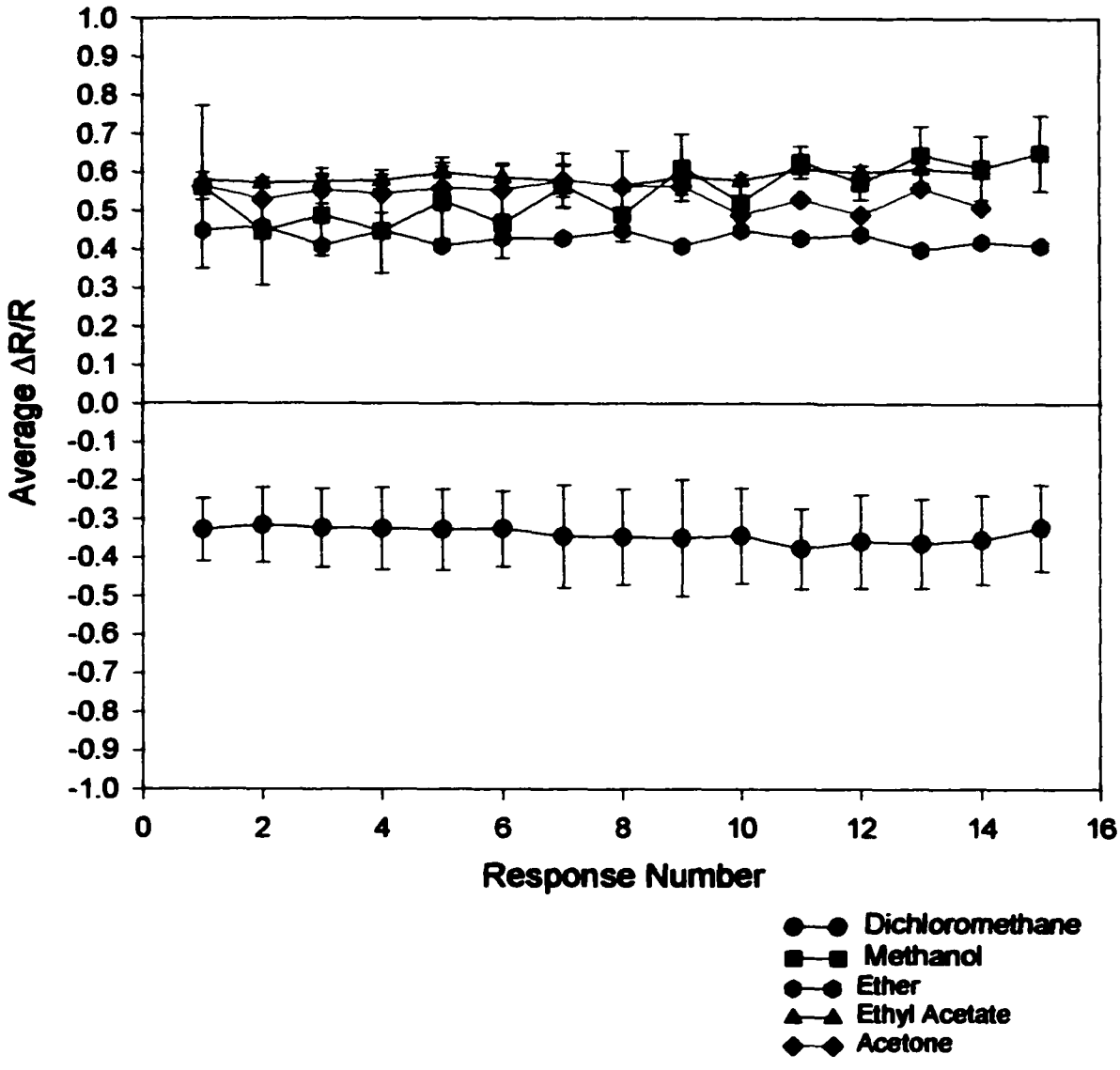

Figure 4.14. The plot shows the average ΔR/R for a series of number of pDPP/ClO_4^- films on IDA electrodes of various dimensions. The data was calculated from plots like those shown in Figure 3.2.13. The average ΔR/R for each plot above is shown in Table 3.1.

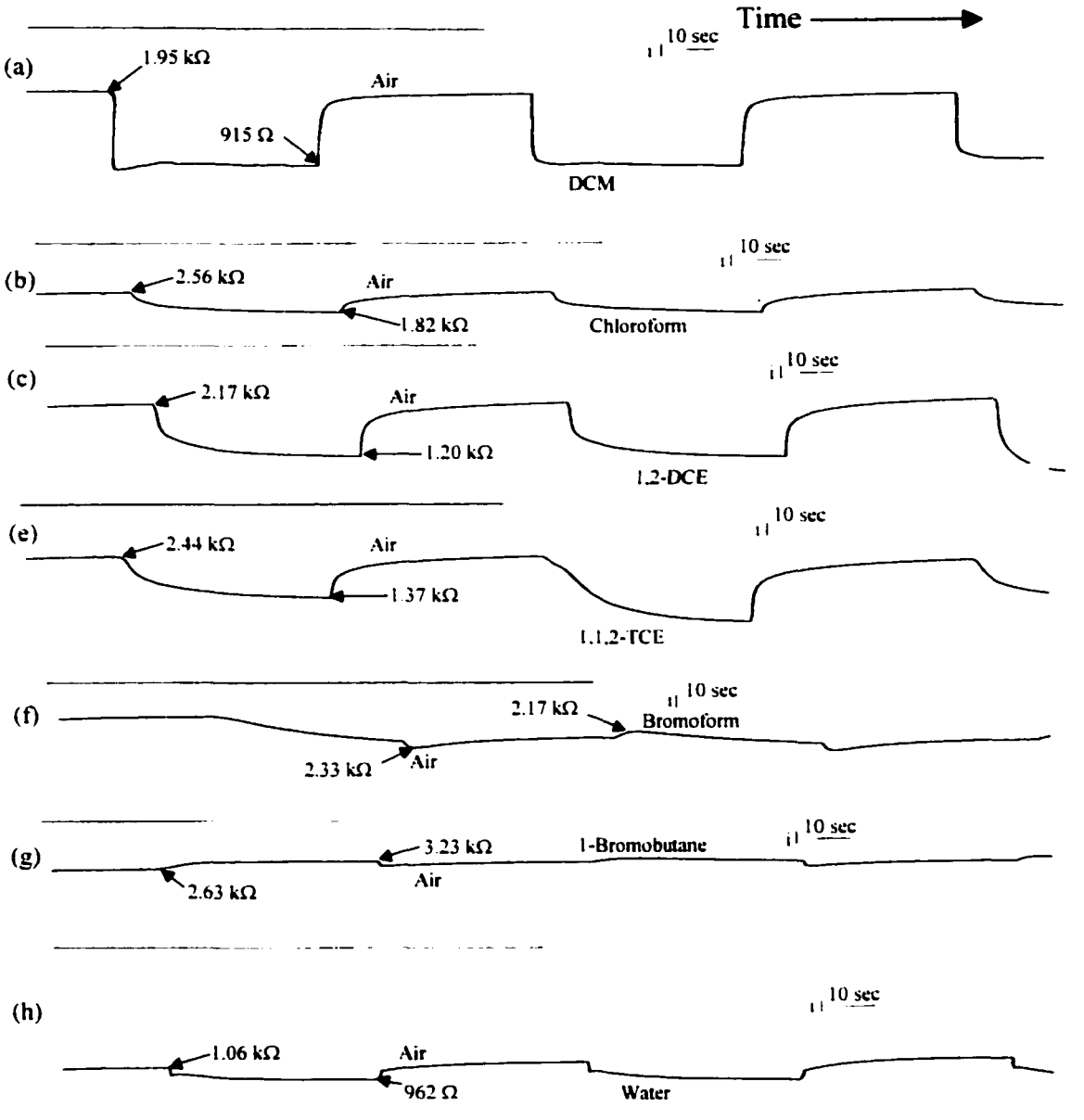

Figure 4.15. The above current-time plots show the current (resistance) changes for a pDPP/ClO_4^- film for exposure to various halogenated organic solvents and for water vapor. The same film was used in all the plots above. The film was grown with the passage of 6mC and was deposited on a 1025.3 IDA. The current (i) scale bar in each plot is 25 μA. The horizontal line above each plot is the current response at open circuit (i.e., R = ∞).

film resistance on the time scale of the plots. For the chlorinated solvent vapors, the resistance change occurred most rapidly for exposure to dichloromethane and more slowly for the other three chlorinated solvents. The shapes of the responses appear quite symmetrical in alternating the film environment between air and vapor-saturated air.

The brominated hydrocarbon vapors show much smaller changes in the film resistance compared to those noted for exposure to chlorinated organic vapors. More importantly, the resistance response of the film *decreased* upon exposure to the brominated hydrocarbon vapors.

Plot (g) in Figure 4.14 shows the response of the pDPP/ClO_4^- film to air saturated with water vapor at room temperature. Interestingly, the film resistance was noted to decrease with respect to the dry film in air. Water vapor affected the film resistance much like the chlorinated organic vapors did. Water vapor had the opposite effect on the pDPP/$CF_3SO_3^-$ films, decreasing the film resistance.

DISCUSSION

The sensing capabilities of the pDPP films, as demonstrated by the data presented in this study, are promising. The responses to the alternating exposure of solvent vapors and air, as seen in Figures 4.10 and 4.13, were found to be repeatable and show good stability over the course of the experiments. The signals produced by the resistance changes in the films were both rapid and large. Slight transient behavior in the baseline resistances of the films was noticed for most experiments involving repeated alternating exposure to the vapors and air. A deviation in the baseline resistance with time was most evident with sensing of methanol vapor. This change in baseline resistance has been

recognized in similar sensing studies and such behavior was reported as being unacceptable for sensing responses.[109] However, others have successfully corrected for the transient baseline mathematically.[88]

Several differences in the pDPP films' resistance responses, as a result of variations in the analyte vapor composition and the polymer growth conditions, were noted which are advantageous for vapor sensing. First, consider the shape of the plots in Figure 4.10 and 4.13. For the pDPP/$CF_3SO_3^-$ films, plots (b)-(e) in Figure 4.10 have very square shape responses to the alternating exposure to the vapors and air. However, the film response to dichloromethane in plot (a) shows a jagged-shaped behavior. The response to the dichloromethane vapor by the pDPP/ClO_4^- film shown in Figure 4.13a does not exhibit such a dramatic difference in shape from the film's response to the other vapors tested. Dichloromethane vapor obviously interacts differently with the two polymer films. The other vapors produced signal responses that were all much more similar in shape to each other. Solely by the shape of the plots in Figure 4.10, one could identify the interaction of dichloromethane vapor with the pDPP/$CF_3SO_3^-$ films.

The films were also found to differentiate at least one of the organic vapors based upon the relative resistance responses calculated from plots like those in Figures 4.10 and 4.13. Consider Figure 4.12. The pDPP/$CF_3SO_3^-$ film was able to differentiate between the methanol and the dichloromethane vapors based on the relative response magnitude. The average $\Delta R/R$ value for the film response to dichloromethane vapor was about 0.2, half that measured for the film exposure to methanol. Both of these solvents can readily be differentiated from each other upon comparison of the induced relative resistance change. The values of $\Delta R/R$ for acetone, ether, and ethyl acetate, given the error bars, are

not distinguishable from each other. With a ΔR/R value of about 0.65, these three solvents vapors produced a greater relative resistance increase with the pDPP/$CF_3SO_3^-$ film than either methanol or dichloromethane.

The pDPP/ClO_4^- films produced a different response pattern to the solvent vapors than was noted with the pDPP/$CF_3SO_3^-$ films. The pDPP/ClO_4^- films showed excellent differentiation for dichloromethane, but no ability to distinguish between the other four vapors. Here, the interaction with the dichloromethane vapor decreased the film resistance with an average ΔR/R value of -0.34 (see Figure 4.14). Of particular importance is the opposite sign of the response. This readily distinguishes the film interaction with dichloromethane vapor from the other vapors tested. As with the pDPP/$CF_3SO_3^-$ films, the other four vapors increased the absolute film resistance.

The type of response of the pDPP/ClO_4^- film produced by dichloromethane is not unique to this solvent. The data in Figure 4.15 showed that the decrease in film resistance occurred with several small, chlorinated organic vapors. Analogous small, brominated organic vapors, however, did not have the same effect on the film's resistance response. The data suggest the possibility of devising a sensor specific to small, chlorinated organics. Organic molecules of this type have been identified as environmental contaminants in aqueous systems.[116,117] A sensor based on the type of response exhibited by pDPP/ClO_4^- films may be useful in devising an inexpensive and easily employed means of analyzing contaminated water systems.

The film reaction to water vapor may, however, prove to be deleterious for this application. Exposure of the pDPP/ClO_4^- films to water vapor also decreased the film resistance (see Figure 4.15g). This makes it difficult to differentiate the resistance

response of the two vapors based on the direction of $\Delta R/R$. However, "quick and dirty" experiments that involved a miniscule amount of dichloromethane in a large amount of water gave $\Delta R/R$ values that were significantly larger than those recorded with water vapor alone. The larger $\Delta R/R$ responses were similar to the resistance changes with dichloromethane vapor alone. The difference in the absolute resistance magnitude for exposure to dichloromethane vapor and water vapor are readily noted in the plots in Figure 4.15.

Both of the pDPP films can readily discriminate the dichloromethane vapors from the other organic vapors studied. With the pDPP/$CF_3SO_3^-$ films, the $\Delta R/R$ values for dichloromethane are small compared to the other vapor responses. For the pDPP/ClO_4^- films, the difference in sign of the $\Delta R/R$ response makes identification of dichloromethane vapor obvious. The pDPP/$CF_3SO_3^-$ film can also differentiate methanol vapor from ether, ethyl acetate, and acetone. Consideration of both film responses to the analyte vapors, as would be done with a sensor array configuration, improves the ability to distinguish methanol and dichloromethane vapors from each other as well as from the other vapors tested.

Several papers have suggested that the interaction of the solvent vapors and a conducting polymer film is a result of charge donation or acceptance between the polymer-analyte vapor pair.[111] The charge-transfer between the analyte vapors and the polymer effectively changes the concentration of positive charge carriers in a polymer film; thus changing the film conductivity.[111]

According to this type of analysis, the conductivity change of a conducting polymer film upon exposure to a vapor should depend largely on the initial value of the

polymer work function and the Mulliken electronegativity of the analyte molecule. The Mulliken electronegativity, χ_M, is defined as $\chi_M = \frac{1}{2}(I_P - E_A)$, where I_P is the ionization potential of the vapor molecule and E_A is the electron affinity.[111] The E_A of most organic molecules is very low, i.e., $I_P >> E_A$, such that $\chi_M = \frac{1}{2}I_P$.[111] Therefore, a particular polymer will respond to a series of vapors according to I_P of the vapor molecule.

The work function of a polymer depends largely on the conditions by which the film was grown and subsequently exposed.[111,113] Of particular importance are the oxidation state of the polymer, the solvent from which the film is polymerized, and the type of anion with which it is doped.[111,113] Blackwood and Josowicz have demonstrated how a particular analyte vapor could behave as either a charge donor or acceptor to a particular polymer depending on the growth-solvent and dopant ions.[111] The varying interactions are partially attributed to changes in the film morphology, which is due in part to the use of different counteranions in film growth. The type of dopant employed for the film growth greatly affects the morphology.[113] Morphology changes can affect the relative concentration of surface-to-bulk interactions of the vapor molecules and the polymer.[113] Primarily, however, Blackwood and Josowicz show that it is the relative difference between the initial work function of the polymer and the ionization potential of the vapor molecule that determines the magnitude and direction of the resistance change in the polymer vapor interactions.[111]

The responses of the films employed in this work correlate well with the above theory. The SEM images of the pDPP/$CF_3SO_3^-$ and pDPP/ClO_4^- films (Figures 4.7 and 4.8) show that the film morphologies differ. The pDPP/$CF_3SO_3^-$ and pDPP/ClO_4^- films also produced significantly different responses to the vapors tested. As mentioned above,

the work function of the polymers can differ depending on the conditions of polymer growth; i.e., due to the different counteranions used.[111] This can greatly affect the film morphology and the initial work function of the dry films. Based on the differences in the film morphology and the films' resistance response to the vapors, let us assume then that the work functions of these two types of films are slightly different. The resistance change at each film will then depend on the relationship between the magnitude of the I_P values of the analyte vapors[118] (see Table 4.2) and the work function of the polymer.

Consider first the plots in Figure 4.12. Exposure of the pDPP/$CF_3SO_3^-$ films to all the vapors listed increased the resistance. Thus, based on the Blackwood and Josowicz theory, the positive charge carrier concentration in the polymers decreased because the analyte vapors behaved as charge donors. Comparing the magnitude of the response with the I_P values of the analyte vapor, it can be seen that the $\Delta R/R$ generally increases with decreasing I_P. The $\Delta R/R$ for ethyl acetate, ether, and acetone are too close to confidently differentiate. Note that the I_P values of these compounds are also quite close to each other. The magnitude of response of this film thus seems to be related to the ionization potential of the vapor molecules. The dichloromethane vapor has a rather large I_P value and induces only a small $\Delta R/R$ on the film. If it were solely the difference in the work function and $\frac{1}{2}I_P$ that influences the nature of the response in these film-vapor interactions, it would indicate the polymer has a rather large work function and is a strong charge acceptor.

Figure 4.14 on the other hand shows a distinct change in the charge-donor/acceptor nature of the polymer film. Four of the vapors, having I_P values between

SOLVENT	IONIZATION POTENTIAL (I_P)
Water	12.6
Carbon Tetrachloride	11.5
Chloroform	11.42
Dichloromethane	11.4
1,2-Dichloroethane	11.1
Methanol	10.84
Bromoform	10.53
Dibromobutane	10.13
Ethyl Acetate	10.11
Acetone	9.69
Ether	9.6

Table 4.2. The above is a list of the ionization potentials (I_P) for the solvent vapors employed in this study.

9.6 and 10.84, cause resistance increases in the polymer. These four vapor molecules are charge donating to the polymer; their I_P values must be smaller than the corresponding value of the film work function. Dichloromethane (I_p = 11.4) behaved as a charge acceptor, *decreasing* the $\Delta R/R$ of the film; increasing the concentration of positive charge carriers on the polymer. If only the difference between the initial work function of the polymer and the I_P of the vapor is affecting the response, then it may be noted that the pDPP/ClO_4^- film has a work function value that lies between the corresponding values of the I_P of dichloromethane and the other four vapors. This also indicates that the work function is smaller for the pDPP/ClO_4^- films than the pDPP/$CF_3SO_3^-$ films.

Now consider the responses noted in Figure 4.15. The work function of the pDPP/ClO_4^- polymer must have a value equivalent to an I_P value between 10.84 and 11.1. This would explain, in part, the different sign of the resistance change for the chlorocarbon and water. The I_P values of the chlorinated solvent vapors and water vapor are greater than 11 and are charge acceptors (i.e., $I_P > WF_{polymer}$). The other vapors tested, including the brominated organic vapors, had I_P values less than 10.9 and behave as charge donors; increasing the film resistance.

The difference in polymer work function and the I_P of the vapor molecules is likely not the only factor influencing the magnitude and direction of the resistance change in the polymer. If that were the case, then water vapor should have produced a larger resistance change then dichloromethane. Other factors such as vapor pressure and solubility of the vapor in the polymer probably also affect the resistance response.

Investigation of additional pDPP film sensors incorporating other dopant ions may reveal further selectivity for certain organic vapors as seen with the two films

studied here. This may be useful in development of a sensor array that could be used for sensing chlorinated organic solvents in aqueous environments. Also, additional films doped with different anions may provide insight into how the film growth conditions affect the resistance change and thus the sensing capabilities of the films.

CONCLUSIONS

The pDPP/ClO_4^- and pDPP/$CF_3SO_3^-$ films used in this investigation have shown promise for the development of organic conducting polymer chemiresistor sensors for select organic vapors. In particular, the films can be used to distinguish dichloromethane readily from a variety of other organic solvents. This was achieved by comparison of the average relative resistance change of the film when alternately exposed to air and vapor saturated air. While several reports demonstrate the ability to distinguish the polymer-analyte interaction of a variety of vapors based on the magnitude of the relative resistance change, there have been no reports of a single polymer film showing the response selectivity for chlorinated organic vapors as does the pDPP/ClO_4^- films prepared in this work.

The response patterns to the various solvents differ for the pDPP films, depending upon the dopant anion incorporated into the film during growth. The difference is most notable for dichloromethane where the resistance of the pDPP/ClO_4^- film decreased, while the resistance of the pDPP/$CF_3SO_3^-$ film increased upon exposure to its vapor.

The decrease in resistance of pDPP/ClO_4^- is not unique to dichloromethane; a similar response was also noted with several small, chlorinated hydrocarbons.

Interestingly, small, brominated hydrocarbons did not produce similar responses, rather they caused an increase in pDPP/ClO_4^- film resistance.

Blackwood and Josowicz correlated the difference in the work function of the sensing polymer and ionization potential of the analyte vapor molecules to describe the nature of the charge donor/acceptor properties of the polymer-vapor molecule pair.[111] The responses by the pDPP/ClO_4^- and pDPP/$CF_3SO_3^-$ films in this study appear to agree with the findings of Blackwood and Josowicz. The use of different counterions during polymer growth could account for the differences in the initial work function of the dry films and thus the differences in resistance change in the polymers. Assuming only the work function and the ionization potential affect the conductivity responses, the data indicate that the pDPP/ClO_4^- work function is slightly less than the pDPP/$CF_3SO_3^-$ polymer's work function. The lower apparent work function of the pDPP/ClO_4^- film advantageously allows it to differentiate between the chlorinated organics vapors (which have high I_P values) and most other organic vapors. Few common organic molecules have I_P values as large as those of chlorinated organics.

Because of the specific interaction of these materials with chlorinated hydrocarbons they could possibly be developed and incorporated into sensors for aqueous systems that have been contaminated with these compounds via headspace analysis.

As a stand-alone sensor, these pDPP films have the disadvantage of also responding to water in a qualitatively similar way. Like the chlorinated organic vapors, water has a very large I_P value. However, the magnitude of the resistance change to water vapor was considerably smaller than that noted for most of the chlorinated

hydrocarbon vapors (possibly due to differenced in vapor pressure of the liquids) and comparisons may be made via this response as a qualitative sensor.

An array-type sensor composed of this material may prove to be highly selective for many vapors. Incorporation of various dopants and modifying growth conditions could possibly fine tune the polymer work function and allow for the sensing of a large number of vapors.

CHAPTER 5

Chemical Locking of Single Redox Concentration Gradients in Conducting Polymers

INTRODUCTION

In this chapter, the preliminary results of the investigation into *permanently* locking a spatially defined redox concentration gradient in conducting redox polymer films are described. A few researchers have previously reported results for *physically* "locking" single and serial redox concentration gradients in redox conducting films.[119-123] In those reports, redox concentration gradients were "frozen" by thermally suppressing the ionic conductivity of the films. Using this approach, the ionic motion was sufficiently restrained on the time scale of their experiments but only under a limited range of operational conditions. We believe the limitations that exist in these thermally locked systems (vide infra) could be overcome by the method reported here.

Our work has focused on permanently fixing redox concentration gradients by chemically grafting counterions to pendant sites on customized redox polymers. Thus, limitations resulting from finite ion motion in the thermally locked gradients may be circumvented.

BACKGROUND

Electronic conduction in fixed-site redox polymers occurs by an electron hopping process between discreet redox-active sites attached to an electrochemically inactive

polymer backbone. Figure 5.1 illustrates the electron-hopping process for a redox polymer having metal ion redox-active centers. The mixed valent state of redox-active sites allows for the electronic conductivity to occur. The mixed valent sites are usually uniformly distributed throughout the film. However, it is possible to form alternative distributions of redox sites in the polymers by electrochemical means. These spatially ordered arrangements could form microstructures that impart interesting electronic properties to a polymer film. For example, diode-like electronic behavior and electrochemically-generated luminescence have been reported as a result of redox microstructure formation.[119-121]

The microstructures discussed here take the form of redox concentration gradients. Using an electrode-polymer-electrode configuration, concentration polarization of redox states can be electrochemically induced in a polymer film (Figure 5.2). The microstructure can be maintained by holding the potential bias between the electrodes or by suppressing the net ionic motion in the films via physical or chemical means. Eliminating ionic motion in the polymer films would prevent the relaxation of the redox concentration gradients.

A number of reports detail the formation and locking of redox concentration gradients in various fixed-site redox polymers.[119,120,122,123] Both single and serial redox gradients (Figure 5.2) were electrochemically generated and studied. Ionic and electronic conductivities of the films were examined for uniform non-mixed valent,

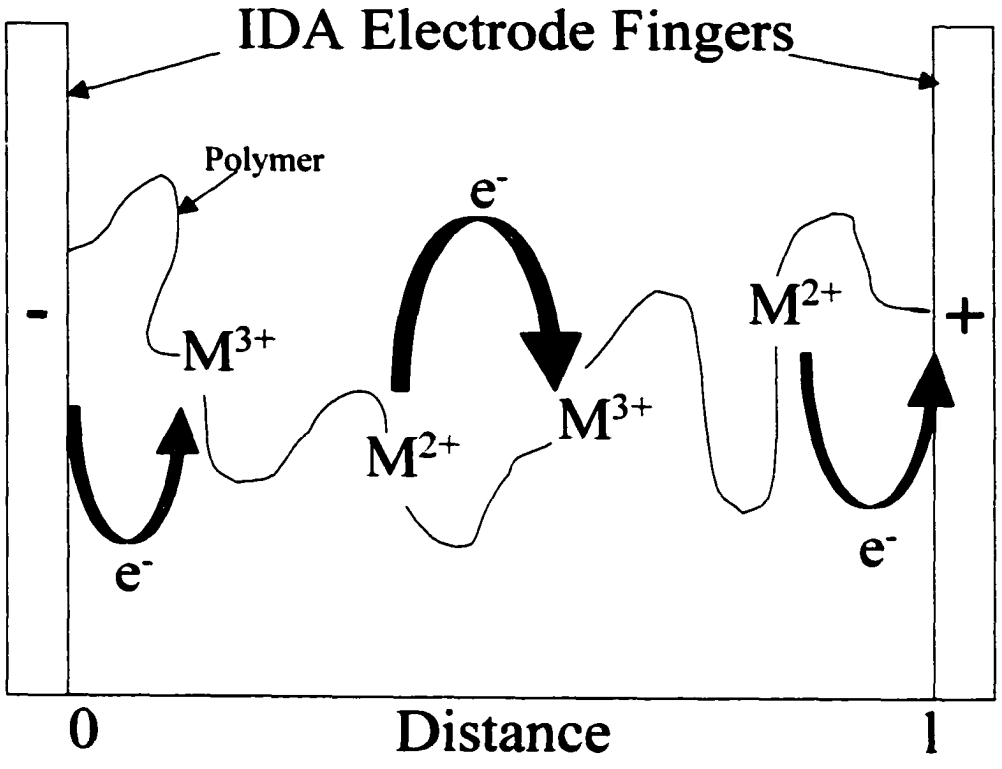

Figure 5.1. Diagram depicting the electron-hopping process in a redox polymer.

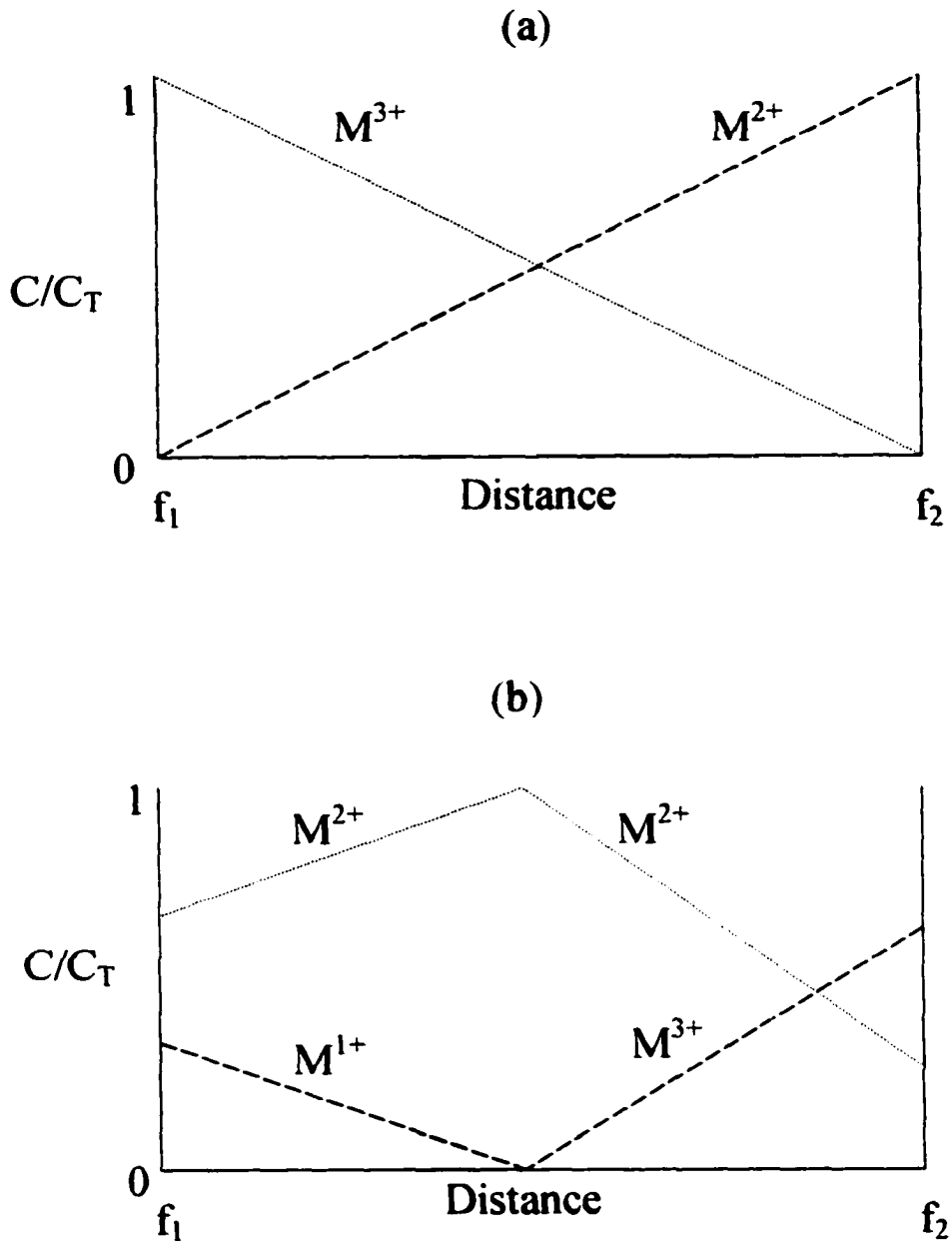

Figure 5.2. The diagrams depict the concentration gradients of the redox states in a polymer film between two fingers (f_1 and f_2) of an IDA. C/C_T is the relative concentration of the oxidized states. The dashed lines represent the concentration of the species with distance. Diagram (a) shows a single ($M^{3+/2+}$) gradient and diagram (b) shows a serial gradient for $M^{2+/1+}$ and $M^{3+/2+}$.

uniform mix valent, and mixed valent gradient states (Figure 5.3). In the solvent swollen films, both electronic and ionic conductivities were significant. Drying the films drastically reduced the measured ionic conductivity. Nonetheless, a small degree of ionic conductivity still occurred in the films. Further suppression of the ionic conductivity was achieved by modestly reducing the temperature of the films (ca. -20°C, depending on the film employed). Drying and cooling the films containing a redox gradient or gradients preserved the electronic microstructure without the need of a potential bias. This preservation of the gradients was, however, not permanent and was subject to limitations.

Terrill et al. and Maness et al. used two distinct systems of conducting redox films. One involved the use of viologen-based films.[119,120,122,123] These films were either monomeric or polymeric and the affect of a single redox gradient on the electronic properties of the films was examined. Both single and serial gradient microstructure formation and the affect they had on the properties of $Ru(bpy)_3$-based films (bpy = bipyridine) were examined in their other system.

Both the viologen-based films and the $Ru(bpy)_3$-based films demonstrated interesting electronic properties due to the concentration redox gradients. In addition, the $Ru(bpy)_3$-based films were capable of exhibiting electrochemically generated luminescence (ECL) when they possessed a serial gradient configuration (i.e., $Ru^{3+/2+}$ and $Ru^{2+/1+}$). The light emission is a result of the following reaction:

$$Ru^{3+} + Ru^{1+} \rightarrow {}^{*}Ru^{2+} + Ru^{2+} \rightarrow 2Ru^{2+} + h\nu$$

Light emission occurred from the junction of the two gradients. Degradation of the gradient results in loss of light production. Thus, the preservation of the redox

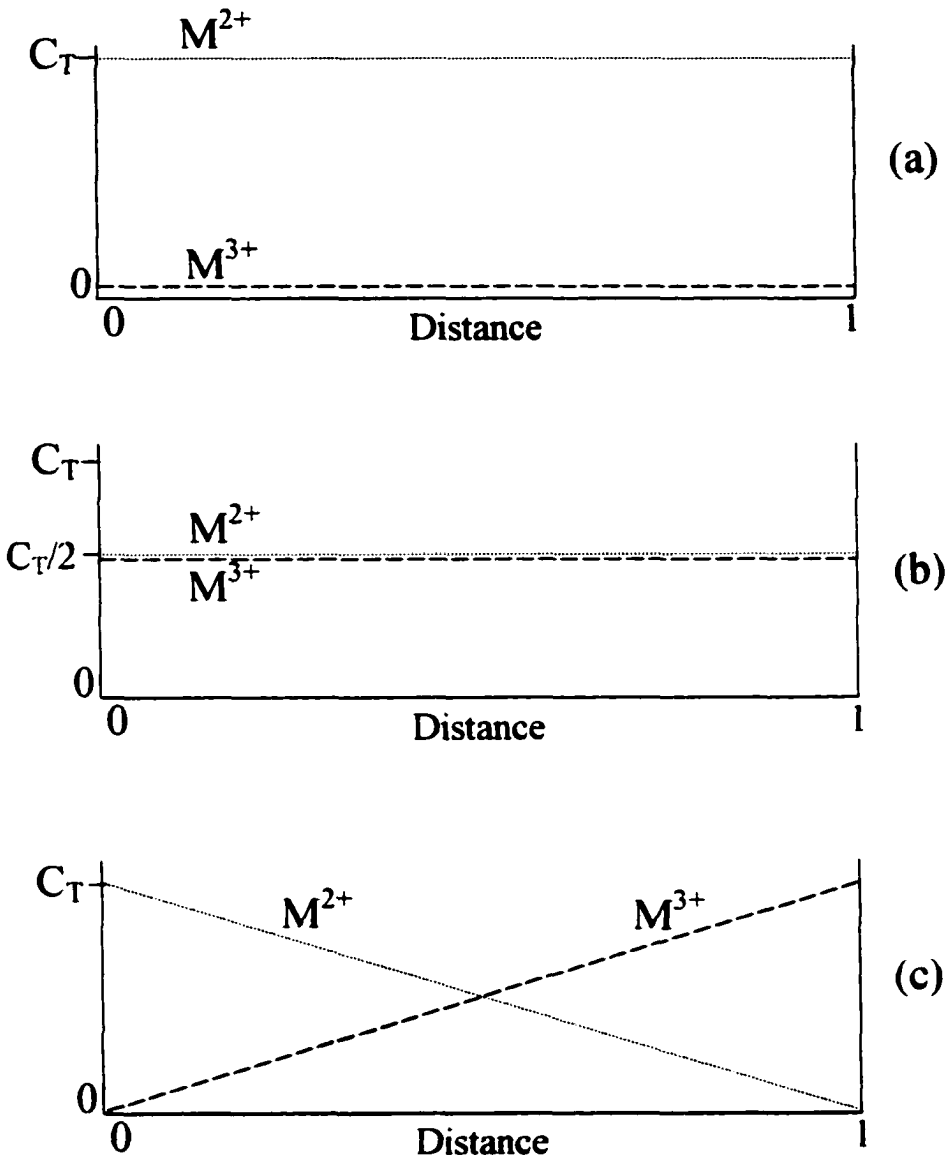

Figure 5.3. The above concentration-distance profile diagrams demonstrate spatial compositions of redox states in a redox polymer. These forms are (a) uniform, non-mixed valent, (b) uniform mixed valent, and (c) mixed valent gradient. M^{x+} indicates the oxidation state of the metal centers in the redox polymer. C_T is the total concentration of redox sites at a particular distance.

concentration gradients formed in these ECL films is integral to the development of practical light emitting devices employing these materials.[119,120] The electronic behavior of the films studied by Terrill,[122,123] Maness,[119,120] and Masuri[121] is generalized as follows. The non-mixed valent form of the polymers was not electronically conducting but solely ionically conducting due to the lack of sufficient donor and acceptor sites. The uniform mixed valent state of the films (i.e., films containing a significant population of at least two oxidation states) displayed both ionic and electronic conductivities. However, the dry, solvent-free state of the uniform, mixed-valent films has drastically suppressed ionic conductivity with respect to their electronic conductivity. If the dry film contains a preformed redox concentration gradient, the reduced ionic motion maintained the gradient under modest voltage bias (in a forward or reverse direction of the established gradients) for short times. The redox concentration gradient in a solvent swollen film relaxes to a uniform, mixed valent state without an applied potential bias. However, even dry, gradient-containing films were found to demonstrate small current hysteresis and slow transient behavior with both potential cycling and steps. This behavior has been attributed to the existence of a small degree of counterion migration that permits the occurrence of interfacial electrolysis and change in the redox concentration gradients.

Cooling of the film further suppressed the ionic conductivity of the dry films such that the gradients could be unperturbed by greater voltage bias. The dry, viologen-based films were seen to lose the current hysteresis that was indicative of minor ion rearrangement when the temperature of the film was reduced to ca. -10°C. This gave further evidence for quenching of the ionic conductivity.

Unfortunately, drying and cooling of the films were found to have limitations in maintaining the integrity of the gradients. Ionic motion and the subsequent degradation of the gradients could be induced in $Ru(bpy)_3$-based films operating under reverse bias for prolonged times (ca. 10 min.). The resulting change in the electronic behavior of th films was consistent with gradient relaxation.

Our approach to locking the redox concentration gradients utilizes unpolymerized acrylate groups on the polymer to chemically graft charge-compensating anions permanently in place once the gradient has been established. Drop cast films of the monomer solution on interdigitated array (IDA) electrodes are dried and thermally polymerized. In previous studies, it was found that cast films of a monomer similar to those used here, polymerized slowly, ca. 10 hrs at 150°C. It was determined that approximately 1.5 of the 6 acrylate groups per monomer were used in forming the polymer structure.[124] That leaves a significant portion of the pendant acrylate groups available for polymerization with incorporated polymerizable counterions.

These polymerizable anions would be electrochemically exchanged into the films by cycling the redox state of the polymer. Then, while still in the electrolyte solution, a redox concentration gradient would be formed by a potential bias applied to the combs of the IDA. After gradient formation, the film is removed from solution and allowed to dry. The gradient would be maintained in the dry film by the application of a potential bias using a bipotentiostat or a battery. While still applying the potential bias, the film would then be heated a second time. This second polymerization process would graft the incorporated anions to the polymer as well as further polymerize the film itself. The grafted anions would then permanently fix the redox concentration gradient in the film.

This gradient should be stable within the film regardless of exposure to solvents, temperature variations, and a wide range of voltage biases. In chemically grafting the anions to the polymer, limitations of thermally "frozen" redox concentration gradients should be overcome.

Certain properties were required of the polymerizable counterions. The anion must polymerize with the pendant acrylate groups on the polymer film and do so under conditions that will maintain the general structure and properties of the film. The anions chosen for use as counterions possess pendant acrylate or vinyl moieties. These functional groups should thermally polymerize with the acrylate groups on the polymer at temperatures that will not have any deleterious affect on the films. In addition, the anions must be electrochemically inactive over the potential range of the film voltammetry.

To assist in properly matching the redox behavior of the polymerizable anions with the film voltammetry, particular monomers were employed. The monomers used are shown in Figure 5.4. Monomer **I** is a trisbipyridine-based complex with a total of six polymerizable acrylate groups. The complex has a 2+ overall charge and is associated with two PF_6^- ions for purpose of charge neutrality. The PF_6^- ions can be electrochemically replaced by the polymerizable anions prior to establishing a redox concentration gradient. Employing Fe (instead of Ru) shifts the $M^{3+/2+}$ redox potential of the monomer (and the subsequently polymer films) by ca. -200 mV. The more negative the oxidation of the redox couple, the more options available with regards to selection of polymerizable anions.

Monomer **II** is a bisbipyridine-based complex. In the work here, the trans-complex of **II** is used instead of the cis-complex as the trans-complex gave qualitatively

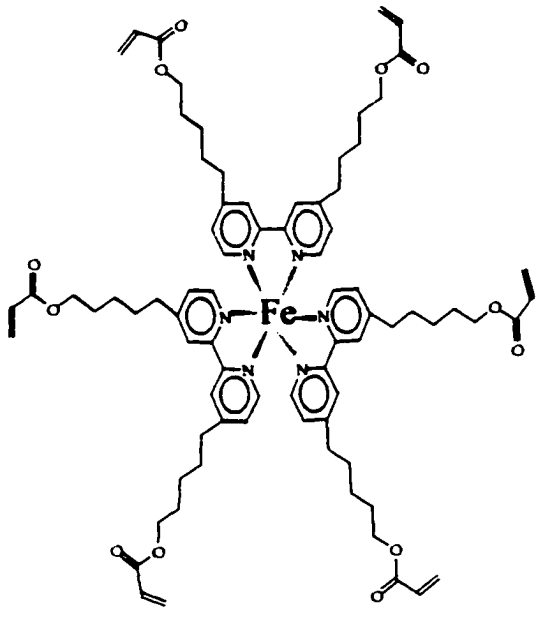

I

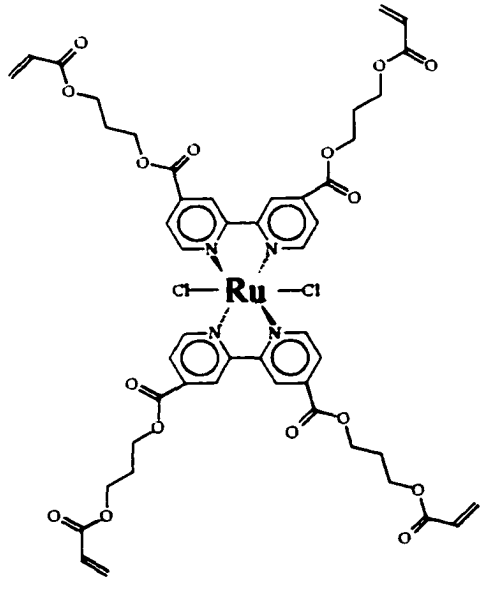

II

Figure 5.4. Structures of the (I) tris((4,4'-pentyl-1-acrylato)-2,2'-bipyridine)iron(II) and (II) bis(4,4'-dicarb((acrylatoprop-1-oxy)-2,2'-bipyridine)dichlororuthenium(II) monomers.

better film formation and film voltammetry.[103,125] Because the overall oxidation state of monomer **II** is zero, there are no associated anions that need to be exchanged prior to establishing the gradient. Instead, the polymerizable anions are incorporated during the gradient forming process.

EXPERIMENTAL

Chemicals and Equipment. A Pine Instruments RDE4 bipotentiostat, modified to provide a potential range of ±5 V, was utilized for both film voltammetry and gradient formation. A Keithley 178 digital multimeter was used in conjunction with the RDE4 to closely monitor the potentials applied to the films. Voltammetry of gradient-locked films was achieved using an EG&G Princeton Applied Research Model 173 potentiostat/galvanostat. Temperature controlled experiments were performed with a Fisher Scientific model 1013S Isotemp Refrigerated Circulator. Reagent grade (95%) ethanol was used in the circulator for temperatures below 5°C and tap water was used for temperatures above 5°C.

All chemicals used were purchased from Aldrich unless otherwise noted. 4-styrenesulfonic acid, potassium salt (KSS) and 4-styrenesulfonic acid, sodium salt (NaSS) were purchased from Polysciences, Inc. All solvents were A.C.S. grade or better. Optima grade acetonitrile was purchased from Fisher Scientific.

Synthesis of Polymerizable Electrolytes. In order to achieve a useful degree of solubility of the polymerizable anions in acetonitrile, the anions were metathesized into tetraalkylammonium salts. Acetonitrile was the solvent of choice because of its large

potential window and because the solvent readily swells the polymer films. Swelling of the films should facilitate ion transport and the incorporation of counterions.

4-styrenesulfonic acid, tetramethylammonium salt (TMASS) was prepared by ion exchange chromatography. Rexyn 101 (H^+) beads were soaked and rinsed in distilled water. After rinsing, a five-fold molar excess of tetramethylammonium hydroxide (25% w/v in water), with respect to the exchange sites on the beads, was added to the moist exchange resin. The beads were soaked in the solution for 2 hours. A column was then loaded with the beads and the aqueous solution. The loaded column was rinsed with distilled water until the pH of the effluent from the column was ca. 7. A solution of aqueous KSS was then slowly (ca. 0.5 ml/min) passed through the column and the effluent collected. Note that there was an eight-fold excess of exchange sites on the column in relation to the moles of KSS in the sample. The effluent was collected and then slowly evaporated in a large covered evaporation dish. An off-white solid remained in the dish. The collected solid was dried overnight under vacuum. The solid was recrystallized by dissolving in a minimum of hot isopropanol and allowed to cool. Once cooled to room temperature, ethyl acetate was added to solution until just cloudy. The solution was then cooled to 0°C. After ca. 12 hours, short needle-like crystals are filtered from solution and rinsed with cold ethyl acetate. NMR was used to check the purity of the TMASS. This was done by comparing the integration of the tetramethylammonium peak to the integrated values of the vinyl peaks.

Attempts at preparing tetraethylammonium, tetrapropylammonium, and tetrahexylammonium salts of 4-styrenesulfonate were also made. However, these salts

were not successfully prepared with sufficient purity to use as electrolytes because they did not crystallize from solution, but instead form yellowish oils.

Synthesis of Tetramethylammonium (3-Sulfopropylacrylate) (TMA(3-SPA)). Potassium (3-sulfopropyl acrylate) K(3-SPA) was dissolved in a minimum of distilled water. A cation exchange column of Rexyn 101 (H^+) was functionalized with TMA^+ as described above. The column contained an eight-fold excess of TMA^+ with respect to moles of K^+ in the sample. The $K(3\text{-}SPA)_{(aq)}$ solution was slowly passed through the column. The effluent was collected and rotoevaporated dry with gentle heating. A thick, slightly tan oil was left on the walls of the flask. This was dried under vacuum, leaving tan crystals on the flask walls. The TMA(3-SPA) was recrystallized by dissolving the solid in a minimum of hot ethanol/acetonitrile (50/50, v/v) and cooling to 0°C.

Synthesis of Bis(4,4'-dicarbo(acrylatoprop-1-oxy)-2,2'-bipyridine)dichloro ruthenium (II) ($Ru(4,4'\text{-}DEAB)_2Cl_2$). The synthesis of this complex was done in a manner identical to the procedure given by Schmittle for the synthesis of bis(4,4'-bis(ethoxycarbonyl)-2,2'bipyridine) dichloro ruthenium (II).[103] 45.8 g of $Ru(DMSO)_4Cl_2$, 0.42 g of LiCl, and 0.094 g of 4,4'-DEAB were dissolved in warm isopropanol. Once dissolved, the solution was heated at reflux for 3 hours. The solution turns from yellow to dark red/black. The solution was cooled to 25°C and rotovaped to dryness. The remaining dark solid was dissolved in dichloromethane and the mixture filtered to remove excess LiCl. The trans- and cis- complexes were separated using flash silica chromatography. The mobile phase was a gradient elution with dichloromethane/acetone from 100:0 to 85:15. A purple fraction (cis-complex) and a green fraction (trans-complex) were collected and rotary evaporated to dryness.

Synthesis of Tris((4,4'-pentyl-1-acrylato)-2,2'-bipyridine) Iron(II) Bis(hexafluorophosphate) ($Fe(4,4'\text{-}PAB)_3(PF_6)_2$). The synthesis is shown schematically in Scheme 5.1.

4,4'-Bis-(5-bromo-pentyl)-2,2'-bipyridine (I). In a 1.0 L three-neck flask, ca. 30 ml of dry THF was cooled with a dry ice/acetone bath. The flask was purged with N_2. 7.8 ml (0.056 moles) of diisopropylamine was syringed into the flask and allowed to cool. After about 30 minutes, 28.0 ml of N-butyllithium (2.0M in cyclohexane, 0.056 moles) was syringed into the solution in the flask and cooled for 30 minutes. 5.01 g (0.0273 moles) of 4,4'-dimethyl-2,2'-bipyridine (4,4'-DMB) was dissolved in ca. 350 ml of dry THF and added drop-wise under nitrogen to the cooled lithium diisopropylamide solution. The solution in the three-neck flask turned dark red. The solution was stirred for 2 hours while cooled with a dry ice/acetone bath. After two hours, 13.0 ml of 1,4-dibromobutane (purged with N_2) was quickly syringed into the solution. The solution was continuously stirred and the temperature maintained with a dry ice/acetone bath for two hours before warming to room temperature whereupon it was stirred under N_2 for an additional 12 hours. Over the course of the reaction, the solution turned from a dark red to a light yellow upon warming.

The yellow solution was rotoevaporated to dryness; yielding a tan solid. The bromoalkylated product (**I**) was extracted into dichloromethane and the salts into water. The volume of the dichloromethane solution was reduced on a rotoevaporator until a tan slurry was obtained. Warm ether was added to the slurry and stirred. The mixture was filtered and the white filtrate was rinsed 2 times with ether. The filtrate was rotoevaporated to dryness. The remaining solid was washed three times with a total of

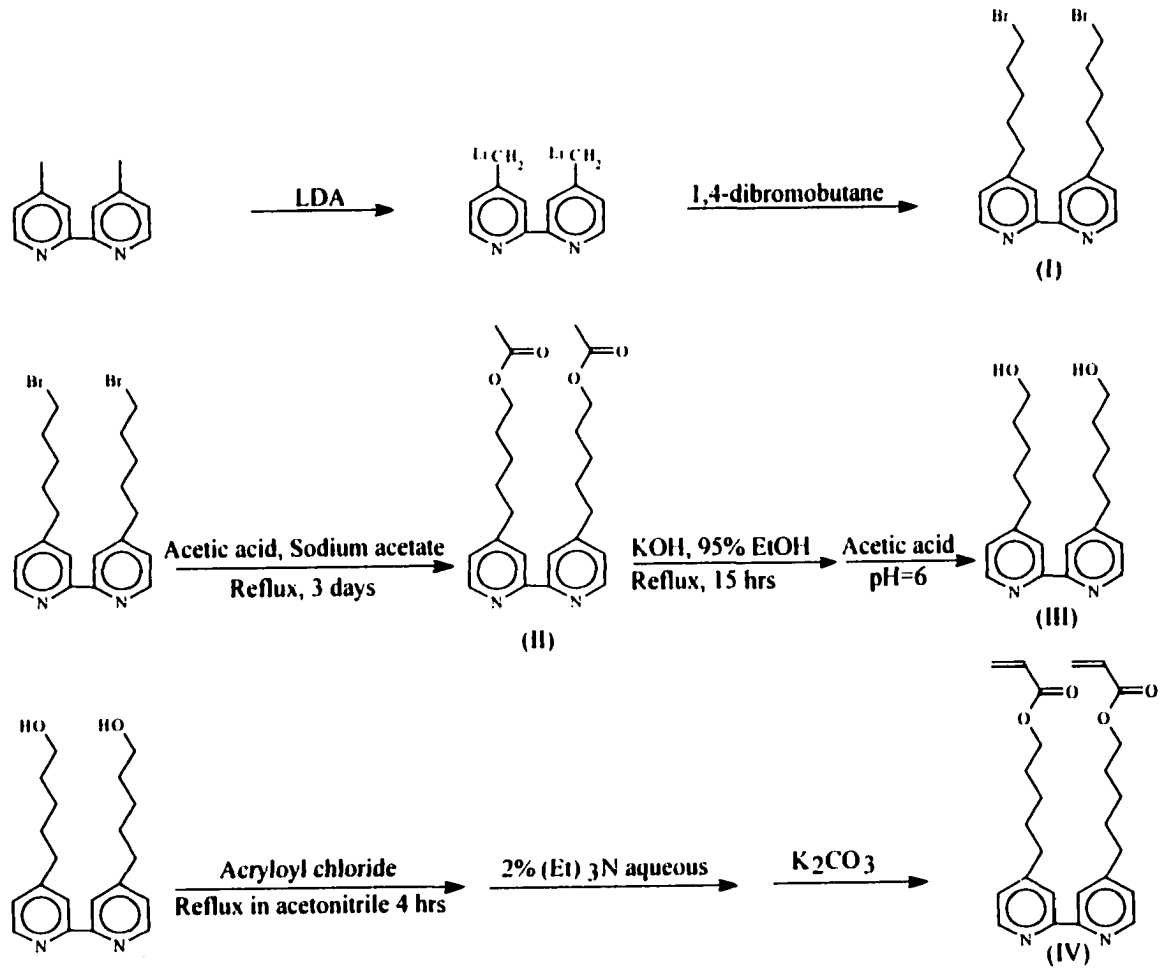

Scheme 5.1. Synthesis of 4,4'-PAB ligand.

ca. 250 ml of hexane. The hexane fractions were decanted off the brown oily solid and collected. The volume of the hexane solution was reduced by rotoevaporation until a white solid appeared. The flask was then placed in a NaCl/ice water bath. Cooling the solution produced a white precipitate. The mother liqueur was decanted off and filtered through a cooled frit into a round bottom flask. More hexanes were added to the white precipitate and the solution heated to dissolve the solids and then cooled again in an ice bath. This was repeated two more times. Approximately half of the hexane solution was rotoevaporated; leaving an oily slurry (**I**) in the flask.

Acetic acid 5-[4'-(5-acetoxy-pentyl)-2,2'-bipyridinyl-4-yl]-pentyl ester (**II**). The oily slurry (**I**) was dissolved in glacial acetic acid (Malinckrodt) and ca. 6 g of sodium acetate added to the solution. The solution was heated to reflux and stirred under N_2 for 72 hours. This solution turned orange and fine, white solids were in the flask. The white solids dissolved upon addition of 200 ml of distilled water to the solution. Ammonium hydroxide (Malinckrodt) was then added to the solution until pH = 5. Dark brown oil formed in the flask. The solution and oil were transferred to a separation funnel. The oily brown product was extracted from the aqueous solution into dichloromethane. The extraction was complete when the aqueous layer became clear. The dichloromethane solution was rotoevaporated until ca. 20 ml of brown oil remained. The product (**II**) was partially isolated by liquid chromatography (silica gel, 10% acetone/dichloromethane). The collected fractions were combined and rotoevaporated down until a pale yellow oil remained. The oil was dissolved in hexanes and cooled to 0°C; forming fine crystals. NMR verifies the solid was the desired product (**II**). ^{1}H NMR (δ in ppm from TMS,

$CDCl_3$; multiplicity, integration): 1.4(m, 5H); 1.7(m, 9H); 2.0(s, 5H); 2.7(t, 4H); 4.1(t, 3H); 7.2(d, 2H); 8.3(s, 2H); 8.6(d, 2H).

5-[4'-(5-Hydroxy-pentyl-2,2'-bipyridinyl-4-yl]-pentan-1-ol (**III**). The diacetate product (**II**) was dissolved in 300 ml of 95% ethanol with a molar excess of KOH. The solution was heated to reflux and stirred under N_2 for 15 hours. The pH of the cooled solution was neutralized to pH 6 with addition of glacial acetic acid (Malinckrodt). This solution was then rotoevaporated dry. A white solid (**III**) remained in the flask.

Acrylic acid 5-[4'-5-acryloyloxy-pentyl)-2,2'-bipyridinyl-4-yl]-pentyl ester (**IV**). 300 mg of (**III**) was added to 150 ml of acetonitrile and stirred under N_2. An excess of acryloyl chloride (8 ml) was syringed into the solution, which was then heated at reflux for 4 hours. The solution was rotoevaporated to obtain a dark brown, oily solid. 100 ml of 2% (v/v) triethylamine in water was added, and extracted 4 times with dichloromethane. The combined dichloromethane extractions were rotoevaporated to ca. 15 ml. The product (**IV**) was isolated by liquid chromatography (silica, 5-15% acetone/dichloromethane). The solutions were rotoevaporated dry and the product (**IV**) identified by NMR. ^1H NMR (δ in ppm from TMS, $CDCl_3$; multiplicity, integration): 1.5(m, 4H); 1.7(m, 8H); 2.7(t, 4H); 5.9(m, 2H); 6.1(m, 2H); 6.4(m, 2H); 7.2(d, 2H); 8.3(s, 2H); 8.6(d, 2H).

Tris-[acrylic acid 5-[4'-(5-acryloyloxy-pentyl)-2,2'-bipyridinyl-4-yl]-pentyl ester] iron(II) hexafluorophosphate. The $Fe(II)((4,4'\text{-}PAB)_3(PF_6)_2$ complex was prepared by dissolving ca. 4 mg of the ligand (**IV**, Scheme 5.1) in a minimum of ethanol. A two-fold molar excess of an aqueous solution of $Fe(II)(NH_4)_2(SO_4)_2$ was added dropwise to the ethanol solution. To this red solution, an excess of NH_4PF_6 (aq) was added. The

complex was extracted into dichloromethane until the aqueous layer was clear. Rotoevaporating off the dichloromethane resulted in the iron complex.

Cells and Electrodes. For all electrochemical experiments, a single compartment cell was used and a three- or four-electrode configuration was employed. For temperature controlled experiments using the Isotemp Refrigerated Circulator, a jacketed single compartment cell was used to house the film-coated electrode.

The IDA working electrodes were purchased from Abtech Scientific, Inc. The electrodes were platinum on a glass substrate (Figure 5.5b). A variety of arrangements were obtained which have different gap widths between fingers, different finger lengths, and a different number of fingers. The finger height for all the IDAs was reported to be 0.10 μm. A number notation gives the physical arrangement for a certain IDA. For example, the numbers 0525.3 denote that the IDA has a 5 μm gap between fingers, there are 25 fingers on each comb (50 fingers total make up the IDA), and the fingers are 3 mm in length. All the IDAs used in these studies had a finger width of 5 μm. The above number notations will identify IDA configurations when necessary. A clip produced in our lab accomplished electrical contact to the IDAs. Figure 5.5a shows the design and construction of the clip. A Ag/Ag^{+}(0.10M $AgNO_3$, DMSO) reference electrode made in our lab was used in all electrochemical experiments unless otherwise stated. The auxiliary electrode was a platinum wire. In all solution voltammetry experiments conducted on polymer films deposited on IDA electrodes, the two sets of fingers were shorted together unless otherwise noted.

Film Formation. Films of the redox monomers were drop cast onto the working electrodes. Monomer solutions were added dropwise to an electrode surface and the

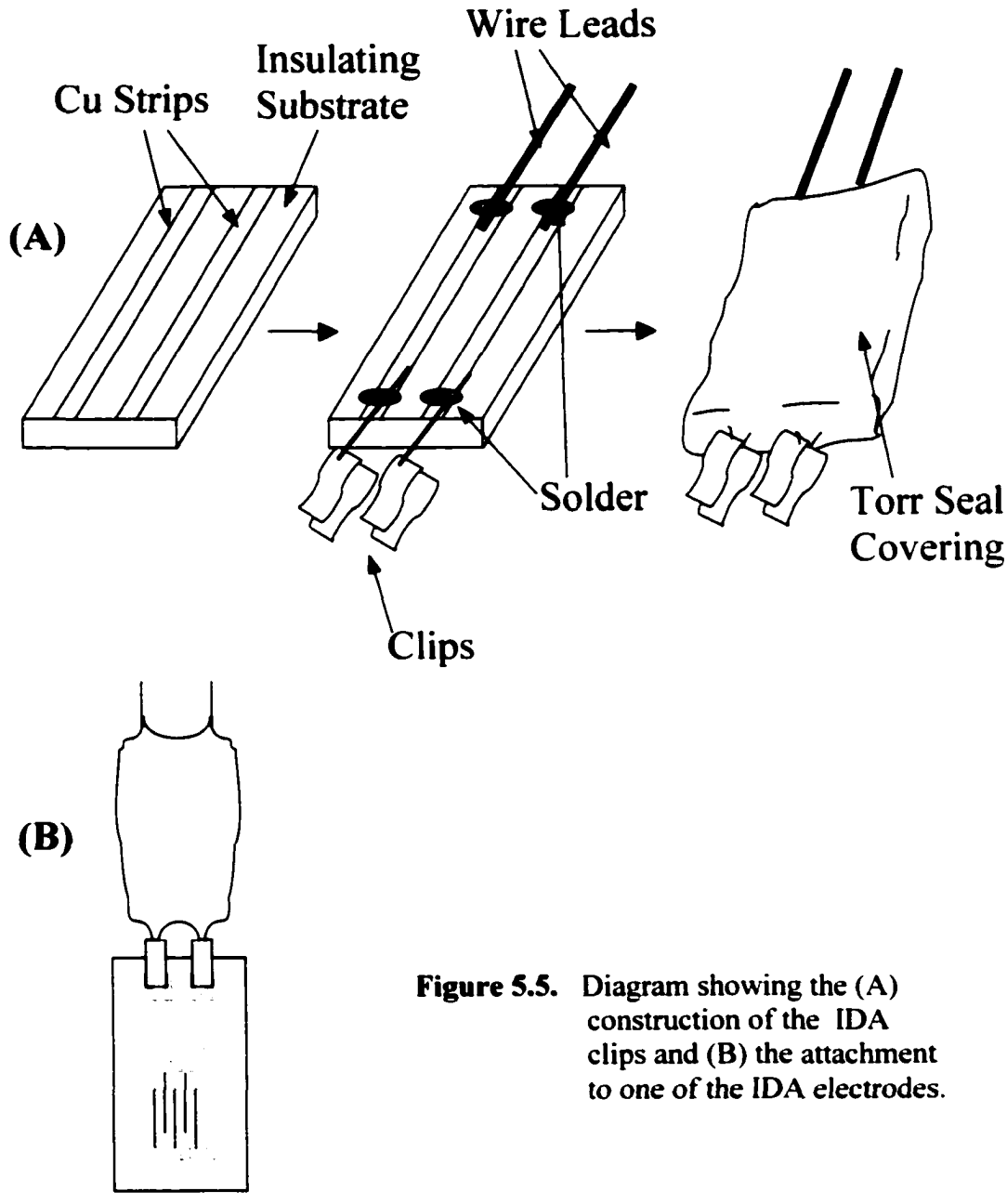

Figure 5.5. Diagram showing the (A) construction of the IDA clips and (B) the attachment to one of the IDA electrodes.

solvent allowed to evaporate at room temperature. The electrodes were kept covered during the evaporation process to prevent incorporation of foreign particles into the film. Once dry, a thin film of monomer covered the electrode. A thicker region of monomer typically surrounded the film, as was often seen with drop cast films. Repeating the above process produced thicker films.

To minimize the presence of solid contaminants, the monomer was first dissolved in dry acetonitrile and filtered through a Whatman 0.1 μm TF syringe filters having polypropylene casings. This acetonitrile solution was rotoevaporated to dryness for use with the desired casting solvent. Solvents for the monomer solutions were dried over molecular sieves and filtered through alumina prior to use. This method was found to provide clean casting solutions that produced films with good uniformity.

Monomer films were thermally polymerized. Given the high number of acrylate groups on each monomer, the films should ready crosslink. The degree of polymerization was crucial for producing a quality film. If the film was overly crosslinked, it exhibits minimal redox activity (if any) due to hindered movement of counter ions within the film. This situation would make redox gradient formation in the films difficult. Conversely, if the film was not sufficiently polymerized, it would dissolve either during the rinsing process or during attempts to perform electrochemistry.

Gradient Formation in Polymer Films. After electrochemically exchanging one of the vinyl-containing anions into a redox polymer film on an IDA electrode, a single $M^{3+/2+}$ (where M = Fe or Ru) redox gradient was established. Using a bipotentiostat, one channel applied a potential to maintain a reduced state of the film around that finger set. The second channel was then cycled or stepped out to a potential

that was more oxidative than the $E_{1/2}$ of the film on the IDA. The potential difference between channel one and channel two ranged between 500 and 800 mV, depending on the reduction potential applied to channel one and the particular film and electrolyte/solvent system used. While maintaining the potential difference, the current response at each set of fingers on the IDA was monitored. The film remained in solution with the applied potential difference until the current measured at each comb reached a steady state. The time to reach steady state was typically between 15 and 30 minutes.

Upon reaching steady state, the film was removed from the electrolyte solution. The potential bias was still maintained between the combs of the IDA. The film and electrode were rinsed with the solvent used in establishing the gradient. Excess solvent was removed from the electrode by dabbing the edge of the IDA with a Kimwipe. The film was then allowed to air dry.

When dry, the electrical connections to the electrodes were transferred from the bipotentiostat to a 1.5 V battery so that the electrode could be moved as needed without relaxation of the redox gradient. The large potential drop between the combs when attached to the battery was theoretically large enough to maintain the gradients, but not large enough to cause any electrochemistry on the dry films.

Visual examination of the gradient was accomplished with an optical microscope. The films were inspected for color variations around the fingers of the IDA. Color variations are expected upon formation of a redox gradient because the reduced and oxidized forms of the film are different colors.

Locking of Redox Gradients. Films containing polymerizable anions and having a visible redox gradient were polymerized in a vacuum oven at temperatures

sufficient to thermally co-polymerize the incorporated counter anions with the free acrylate sites on the polymer. The polymerization was carried out with the 1.5 V battery attached to the IDA to maintain the potential bias across the film.

Initial attempts to lock the concentration gradient of anions in the film involved placing the IDA, battery, and connecting wires in a large beaker and placing the whole assembly in the vacuum oven. This proved to be a viable option for many of the experiments. However, occasionally the battery leaked during heating. Later gradient-locking polymerizations made use of a thin copper bus that allowed for the battery to remain outside of the vacuum oven.

After attempting to lock the gradient via thermal polymerization, electrodes were removed from the oven and allowed to cool to room temperature on the bench top. The external potential was applied throughout the process. Once cool, the films were examined again under the microscope to visually note changes in the redox gradient. The battery was removed and the films were connected to the bipotentiostat for analysis of their electrical behavior (i.e., voltammetry, resistance, etc.).

RESULTS

Casting Films of $Fe(4,4'\text{-}PAB)_3(PF_6)_2$. Solutions of the monomer in acetonitrile drop cast onto the surface of a working electrode and allowed to dry in the air produced smooth and glassy looking films. They were translucent, red, and appeared to be quite uniform in thickness with the exception of a thicker ring of material around the periphery of the film, as mentioned above. The monomer solution concentration was typically ca. 10 mM and films were deposited with one or two drops of the monomer solution

dispersed from a disposable pipette. This proceedure produced thin films that covered the active electrode area.

In some cases, monomer films were seen to bead up on the electrode as the solution dried. Using thoroughly dried monomer solutions and IDAs greatly improved the quality of the cast films. Uniform films were cast onto glassy carbon, indium tin oxide-coated glass, platinum IDA's on glass, and glass slides.

Casting Films of $Ru(4,4'\text{-}DEAB)_2Cl_2$. Solutions of the monomer were prepared between 10 and 15 mM in 1,2-dichloroethane. Dichloromethane was also used, but the resulting films were not as smooth or uniform as those obtained from solutions of 1,2-dichloroethane. Films cast from dichloromethane solutions had a tendency to pool up and bead during evaporation of the solvent (probably due to water condensation due to evaporative cooling). This was often eliminated by tilting and rolling the electrode as the solvent evaporated. This tilting procedure was not needed when using solutions of 1,2-dichloroethane.

Acetonitrile solutions were found to produce films of very poor quality. These films almost always beaded up upon solvent evaporation: even with tilting and rolling of the electrode as the solvent evaporated.

Dry $Ru(4,4'\text{-}DEAB)_2Cl_2$ films were green-black and had a smooth, glossy appearance. Like the $Fe(4,4'\text{-}PAB)_3(PF_6)_2$ films, the $Ru(4,4'\text{-}DEAB)_2Cl_2$ monomer films had a thicker ring of material around the edge of the film, while the center portion of the films appeared to be rather uniform in thickness.

Initial Film Polymerization. The conditions employed for monomer polymerization were determined by trail and error. Optimum conditions were achieved

with film polymerization taking place in a vacuum oven at reduced pressure. For $Fe(4,4'\text{-}PAB)_3(PF_6)_2$ films, the oven temperature was 70°C and the duration of the polymerization was ca. 2 hours. The resulting films adhered to the working electrodes in solution and they demonstrated good voltammetry. The $Ru(4,4'\text{-}DEAB)_2Cl_2$ films formed best if polymerized at 80°C for 6 to 7 hours. The different time and temperature required for producing polymer films from the two monomers might be a result of differences in the ligand structure and the number of polymerizable functionalities on each.

After successful film formation in the vacuum oven, the electrode and film were rinsed with solvent to remove unpolymerized material and to ensure that the film had sufficiently polymerized. Rinsed films were then air dry on the bench top for 12 hours. Inspection after drying was imperative as cracks occasionally formed in the films. The films on IDA electrodes were considered usable for gradient formation as long as the cracks did not extend over the fingers.

Attempts at using a conventional oven (i.e., at atmospheric pressure) for the initial film polymerization did not yield usable films. Temperatures between 70 and 170°C were used for durations lasting between one to four hours. In all such attempts, the films were found to pool up and/or bead up on the electrodes during the heating process. The thick beaded material remaining on the electrode would either wash away completely from the IDA when rinsed with solvent (i.e., water or acetonitrile) or else they would be over polymerized and not display any electrochemistry when cycled in an appropriate electrolyte solution.

Polymerization of the monomer film using a UV light source also proved unsuccessful. Films were placed in a glass cell having a quartz window to allow exposure to the UV radiation. The chamber was continually purged with N_2 to minimized film heating from the UV source. In every attempt, insufficient polymerization appeared to have occurred as the film material washed off of the electrode during the rinsing process. Even films that were exposed to the UV radiation for 12 hours were still soluble.

Cyclic Voltammetry of Fe(4, 4'-PAB)$_3$(PF$_6$)$_2$ Polymer Films in Solutions Containing TBAPF$_6$. Figure 5.6 shows a typical voltammogram of a Fe(4, 4'-PAB)$_3$(PF$_6$)$_2$ film in 0.1 M TBAPF$_6$/acetonitrile. The magnitude of the current response was large and the redox behavior stable. The magnitude and reversibility of the current response suggest facile transport of counterions in the film. The voltammetry in Figure 5.6 is for a film cast onto a platinum IDA electrode. Identical voltammetry was noted for films on carbon disk electrodes.

Cyclic Voltammetry of Fe(4, 4'-PAB)$_3$(PF$_6$)$_2$ Polymer Films in Solutions Containing a Polymerizable Anion. Initially, styrenesulfonate (SS^-) anion seemed to be a plausible candidate for locking redox gradients in the Fe(4, 4'-PAB)$_3$(PF$_6$)$_2$ films. The anion was an optimistic choice due to its relatively small size and the possibility of co-polymerizing its pendant vinyl group with the unreacted acrylate groups within the polymer. Unfortunately, the anion underwent an irreversible oxidation in the same potential region as the films' $Fe^{3+/2+}$ redox process. Since it is necessary that the anions

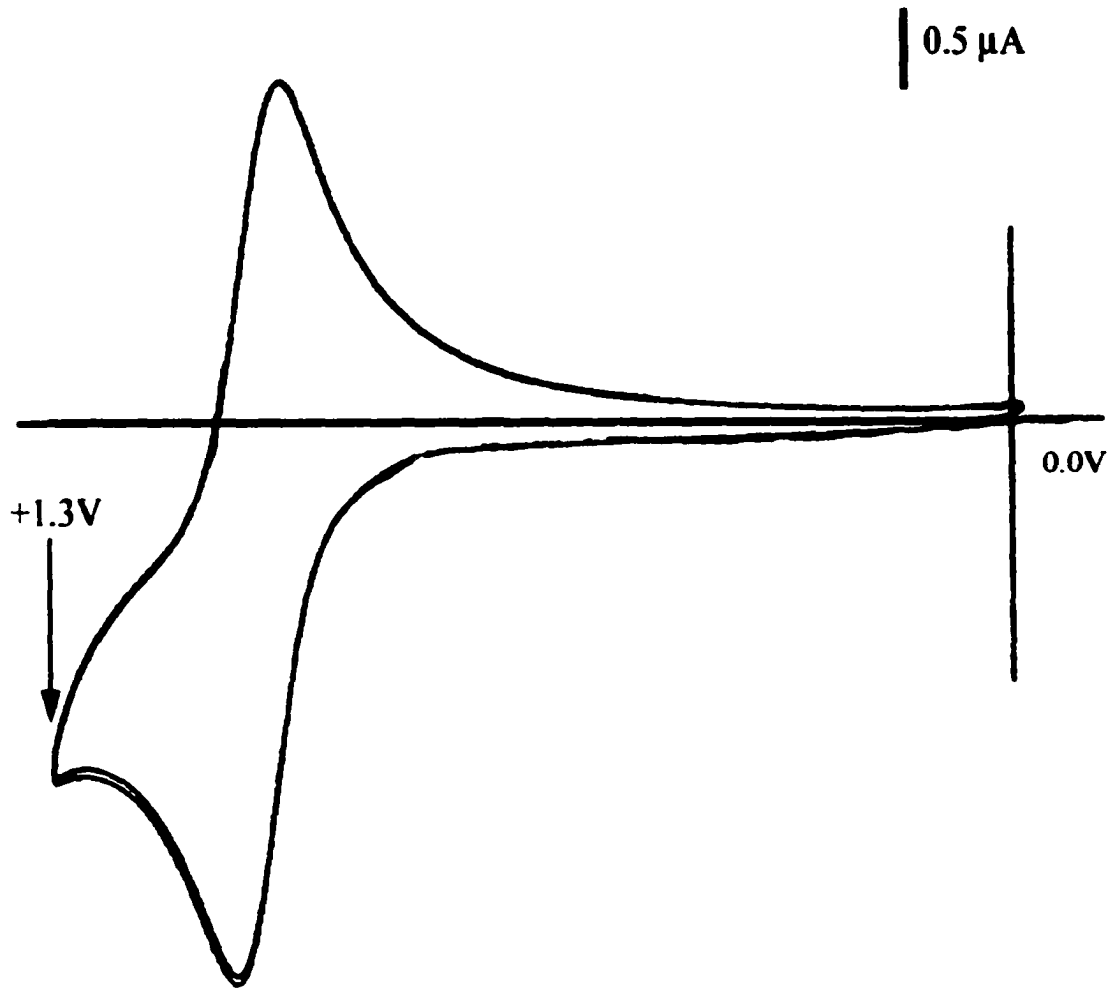

Figure 5.6. Cyclic voltammogram of a $Fe(4,4'\text{-}PAB)_3(PF_6)_2$ film on a 0550.5 platinum IDA electrode cycled in a 0.1M $TBAPF_6$/acetonitrile solution. Scan rate was 50mV/s.

be electrochemically inactive at potentials needed to form the redox gradient, the SS^- anion was deemed unsuitable for use with the $Fe(4,4'\text{-}PAB)_3(PF_6)_2$ films.

Another anion investigated was 3-sulfopropyl acrylate (3-SPA). The background voltammetry of TMA(3-SPA) in acetonitrile gave no indication of redox chemistry out to a potential of ca. +1.7 V vs Ag/Ag^+ (0.10M $AgNO_3$, DMSO). Given the $E_{1/2}$ of +1.02 V for the $Fe(4, 4'\text{-}PAB)_3(PF_6)_2$ films, the 3-SPA anion should be incorporated into the film without undergoing redox chemistry. The acrylate functionality on the counteranion should then readily polymerize with the remaining acrylate functionalities on the polymer.

It turns out that the incorporation of 3-SPA anions into $Fe(4,4'\text{-}PAB)_3(PF_6)_2$ films is not so straightforward. Figure 5.7 shows a voltammogram of an $Fe(4,4'\text{-}PAB)_3(PF_6)_2$ film cycled in a 70 mM solution of TMA(3-SPA) in acetonitrile. On the initial anodic potential sweep, a large oxidation peak can be seen with a maximum at ca. +1.0 V. Essentially no cathodic peak was noted on the return scan. Following scans show a considerable decrease in the anodic current with each scan and no evidence of any cathodic current. The $Fe(4,4'\text{-}PAB)_3(PF_6)_2$ films cycled in the TMA(3-SPA)/acetonitrile solution apparently undergo an irreversible process that hampers further voltammetry. However, the film did not show any significant changes noticeable by viewing with a microscope to indicate any change in oxidation state of the film. Similar behavior was observed for films on glassy carbon electrodes.

Two possible processes were considered to explain the diminishing film voltammetry seen in Figure 5.7. The first is the irreversible incorporation of the anions into the film. This may be due to the physical "entrapment" of the anion by the polymer

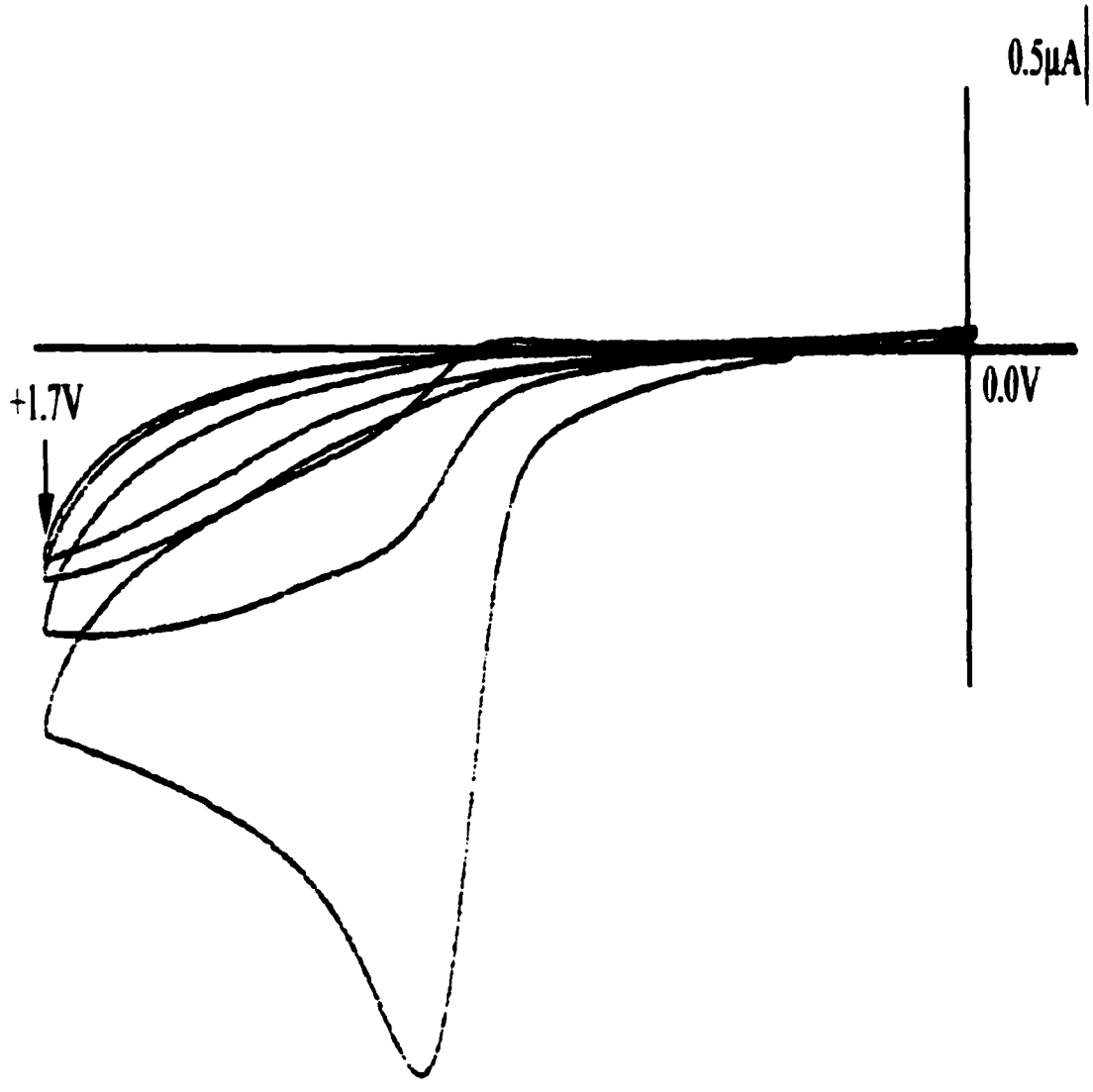

Figure 5.7. Cyclic voltammogram of a $Fe(4,4'\text{-}PAB)_3(PF_6)_2$ film cycled in a 70mM TMA(3-SPA)/acetonitrile solution. Scan rate was 50mV/s.

structure of the film. The second possibility was that of a chemical or electrochemical reaction of the anion with the polymer that passivated the voltammetry (i.e., polymerization of the anion with acrylate sites on the polymer or an activated chemical process due to the presence of the film). Since the background voltammetry of the anion gave no sign of any significant redox chemistry, the likelihood of electrochemical process between the anion and the film seemed doubtful.

Voltammetry of the TMA(3-SPA) electrolyte and the $Fe(4,4'\text{-}PAB)_3(PF_6)_2$ monomer together in acetonitrile was investigated for any chemical or electrochemical process that would result in passivation of the $Fe^{3+/2+}$ redox behavior. The voltammograms in Figure 5.8 clearly show the stable and reversible voltammetry of the monomer. That the voltammetry of the monomer was not affected by the presence of the TMA(3-SPA) suggests no chemical or electrochemical interaction caused decay of the $Fe(4,4'\text{-}PAB)_3(PF_6)_2$ film voltammetry shown in Figure 5.7. We speculate that changes in the physical structure of the film affected the voltammetry; that is, ion transport was sterically hindered in the films. The decaying current response and the increasing separation of the peak potentials may have been due to sterically induced ion and charge trapping in the polymers.

Changing the solvent in which an electroactive polymer is cycled has been reported to have a profound effect on the film voltammetry.[40] This was also found to be the case with the $Fe(4,4'\text{-}PAB)_3(PF_6)_2$ films. These films were cycled in solutions of TMA(3-SPA)/water instead of TMA(3-SPA)/acetonitrile. The film voltammetry gave both oxidation and reduction peaks without any significant current decay with extended cycling. However, the voltammetry showed a large peak separation and there was a

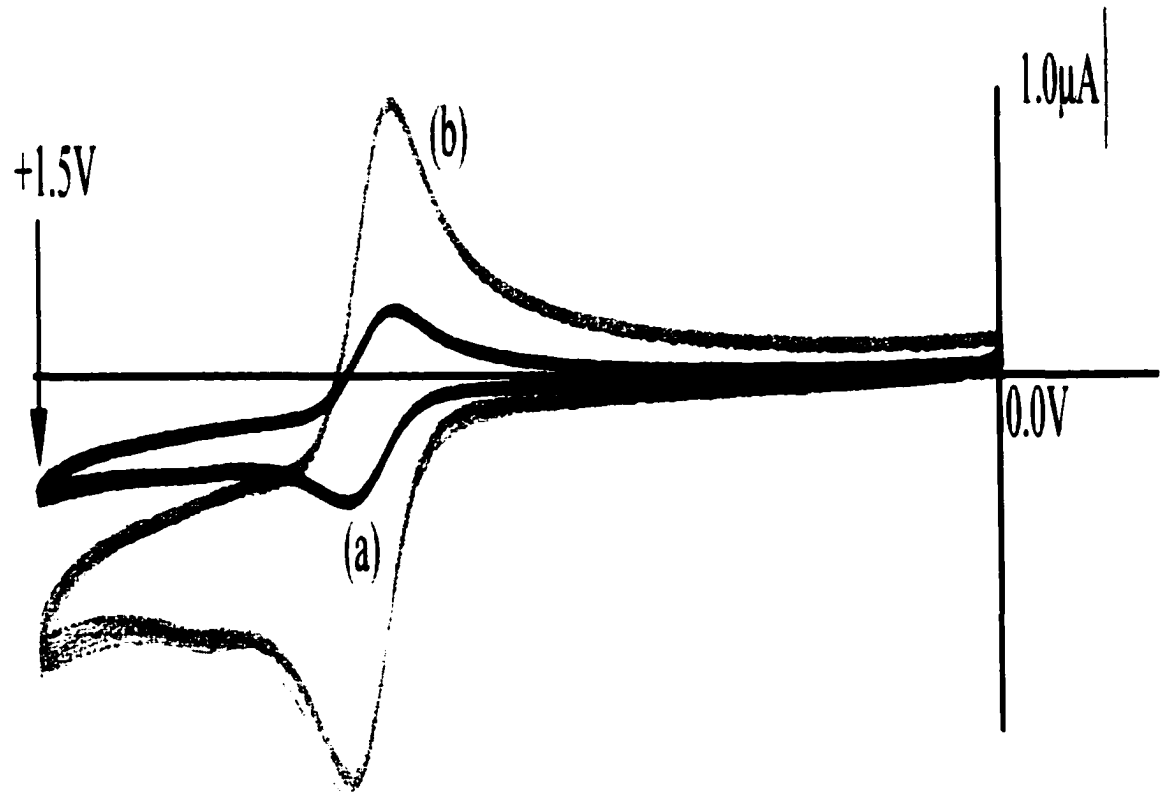

Figure 5.8. Cyclic voltammograms of (A) a bare platinum button electrode (area = 0.071cm^2) and (B) a bare glassy carbon button electrode (area = 0.28cm^2) cycled at 50mV/s in a Fe(4,4'-PAB)$_3$(PF_6)$_2$ monomer/TMA(3-SPA)/acetonitrile solution.

hysteresis or "crossover" in the oxidation peak (Figure 5.9a). This type of behavior typically results from variable kinetics in the electron transport in the film, possibly due to variations in the characteristics of the films. Slowing the scan rate of the experiment from 50 mV/sec to 10 mV/sec eliminated the "crossover". The peak separation, however, remained very large (ca. 200 mV).

The addition of ca. 5% acetonitrile to the aqueous TMA(3-SPA) solution slightly decreased the ΔE_p (ca. 80 mV) and allowed the use of slightly faster scan rates (20 mV/sec, Figure 5.8b). Addition of acetonitrile did not appear to have any adverse effects on the film voltammetry.

Transferring films that gave stable voltammetric responses in the TMA(3-SPA)/water solutions into a TMA(3-SPA)/acetonitrile solution resulted in decaying voltammetry similar to that shown in Figure 5.7. The original voltammetry could not be revived even upon transfer back to a TMA(3-SPA)/water solution or to a TMA(3-SPA)/water/acetonitrile solution. Gradient locking experiments using the Fe(4, 4'-PAB)$_3$(PF$_6$)$_2$ films were thus performed in the aqueous/acetonitrile solutions containing the 3-SPA anion.

Cyclic Voltammetry of Ru(4,4'-DEAB)$_2$Cl$_2$ Polymer Films in Solutions Containing TBAPF$_6$. Figure 5.10 shows the voltammetry of a typical Ru(4,4'-DEAB)$_2$Cl$_2$ film cycled in TBAPF$_6$/acetonitrile. The current response is large, stable, and reversible. This behavior was noted for films on both glassy carbon and platinum IDA electrodes. The $E_{1/2}$ of the $Ru^{3+/2+}$ couple is +675 mV vs Ag/Ag^+ (0.10 M $AgNO_3$, DMSO). This value is ca. 350 mV more negative than the $E_{1/2}$ of the $Fe^{3+/2+}$ couple in the

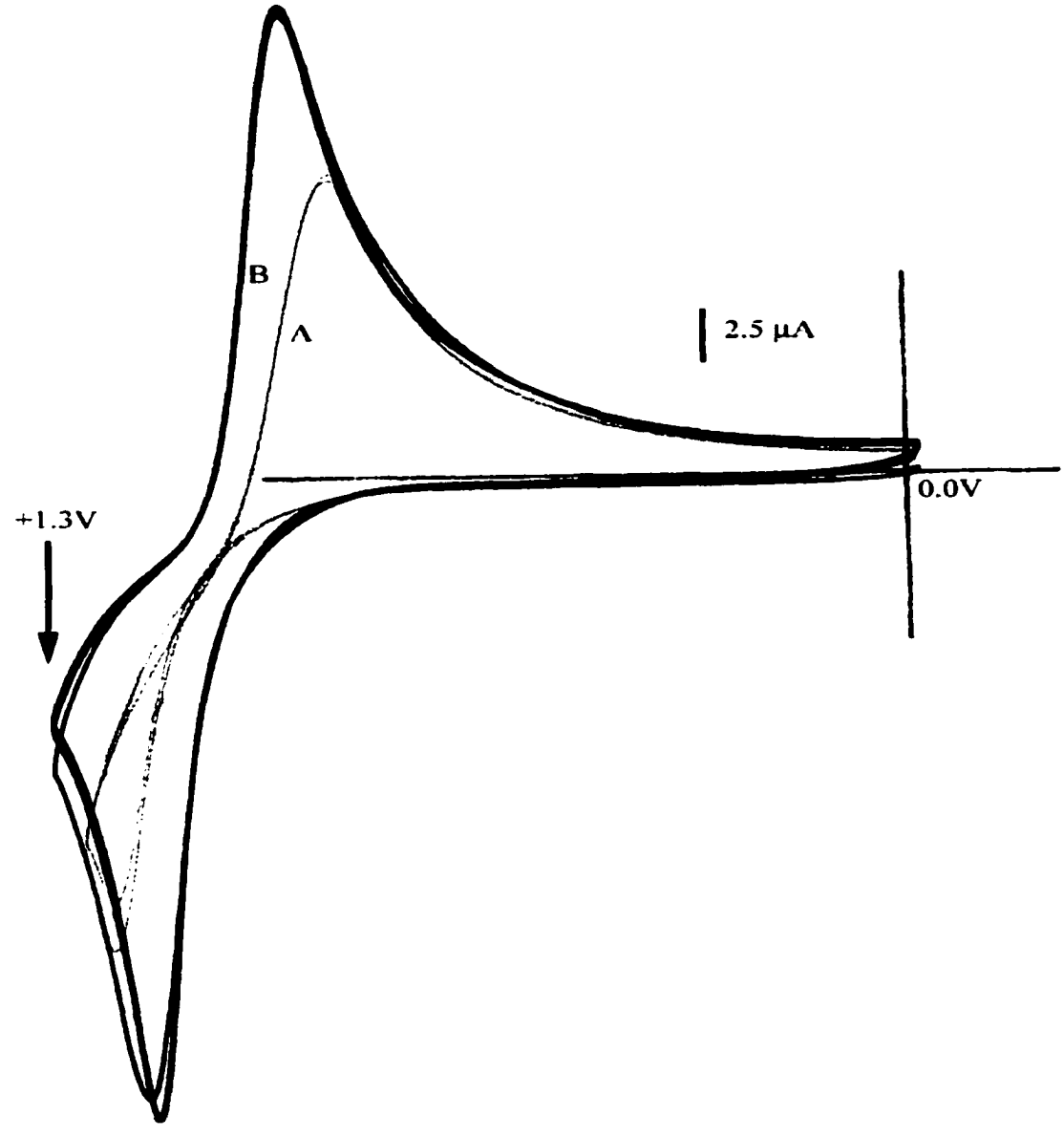

Figure 5.9. Cyclic voltammograms of $Fe(4,4'\text{-}PAB)_3(PF_6)_2$ films on glassy carbon button electrodes. One film (A) was cycled in 0.10M TMA(3-SPA)/water and in the other (B) was cycled in TMA(3-SPA)/water/acetonitrile (70:30, v/v). Note the "crossover" in the current response for the oxidation peak in plot A. The scan rate for both voltammograms was 20mV/s.

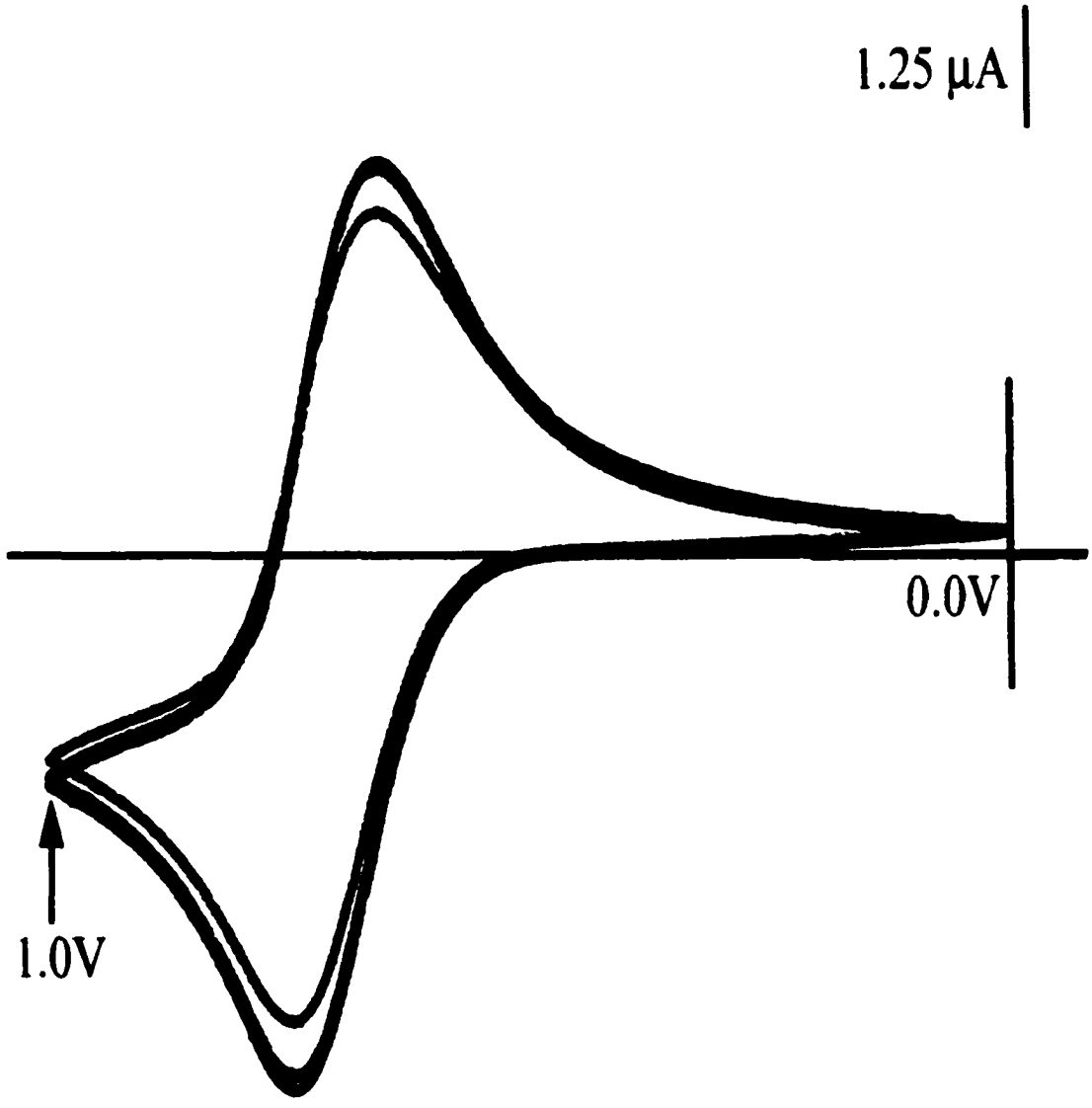

Figure 5.10. Cyclic voltammogram of a $Ru(4,4'\text{-}DEAB)_2Cl_2$ film cycled in a 0.1M $TBAPF_6$/acetonitrile solution. The film was cast onto a 0525.3 platinum IDA. The scan rate was 50mV/s.

$Fe(4,4'\text{-}PAB)_3(PF_6)_2$ films, which make it negative enough for SS^- anion to be a viable option for use as a polymerizable anion to lock a $Ru^{3+/2+}$ redox gradient.

Cyclic Voltammetry of $Ru(4,4'\text{-}DEAB)_2Cl_2$ Polymer Films in Solutions Containing 4-Styrenesulfonate. The voltammetry of a $Ru(4,4'\text{-}DEAB)_2Cl_2$ film in TMASS/acetonitrile is shown in Figure 5.11. Although there was a slight decay in the film current with time, the voltammetry was stable on the time scale of the experiments (ca. 15 min.) in these studies. The SS^- anion appeared to readily and reversibly pass into and out of the $Ru(4,4'\text{-}DEAB)_2Cl_2$ films.

The $Ru(4,4'\text{-}DEAB)_2Cl_2$ films were also cycled in solutions of KSS in DMSO/acetonitrile (70:30, v/v). Because of its ready solubility in DMSO and the DMSO/acetonitrile solution, KSS was used as is and there was no need to metathesize it to the tetramethylammonium salt. The voltammetry of the film was similar to that of a film cycled in the TMASS/acetonitrile solution. The $E_{½}$ was unchanged, but the ΔE_p was ca. 20 mV greater. The slightly larger peak separation may be a result of changes in film swelling, and thus the ion transport kinetics, using the different solvent system. The change of cation and solvent appeared not to have any other noticeable effect on the film redox behavior.

Gradient Formation in $Ru(4,4'\text{-}DEAB)_2Cl_2$ and $Fe(4,4'\text{-}PAB)_3(PF_6)_2$ Polymer Films. In applying the potential gradient to the IDA and film, the initial current response spiked and then decayed to a small value as the films reached a steady redox state. It was typical for the films to give small steady-state current responses (ca. 1×10^{-7} A to 1×10^{-8} A). These steady-state current values varied considerably between films (up to several 100's of nA). The variations are likely due to different film thickness and degrees of

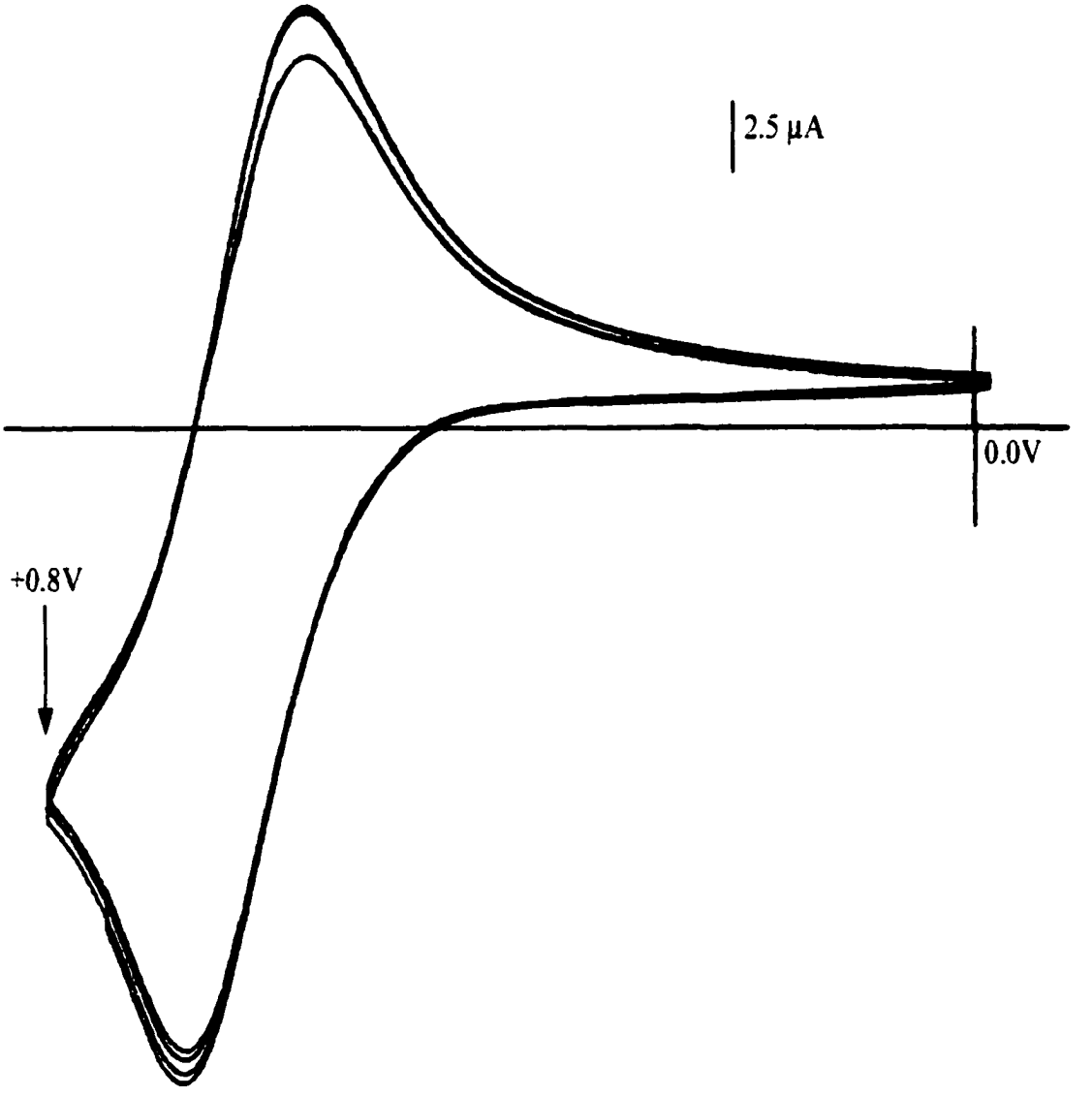

Figure 5.11. Cyclic voltammogram of a Ru(4.4'-DEAB)$_2$Cl$_2$ film on a 0550.5 platinum IDA cycled in 70 mM TMASS/acetonitrile solution. The scan rate was 50mV/s.

polymerization. These film variations could affect the concentration of incorporated anions in the film and the structure of the gradients themselves. For example, a polymer with a high degree of crosslinking would sterically hinder ion transport and ion rearrangement within itself and complete concentration gradients may not occur.

Upon removing a redox gradient-containing film from solution and air-drying, the measured current response showed a current spike that decayed away to a value equivalent to or less than the steady state current measured in solution. In a few cases, the steady state current was too small to measured.

With backlighting under the microscope, alternating regions of reduced and oxidized polymer could be identified in gradient containing films. The Fe(4,4'-PAB)$_3$(PF$_6$)$_2$ films appear red in the reduced state and a pale yellow in the oxidized state. The Ru(4,4'-DEAB)$_2$Cl$_2$ films were green at reduced potentials and pinkish-brown when oxidized. Figure 5.12 is an example of a visible redox gradient in a Ru(4,4'-DEAB)$_2$Cl$_2$ film. It should be noted that not all visible gradients appear as uniform as that depicted in Figure 5.12. In some cases, the gradient appears to be less symmetrical. That is, there seems to be more of the film either reduced or oxidized between the fingers. The cause of this asymmetry was not certain.

When using PF_6^- as the counterion, a visible gradient was always produced in either of the film types used here. This was however, not the case when employing the polymerizable anions. Often, there was no visible gradient identified in the dried films. The lack of a gradient may suggest that the film had undergone some undesirable process that interfered with establishing the $3^+/2^+$ redox gradient. However, interfering chemical

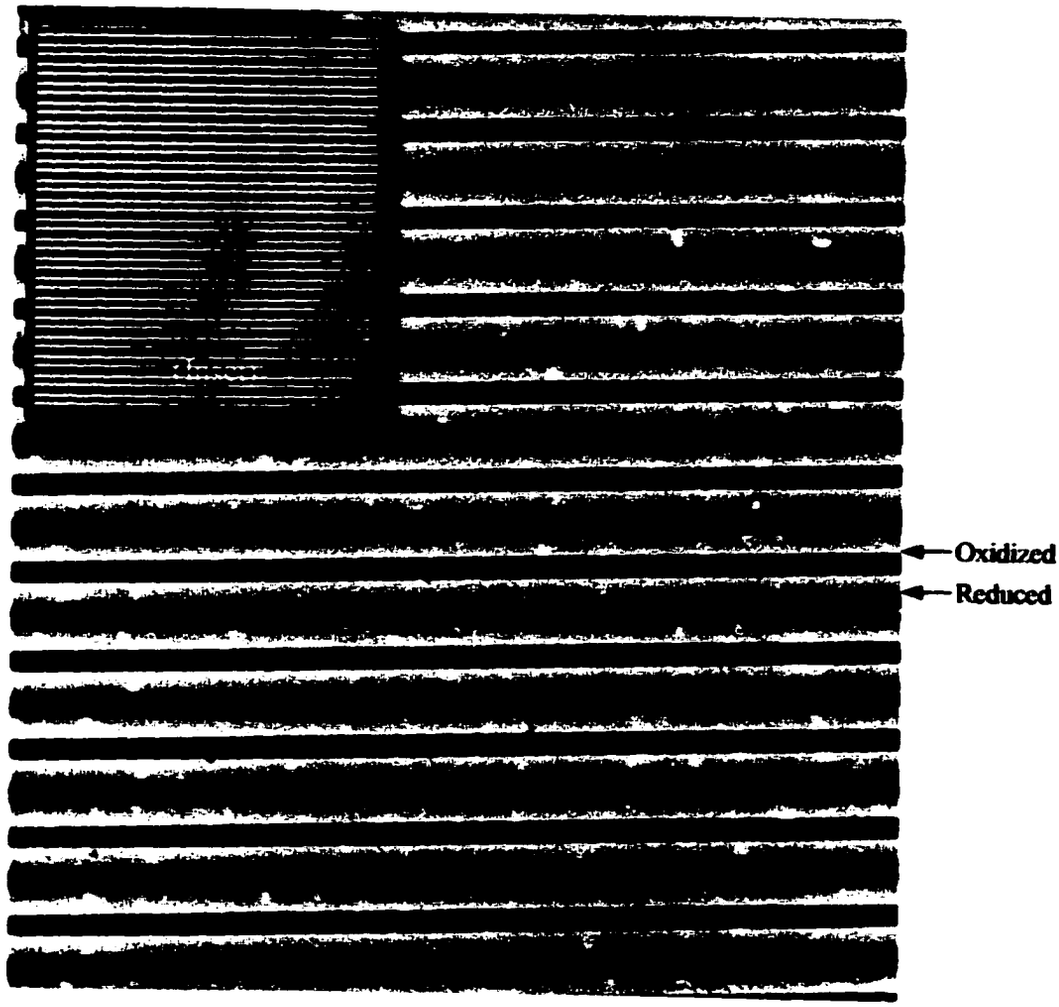

Figure 5.12. Photograph of $Ru(4,4'\text{-}DEAB)_2(Cl)_2/SS^-$ film with locked redox gradient. The film is on a platinum IDA with a 5 μm gap between 5 μm wide fingers. The film is magnified 400 times. The inset photo is of the identical film with 50 times magnification. The dark regions around the fingers are the reduced state of the film and the lighter regions are the oxidized form of the film.

or electrochemical processes should have been noted in the film voltammetry prior to application of the redox gradient.

Visible redox gradients in both the $Ru(4,4'\text{-}DEAB)_2Cl_2$ films and the $Fe(4,4'\text{-}PAB)_3(PF_6)_2$ films were found to have finite lifetimes when in the dry state at room temperature. After ca. three days of sitting on the bench top without a voltage bias, the gradient was no longer visible under microscope examination. When newly formed and dry, the gradient-containing films had small, but measurable current responses (ca. tens of nA or less) when a potential bias of up to 5 V was applied between the finger sets. After loss of the visible gradient, application of the same voltage bias produced no current.

Locking of the Redox Gradient in the Films. When a visible redox gradient formed in films incorporating a polymerizable counteranion, the films were placed in a vacuum oven at elevated temperatures in order to permanently lock the gradient in the film. After polymerization, the films were inspected under the microscope for a preserved visible gradient. Quite often, the film removed from the oven had no visible redox gradient and the film resistance increased from that prior to the locking procedure. These films were very often difficult to remove from the IDA. The films had apparently become highly polymerized but the redox gradient did not remain visible within the film. This was noted to occur with both the $Ru(4,4'\text{-}DEAB)_2Cl_2$ and the $Fe(4,4'\text{-}PAB)_3(PF_6)_2$ films studied in this work.

Fortunately, not all of the redox gradients disappeared with polymerization. Some of the films maintained a visible gradient throughout this second polymerization

process. However, the gradient appeared more faint than it did prior to the locking process.

Figure 5.13a shows the current response of a redox gradient-containing film after polymerization to lock the ion gradient. The sawtooth plot shows a small, symmetrical current response. At +5 V, the current measured was ca. 76 nA, corresponding to a film resistance of ca. 66 MΩ. Prior to thermally locking the redox gradient, the film had a resistance of 0.8 MΩ. In nearly every case in which the gradient was preserved, the film became very resistive ($>1\times 10^9$ Ω).

Figure 5.13b shows the data in 5.13a plotted as current vs. potential. The plot displays a nonlinear current response having increasing current with increasing potential. The shape of the plot is reminiscent of the voltammograms of both uniform and redox gradient-containing mixed valent films as reported by Terrill el al.[122,123] This agreement in plots, at the very least, suggests that there is suppression of the ionic conductivity in our films.

Without an applied potential bias, the film was then wet with acetonitrile and allowed to dry. The subsequent voltammetry of the dry film (Figure 5.13c) showed an ohmic response instead of the curved plot shown in Figure 5.13b. The current response at +5 V has also increased. After half an hour of cycling, the current response decreased slightly. Still, the response remained linear instead of returning to the non-linear response noted prior to wetting. The transient behavior of the film voltammetry with wetting and drying may suggest the lack of a completely locked redox concentration gradient. However, the resulting ohmic response is what one would expect to see for

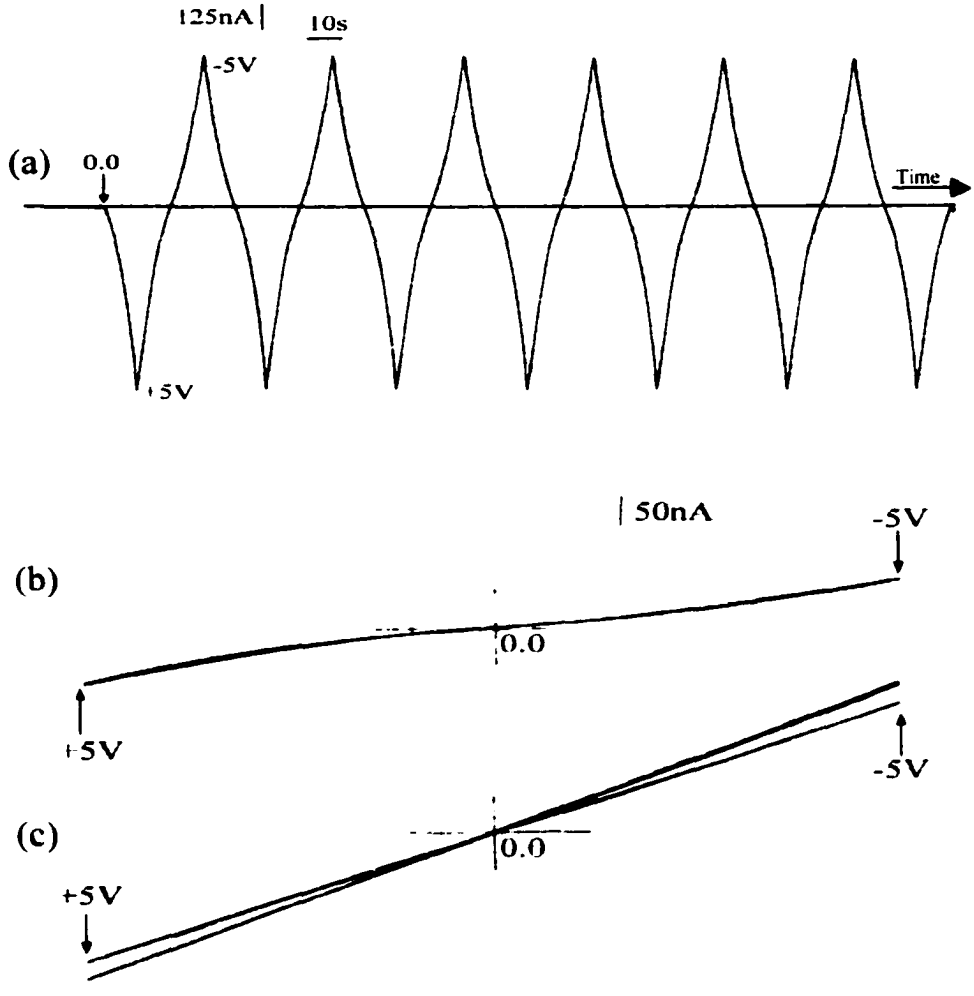

Figure 5.13. Voltammograms of a dry, locked Ru(4,4'-DEAB)$_2$Cl$_2$ film. The gradient was formed in a 50 mM NaSS/dimethylsulfoxide/acetonitrile (70:30, v/v) solution with a potential bias of 590mV between the finger sets of the 0050.5 IDA. Plot (a) is the current vs. time plot of the film cycled between ±5V. The current at ±5V can be seen to lightly decrease with each cycle. Plot (b) is the data in (a) plotted as current vs. potential. Plot (c) is the voltammetry of the film *after* a drop of acetonitrile was added to the film surface and allowed to dry. The current at 5V is noted to decay significantly over time (ca. 30mins). The scan rate used in each plot was 50mV/s.

films containing a locked redox concentration gradient[123] and having only electronic conductivity.[29]

For comparison with the response shown in Figure 5.13b, a dry film containing a redox concentration gradient (*not locked*) was cycled between ±1 V (Figure 5.14). The current response was seen to decrease with time. Some degree of ionic motion may have still existed in the films in Figures 5.13 and 5.14 and the increase in film resistance (or decrease in current) may be an indication of some degree of loss of mixed valency in the films. According to Terrill et al., a loss of the uniform, mixed valent nature of the polymer should result in an increase in film resistance.[123] Voltammetry of the films used in these studies indicated a similar trend. Gradient-locked films had larger resistance values than non-locked, gradient-containing films and films in the single valent state have even larger resistances than gradient-locked films.

After attempting to establish a "locked" redox gradient in the polymer films, some of them were subjected to potential cycling in the electrolyte solution used to establish the redox gradients. Not surprisingly, the resulting voltammetry differed from that recorded prior to establishing the redox gradients in the films. After undergoing the gradient-locking process, the film voltammetry showed increased peak separations and decreased current responses. Based solely on the greater degree of polymerization that likely exists in the "locked" gradient-containing polymer film, the change in voltammetry is expected. What was unexpected was the loss of the visible redox gradient in the "locked" films after potential cycling in solution. The films appeared to be in a completely reduced oxidation state. The final applied potential prior to removing the films from solution was 0.0 V, a potential that could reduce the polymers used in these

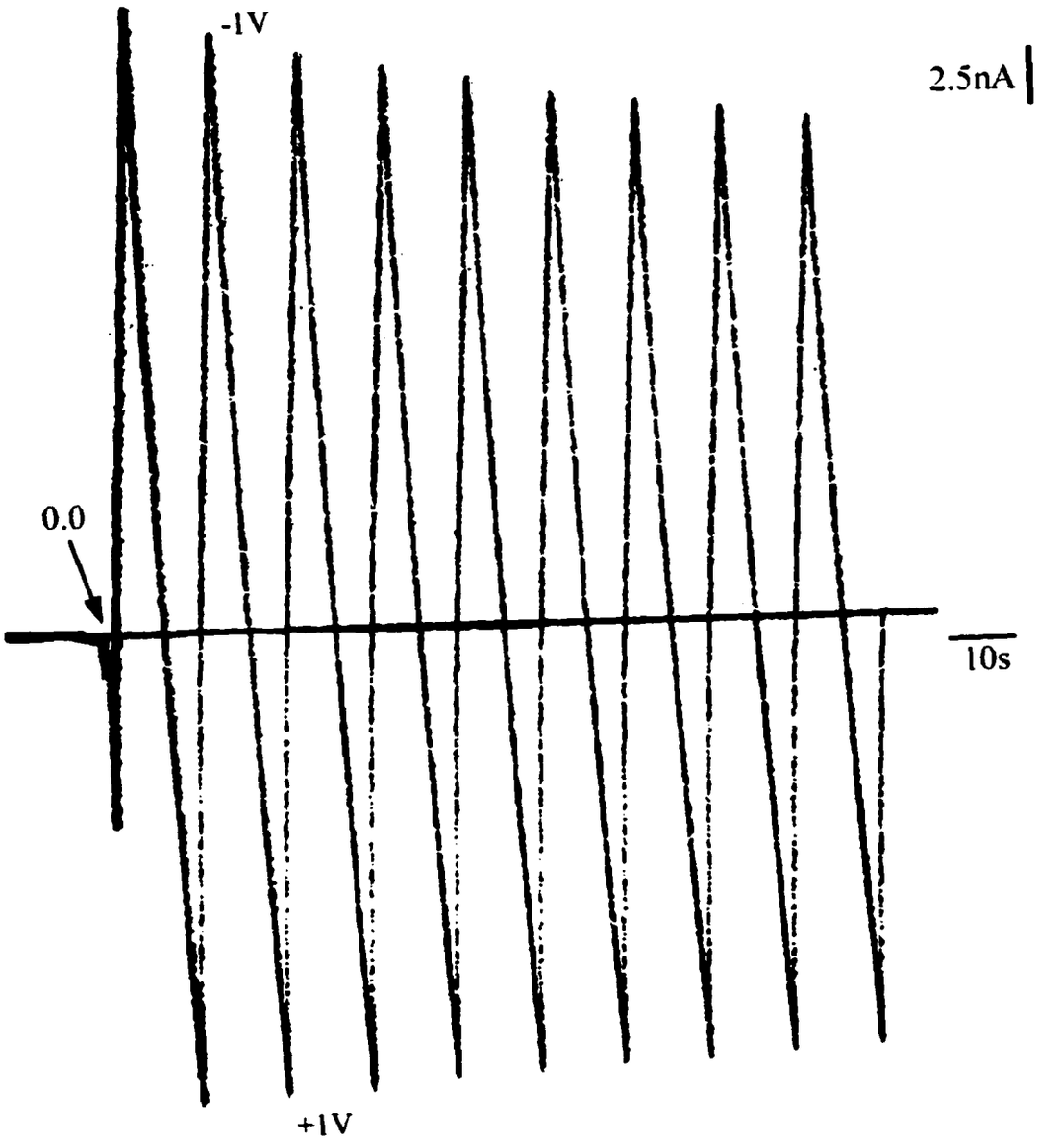

Figure 5.14. Current vs. time plot for a $Ru(4,4'\text{-}DEAB)_2Cl_2$ film on a 0550.5 platinum IDA. The dry, unlocked, gradient-containing film was cycled in air at 50mV/s. The sweep rate was 10s/cm. The film was cycled between ±1.0V.

studies. The loss of the visible gradient would seem to indicate a change in the redox states of the polymer. This could not occur if ionic motion could not take place in the polymer. Rearrangement of incorporated anions may have taken place if the anions had not polymerized with the polymer. It may also be possible that the anions had chemically bonded with the polymer but cations from solution were capable of passing to the trapped anionic sites to compensate for the negative charge; allowing the polymer site to be reduced.

Films Demonstrating Long Term and Robust Electronic Properties. The film characteristics discussed above were commonly noted and unfortunately did not provide much evidence for a permanently locked redox gradient. However, a small number of the films demonstrated behavior that was unique from that of the films described above. These instances all involved the $Ru(4,4'\text{-}DEAB)_2Cl_2$ films incorporating the SS^- counteranion. The films and the redox gradients were prepared identically as the films described above. Potential differences applied across the finger sets for establishing the gradients are shown in Table 5.1.

When these films were removed from the electrolyte solution after setting up the redox concentration gradient, the current response of these films was found to increase by over two orders of magnitude as the film dried. This behavior contrasts with the films discussed above in which the current spiked and then decayed to a very small value (a few nA).

Although faint, a gradient was visible in all the films listed in Table 5.1. The thinness of some of the films may have made it difficult to see the color contrast. Even after the thermal polymerization to fix the gradient, they were still faintly visible.

Dimension of IDA	Electrolyte	Solvent	Potential Difference Between Finger Sets ΔE_{App} (mV)	Resistance of Dry Films (kΩ)		Quality of Visible Gradient
				Before Locking	After Locking	
0550.5	TMASS	ACN	405	3.61	3.43	Faint
0550.5	TMASS	ACN	454	3.75	3.69	Faint
0550.5	TMASS	ACN	500	_____	3.70	Good
0525.3	TMASS	ACN	782	1.91	1.45	Faint
0550.5	KSS	DMSO/ACN	804	_____	3.58	Very Faint

Table 5.1. Films that produced locked visible gradients and electronic properties.

Interestingly, the resistances of the films after locking the gradients in place did not change significantly from that measured prior to the locking process. Table 5.1 shows the resistance values for these redox gradient-containing films.

Voltammetry of the dry, gradient-locked films was done with potentials ranging up to ±29 V. Figure 5.15 shows a plot of the current vs. time for the voltammetry of one of the gradient-locked films listed in Table 5.1. The sawtooth plots for this film, and all of the locked films listed remained stable and repeatable. No change was noted in shape or magnitude of the response with continued cycling. Compare this with a dry Ru(4,4'-DEAB)$_2$Cl$_2$ film that contained a redox gradient but was not thermally locked in place (Figure 5.13). The sawtooth plot in Figure 5.14 shows a large obvious current hysteresis with each cycle as the gradient relaxes under the applied potentials. This type of hysteresis was not present with the film cycled in Figure 5.15. The shape of the plot in Figure 5.15 shows additionally interesting behavior in the current response. It was noted that the slope of the current increase decreased with greater applied voltage. In similar experiments by Terrill et al,[122,123] the slope of the current became increasingly larger as the applied voltage to the dry, locked films increased. Terrill's reported response was similar to that noted in Figure 5.13a and b, not to that in Figure 5.15.

Wetting the films listed in Table 5.1 in either pure solvent or electrolyte solutions did not affect the dry film conductivity. For example, one of the gradient-locked films was subjected to potential cycling in a TMASS/acetonitrile solution. The voltammetry differed from that seen prior to setting up the redox gradient, as may be expected, if only from the greater polymerization of the film. The voltammetry was much smaller in magnitude and there was a greater difference in the peak potentials (Figure 5.16). The

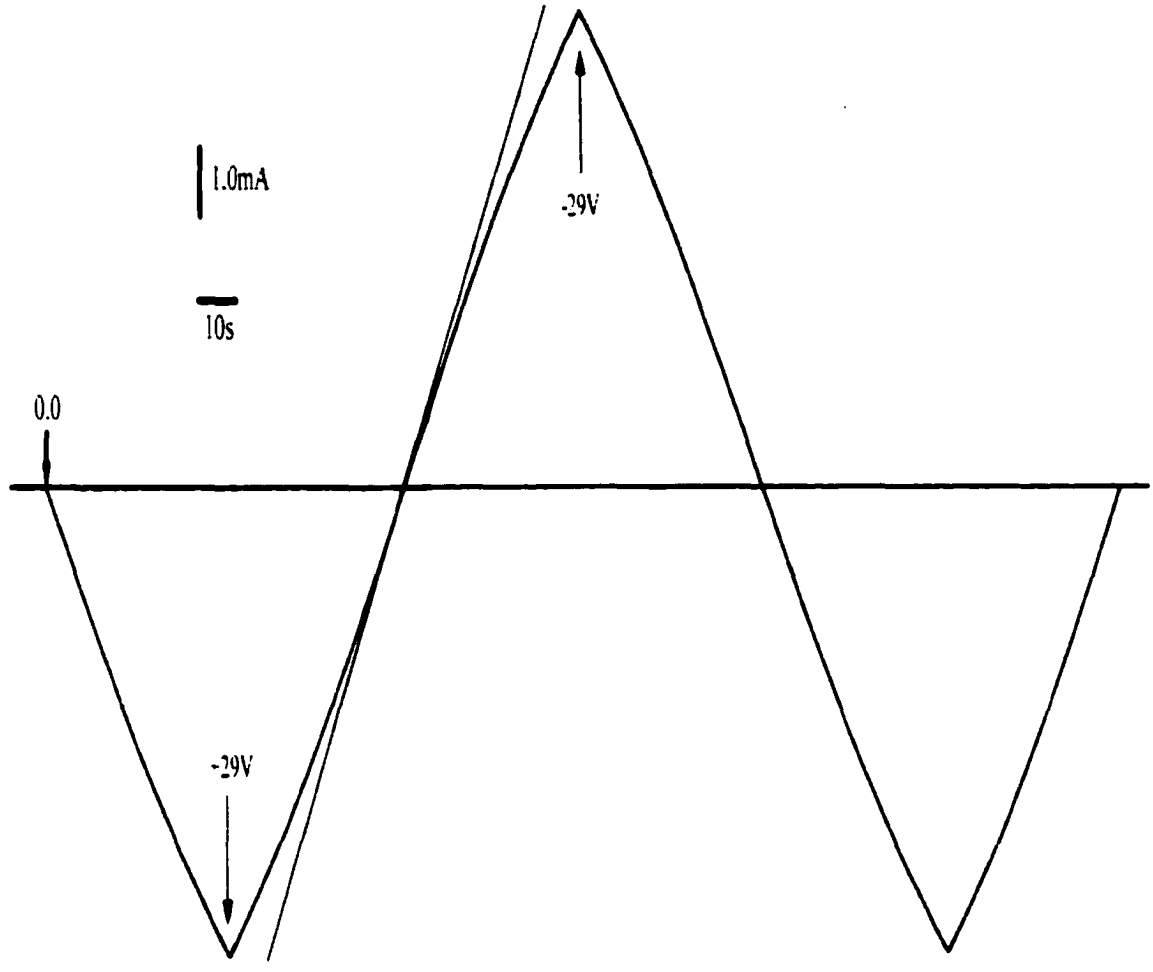

Figure 5.15. Current vs time plot for a dry locked gradient-containing Ru(4,4'-DEAB)$_2$Cl$_2$ film on a 0550.5 platinum IDA. The SS^- anion was used to fix the redox gradient in place. The film was cycled between ±29V. The sweep rate was 10s/cm and the scan rate for the potential was 200mV/cm.

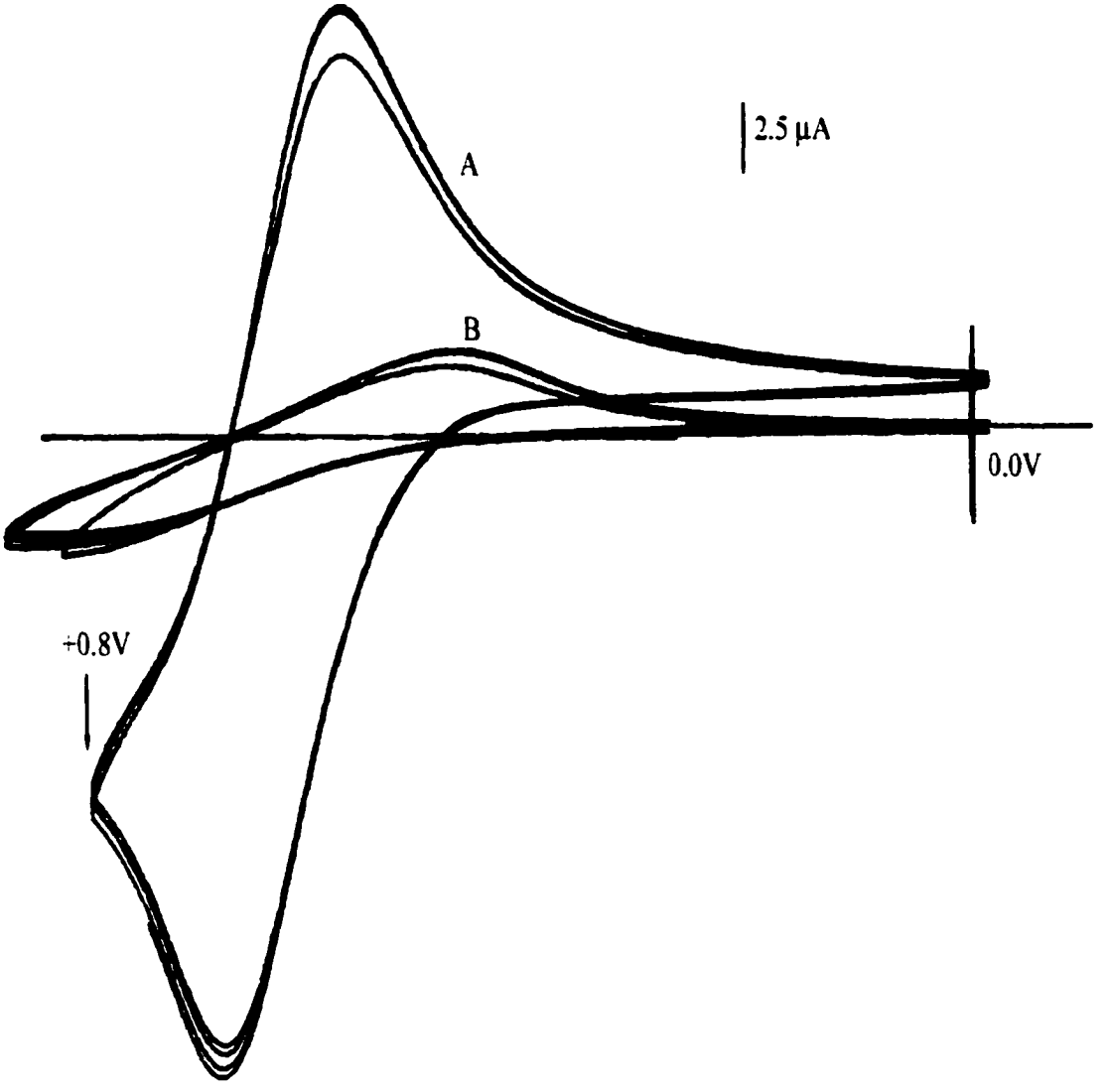

Figure 5.16. Cyclic voltammograms of a $Ru(4,4'\text{-}DEAB)_2Cl_2$ film on a 0550.5 platinum IDA cycled in a 70mM TMASS/acetonitrile solution before establishing the redox concentration gradient (A) and after locking the redox gradient in place and drying the film (B). The scan rate for both voltammograms was 50mV/s.

occurrence of *any* voltammetry in the solution suggests that there are still some accessible sites for ion transport to compensate charge variations in the films. It may be that cation transport can occur in order to compensate for the grafted anions inside the polymer, thus allowing for electrochemistry of the metal centers. Removing the film from the solution and reexamining the presence of the visible gradient and the electronic properties of the film showed that the electrochemical process had not changed these characteristics of the film. The gradient was still visible and the resistance of the film was unchanged. This was true for all the films listed in Table 5.1.

Films that did not show the high conductivity of the films in Table 5.1, but showed a visible gradient and underwent the polymerization process to lock the gradient (such as those in Figure 5.14), did not show the preservation of the visible gradient and the electronic properties after performing the wet voltammetry. Cycling the supposedly locked gradient-containing film in solution resulted in large changes in the film voltammetry and the gradient was no longer seen. Even the addition of acetonitrile alone to such a film and allowing to dry, changed the subsequent electrochemistry of the again dry film (Figure 5.13c).

It was proposed that the low resistance of the locked films in Table 5.1 might have been due to shorts in the film that occurred during the introduction of the redox gradients and not the result of a gradient microstructure. The presence of a short was investigated through applying a voltage (1.5 V) between the finger sets of the IDA and covering the film with a low boiling point solvent, i.e., n-pentane. If a short existed, bubble formation in the n-pentane due to resistive heating would be witnessed. Two of the films in Table 5.1 produced bubbles in the solvent; the others did not. The source of

the bubbles was a small crack or opening in the films. These hot spots were touched with a pointed wood applicator to remove the region of the film around the source of the bubbles. The removal of the film halted the formation of the bubbles but did not change the resistance measurement in the film. Apparently, these hot spots did not affect the measured electronic properties of the films.

Investigation of the resistive properties of the films with temperature was explored. The results are shown in Figure 5.17. It was found that the current (at 1.5 V applied voltage) decreased with an increase in the temperature of the film. This is suggestive of metallic resistance-temperature behavior and was noted for the films submerged in a range of solvents. The current-temperature relationship corresponds with the shape of the sawtooth voltammetry shown in Figure 5.15 if one assumes that there was a degree of resistive heating occurring in the dry film at the large applied potentials.

The plots defined by the circles in Figure 5.17 show excellent agreement in the current-temperature data. The other plots, though the slopes are similar, are offset. The circle plots are for films that were prepared from the identical monomer solution at the same time under exactly identical conditions. It is likely the films' thickness and degree of polymerization were better matched to each other than to the other films represented. This may explain the close agreement in the resistance values and the data in Figure 5.17. This gives support to the presence of a locked gradient in the films. If this unique film behavior was a result of shorting or some other anomaly of contamination, it would seem unlikely that the data of the two circle plots would agree so closely.

The temperature experiments and the submersion of the films in the various solvents did not affect the electronic properties of the dry films.[126] Some of the films did

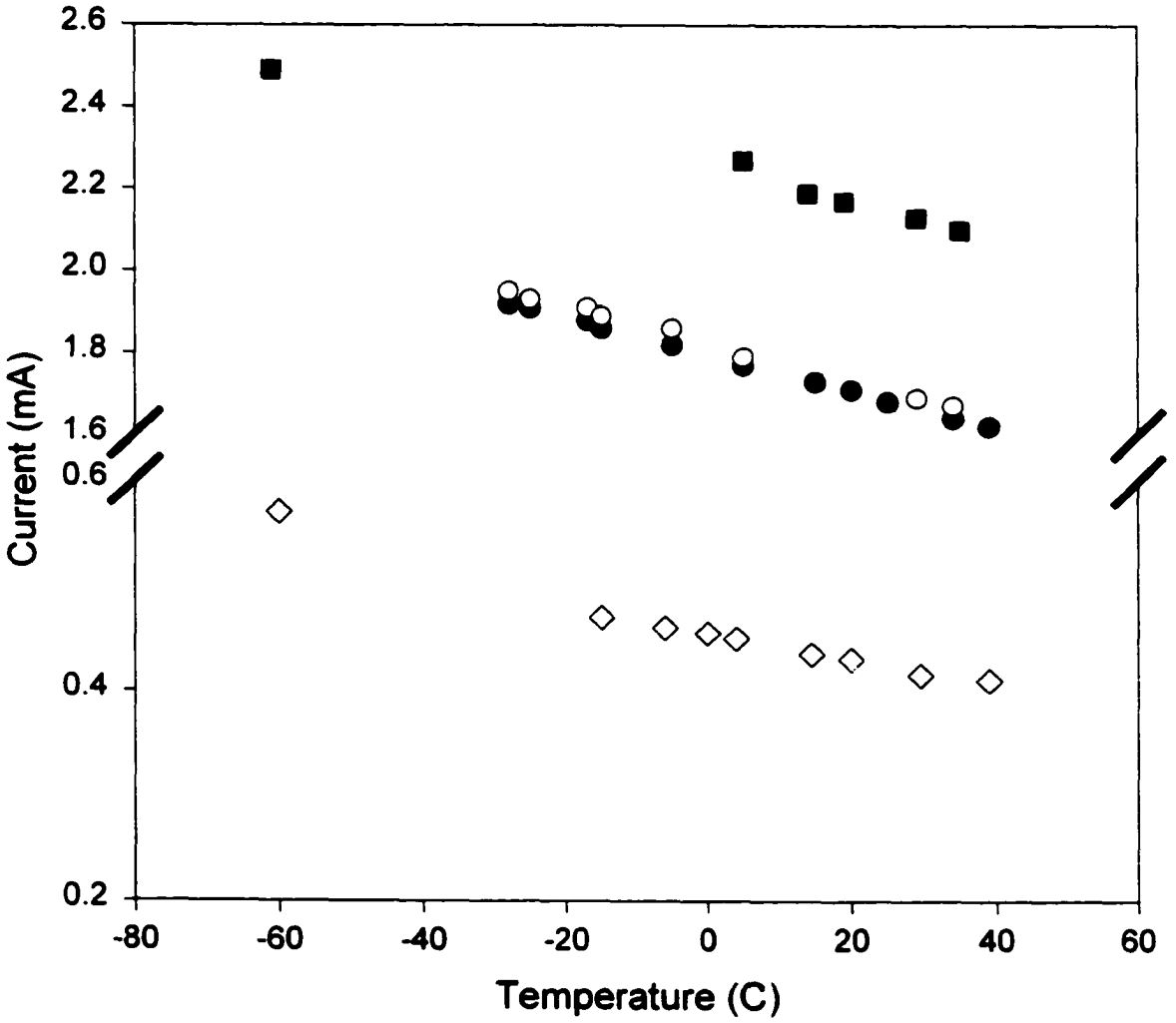

Figure 5.17. Current vs. temperature plots for $Ru(4,4'\text{-}DEAB)_2Cl_2$ films that have a fixed visible redox gradient.

show signs of cracking and loss of material on the film edges, but the resistance and voltammetry remained essentially unchanged. The films appeared to be quite robust.

The films in Table 5.1 were left on the bench top without any applied potential. Figure 5.18 shows the resistance of one of the films for the first 800 hours. The value remained essentially unchanged. In fact, at the time of this writing, the resistance of the film has remained unchanged for more than 6000 hours! The gradient was still faintly visible under magnification and appeared unchanged. The other films in Table 5.1 also maintained their electronic properties for several months and showed no sign of change. Given the conditions that the films were exposed to and the persistence of the electronic properties and visible gradient, there is strong evidence that these films had a truly locked redox gradient.

DISCUSSION

The currently available data for the attempts at locking the redox concentration gradients in the redox polymer films unfortunately does not absolutely verify the existence of chemically locked redox gradients. The bulk of the attempts appeared to be unsuccessful at fully locking a redox gradient. That is not to say that a gradient in the film did not exist but that there appeared to be at least some minimal amount of ionic motion still present in the supposedly "locked" gradient-containing films.

As mentioned above, only some of the films formed a visible gradient. In our work, redox gradients could be seen in the films because of the color difference between the reduced and oxidized states of the polymer films. Visible gradients could be readily prepared in films incorporating common electrolytes solutions such as $TBAPF_6$. Using

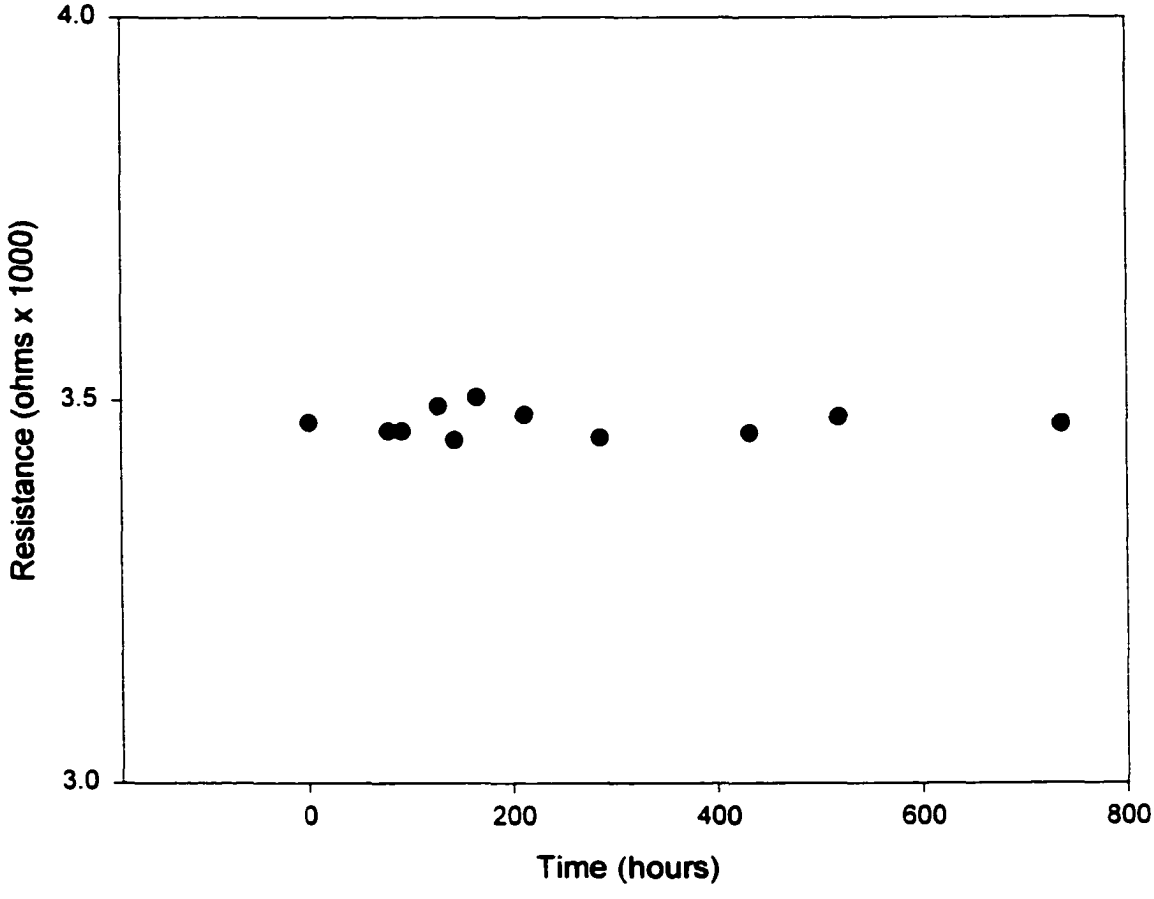

Figure 5.18. Plot of the resistance vs. time for a locked gradient containing Ru(4,4'-DEAB)$_2$Cl$_2$ film. The film remained under ambient lab conditions without any potential bias to support the redox gradient.

an electrolyte containing a polymerizable anion (either SS^- or 3-SPA^-) produced less satisfactory results when looking for a visible gradient. The inability to consistently form visible gradients with the polymerizable anions in the films is not yet explainable. However, interactions between the anions and the films could result in poor gradient formation. For example, impeded ion motion or rearrangement of counterions due to steric hindrance within the film may result in the formation of poor redox gradients. That is, the distribution of redox sites could not become strongly polarized between neighboring fingers as portrayed in Figure 5.2a. Instead, only a partial polar distribution of redox states would form (Figure 5.19). Without complete gradient formation, color variations around the electrode fingers due to the change in the redox state of the polymer would likely be difficult to visually identify.

For films that had visible redox gradients, resistance values between the two combs of the IDAs were quite large. The measured resistances were on the order of ca. 1×10^9 Ω. The corresponding current measurements were in the tens to hundreds of nA. These were similar in magnitude to the current values reported by Terrill et al. in similar studies.[123]

Most "locked" gradient-containing films (see Figure 5.13a and b) gave current responses to potential sweeps similar to those reported by Terrill et al.[122,123] Terrill et al. postulated a small degree of ionic motion in their dry, gradient-containing films. At room temperature, some current hysteresis to voltage changes was noted and it was believed to result from ionic conductivity. Reducing the temperature of the films greatly reduced the measured current hysteresis. With our films, we typically saw a dramatic decrease in the current response with time for the dry, gradient-containing (*but unlocked*) films (Figure

5.14). Thermally locking the redox gradients in the films greatly minimized the current decay noted with the dry, unlocked, gradient-containing films. The decay, however, was not completely eliminated and still occurred, though to a lesser degree. By comparison with Maness's work,[119,120] the slower current decay of the locked films with the larger current decay of the unlocked films suggests a minimization (but not elimination) of ionic mobility.

A few unique instances were presented for films in which the current response of the films did not decrease upon drying of the gradient containing film, but showed a large current increase. The large current response corresponds to film resistances about 6 orders of magnitude smaller than the resistance of most gradient-containing films produced in this work. These films were seen to contain faint visible redox gradients and they retained the gradient during the thermal process to lock them in place. According to Terrill's work,[122] gradient-locked films should have rather large resistances with respect to the uniform, mixed valent state of the film. However, the presence of a visible color gradient in our films suggests otherwise. The electronic behavior of these films was found to be stable under quite severe conditions. Wetting by solvents had no effect on the film voltammetry, nor did the application of large potentials. There was no appearance of current hysteresis like that seen with most films (Figure 5.13 and 5.14).

The dry, gradient-"locked" films in Table 5.1 gave current responses to applied potentials that differed from that noted for most gradient-"locked" films (Figures 5.13a and 5.14) produced in this study and from that reported by Terrill et al. and Maness et al.[119,120,122,123] Instead of increasing with applied potential, the current response decreased (Figure 5.15). This behavior may be explained by resistive heating in the film

during the potential sweep. Increasing the temperature of the film resulted in a decrease in the current passing between the combs of the IDA (Figure 5.17). Conversely, Maness et al. and Terrill et al. found their films to increase in conductivity with an increase in temperature.[119,123]

The films in Table 5.1 were also found to maintain their electronic properties and visible color gradient under ambient conditions for extended periods of time without the aid of a potential bias. This suggests that the gradient formation was stable and permanent. These characteristics would be expected from a chemically locked redox gradient in these films.

Unfortunately, the reproducibility of films containing the gradient microstructures was low. This was particularly true for films that had low resistances and high stability. Assuring better and more uniform film formation and quantitative verification of the formation of a redox concentration gradient would likely increase the reproducibility of the film behavior.

CONCLUSIONS

The preliminary studies presented here have not provided hard evidence for the chemical locking of redox gradient microstructures in the redox polymer films. There is, however, evidence suggesting that the process presented in this chapter may be a viable means of permanently locking in place the redox gradients.

We've identified interesting and unique behavior in several of the redox gradient-containing films. The permanency of the electronic behavior and the presence of the

visible gradients is optimistic evidence for the presence of the chemically locked redox gradients.

The main issue to be addressed in future work is that of reproducibility. A more established film production method and analysis of film structure is needed to ensure the films are of identical thickness and polymerization. This would allow for greater uniformity in the films and the resulting redox gradient. The chemical locking of redox gradients can be extended to serial gradients as well as a single gradient. Formation of permanent serial gradients would allow for the study of unique electrical properties (i.e., diode-like behavior) in thin films and allow for long-lived light emitting devices that would have generous operating parameters.

REFERENCES

(1) Josowicz, M.; Janata, J.; Ashley, K.; Pons, S. *Anal Chem* **1987**, *59*, 253-258.

(2) Miasik, J. J.; Hooper, A.; Tofield, B. C. *Journal of the Chemical Society-Faraday Transactions I* **1986**, *82*, 1117-&.

(3) Dobay, R.; Harsanyi, G.; Visy, C. *Anal. Chim. Acta* **1999**, *385*, 187-194.

(4) Foulds, N.; Lowe, C. R. *J. Chem. Soc.-Faraday Trans.* **1986**, *82*, 1259-1264.

(5) Hoa, D. T.; Kumar, T. N. S.; Punekar, N. S.; Srinivasa, R. S.; Lal, R.; Contractor, A. Q. *Anal Chem* **1992**, *64*, 2645-2646.

(6) van de Leur, R. H. M.; van der Waal, A. *Synth. Met.* **1999**, *102*, 1330-1331.

(7) Sukeerthi, S.; Contractor, A. Q. *Indian J. Chem. Sect A-Inorg. Phys. Theor. Anal. Chem.* **1994**, *33*, 565-571.

(8) Vidal, J. C.; Garcia, E.; Castillo, J. R. *Anal. Chim. Acta* **1999**, *385*, 213-222.

(9) Vigmond, S. J.; Kallury, K. M. R.; Ghaemmaghami, V.; Thompson, M. *Talanta* **1992**, *39*, 449-456.

(10) Partridge, A. C.; Jansen, M. L.; Arnold, W. M. *Mater. Sci. Eng. C-Biomimetic Supramol. Syst.* **2000**, *12*, 37-42.

(11) Endres, H. E.; Drost, S.; Hutter, F. *Sens. Actuator B-Chem.* **1994**, *22*, 7-11.

(12) Imisides, M. D.; John, R.; Wallace, G. G. *Chemtech* **1996**, *26*, 19-25.

(13) Momma, T.; Nishimura, K.; Osaka, T.; Kondo, N.; Nakamura, S. *J. Electrochem. Soc.* **1994**, *141*, 2326-2331.

(14) Goward, G. R.; Leroux, F.; Nazar, L. F. *Electrochim. Acta* **1998**, *43*, 1307-1313.

(15) Croce, F.; Panero, S.; Passerini, S.; Scrosati, B. *Electrochim. Acta* **1994**, *39*, 255-263.

(16) Chandrasekar, P. In *Conducting Polymers; Fundamentals and Applications. A Practical Approach*; Kluwar Academic Publishers: Boston, 1999; pp 573-589.

(17) Waltman, R. J.; Diaz, A. F.; Bargon, J. *J. Electrochem. Soc.* **1984**, *131*, 1452-1456.

(18) Novak, P.; Muller, K.; Santhanam, K. S. V.; Haas, O. *Chem. Rev.* **1997**, *97*, 207-281.

(19) Burgmayer, P.; Murray, R. W. *J. Am. Chem. Soc.* **1982**, *104*, 6139-6140.

(20) Burgmayer, P.; Murray, R. W. *J. Electroanal. Chem.* **1983**, *147*, 339-344.

(21) Burgmayer, P.; Murray, R. W. *J. Phys. Chem.* **1984**, *88*, 2515-2521.

(22) Schlenoff, J. B.; Chien, J. C. W. *J. Am. Chem. Soc.* **1987**, *109*, 6269-6274.

(23) Although not true semiconductors, it is typical to discuss the electronic conductivity of conducting polymers as if they were.

(24) Hayes, W. *Contemp. Phys.* **1985**, *26*, 421-441.

(25) Hendrickson, S. M. In *Ph. D. Dissertation*; Colorado State University, 1997.

(26) Bredas, J. L.; Street, G. B. *Accounts Chem. Res.* **1985**, *18*, 309-315.

(27) Redding, J. L.; Reynolds, J. R. *Advances in Polymer Science*; Springer-Verlag: Berlin, 1999; Vol. 145.

(28) Frommer, J. E.; Chance, R. R. In *Electrical and Electronic Properties of Polymers: A State-of-the-Art Compendium*; Kroshwitz, J. I., Ed.; John Wiley and Sons: New York, 1988; pp 56-101.

(29) Wilbourn, K.; Murray, R. W. *J. Phys. Chem.* **1988**, *92*, 3642-3648.

(30) Malinauskas, A. *Polymer* **2001**, *42*, 3957-3972.

(31) Mirmohseni, A.; Oladegaragoze, A. *Synth. Met.* **2000**, *114*, 105-108.

(32) Caruso, F. *Adv. Mater.* **2001**, *13*, 11-+.

(33) Gangopadhyay, R.; De, A. *Chem. Mat.* **2000**, *12*, 608-622.

(34) Sadki, S.; Schottland, P.; Brodie, N.; Sabouraud, G. *Chem. Soc. Rev.* **2000**, *29*, 283-293.

(35) Baker, C. K.; Qiu, Y. J.; Reynolds, J. R. *J. Phys. Chem.* **1991**, *95*, 4446-4452.

(36) Janata, J. *Anal Chem* **1991**, *63*, 2546-2550.

(37) Warren, L. F.; Walker, J. A.; Anderson, D. P.; Rhodes, C. G.; Buckley, L. J. *J. Electrochem. Soc.* **1989**, *136*, 2286-2295.

(38) Diaz, A. F.; Martinez, A.; Kanazawa, K. K. *J. Electroanal. Chem.* **1981**, *130*, 181-187.

(39) McCullough, R. D. *Adv. Mater.* **1998**, *10*, 93-+.

(40) Delabouglise, D. *Synth. Met.* **1992**, *51*, 321-327.

(41) Feldheim, D. L.; Krejcik, M.; Hendrickson, S. M.; Elliott, C. M. *J. Phys. Chem.* **1994**, *98*, 5714-5720.

(42) Tsai, E. W.; Basak, S.; Ruiz, J. P.; Reynolds, J. R.; Rajeshwar, K. *J. Electrochem. Soc.* **1989**, *136*, 3683-3689.

(43) Diaz, A. F.; Castillo, J.; Kanazawa, K. K.; Logan, J. A.; Salmon, M.; Fajardo, O. *J. Electroanal. Chem.* **1982**, *133*, 233-239.

(44) Feldheim, D. L.; Hendrickson, S. M.; Krejcik, M.; Elliott, C. M. *Chem. Mat.* **1995**, *7*, 1124-1131.

(45) Zotti, G.; Zecchin, S.; Schiavon, G.; Groenendaal, L. *Chem. Mat.* **2000**, *12*, 2996-3005.

(46) Duffitt, G. L.; Pickup, P. G. *J. Chem. Soc.-Faraday Trans.* **1992**, *88*, 1417-1423.

(47) Ren, X. M.; Pickup, P. G. *J. Phys. Chem.* **1993**, *97*, 5356-5362.

(48) Zhou, Q. X.; Kolaskie, C. J.; Miller, L. L. *J. Electroanal. Chem.* **1987**, *223*, 283-286.

(49) Josowicz, M. *Analyst* **1995**, *120*, 1019-1024.

(50) Paulse, C. D.; Pickup, P. G. *J. Phys. Chem.* **1988**, *92*, 7002-7006.

(51) Kaufman, J. H.; Kanazawa, K. K.; Street, G. B. *Phys. Rev. Lett.* **1984**, *53*, 2461-2464.

(52) Song, M. K.; Park, J. K.; Yeo, I. H.; Rhee, H. W. *Synth. Met.* **1999**, *99*, 219-225.

(53) Naoi, K.; Lien, M.; Smyrl, W. H. *J. Electrochem. Soc.* **1991**, *138*, 440-445.

(54) Lien, M.; Smyrl, W. H.; Morita, M. *J. Electroanal. Chem.* **1991**, *309*, 333-340.

(55) Zhong, C. J.; Doblhofer, K. *Electrochim. Acta* **1990**, *35*, 1971-1976.

(56) Reynolds, J. R.; Pyo, M.; Qiu, Y. J. *Synth. Met.* **1993**, *55*, 1388-1395.

(57) Li, Y. F.; Liu, Z. F. *Synth. Met.* **1998**, *94*, 131-133.

(58) Arca, M.; Mirkin, M. V.; Bard, A. J. *J. Phys. Chem.* **1995**, *99*, 5040-5050.

(59) Bose, C. S. C.; Basak, S.; Rajeshwar, K. *J. Phys. Chem.* **1992**, *96*, 9899-9906.

(60) Lim, J. Y.; Paik, W. K.; Yeo, I. H. *Synth. Met.* **1995**, *69*, 451-454.

(61) Mao, H.; Pickup, P. G. *J. Phys. Chem.* **1989**, *93*, 6480-6485.

(62) Ren, X. M.; Pickup, P. G. *Electrochim. Acta* **1996**, *41*, 1877-1882.

(63) Bach, C. M. G.; Reynolds, J. R. *J. Phys. Chem.* **1994**, *98*, 13636-13642.

(64) Krishna, V.; Ho, Y. H.; Basak, S.; Rajeshwar, K. *J. Am. Chem. Soc.* **1991**, *113*, 3325-3333.

(65) Shinohara, H.; Kojima, J.; Aizawa, M. *J. Electroanal. Chem.* **1989**, *266*, 297-308.

(66) Pickup, P. G.; Osteryoung, R. A. *J. Electroanal. Chem.* **1985**, *195*, 271-288.

(67) Bard, A. J.; Faulkner, L. R. *Electrochemical Methods*; Wiley: New York, 1980.

(68) Vorotyntsev, M. A.; Vieil, E.; Heinze, J. *J. Electroanal. Chem.* **1998**, *450*, 121-141.

(69) It is important to emphasize that the ring potential be chosen such that it is well onto the limiting current plateau of the cation reduction so that small variations in potential from iR drop do not effect the ring current.

(70) The magnitude of $i_{r,0}$ in equation 2 is proportional to $\omega^{1/2}$ where is the electrode rotation rate; the quantities $i_d(t)$ and $i_r^*(t)$ are, on the other hand, independent of . Consequently, the signal-to-background in these experiments increases as decreases. In all experiments reported here, was maintained at 400 rpms, which is the lowest rotation rate available with the PIR rotator. While they are independent of , the values of $i_d(t)$ and i_r^* do depend on the polymer thickness and the potential scan rate, . At fast scan rates, a collection of problems can arise from iR drop, from ion/electron transport rates within the polymer film, and from maintaining insufficient flux of dopant ions from solution to the polymer interface (see text). A scan rate of 50 mV/s was determined to be an optimum compromise and was used in all of the studies reported here unless otherwise noted.

(71) The quantity $\beta^{2/3}$ is experimentally the ratio of the independently determined ring and disk currents measured from the mass transport-limited oxidation or reduction

of some arbitrary solution species. Since the limiting currents at either electrode are proportional to the flux of species to the respective surface, knowing the limiting flux at one electrode and β, the flux at the other electrode can be calculated.

(72) While it would be interesting to quantitate the potential dependence of f_{C^+} under flux-limited conditions, the small absolute and relative concentrations of the minor component make such studies virtually impossible because of the poor overall signal-to-noise. Nonetheless, the dependence is qualitatively obvious.

(73) The Cc^+ was modeled using CAChe™ Editor, Release 3.9. The CMP^+ and DMP^+ measurements were done with Biograf by BioDesign, Inc., Version 2.2.

(74) Lacroix, J. C.; Kanazawa, K. K.; Diaz, A. *J. Electrochem. Soc.* **1989**, *136*, 1308-1313.

(75) Kalaji, M.; Peter, L. M.; Abrantes, L. M.; Mesquita, J. C. *J. Electroanal. Chem.* **1989**, *274*, 289-295.

(76) Kalaji, M.; Nyholm, L.; Peter, L. M. *J. Electroanal. Chem.* **1991**, *313*, 271-289.

(77) Salzer, C. A.; Elliott, C. M.; Hendrickson, S. M. *Anal Chem* **1999**, *71*, 3677-3683.

(78) Bahr, S. R.; Boudjouk, P. *J. Org. Chem.* **1992**, *57*, 5545-5547.

(79) Size estimates were made using CAChe™ Editor, Release 3.9.

(80) There is some speculation that the growth potential can have some affect on the ion transport. However, growth potential was not considered as a variable parameter in this study.

(81) Duffitt, G. L.; Pickup, P. G. *J. Phys. Chem.* **1991**, *95*, 9634-9635.

(82) Slater, J. M.; Watt, E. J. *Analyst* **1991**, *116*, 1125-1130.

(83) Slater, J. M.; Watt, E. J. *Analytical Proceedings* **1992**, *29*, 53-56.

(84) Torres-Rodrigues, L. M.; Billon, M.; Roget, A.; Bidan, G. *Synth. Met.* **1999**, *102*, 1328-1329.

(85) Charlesworth, J. M.; Partridge, A. C.; Garrard, N. *J. Phys. Chem.* **1993**, *97*, 5418-5423.

(86) Pearce, T. C.; Gardner, J. W.; Friel, S.; Bartlett, P. N.; Blair, N. *Analyst* **1993**, *118*, 371-377.

(87) Sotzing, G. A.; Briglin, S. M.; Grubbs, R. H.; Lewis, N. S. *Anal Chem* **2000**, *72*, 3181-3190.

(88) Kunugi, Y.; Nigorikawa, K.; Harima, Y.; Yamashita, K. *J. Chem. Soc.-Chem. Commun.* **1994**, 873-874.

(89) Janata, J.; Langmaier, J. *Analytical Proceedings* **1991**, *28*, 372-373.

(90) Sangodkar, H.; Sukeerthi, S.; Srinivasa, R. S.; Lal, R.; Contractor, A. Q. *Anal Chem* **1996**, *68*, 779-783.

(91) Green, M. J.; Hill, H. A. O. *Journal of the Chemical Society-Faraday Transactions I* **1986**, *82*, 1237-1243.

(92) Sung, W. J.; Bae, Y. H. *Anal Chem* **2000**, *72*, 2177-2181.

(93) Umana, M.; Waller, J. *Anal Chem* **1986**, *58*, 2979-2983.

(94) Sadik, O. A.; Brenda, S.; Joasil, P.; Lord, J. *J. Chem. Educ.* **1999**, *76*, 967-970.

(95) Tatsuma, T.; Gondaira, M.; Watanabe, T. *Anal Chem* **1992**, *64*, 1183-1187.

(96) Nishizawa, M.; Matsue, T.; Uchida, I. *Anal Chem* **1992**, *64*, 2642-2644.

(97) Lyons, M. E. G.; Lyons, C. H.; McCormack, D. E.; McCabe, T. J.; Breen, W.; Cassidy, J. F. *Analytical Proceedings* **1991**, *28*, 104-106.

(98) Talaie, A.; Lee, J. Y.; Lee, Y. K.; Jang, J.; Romagnoli, J. A.; Taguchi, T.; Maeder, E. *Thin Solid Films* **2000**, *363*, 163-166.

(99) Atta, N. F.; Galal, A.; Mark, H. B.; Yu, T.; Bishop, P. L. *Talanta* **1998**, *47*, 987-999.

(100) EG&G Princeton Applied Research, Application Note AC-1, Princeton, New Jersey, 1989.

(101) McNeil, C. J.; Athey, D.; Ball, M.; Ho, W. O.; Krause, S.; Armstrong, R. D.; Wright, J. D.; Rawson, K. *Anal Chem* **1995**, *67*, 3928-3935.

(102) Schmittle, J. In *Ph. D. Dissertation*; Colorado State University, 1989.

(103) Schuetzle, D.; Hammerle, R. *Fundamentals and Applications of Chemical Sensors*; American Chemical Society: Washington, D.C., 1986.

(104) Janata, J. *Principles of Chemical Sensors*; Plenum Press: New York, 1989.

(105) Amrani, M. E. H.; Payne, P. A.; Persaud, K. C. *Sens. Actuator B-Chem.* **1996**, *33*, 137-141.

(106) Refer to Chapter 3 of this manuscript.

(107) Bartlett, P. N.; Lingchung, S. K. *Sensors and Actuators* **1989**, *19*, 141-150.

(108) Bartlett, P. N.; Lingchung, S. K. *Sensors and Actuators* **1989**, *20*, 287-292.

(109) Hanawa, T.; Kuwabata, S.; Yoneyama, H. *Journal of the Chemical Society-Faraday Transactions I* **1988**, *84*, 1587-1592.

(110) Blackwood, D.; Josowicz, M. *J. Phys. Chem.* **1991**, *95*, 493-502.

(111) Freund, M. S.; Lewis, N. S. *Proc. Natl. Acad. Sci. U. S. A.* **1995**, *92*, 2652-2656.

(112) Topart, P.; Josowicz, M. *J. Phys. Chem.* **1992**, *96*, 8662-8666.

(113) It was noted in SEM micrographs of the bare IDA electrodes that the dimensions of the 0525.3 IDAs were not as reported by Abtech Scientific. These devices had finger widths of ca. 7 μm and a gap width of ca. 3 μm. These devices will still, however, be identified by the designation 0525.3.

(114) Diaz, A. F.; Castillo, J. I.; Logan, J. A.; Lee, W. Y. *J. Electroanal. Chem.* **1981**, *129*, 115-132.

(115) Scherer, M. M.; Richter, S.; Valentine, R. L.; Alvarez, P. J. J. *Crit. Rev. Microbiol.* **2000**, *26*, 221-264.

(116) Mackay, D. M.; Cherry, J. A. *Environ. Sci. Technol.* **1989**, *23*, 630-636.

(117) Lide, D. R., Ed. *Handbook of Chemistry and Physics*; 72 ed.; CRC Press: Ann Arbor, 1991.

(118) Maness, K. M.; Terrill, R. H.; Meyer, T. J.; Murray, R. W.; Wightman, R. M. *J. Am. Chem. Soc.* **1996**, *118*, 10609-10616.

(119) Maness, K. M.; Masui, H.; Wightman, R. M.; Murray, R. W. *J. Am. Chem. Soc.* **1997**, *119*, 3987-3993.

(120) Masui, H.; Murray, R. W. *J. Electrochem. Soc.* **1998**, *145*, 3788-3793.

(121) Terrill, R. H.; Hatazawa, T.; Murray, R. W. *J. Phys. Chem.* **1995**, *99*, 16676-16683.

(122) Terrill, R. H.; Hutchison, J. E.; Murray, R. W. *J. Phys. Chem. B* **1997**, *101*, 1535-1542.

(123) Elliott, C. M.; Pichot, F.; Bloom, C. J.; Rider, L. S. *J. Am. Chem. Soc.* **1998**, *120*, 6781-6784.

(124) The cis- and the trans- complexes of the Ru complex have been separated and

identified according to the methods by Schmittle.

(125) Elliott. C. M.; Kopelove, A. B.; Albery, W. J.; Chen, Z. J. *Phys. Chem.* **1991**, *95*, 1743.

APPENDIX I

The Collection Efficiency, N

The rotation of a cylindrical electrode in a solution establishes a controlled hydrodynamic motion of solvent and solution species in the near region of the electrode. The solution is drawn to the surface of the electrode and is then is forced outward in a radial direction along the electrode surface. In the case of a rotating ring-disk electrode, this provides for the movement of solution from the center disk region, across the insulating gap, and then over the ring. In this manner, the disk can become the generator (source of primary electrochemistry) and the ring the collector (site of secondary electrochemistry). The efficiency of the ring electrode to impart a second electrochemical reaction upon the generated redox species from the disk is related solely to the geometry of the ring-disk electrode. Stated simply, the larger the distance from the edge of the disk to the inside edge of the ring the smaller the value of the collection efficiency, N. Decreasing the thickness of the ring decreases the value of N.

For the electrode we employ in these studies, the insulating gap between the disk and the ring is rather large at 1.4mm. This larger gap was created to keep electrochemically grown films from extending over the gap and shorting the two working electrodes (i.e., the ring and the disk). As a result of the larger gap, the collection efficiency of this particular electrode is rather small.

A rather involved mathematical approach exists for determination of the collection efficiency[67]. However, a more simplistic experimental means provides accurate determinations. Using the ferrocene/ferricinium couple, the value of N for the electrode was determined by measuring the limiting ring current and limiting disk current. Limiting currents are noted, as the motion of the analytes to the electrode surface is not diffusion limited; a result of the electrode rotation at these scan rates. With rotation of the electrode, the disk is cycled out to a sufficiently positive potential to oxidize the ferrocene to ferricinium. Meanwhile, the ring is held at a potential sufficient to reduce ferricinium back to ferrocene. By comparison of the disk current to the ring current the value of N can then be readily measured. This value is constant regardless of the solvent or electrolyte system used. In this work, it was found to be unchanged with the presence of the polymer film. For the particular electrode used in these studies, N had a value of 0.12 (or 12%).

For a more thorough discussion of the collection efficiency, refer to reference 67.

APPENDIX II

Asyst Program

The following is the Asyst program used for collection of the cyclic voltammetry data in the RRDE studies. The program has been modified to perform data averaging in order to improve the signal-to-noise in the collected data. Three channels were used for data collection: Channel 1 for disk potential (E_d), channel 2 for disk current (i_d), and channel 3 for the ring current (i_r). The data was collected from a Pine RDE4 bipotentiostat. The bipotentiostat was modified to generate sweep potentials from ±2V to ±5V. A Data Translation DT2801-A acquisition board with 12-bit resolution and a throughput of 27.5 kHz was used for data collection.

```
                        \ rrde2
                        \ data acq for rrde expts
                        \ cycled disk and const. E on ring
                        \ for external bi-potentiostat
                        \ uses channel 1 ED, 2 iD, 3 iR
                        \ v1.0 written 1/97 by SMH
                        \ v1.1 data averaging loop appended
                        \ 11/97 by BJW and CAS
                        \ adaptation of EQCM.CV and cax2.
dt2800                  \ initialize DT2801-A (board driver)
```

```
integer scalar last             \ dummy variable 'last' to 'forget'
                                \ declare variables
integer scalar adpoints         \ total # of data points
real scalar adpoints3           \ array dimension for ED, iD & iR
integer scalar adgain           \ a/d board gain settings
real scalar apadrate            \ Apparent sampling rate in Hz
real scalar adrate              \ Real sampling rate in Hz
real scalar vrange              \ voltage range from gain setting
real scalar vrange1             \ mid-point of voltage range
real scalar potential           \ potentiostat disk potential setting
real scalar currD.set           \ potentiostat disk i setting
real scalar currR.set           \ potentiostat ring i setting
real scalar time1               \ time of forward E step
real scalar STN                       \ # of points for signal:noise
correction
real scalar STN3                    \ size of array holding data for
averaging
integer scalar count1           \ loop variable for data collection
integer scalar count2           \ loop variable for S:N data collection
token ED.out                    \ ED.out is disk potential data
token iD.out                    \ iD.out is disk i data
token iR.out                    \ iR.out is ring i data



: set.var                           \ define routine 'set.var'
echo.off
cr ." Enter the time for the cycle(s) (sec): "
#input
```

```
time1 :=
cr ." Enter the sampling rate in Hz wanted: "
#input
apadrate :=
cr ." Enter the number of data points to be collected for S:N
correction: "
#input
STN :=
cr ." Enter the E range for disk (0=+-10V, 1=+-5V, 2=+-2.5V 3=+-1.25V):
"
#input
adgain :=
cr ." Enter the potentiostat disk current setting: "
#input
currD.set :=
cr ." Enter the potentiostat ring current setting: "
#input
currR.set :=
apadrate STN * adrate :=              \ Set real aquis rate

echo.on
;
set.var                               \ now actually execute 'set.var'

time1 apadrate * adpoints :=          \ adpoints are the total number of
                                      \ data points to be taken
STN 3 * STN3 :=                       \ array dimension for ED, iD & iR
```

```
\ define 1D arrays for use in signal-to-noise data processing

integer dim[ STN ] array ED.buffer
integer dim[ STN ] array iD.buffer
integer dim[ STN ] array iR.buffer
integer dim[ adpoints ] array ED.tempo
integer dim[ adpoints ] array iD.tempo
integer dim[ adpoints ] array iR.tempo

\ define 1D array "data.buffer" to have a dimension of adpoints3
integer dim[ STN3 ] array data.buffer

1 3 a/d.template rrde.template        \ set up the a/d 'template'
                                      \ set channels 1-3 for data acq
                                      \ ch 1 = ED, ch 2 = iD, ch 3 = iR
data.buffer template.buffer


: go                                  \ subroutine 'go' to acquire data
0 data.buffer :=                      \ clear data.buffer array
0.1 conversion.delay                    \ set board conv time at minimal
value
adgain a/d.gain                       \ set a/d gain for board
                                      \  (determined by disk potential
range)

adrate inv 1000.  *  sync.period      \
```

```
cr ." Press any key to begin data acquisition."  pckey
cr  ." Data being acquired..."    cr

0 count1 :=
begin
  a/d.init
  0 data.buffer :=                                  \ start of outer data
aquisition loop
  0 count2 :=
  begin                                            \ start of nested data
aquistion loop
    a/d.in>array
    1 count2 + count2 :=
    synchronize
    STN count2 =
  until
1 count1 + count1 :=

  data.buffer sub[ 1 , STN , 3 ] ED.buffer :=      \ separate array
data.buffer
  ED.buffer mean
  ED.tempo [ count1 ] :=
  0 ED.buffer :=

  data.buffer sub[ 2 , STN , 3 ] iD.buffer :=      \ into 3 different
arrays
  iD.buffer mean
  iD.tempo [ count1 ] :=
  0 iD.buffer :=
```

```
  data.buffer sub[ 3 , STN , 3 ] iR.buffer :=
  iR.buffer mean
  iR.tempo [ count1 ] :=
  0 iR.buffer :=

  adpoints count1 =
until

ED.tempo becomes> ED.out                \ transfer temp array data into
tokens
iD.tempo becomes> iD.out
iR.tempo becomes> iR.out




\ determine vrange for a/d gain
0 adgain =
if 20. vrange := then
1  adgain =
if 10. vrange := then
2 adgain =
if 5. vrange := then
3 adgain =
if 2.5 vrange := then
vrange  2.0  /  vrange1 :=              \ for bipolar middle voltage
```

```
\ convert & scale data
ED.out 4095. / vrange * vrange1 - becomes> ED.out
iD.out 4095. / vrange * vrange1 - currD.set * becomes> iD.out
iR.out 4095. / vrange * vrange1 - currR.set * becomes> iR.out
;

: plotcvd
3 color
ed.out neg id.out neg
xy.auto.plot
;

: plotcvr
3 color
ed.out neg ir.out neg
xy.auto.plot
;

: ploted
3 color
ed.out neg
y.auto.plot
;

: plotiD                                    \ routine to plot iD data
3 color
iD.out neg
y.auto.plot
;
```

```
: 2ndiD                                    \ routine to add iD curve to plot
iD.out neg
y.data.plot
;

: plotqD                                   \ routine to plot QD data
3 color
iD.out neg
integrate.data
y.auto.plot
;

: 2ndqD                                    \ routine to add QD curve to plot
iD.out neg
integrate.data
y.data.plot
;

: plotq2D                                  \ routine to plot integrated QD
data
3 color
iD.out neg
integrate.data integrate.data
y.auto.plot
;
                                           \ routine to add Q2D curve to
plot
: 2ndq2D
```

```
iD.out neg
integrate.data integrate.data
y.data.plot
;

: intiD                                    \ routine to list QD data
iD.out neg
integrate.data
cr ." Integrated iD = " .
;

: int2iD                                     \ routine to list integrated QD
data
iD.out neg
integrate.data integrate.data
cr ." Twice integrated iD = " .
;

: plotiR                                   \ routine to plot iR data
3 color
iR.out neg
y.auto.plot
;

: 2ndiR                                    \ routine to add iR curve to plot
iR.out neg
y.data.plot
;
```

```
: plotqR                                    \ routine to plot QR data
3 color
iR.out neg
integrate.data
y.auto.plot
;

: 2ndqR                                     \ routine to add QR curve to plot
iR.out neg
integrate.data
y.data.plot
;

: plotq2R                                     \ routine to plot integrated QR
data
3 color
iR.out neg
integrate.data integrate.data
y.auto.plot
;
                                            \ routine to add Q2R curve to
plot
: 2ndq2R
iR.out neg
integrate.data integrate.data
y.data.plot
;

: intiR                                      \ routine to list QR data
```

```
iR.out neg
integrate.data
cr ." Integrated iR = " .
;

: int2iR                                    \ routine to list integrated QR
data
iR.out neg
integrate.data integrate.data
cr ." Twice integrated iR = " .
;

: create.file                               \ subroutine to store data to
diskfile
file.template
1 comments
integer dim[ 1 ] subfile
real dim[ adpoints ] subfile
3 times
end
;
                                           \ definitions for file read/write
12 string filename
60 string comment1
integer dim[ 1 ] array npoints

: sto.ca                                   \ routine to store data
cr ." Enter file name to save data in: "
"input
```

```
filename ":=
cr ." Type in one comment (60 chars): "
"input
comment1 ":=
create.file
filename defer> file.create
filename defer> file.open
adpoints npoints [ 1 ] :=
comment1 1 >comment
1 subfile npoints array>file
2 subfile ED.out array>file
3 subfile iD.out array>file
4 subfile iR.out array>file
file.close
cr ." File written to and closed."
;

: write.ca                              \ routine to output ascii data
cr ." Enter file name to save data in: "
"input defer> out>file                  \ send ascii output to console &
file
cr ." Type in one comment (60 chars): "
"input
cr ." Number of data points: " npoints  .
cr ." Disk potential data array: " ED.out .
cr ." Disk current data array: " iD.out .
cr ." Ring current data array: " iR.out .
cr ." Ascii data file written."
out>file.close
```

```
;

: sto123.ca                          \ routine to write current and
load.overlay 123io.sov               \ charge data to lotus file
cr ." Enter file name to save data in: "
"input
filename ":=
filename defer> 123file.create       \ create and open file
filename defer> 123file.open
1 1 123write.across                  \ write from row1 col1
cr ." Type in one comment (60 chars): "     \ input comments
"input ">123file                     \ write comments to file
2 2 123write.down                    \ write in row2 col2
adpoints npoints [ 1 ] :=
npoints array>123file                \ write number of data points
3 2 123write.down
ED.out array>123file                 \ wrue the disk pot data in r3 c2
3 3 123write.down
iD.out array>123file                 \ write the disk cur data in r3 c3
3 4 123write.down
iR.out array>123file                 \ write the ring cur data in r3 c4

123file.close                        \ close file
release.overlay                      \ reset overlay
cr ." File written to and closed."
;

: asysttol23.ca                      \ routine to convert ca file to
                                     \ lotus file
```

```
load.overlay 123io.sov                  \ save cur in col1 and charge in
col2
cr ." Enter file name to get chronoamp data from: "
"input
filename ":=
filename defer> file.open
1 subfile npoints file>array
npoints [ 1 ] adpoints :=
2 subfile  file>unnamed.array becomes> ED.out
3 subfile  file>unnamed.array becomes> iD.out
4 subfile  file>unnamed.array becomes> iR.out
cr ." File comment: "
1 comment> comment1 ":=
file.close
cr ." File read and closed."  cr cr
cr ." Enter file name to save data in: "
"input
filename ":=
filename defer> 123file.create          \ create and open file
filename defer> 123file.open
1 1 123write.across                     \ write from row1 col1
comment1 ">123file
2 1 123write.down
adpoints npoints [ 1 ] :=
npoints array>123file                   \ write number of data points
3 2 123write.down
ED.out array>123file                    \ write the disk pot in r3 c2
3 3 123write.down
iD.out array>123file                    \ write the disk cur data in r3 c3
```

```
3 4 123write.down
iR.out array>123file                    \ write the ring cur data in r3 c4

123file.close                           \ close file
release.overlay                         \ reset overlay
cr ." File written to and closed."
;

: get.ca                                  \ routine to retrieve chronoamp
data
cr ." Enter file name to get chronoamp data from: "
"input
filename ":=
filename defer> file.open
1 subfile npoints file>array
npoints [ 1 ] adpoints :=
2 subfile  file>unnamed.array becomes> ED.out
3 subfile  file>unnamed.array becomes> iD.out
4 subfile  file>unnamed.array becomes> iR.out
cr ." File comment: "
1 comment>  cr "type cr
file.close
cr ." File read and closed."  cr cr
;

1 3 a/d.template rrde.template            \ set up the a/d 'template'
data.buffer template.buffer                 \ set channels 1-3 for data
acq
```

```
: menu
cr ." RRDE- commands: "
cr ." Enter 'go' to run rrde experiment. "
cr ."    ploti, plotq or plotq2 to plot i, Q or Q2 vs t."
cr ."      2ndi, 2ndq or 2ndq2 to add curves to plot.   (change color
first.)"
cr ."    inti or int2i to list integrated data."
cr ."    sto.ca to store ca data, write.ca to write ascii data."
cr ."    get.ca retrieve data."
cr ."    sto123.ca to store open data to a lotus file"
cr ."    asysttol23.ca to convert ca data to a lotus file"
cr ." 'menu' to get this menu."
;

screen.clear
menu
```